Chem. Chem. Technol., 2019,
Vol. 13, No. 3, pp. 275–279

Chemistry

SPECTROPHOTOMETRIC DETERMINATION OF RUTHENIUM UTILIZING ITS CATALYTIC ACTIVITY ON OXIDATION OF HEXACYANOFERRATE(II) BY PERIODATE ION IN WATER SAMPLES

Abhishek Srivastava[1, *], Vivek Sharma[1], Anjali Prajapati[1], Neetu Srivastava[2], R. M. Naik[3]

https://doi.org/10.23939/chcht13.03.275

Abstract. The catalytic effect of ruthenium chloride on the outer sphere electron transfer of hexacyanoferrate(II) by periodate ion in aqueous alkaline medium has been effectively employed to determine ruthenium(III) at micro level. The optimum reaction condition has been established and fixed time procedure is adopted. A linear relationship between changes in absorbance and added Ru(III) concentration has been utilized for the trace level determination of Ru(III). The results reveal that the addition of interfering ions (up to 71 times higher concentration of Ru) does not have significant effect on the catalytic activity of Ru(III) on oxidation of hexacyanoferrate(II) by periodate ion. Polyaminocarboxylates (HEDTA, EDTA and IDA) suppress its catalytic power to maximum, if tolerance limit is more than 14.29 times. Due to the reproducibility, stability and selectivity, this method can also be quantitatively applied in different types of water samples for determination of ruthenium(III) at micro level.

Keywords: kinetics, mechanism, hexacyanoferrate(II), periodate, ruthenium(III).

1. Introduction

Ruthenium, a noble metal, is found in crustal materials at very low concentration (few ppb) [1], whereas meteorites and chondrite contain much higher percentage of ruthenium [2]. However, ruthenium compounds are highly toxic and carcinogenic, different studies have been reported for materials containing ruthenium complexes in electronic, electrochemical and electrical industries [1, 2]. The complexes of ruthenium have found applications in pharmaceutical industries in the detection and determination of protein, antibiotic, chloramphenicol, and cefprozil [3-5]. Ruthenium along with its complexes exhibits excellent catalytic property in both alkaline and acidic medium for the reactions having environmental and commercial applications [6-18]. To fight against the deadly disease of cancer a number of ruthenium bearing complexes have been prepared and their antitumor properties are tested [19-21]. The life span of hosts bearing tumor increases by the intake of certain ruthenium compounds in spite of low cytotoxicity of ruthenium agents. Due to high catalytic activity of ruthenium, alloys of ruthenium are used as catalyst in fuel cells. Pt-Ru bimetallic alloy show the highest activity for the methanol oxidation reaction in methanol fuel cells [22]. Nanoparticles of Ru-Pt have also been used as an effective catalyst for carbon monoxide – tolerant fuel cell [23]. Thus, the potential application of ruthenium and its complexes in various areas, especially in pharmacology [24] and metallurgy [25] has made a challenge to develop a rapid, selective, simple and inexpensive method for the determination of ruthenium in different type of samples at trace level. The catalytic and inhibition properties have been extensively used for the growth and development of analytical methods for the trace level determination of different elements and compounds. The processes for the ruthenium determination viz. spectrophotometry, cyclic voltametry, atomic absorption spectrophotometry, mass spectrometry, HPLC, atomic absorption spectrometry, and X-ray fluorescence, have been used by investigators. Despite of good sensitivity and selectivity most of these methods are complicated, time consuming and require expensive chemicals. Therefore, the catalytic kinetic methods (CKMs) employing spectrophotometric monitoring (SPM) under pseudo condition still remain a popular method for achieving ruthenium(III) estimation at trace level [26-38]. A comparison of known CKMs along with reaction condition, types of sample and dynamic range of detection (DRD) are summarized in Table 1 [28, 29, 32-38].

[1] Department of Chemistry, G.L.A. University, Mathura, U.P., India
[2] Department of Chemistry, D.D.U. Gorakhpur University, Gorakhpur, 273001, U.P., India
[3] Department of Chemistry, Lucknow University, Lucknow, 226007, U.P. India
[*] *aabhichem@gla.ac.in*

Table 1

A comparative study of determination of ruthenium(III) involving different reactions

Major reactants	D.R.D. (χd) $ng \cdot ml^{-1}$	Methods used and reaction conditions	Samples used	Ref. No.
Thymol blue and potassium bromate	1 to 25	CKM, SPM, λmax 544 nm, temp. 308 K	Synthetic samples	32
Tren and hexacyanoferrate(III)	10.11 to 252.67	CKM, SPM, λmax 420 nm, temp. 318 K, time 10 min	Water samples	28
Benzylamine and $[Fe(CN)_6]^{3-}$	10 to 121 (6.90)	CKM, SPM, λmax: 420 nm, temp. 308 K, time 5 min	Synthetic samples	34
Phenosafranine and $NaIO_4$	Nanogram range	CKM, SPM, λmax 520 nm	Synthetic water samples	36
L-Phenylalanine and $KMnO_4$	0.101 to 2.526 (0.08)	CKM, SPM, λmax 526 nm, temp. 318 K, time 5 min	Tap water, synthetic mixtures	29
Ce(IV) and As(III)	0.45 to 9.00 (0.08)	CKM, SPM, λmax 625 nm, PC-ANN used	Synthetic samples	37
Hematoxylin and H_2O_2	5 to 120	CKM, SPM, λmax 440 nm, temp. 308 K	Synthetic mixtures	35
Acridine orange and chlorite	1 to 10	CKM, SPM, λmax 490 nm, temp. 298 K, time 5 min	Synthetic water samples	35
Safranin O and potassium metaperiodate	0.80 to100.0 (0.25)	CKM, SPM, λmax 521 nm, temp. 308 K, time 5 min	Synthetic water samples	33

In order to extend our efforts for development of CKMs for the determination of ruthenium(III) [28-29], the present study proposed a new, rapid, selective, sensitive, and less expensive method to determine Ru(III) by applying its catalytic property on oxidation of hexacyanoferrate(II) by periodate ion in highly basic condition. The proposed method permits to determine the [Ru(III)] down to 10 $ng \cdot ml^{-1}$ with very good accuracy and reproducibility. The minute amount of ruthenium is also added in certain areas of rivers, lakes and oceans as industrial wastes. In the present study we have developed a selective CKM for Ru(III) determination in water samples.

2. Experimental

2.1. Reagents

Analytical grade chemicals and double distilled water were used throughout the investigation. Potassium hexacyanoferrate(II) (Sigma) was used as such for the preparation of stock solution and kept in dark colored container to prevent photo-degradation. The 1.0M solution of sodium metaperiodate (Merck) was prepared, to prevent decomposition it was always wrapped with aluminium foil. Calculated amount of ruthenium(III) chloride (Alfa) was used for the preparation of its stock solution (100 $\mu g \cdot ml^{-1}$) in 0.5M HCl. The potassium iodide (S. D. Fine) solution was used to check the possible oxidation of ruthenium(III) in hydrochloric acid. Sodium chloride (Merck) solution was used to fix ionic strength (0.1M) of reaction mixture. pH of the reactants were fixed separately at 9.50 ± 0.02 using sodium hydroxide and perchloric acid. Standardization of pH meter was done by standard BDH buffers.

2.2. Apparatus

The progress of catalytic reaction was examined using Sisco single beam visible spectrophotometer, model GIGI-110 equipped with self designed thermostated cell chamber. The pH was maintained by Elico LI-120 digital pH meter. The glassware was cleaned thoroughly with detergent, rinsed with dilute EDTA, dipped in 10% HNO_3 for minimum 10 min and finally washed thoroughly with double distilled water. The spectrophotometer cuvettes were cleaned by soaking in 15% HNO_3 to discharge ruthenium traces adsorbed on cell walls.

2.3. Procedure

Except the Ru(III) concentration, the concentration of the reactants, pH and ionic strength were judiciously chosen from the kinetic examination of the catalytic electron transfer reaction [39]. The reaction conditions under which the catalytic activity of Ru(III) was optimum were selected for quantitative analysis. All the standard solutions were thermally equilibrated at 303.0 ± 0.1 K. The pseudo-first-order conditions were applied to study the reaction by taking minimum 10 times excess of periodate over hexacyanoferrate(II). The progress of the electron transfer of hexacyanoferrate(II) by periodate was monitored using "fixed time procedure" in highly alkaline medium by computing the increase in absorbance at 420 nm. The change in absorbance at a definite time interval were computed to plot the calibration curve

between Ru(III) concentration and change in absorbance. To prevent the complications arising due to possible interference by the reagents and products present in the reaction system, the inceptive rate was followed to determine Ru(III).

3. Results and Discussion

The optimum reaction condition has been established and fixed time procedure was adopted to obtain regression equations. The graphs plotted between ΔAt (change in absorbance at *t*, min) *versus* [Ru(III)] (Fig.1) exhibited the linear dependency on [Ru(III)] in the concentration range of $(1–20)\cdot10^{-7}$ M (10–202 ng·ml^{-1}), which is in good agreement with theoretical concept. The calibration equations relating Δ*At* (*t* =2, 5 and 7 min) and [Ru(III)], detection limit and correlation coefficients (r^2), are summarized in Table 2.

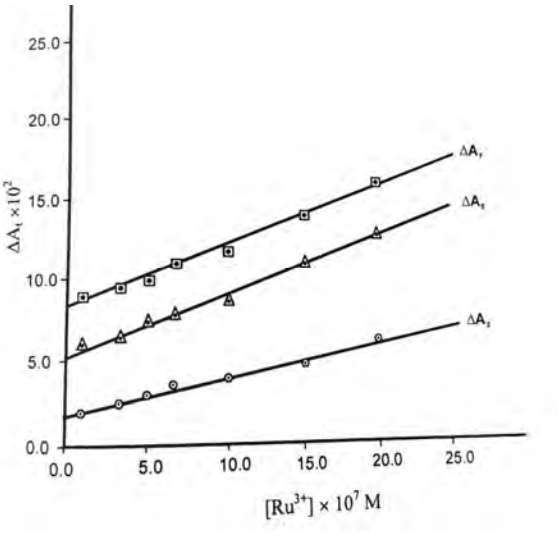

Fig. 1. Plot between Δ*At* (change in absorbance at *t*, min) *vs.* [Ru(III)]

Table 2

Determination of ruthenium(III) at $[Fe(CN)_6]^{4-} = 2.25\cdot10^{-4}$, $[NaIO_4] = 7.5\cdot10^{-3}$, pH = 9.5 ± 0.02, *T* = 303 ± 0.1 K, *I* = 0.1M (NaCl)

Calibration equations	Linear range, M	Detection limit, μg·ml^{-1}	Correlation coefficient r^2
$\Delta A_2 = 2.25\cdot10^4[Ru^{3+}] + 0.018$	$(1–20)\cdot10^{-7}$	0.0081	0.9972
$\Delta A_5 = 3.28\cdot10^4[Ru^{3+}] + 0.053$	$(1–20)\cdot10^{-7}$	0.0053	0.9921
$\Delta A_7 = 4.31\cdot10^4[Ru^{3+}] + 0.078$	$(1–20)\cdot10^{-7}$	0.0038	0.9892

Table 3

Computation of recovered ruthenium(III) in spiked water with % error at $[Fe(CN)_6]^{4-} = 2.25\cdot10^{-4}$, $[NaIO_4] = 7.5\cdot10^{-3}$, pH = 9.5 ± 0.02, *T* = 303 ± 0.1 K, *I* = 0.1M (NaCl)

Ru(III) taken, ng·ml^{-1}	ΔA_2		ΔA_5		ΔA_7	
	Ru(III) found, ng·ml^{-1} ± S.D. ng·ml^{-1}	Error, %	Ru(III) found, ng·ml^{-1} ± S.D. ng·ml^{-1}	Error, %	Ru(III) found, ng·ml^{-1} ± S.D. ng·ml^{-1}	Error, %
10.11	10.08 ± 0.09	-0.30	9.96 ± 0.08	-1.51	9.91 ± 0.10	-2.02
33.35	33.66 ± 0.13	0.93	33.98 ± 0.21	1.85	33.82 ± 0.18	1.39
50.54	51.02 ± 0.28	0.95	51.09 ± 0.33	1.08	51.11 ± 0.62	1.12
67.72	66.98 ± 0.46	-1.09	67.02 ± 0.51	-1.04	66.82 ± 0.88	-1.35
101.07	102.13 ± 0.39	1.05	102.45 ± 0.56	1.35	102.82 ± 0.76	1.70
121.28	119.96 ± 0.53	-1.09	117.08 ± 0.25	-3.59	118.06 ± 0.44	-2.73
151.601	153.24 ± 0.76	1.08	152.41 ± 0.26	0.53	154.21 ± 0.32	1.69
181.93	181.06 ± 0.65	-0.48	180.26 ± 0.61	-0.93	180.06 ± 0.68	-1.04
202.14	200.86 ± 0.23	-0.63	198.25 ± 0.38	-1.96	199.61 ± 0.21	-1.27

The precision, accuracy and reproducibility of the present method for Ru(III) determination was tested by adding calculated amount of Ru(III) in double distilled water and conducting experiments for recovery. The percentage errors and standard deviation for the recovered ruthenium(III) concentration are given in Table 3. The error corresponding to regression equation ΔA_2 is less than that of ΔA_5 and ΔA_7 (Table 3) because ΔA_2 is a close study of the initial rate than ΔA_5 or ΔA_7. Therefore, a fixed time interval of 2 min was preferred for further measurement, which shows a good agreement between short time of analysis and reproducibility. The results in Table 3 show excellent reproducibility of the proposed method. The regression equation ΔA_2 is therefore advocated for trace level determination of Ru(III).

Table 4

Impact of various cations and anions on determination of $1.4 \cdot 10^{-7}$ M $[Ru^{3+}]$ using ΔA_2 calibration curve $[Fe(CN)_6]^{4-} = 2.25 \cdot 10^{-4}$, $[NaIO_4] = 7.5 \cdot 10^{-3}$, pH = 9.5 ± 0.02, T = 303 ± 0.1 K, I = 0.1M (NaCl)

Foreign ions	Concentration taken, $M \cdot 10^5$	Tolerance level ([interfering ion]/ $[Ru^{3+}]$)
Ca^{2+}	1.45	103.57
Co^{3+}	1.75	125.00
Ba^{2+}	1.25	89.29
SCN^-	1.25	89.29
$S_2O_3^{--}$	1.6	114.29
CH_3COO^-	1	71.43
Cl^-	1.75	125.00
Br^-	1.3	92.86
NO_3^-	1.4	100.00
EDTA	0.20	14.29
HEDTA	0.20	14.29
IDA	0.20	14.29

Table 5

Application of developed method in tap water samples using ΔA_2 calibration curve $[Fe(CN)_6]^{4-} = 2.25 \cdot 10^{-4}$, $[NaIO_4] = 7.5 \cdot 10^{-3}$, pH = 9.5 ± 0.02, T = 303 ± 0.1 K, I = 0.1M (NaCl)

Samples of tap water	$[Ru^{3+}]$ added, $ng \cdot ml^{-1}$	$[Ru^{3+}]$ found, $ng \cdot ml^{-1}$	Recovery, %
Sample 1	10.33	10.51	101.74
Sample 2	12.84	13.28	103.43
Sample 3	16.54	17.02	102.90

3.1. Study of Interferences (Sensitivity)

The sensitivity of the proposed method was studied under optimum reaction condition by addition of various cations, anions and poly-aminocarboxylates to fixed ruthenium(III) concentration ($1.5 \cdot 10^{-7}$ M). The tolerance limit of the added ions was considered not more than ±5 % relative error. The results (Table 4) reveals that the catalytic activity of Ru(III) was not significantly affected by most common ions up to 71 times higher concentration. Polyaminocarboxylates (HEDTA, EDTA and IDA) containing free amino and carboxylic groups form strong co-ordinate complexes with Ru(III), which suppress its catalytic power to maximum, if tolerance limit is more than14.29 times.

3.2. Analytical Application of Developed Method

To test the applicability and reliability, the proposed method was applied to determine the [Ru(III)] in three different samples of tap water having Ru(III) concentration in increasing order.

Because of very low content of Ru(III) in tap water it was added to the water samples so that the concentration of Ru(III) will be in detection range of proposed method (Table 3). The recovery results in Table 5 indicates the quantitative and higher recovery of Ru(III) in every case, which may be due to the synergistic effect of other cations present in tap water. Thus, the developed method can be effectively used for the quantitative determination of ruthenium(III) in mixtures of several metal ions in comparatively higher concentration (Table 3).

4. Conclusions

The experimental data confirms the reproducibility, stability and selectivity of the developed method to determine Ru(III) quantitatively in different types of water samples using readily available and inexpensive reagents. The proposed catalytic spectrophotometric method has good sensitivity with low detection limit as compared to other developed CKM-SPM. In most of other methods, substrates used are expensive and rarely available while other few used quencher and activator for analysis. Over all, the developed method can be effectively applied for the trace level ruthenium(III) analysis in tap water.

References

[1] Balcerzak M.: Rev. Anal. Chem., 2002, **32**, 181. https://doi.org/10.1080/10408340290765524
[2] Druskovic V., Vojkovic V., Jelic T.: Croatica Chem. Acta, 2005, **78**, 617.

[3] Berggren K., Steinberg T., Lauber W. *et al.*: Anal. Biochem., 1999, **276**, 129. https://doi.org/10.1006/abio.1999.4364
[4] Lindino C., Bulhoes L.: J. Braz. Chem. Soc., 2004, **15**, 178. https://doi.org/10.1590/S0103-50532004000200004
[5] Alarfa N., El-Razeq S.: J. Pharm. Biomed. Anal., 2006, **41**, 1423. https://doi.org/10.1016/j.jpba.2006.03.011
[6] Zhou Z., Zhang I.: Adv. Mater. Res., 2013, **602-604**, 1289. https://doi.org/10.4028/www.scientific.net/AMR.602-604.1289
[7] Zhou Z., Zhang I.: Appl. Mechanics Mater., 2012, **217-219**, 2397. https://doi.org/10.4028/www.scientific.net/AMM.217-219.2397
[8] Byadagi K., Nandibewoor S., Chimatadar S.: Acta Chim. Slov., 2013, **60**, 617.
[9] Sharanabasamma K., Angadi A., Tuwar S.: The Open Catal. J., 2011, **4**, 1. https://doi.org/10.2174/1876214X01104010001
[10] Keyvanfard M.: World Acad. Sci. Eng. Tech. 2008, 43.
[11] Hosamani R., Nandibewoor S.: J. Chem. Sci., 2009, **121**, 275. https://doi.org/10.1007/s12039-009-0030-y
[12] Srivastava S., Chaudhary L., Singh K.: Int. J. Res. in Phys. Chem., 2012, **2**, 6.
[13] Babasaheb D., Bhosale A., Gokavib G.: Adv. Appl. Sci. Res. 2012, **3**, 785.
[14] Mishra K., Chaturvedi R., Shukla M.: Ind. J. Chem. 2010, **49A**, 185.
[15] Kumar A., Reddy P., Reddy V.: Int. J. ChemTech. Res., 2013, **5**, 1442.
[16] Ritika M., Barhate V.: Int. J. ChemTech. Res., 2013, **5**, 1578.
[17] Sateesh B., Shastry V., Shashidhar S., Manoj K.: Int. J. Chem. Sci., 2014, **14**, 1109.
[18] Fawaz A.: J. Chem. Sci., 2016, **128**, 733. https://doi.org/10.1007/s12039-016-1067-3
[19] Gorakh S., Antonio D., Jyoti G. *et al.*: Chem. Commun., 2013, **49**, 11533. https://doi.org/10.1039/c3cc46239k
[20] Lakomska I., Fandzloch M., Muziol T. *et al.*: Dalton Trans., 2013, **42**, 6219. https://doi.org/10.1039/c2dt32216a
[21] Sharma A., Gangrade, Bakshi D., John J.: Int. J. ChemTech. Res., 2014, **4**, 828.
[22] Schoekel A., Melke J., Burns M. *et al.*: J. Power Sources, 2016, **301**, 210. https://doi.org/10.1016/j.jpowsour.2015.09.119
[23] Hsieh Y., Zang Y., Su D. *et al.*: Nat. Commun., 2013, 2466. https://doi.org/10.1038/ncomms3466
[24] Messori L., Camarri M., Ferraro T. *et al.*: A.C.S. Med. Chem. Lett., 2013, **4**, 1124. https://doi.org/10.1021/ml400390c
[25] Brunken S., Kratzig A., Bogdanoff P. *et al.*: Thin Solid Films, 2013, **527**, 16. https://doi.org/10.1016/j.tsf.2012.12.037
[26] Madan P., Barhate V.: Int. J. Sci. Res., 2016, **5**, 778.
[27] Shelar S., Bhor R., Anuse M., Naval R.: Sep. Sci. Tech., 2015, **50**, 1190. https://doi.org/10.1080/01496395.2014.983245
[28] Prasad S., Naik R., Srivastava A.: Spectrochim. Acta A, 2008, **69**, 193. https://doi.org/10.1016/j.saa.2007.03.030
[29] Naik R., Srivastava A., Prasad S.: Spectrochim. Acta A, 2008, **70**, 958. https://doi.org/10.1016/j.saa.2007.10.011
[30] Zhou Z., Zhang L.: Appl. Mech. Mater., 2012, **204-208**, 4067.
[31] Sreekanth B., Jonnalagadda, Brijesh P.: Anal. Lett., 2011, 1868.
[32] Jonnalagadda S., Chinake C., Love I.: Fresenius Anal. Chem., 1994, **349**, 829. https://doi.org/10.1007/BF00323114
[33] Keyvanfard M., Rezaei B.: Can. J. Anal. Sci. Spectrosc., 2005, **50**, 221.
[34] Crouch S., Scheeline A., Kirkor E.: Anal. Chem., 2000, **72**, 53. https://doi.org/10.1021/a1000004b
[35] Prasad S.: Asian J. Chem., 2002, **14**, 799.
[36] Prasad K., Rao N.: React. Kinet. Catal. Lett., 1995, **56**, 273. https://doi.org/10.1007/BF02076032
[37] Khayamian T., Ensafi A., Atabati M.: Anal. Lett., 2002, **35**, 2039. https://doi.org/10.1081/AL-120014292
[38] Bhagwat V., Vijay R., Jonnalagadda S., Pare B.: Indian J. Chem. Technol., 2006, **13**, 644.
[39] Naik R., Srivastava A., Asthana A.: J. Iran. Chem. Soc., 2008, **5**, 29. https://doi.org/10.1007/BF03245812

Received: February 05, 2018 / Revised March 23, 2018 / Accepted: July 12, 2018

СПЕКТРОФОТОМЕТРИЧНЕ ВИЗНАЧЕННЯ РУТЕНІЮ З ВИКОРИСТАННЯМ ЙОГО КАТАЛІТИЧНОЇ АКТИВНОСТІ НА ОКИСНЕННЯ ГЕКСАЦИАНОФЕРРАТА(II) ПЕРІОДАТНИМ ЙОНОМ В ЗРАЗКАХ ВОДИ

Анотація. *Для визначення рутенію(III) на мікрорівні застосовано каталітичний ефект хлориду рутенію на зовнішнє перенесення електронів гексаціаноферрату(II) періодатним йоном у водному лужному середовищі. Встановлено оптимальні умови реакції та необхідний час. Лінійна залежність між поглинальною здатністю та концентрацією Ru(III) використана для визначення слідів Ru(III). Показано, що додавання інтерферентних йонів (в концентраціях, до 71 разів вищих за концентрацію Ru) істотно не впливає на каталітичну активність Ru(III) при окисненні гексаціаноферрату(II) періодатним йоном. Поліамінокарбоксилати пригнічують його каталітичну здатність до максимального значення, якщо допустима межа є більшою за 14,29. Враховуючи відтворюваність, стабільність та селективность цього методу, запропоновано використовувати його для різних типів зразків води для визначення рутенію(III) на мікрорівні.*

Ключові слова: *кінетика, механізм, гексаціаноферрат(II), періодат, рутеній(III).*

Chem. Chem. Technol., 2019,
Vol. 13, No. 3, pp. 280–287

Chemistry

THERMODYNAMIC PROPERTIES OF 2-METHYL-5-ARYLFURAN-3-CARBOXYLIC ACIDS CHLORINE DERIVATIVES IN ORGANIC SOLVENTS

Iryna Sobechko[1], [*], Yuri Horak[2], Volodymyr Dibrivnyi[1], Mykola Obushak[2], Lubomyr Goshko[1]

https://doi.org/10.23939/chcht13.03.280

Abstract. The temperature dependences of the solubility of 2-methyl-5-(2-chloro-5-trifluoromethylphenyl)-furan-3-carboxylic acid and 2-methyl-5-(2,5-dichlorophenyl)-furan-3-carboxylic acid in acetonitrile, dimethyl ketone, isopropanol and ethyl acetate have been experimentally determined. The enthalpies of fusion of the investigated substances, as well as their enthalpies and entropies of mixing at 298 K have been calculated. The dependence of the saturated solution concentration on the values of enthalpy and entropy of solubility at 298 K has been determined. The compensating effect of mixing the investigated acids with all solvents containing the carbonyl group has been established.

Keywords: enthalpy, entropy of solubility, mixing, melting, 2-methyl-5-(2-chloro-5-trifluoromethylphenyl)-furan-3-carboxylic acid, 2-methyl-5-(2,5-dichlorophenyl)-furan-3-carboxylic acid.

1. Introduction

Functionalized aryl derivatives of five-membered heterocycles belong to a class of substances that attract researchers' attention from the standpoint of studying their valuable properties and various modifications of their structure. In particular, the compounds with an arylfuran fragment have become widely used as the modifying agents in the synthesis of polymeric materials [1, 2] and biologically active compounds, since they exhibit a wide spectrum of biological activity [3] and are less toxic than those containing only a functionalized fragment of furan [4]. The compounds with this fragment have begun to be used in therapeutic practice for the treatment of neurodegenerative diseases [5], the treatment of genetic diseases [6], the creation of drugs for the treatment of tobacco dependence in order to reduce the need for nicotine and remove abstinence symptoms [7] and in the treatment of HIV-1 infection as a component of antiretroviral therapy [8]. It should ne noted that polymeric materials with arylfuran fragments are also biologically active [9]. The chitosan polymers modified with chlorine- and nitro-containing arylfurans showed significantly higher antimicrobial activity than unmodified chitosans [10, 11]. Thus, the search for promising reactions involving arylfuran fragments and the need for a deeper understanding of their biochemical functions requires the study of their thermodynamic properties. Naturally, the scientific researches appeared in which thermodynamic properties of individual organic compounds with an arylfuran fragment were examined. The determined values may contribute to solve practical problems concerning the optimization processes of their synthesis and purification. Since most reactions occur in solutions, the optimization of synthesis and purification of compounds with an arylfuran fragment is impossible without the determination of thermodynamic parameters of solubility. Some works regarding the thermodynamic properties of compounds with arylfuran fragment have appeared in recent years [12-17]. The presented work is the continuation of the previous research. Its purpose is to study the thermodynamic properties of 2-methyl-5-(2-chloro-5-trifluoromethylphenyl)-furan-3-carboxylic acid and 2-methyl-5-(2,5-dichlorophenyl)-furan-3-carboxylic acid solubility in organic solvents of different polarity.

2. Experimental

2.1. Materials

2-Methyl-5-(2-chloro-5-trifluoromethylphenyl)-furan-3-carboxylic acid (I) and 2-methyl-5-(2,5-dichlorophenyl)-furan-3-carboxylic acid (II) were synthesized according to Scheme 1 by two stages:

[1] Lviv Polytechnic National University,
12, Bandery St., 79013 Lviv, Ukraine
[2] Ivan Franko National University of Lviv,
6, Kyryla i Mefodiya St. 79005 Lviv, Ukraine
[*] *phys.chem.lp@gmail.com*

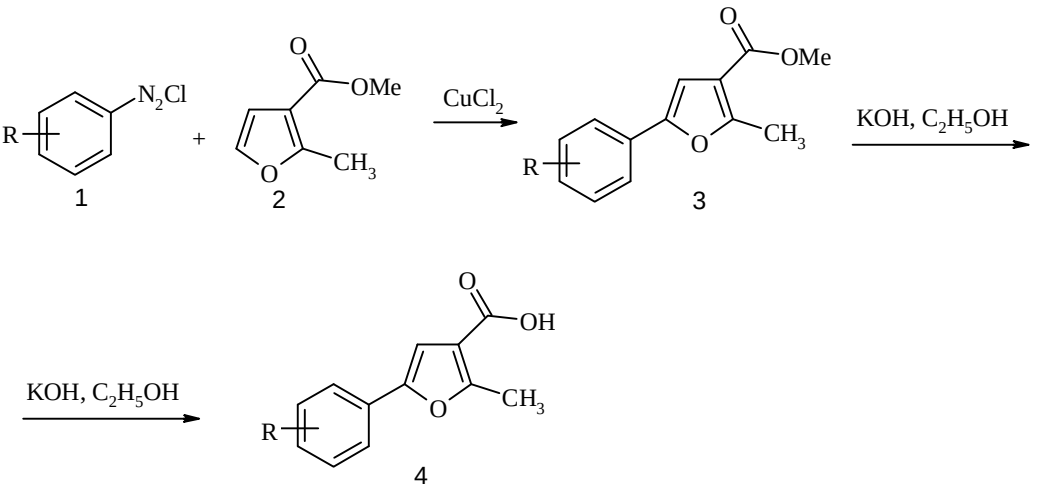

where R = 2-Cl-5-CF_3 (a) and 2,5-Cl_2 (b)

Scheme 1. Synthesis of investigated acids

Arylfuran-containing acids under normal conditions are white crystalline compounds with a molecular weight of 304.7 g/mol (compound I) and 517.6 g/mol (compound II).

At the first stage, methyl esters of 5-aryl-2-methyl-3-furan carboxylic acids (**3a** and **3b**) were synthesized. For this purpose 28 g (0.2 mol) of methyl ester of 2-methyl-3-furan carboxylic acid, 2 g of copper(II) chloride and 80 ml of acetone were added to the three-necked reactor equipped with a stirrer, dropping funnel and bubble counter. A solution of arendiazonium chloride **1**, obtained by diazotization of 0.21 mol of the corresponding amine, was added under vigorous stirring. After nitrogen was released, the product was filtered (compound **3b**) or distilled under vacuum (compound **3a**) and recrystallized from ethanol. At the second stage 5-aryl-2-methyl-3-furancarboxylic acids (**4a** and **4b**) were obtained by saponification of the synthesized esters **3a** and **3b** in the following way. A hot ethanolic solution of potassium hydroxide (4.2 g, 0.075 mol) was gradually added to the hot solution of the corresponding ester (0.05 mol) in ethanol. The mixture was left overnight. After acidification with hydrochloric acid, the precipitate was filtered off, washed with water and repeatedly recrystallized from ethanol. The samples after 4-fold recrystallization were used for research.

Identification of acids was performed using NMR spectroscopy. ^{1}H NMR spectra were recorded by the Bruker DRX 500 (500 MHz, DMSO-d6). Chemical shifts (δ, ppm) are given in relation to the DMSO signal (2.50 ppm).

2-Methyl-5-(2-chloro-5-trifluoromethylphenyl)-furan-3-carboxylic acid: ^{1}H NMR (500 MHz, DMSO) δ 2.67 (3H, s, CH_3); 7.36 (1H, s, 4-H-furan); 7.60 (1H, dd, J_1 = 8.4, J_2 = 1.6, 4-H6CH3); 7.74 (1H, d, J = 8.4, 3-H C_6H_3); 8.05 (1H, s, 6-H C_6H_3); 12.60 (1H, s, COOH).

2-Methyl-5-(2,5-dichlorophenyl)-furan-3-carboxylic acid: ^{1}H NMR (500 MHz, DMSO) δ 2.62 (3H, s, CH_3); 7.31 (1H, s, 4-H furan); 7.44 (1H, dd, 4-H, C_6H_3); 7.59 (1H, d, 3-H, C_6H_3); 7.83 (1H, s, 6-H, C_6H_3); 12.83 (1H, s, COOH).

The compounds purity was determined using a high-performance liquid chromatograph Agilent 1100 HPLC equipped with a diode matrix with a selective detector on a Zorbax SB-C18 column, 4.6×15 mm, eluent A acetonitrile-water with 0.1% TFA (95: 5). No admixtures were found in the samples.

For solubility studies, commonly used organic solvents with a high volatility and sufficiently low boiling point were used: acetonitrile, dimethyl ketone, ethyl acetate and isopropanol (Merck, Germany). A content of the main component was not less than 99.0 wt %. Before use, the solvents were purified by a fractional distillation followed by identification relative to the refractive index (n_D^{20}) and boiling point (T_{boil}). The content of the main component was determined using a gas-liquid chromatograph LXM-8D with a thermal conductivity detector (TCD). Chromatograph columns with a diameter of 0.4 cm and a length of 2 m were filled with a solid phase Chromator N-AW (0.20–0.25 mm) containing 10 % polyethylene glycolidipinate + 1% orthophosphoric acid. Gas carrier was helium. The column temperature was 423 K, the evaporator temperature was 493 K, TCD current was 120 mA.

The determined values differed from those given in the literature by no more than the value of experimental error, and the content of the main component was not less than 99.8 wt% (Table 1).

Table 1

Physicochemical properties of solvents

Solvents	*M*, g/mol	n_D^{20}		T_{boil}, K		Content of the main component, wt %
		determ.	lit.	determ.	lit.	
Acetonitrile	41.05	1.3443	1.3442 [10]	354.6	354.8 [10]	99.9
Dimethyl ketone	58.08	1.3590	1.3591 [10]	329.2	329.3 [10]	99.8
Ethyl acetate	88.11	1.3722	1.3724 [10]	349.9	350.2 [10]	99.9
Isopropanol	60.10	1.3776	1.3776 [10]	355.1	355.3 [10]	99.8

2.2. Solubility

The temperature dependence of the solubility of the investigated acids was determined by gravimetric method, the same as in previous studies [12-17].

The dissolution of the acids was carried out in a sealed glass vessel with a Teflon stirrer, a thermometer and an aperture for sampling. The stirrer speed was 40□50 rpm. The accuracy of thermostatting was ±0.1 K. Saturation of solutions was carried out for not less than 48 h under constant stirring at the experimental temperature. Experiments were carried out at different temperatures. The absence of a hysteresis loop on the solubility curve confirmed the achievement of a state close to equilibrium.

Samples were selected in series of two or three samples and transferred to a pre-weighed sealed weighing bottle, followed by removal of the solvent and re-weighing at the temperature of 333–343 K. The accuracy of the weighing was ±0.0002 g.

2.3. Differential Thermal Analysis

Derivatographic studies of acids were carried out using Q-1500 D derivatograph (Paulik-Paulik-Erday) under a dynamic mode in an atmosphere of air. Heating rate was 5 K/min; platinum crucible was used.

3. Results and Discussion

The experimental results are given in Tables 2 and 3, where m_1 and m_2 are the weights of the solvent and the solute, respectively, and T is the temperature at which solubility was determined. The experimental data were processed using the least squares method and presented in a linear form (1).

$$\ln x_2 = -\frac{\Delta_{sol}H}{RT} + \frac{\Delta_{sol}S}{R} \quad (1)$$

where $\Delta_{sol}H$ and $\Delta_{sol}S$ are partial molar enthalpy and entropy of solubility. Here and below the errors of all values are given for the significance level of 0.95.

The thermodynamic parameters of solubility $\Delta_{sol}H$ and $\Delta_{sol}S$ can be represented by the sum of the corresponding phase transition parameters of crystalline 2-methyl-5-(2-chloro-5-trifluoromethylphenyl)-furan-3-carboxylic acid and 2-methyl-5-(2,5-dichlorophenyl)-furan-3-carboxylic acids in the liquid phase with the parameters of their mixing with the solvent (Eqs. (2) and (3)).

$$\Delta_{sol}H = \Delta_{fus}H + \Delta_{mix}H \quad (2)$$

$$\Delta_{sol}S = \Delta_{fus}S + \Delta_{mix}S \quad (3)$$

To determine the change in enthalpy ($\Delta_{mix}H$) and entropy ($\Delta_{mix}S$) of mixing, it is necessary to consider the enthalpy ($\Delta_{fus}H$) and entropy ($\Delta_{fus}S$) of fusion of the investigated compounds at the average experimental temperature. It is impossible to determine the enthalpy and entropy of acid fusion using the differential thermal analysis due to their increased ability to thermooxidative degradation. Derivatograms show a significant weight loss of acid samples immediately after the melting point has reached (Fig. 1). Therefore, the thermodynamic parameters of solubility were determined by the approximate method of calculation [19, 20]. These works show the constancy of the change in the specific entropy of fusion $\Delta_{fus}S$ (J/g·K) at the melting point for more than 100 organic compounds of different classes. Then $\Delta_{fus}H$ (J/g) is calculated according to the known Eq. (4).

$$\Delta_{fus}H = T_{fus} \cdot \Delta_{fus}S \quad (4)$$

To evaluate the specific entropy of fusion of the investigated acids, we used the experimental results [13-20] obtained by a derivatographic method for arylfurans (Table 4).

The average value of the specific entropy of fusion for derivatives of arylfurans presented in Table 4, is 0.319 ± 0.027 J/g·K). Then, the values of molar entropy and enthalpy of fusion for 2-methyl-5-(2-chloro-5-trifluoromethylphenyl)-furan-3-carboxylic acid can be evaluated as $\Delta_{fus}S$ = 97.2 ± 8.2 J/mol·K, $\Delta_{fus}H_{517.6}$ = 50.3 ± 4.2 kJ/mol; for 2-methyl-5-(2,5-dichlorophenyl)-furan-3-carboxylic acid $\Delta_{fus}S$ = 86.5 ± 7.3 J/mol·K, $\Delta_{fus}H_{556.7}$ = 48.1 ± 4.1 kJ/mol.

Table 2

Temperature dependence of 2-methyl-5-(2-chloro-5-trifluoromethylphenyl)-furan-3-carboxylic acid in organic solvents

T, K	m_1, g	m_2, g	$x_2 \cdot 10^3$	T, K	m_1, g	m_2, g	$x_2 \cdot 10^3$	T, K	m_1, g	m_2, g	$x_2 \cdot 10^3$
Acetonitrile											
287.8	1.5972	0.0020	0.17	304.0	1.6718	0.0038	0.31	317.6	1.0579	0.0045	0.56
287.8	2.2961	0.0027	0.16	306.5	1.0005	0.0026	0.35	317.6	1.6170	0.0067	0.57
297.9	0.6311	0.0011	0.25	306.5	1.0093	0.0026	0.35	321.4	0.2190	0.0010	0.62
297.9	1.3606	0.0025	0.25	306.5	1.3974	0.0036	0.35	321.4	0.3726	0.0017	0.63
297.9	1.4730	0.0028	0.26	307.5	1.5766	0.0045	0.38	321.4	0.4511	0.0021	0.63
298.5	1.4068	0.0027	0.26	307.5	1.6851	0.0047	0.38	321.5	1.0791	0.0050	0.62
298.5	1.4563	0.0027	0.25	312.1	0.7054	0.0022	0.43	321.5	1.3964	0.0067	0.65
298.5	1.6833	0.0032	0.26	312.1	1.6105	0.0055	0.46	321.5	2.1091	0.0098	0.63
302.5	0.5314	0.0011	0.29	312.1	1.6162	0.0053	0.44	322.5	0.6668	0.0032	0.65
302.5	1.5940	0.0032	0.27	316.4	0.8819	0.0032	0.49	322.5	1.7365	0.0087	0.68
302.5	2.2415	0.0048	0.29	316.4	1.5886	0.0060	0.51	322.5	2.3690	0.0117	0.67
304.0	1.4387	0.0034	0.32	316.4	2.0771	0.0076	0.50	326.0	1.7918	0.0106	0.80
304.0	1.4455	0.0034	0.32	317.6	0.8318	0.0033	0.54	326.0	1.9125	0.0111	0.79
$\ln x_2 = (4.46 \pm 0.32) - (3804 \pm 96) \cdot 1/T$											
Dimethyl ketone											
294.4	0.5663	0.0085	2.85	304.3	0.4794	0.0100	3.98	312.9	0.3626	0.0098	5.12
294.4	0.6290	0.0088	2.68	305.5	0.4379	0.0089	3.86	312.9	0.4436	0.0118	5.05
297.0	0.7068	0.0111	2.99	305.5	0.5542	0.0111	3.82	312.9	0.49825	0.0140	5.33
297.0	0.8928	0.0141	3.01	305.5	0.5879	0.0126	4.07	315.8	0.2935	0.0085	5.49
297.0	0.5204	0.0084	3.07	308.4	0.4479	0.0106	4.51	315.8	0.4579	0.0134	5.55
297.5	0.5837	0.0096	3.13	308.4	0.5572	0.0133	4.53	315.8	0.8215	0.0244	5.63
297.5	0.4294	0.0069	3.08	308.7	0.3662	0.0092	4.77	320.0	0.3700	0.0128	6.55
297.5	0.4671	0.0075	3.07	308.7	0.4870	0.0122	4.75	320.0	0.4315	0.0146	6.41
299.4	0.5117	0.0095	3.55	308.7	0.5076	0.0119	4.47	320.0	0.6311	0.0217	6.53
299.4	0.5849	0.0109	3.56	311.1	0.4388	0.0110	4.76	322.9	0.2179	0.0078	6.82
304.3	0.3658	0.0079	4.10	311.1	0.5027	0.0124	4.70	322.9	0.4877	0.018	6.99
304.3	0.3972	0.0082	3.94	311.1	0.6387	0.0168	4.99	322.9	0.5324	0.0195	6.93
$\ln x_2 = (4.40 \pm 0.39) - (3025 \pm 119) \cdot 1/T$											
Ethyl acetate											
300.8	0.4210	0.0048	3.29	308.5	0.5978	0.0087	4.19	315.8	0.7298	0.0135	5.32
300.8	0.7449	0.0086	3.33	311.2	0.4783	0.0074	4.48	315.8	0.8266	0.0151	5.26
300.9	0.4801	0.0054	3.24	311.2	0.5197	0.0080	4.43	315.9	0.8431	0.0158	5.41
300.9	0.6917	0.0080	3.33	311.2	0.5767	0.0090	4.49	315.9	1.1951	0.0221	5.33
300.9	0.8809	0.0101	3.32	311.6	1.0630	0.0164	4.44	318.5	0.4338	0.0090	6.00
304.4	0.6576	0.0082	3.59	311.6	1.0684	0.0164	4.42	318.5	0.4751	0.0100	6.08
304.4	0.7460	0.0092	3.55	313.0	0.4077	0.0069	4.87	318.5	0.5155	0.0108	6.02
304.4	0.7920	0.0095	3.48	313.0	0.4807	0.0080	4.79	323.5	0.4687	0.0118	7.23
307.0	0.7857	0.0107	3.92	313.0	0.5851	0.0098	4.82	323.5	0.4846	0.0122	7.26
307.0	0.8963	0.0122	3.94	313.6	0.5731	0.0102	5.12	323.5	0.5622	0.0136	6.95
307.0	0.9086	0.0123	3.92	313.6	0.6294	0.0114	5.23	327.5	0.4230	0.0118	8.04
308.5	0.4489	0.0062	3.98	313.6	0.7089	0.0129	5.24	327.5	0.5032	0.0139	7.95
308.5	0.5767	0.0080	4.00	315.8	0.7111	0.0130	5.26	327.5	0.5647	0.0157	8.00
$\ln x_2 = (5.47 \pm 0.41) - (3376 \pm 129) \cdot 1/T$											
Isopropanol											
302.7	0.4111	0.0041	1.96	312.4	0.3827	0.0062	3.19	318.0	0.4092	0.0082	3.96
302.7	0.8314	0.0083	1.97	312.4	0.4612	0.0075	3.20	318.0	0.4713	0.0095	3.98
302.7	0.6382	0.0064	1.97	312.4	0.5483	0.0089	3.19	318.0	0.6676	0.0137	4.03
305.0	0.3983	0.0045	2.22	313.5	0.4097	0.0070	3.36	318.4	0.3741	0.0079	4.15
305.0	0.7478	0.0083	2.19	313.5	0.5072	0.0085	3.30	318.4	0.4456	0.0095	4.18
305.0	0.7564	0.0082	2.13	313.5	0.7026	0.0121	3.38	318.4	0.4479	0.0090	3.95
308.6	0.3938	0.0054	2.70	316.2	0.4073	0.0075	3.62	320.9	0.3668	0.0085	4.55
308.6	0.4269	0.0058	2.67	316.2	0.4185	0.0078	3.66	320.9	0.4458	0.0105	4.60
308.6	0.4996	0.0068	2.68	316.2	0.4662	0.0087	3.67	320.9	0.4735	0.0111	4.63
309.8	0.5238	0.0074	2.78	317.1	0.4233	0.0086	4.01	325.5	0.4017	0.0117	5.74
309.8	0.5293	0.0076	2.82	317.1	0.4843	0.0095	3.88	325.5	0.6713	0.0201	5.87
309.8	0.5313	0.0078	2.89	317.1	0.4992	0.0096	3.80	325.5	0.7425	0.0217	5.73
$\ln x_2 = (8.78 \pm 0.35) - (4543 \pm 110) \cdot 1/T$											

Table 3

Temperature dependence of 2-methyl-5-(2,5-dichlorophenyl)-furan-3-carboxylic acid in organic solvents

T, K	m_1, g	m_2, g	$x_2 \cdot 10^4$	T, K	m_1, g	m_2, g	$x_2 \cdot 10^4$	T, K	m_1, g	m_2, g	$x_2 \cdot 10^4$
Acetonitrile											
304.1	1.7584	0.0005	0.43	314.0	4.0253	0.0018	0.68	326.5	2.9971	0.0023	1.16
304.1	1.8033	0.0005	0.42	318.1	1.7062	0.0009	0.80	326.5	3.3645	0.0027	1.22
304.1	3.0456	0.0009	0.45	318.1	1.8319	0.0010	0.83	330.4	2.9830	0.0029	1.47
307.9	1.4604	0.0005	0.52	318.1	2.2592	0.0012	0.80	330.4	3.1800	0.0031	1.48
307.9	1.8749	0.0007	0.53	320.5	2.1442	0.0014	0.99	330.4	3.6235	0.0036	1.50
307.9	1.9603	0.0007	0.54	320.5	2.2392	0.0014	0.95	331.5	2.8957	0.0028	1.46
311.3	2.3067	0.0009	0.59	320.5	2.7723	0.0017	0.93	331.5	3.1059	0.0031	1.51
311.3	2.6456	0.0011	0.63	322.5	1.7379	0.0011	0.96	331.5	3.4128	0.0034	1.51
311.3	2.8480	0.0012	0.64	322.5	1.9867	0.0013	0.99	335.5	2.3662	0.0027	1.73
314.0	2.6318	0.0012	0.69	322.5	2.2074	0.0015	1.03	335.5	2.6048	0.0029	1.69
314.0	2.7298	0.0012	0.67	326.5	2.6295	0.0021	1.21	335.5	3.1141	0.0036	1.75
$\ln x_2 = (4.90 \pm 0.38) - (4546 \pm 123) \cdot 1/T$											
Dimethyl ketone											
298.4	0.7363	0.0014	4.22	309.1	0.7198	0.0021	6.40	317.9	0.9182	0.0041	9.67
298.4	0.8695	0.0017	4.31	309.1	0.9384	0.0027	6.16	317.9	1.1962	0.0050	8.95
300.7	0.4267	0.0009	4.52	312.9	0.3561	0.0013	8.12	318.5	0.6722	0.0030	9.71
300.7	0.5979	0.0012	4.30	312.9	0.4697	0.0017	7.45	318.5	0.7778	0.0034	9.49
300.7	0.7235	0.0015	4.44	312.9	0.5483	0.0020	7.81	318.5	1.0268	0.0045	9.48
305.1	0.3205	0.0008	5.34	313.3	0.9008	0.0031	7.49	322.4	0.4674	0.0023	10.5
305.1	0.3450	0.0009	5.59	313.3	0.9656	0.0034	7.65	322.4	0.7638	0.0039	10.9
305.1	0.5816	0.0015	5.52	313.3	0.9734	0.0034	7.59	322.4	1.1164	0.0054	10.5
308.7	0.4072	0.0012	6.31	313.6	0.8663	0.0033	8.28	323.4	0.4976	0.0026	11.2
308.7	0.4840	0.0014	6.41	313.6	1.0496	0.0038	7.85	323.4	0.7291	0.0040	10.9
309.1	0.6145	0.0018	6.27	317.9	0.7403	0.0030	8.67	323.4	0.8057	0.0043	10.5
$\ln x_2 = (5.33 \pm 0.49) - (3918 \pm 153) \cdot 1/T$											
Ethyl acetate											
301.9	1.6540	0.0023	4.52	316.8	1.5951	0.0039	8.04	324.1	1.2017	0.0039	10.5
301.9	1.6751	0.0023	4.46	316.8	1.6465	0.0041	8.09	324.1	1.3336	0.0043	10.5
301.9	2.7724	0.0038	4.45	316.8	2.0522	0.0052	8.23	324.1	1.7066	0.0057	10.8
304.8	1.4656	0.0022	4.99	318.1	1.2866	0.0033	8.33	327.6	1.6734	0.0060	11.6
304.8	1.7084	0.0026	4.94	318.1	1.8164	0.0048	8.58	327.6	1.8576	0.0067	11.7
304.8	2.0557	0.0031	4.90	318.1	2.1476	0.0057	8.62	327.6	2.3365	0.0085	11.8
312.1	1.1236	0.0023	6.65	321.1	1.5380	0.0045	8.50	331.0	1.6803	0.0069	13.3
312.1	1.9614	0.0040	6.62	321.1	2.0603	0.0060	9.46	331.0	1.8667	0.0076	13.2
312.1	2.5448	0.0053	6.76	321.1	2.7656	0.0082	9.63	331.0	2.0869	0.0085	13.2
316.4	2.9336	0.0071	7.86	321.9	1.3308	0.0039	9.52	332.3	1.0041	0.0044	14.2
316.4	2.9757	0.0071	7.75	321.9	1.8228	0.0055	9.80	332.3	2.0169	0.0088	14.2
316.4	3.2686	0.0081	8.05	321.9	2.4157	0.0072	9.68	332.3	2.2388	0.0098	14.2
$\ln x_2 = (4.84 \pm 0.34) - (3791 \pm 110) \cdot 1/T$											
Isopropanol											
296.9	2.4509	0.0026	2.35	308.5	2.6075	0.0055	4.67	325.5	2.3500	0.0105	9.94
296.9	2.4984	0.0028	2.48	311.3	0.8232	0.0019	5.11	325.5	2.9287	0.0128	9.72
296.9	2.9357	0.0032	2.42	311.3	1.6908	0.0040	5.24	329.8	1.7107	0.0085	11.1
300.5	0.8686	0.0012	3.06	311.3	2.3636	0.0056	5.25	329.8	1.8791	0.0099	11.7
300.5	1.1662	0.0015	2.85	315.2	1.8976	0.0055	6.42	329.8	1.9543	0.0104	11.8
300.5	1.9272	0.0026	2.99	315.2	3.0420	0.0085	6.19	332.2	1.7855	0.0107	13.3
305.6	2.0011	0.0036	3.78	315.2	3.3571	0.0095	6.27	332.2	1.8194	0.0112	13.6
305.6	2.0313	0.0036	3.99	320.5	2.6229	0.0093	7.85	332.2	2.0900	0.0123	13.0
305.6	2.0539	0.0035	3.93	320.5	2.6394	0.0099	8.05	335.5	1.5851	0.0110	15.4
308.5	1.3292	0.0027	4.50	320.5	2.6542	0.0096	8.31	335.5	1.8269	0.0126	15.3
308.5	2.0353	0.0042	4.57	325.5	1.7651	0.0076	9.545	335.5	2.3993	0.0171	15.8
$\ln x_2 = (7.52 \pm 0.39) - (4697 \pm 123) \cdot 1/T$											

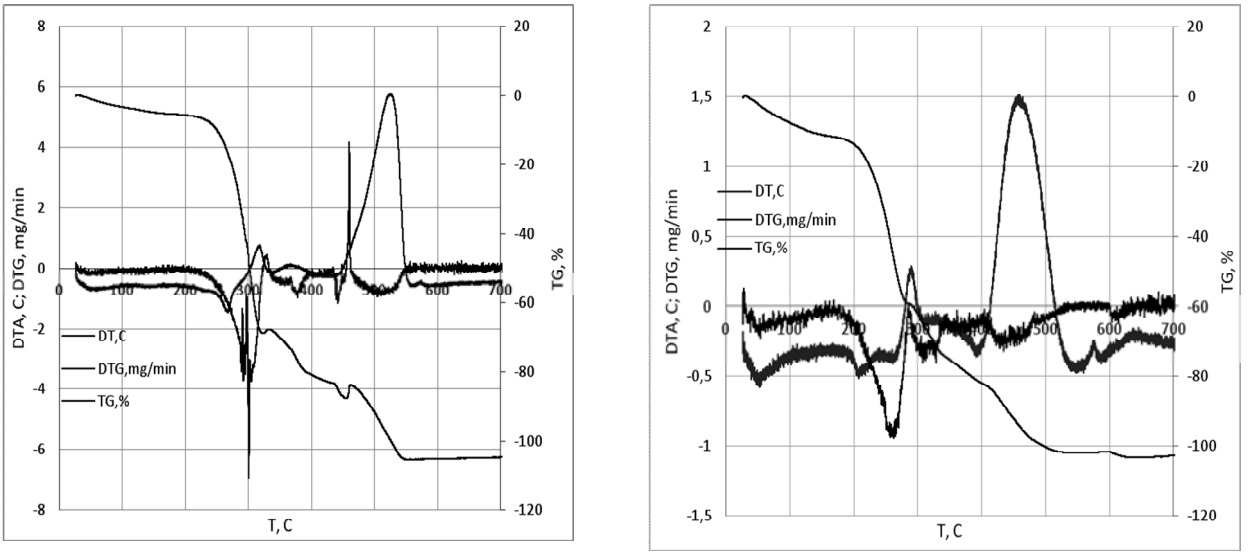

a) b)

Fig. 1. Derivatograms of 2-methyl-5-(2,5-dichlorophenyl)-furan-3-carboxylic acid (a) and 2-methyl-5-(2-chloro-5-trifluoromethylphenyl)-furan-3-carboxylic acid (b)

Table 4

Thermodynamic parameters of arylfurans

Compound	*Mw*, g/mol	T_{fus}, K	$\Delta_{fus}H$, kJ/mol	$\Delta_{fus}S$	
				J/mol·K	J/g·K
2-Methyl-5-phenylfuran-3-carboxylic acid	202.2	458.1±0.5	32.4±1.8	70.7±1.9	0.350
2-Methyl-5-(4-methylphenyl)-furan-3-carboxylic acid	216.2	507.2±1.2	32.7±1.0	64.5±1.5	0.299
5-(2-Nitrophenyl)-furan-2-carboxylic acid	235.2	491.6±1.0	33.59±0.22	68.3±1.0	0.291
3-[5-(2-Nitrophenyl)-furan-2-]-acrylic acid	259.2	447.6±1.0	25.00±0.66	55.9±1.2	0.216
5-(2-Nitrophenyl)-furan-2-oxime	232.2	411.1±1.0	20.1±1.3	48.9±1.6	0.211
5-(3-Nitrophenyl)-furan-2-oxime	232.2	444.9±1.0	26.75±0.48	60.1±1.1	0.259
5-(4-Nitrophenyl)-furan-2-oxime*	232.2	451.1±1.2	22.30±0.17	49.4±1.5	0.213
5-(2- Nitrophenyl)-furan-2-carbaldehyde	217.2	368.3±1.0	33.39±0.70	90.7±1.2	0.417
5-(3- Nitrophenyl)-furan-2-carbaldehyde	217.2	428.6±1.0	36.31±0.44	84.7±1.1	0.390
5-(4- Nitrophenyl) furan-2-carbaldehyde	217.2	479.8±1.0	39.86±0.69	83.1±1.2	0.383
5-(2-Nitro-4-methylphenyl)-furan-2-carbaldehyde	231.2	379.2±1.2	28.10±0.10	74.1±1.2	0.321
5-(2-Nitro-4-oxymethylphenyl)-furan-2-carbaldehyde	247.2	372.0±1.0	35.89±0.07	96.5±1.0	0.390
5-(2-Methyl-4-nitrophenyl)-furan-2-carbaldehyde	231.2	440.4±1.3	34.7±1.1	78.8±1.7	0.341
5-(2-Oxymethyl-4-nitophenyl)-furan-2-carbaldehyde	247.2	490.9±1.5	36.93±0.13	75.2±1.5	0.304
Ethyl-4-(5-formylfuran-2-yl)-benzoate	244.3	386.1±1.5	33.5±1.5	86.7±2.1	0.355
2-Cyano-[3-(4-phenyl)-2-furan]-acrylic acid ethyl ester	267.3	391.5±1.0	34.6±1.8	88.4±2.1	0.331
2-Cyano3-[4-(4-methylphenyl)-2-furan]-acrylic acid ethyl ester	281.3	387.7±1.0	26.8±3.0	69.1±3.2	0.246
2-Cyano-3-[5-(2-nitrophenyl)-2-furan]-acrylic acid ethyl ester	312.3	437.0±1.0	34.93±1.0	79.9±1.3	0.256
2-Cyano-3-[5-(3-nitrophenyl)-2-furan]-acrylic acid ethyl ester	312.3	487.3±1.5	58.7±2.3	120.4±2.7	0.385
2-Cyano-3-[5-(4-nitrophenyl)-2-furan]-acrylic acid ethyl ester	312.3	523.8±1.5	76.6±3.4	146.2±3.7	0.468
2-Cyano-3-[4-(4-methyl-3-nitrophenyl)-2-furan]-acrylic acid ethyl ester	326.3	427.2±1.0	40.9±1.2	95.7±1.6	0.293
2-Cyano-3-[5-(phenyl)-2-furyl]-2-propenamide	238.3	480.8±1.5	37.6±1.7	78.2±2.3	0.328
2-Cyano-3-[5-(4-methylphenyl)-2-furyl]-2-propenamide	252.3	461.0±1.1	40.3±1.6	87.4±2.1	0.346
2-Cyano-3-[5-(2-nitrophenyl)-2-furyl]-2-propenamide	283.2	513.9±1.1	37.43±0.76	72.8±1.3	0.257
2-Cyano-3-[5-(2-nitro-4-methylphenyl)-2- фурил]-2-propenamide	297.2	481.6±1.0	45.3±1.0	94.1±1.4	0.316

Note: * the ratio of *anti*:*sin* isomers is 9:41 (~1:4.55).

Table 5

Thermodynamic parameters of solubility, melting and mixing of investigated compounds in organic solvents at 298 K

Solvent	$\Delta_{fus}H$	$\Delta_{sol}H$	$\Delta_{mix}H$	$\Delta_{fus}S$	$\Delta_{sol}S$	$\Delta_{mix}S$
	kJ/mol			J/mol·K		
2-methyl-5-(2-chloro-5-trifluoromethylphenyl)-furan-3-carboxylic acid						
Acetonitrile	34.5±4.6	31.63±0.80	-2.9±4.7	57.4±8.9	37.1±2.7	-20.3±9.3
Dimethyl ketone		25.15±0.95	-9.4±4.7		36.6±3.2	-20.8±9.5
Ethyl acetate		28.1±1.1	-6.4±4.7		45.5±3.4	-11.9±9.5
Isopropanol		37.77±0.92	3.3±4.7		73.0±2.9	15.6±9.4
2-methyl-5-(2,5-dichlorophenyl)-furan-3-carboxylic acid						
Acetonitrile	31.6±4.4	37.8±1.0	6.2±4.5	46.5±7.9	40.7±3.2	-5.8±8.5
Dimethyl ketone		32.6±1.3	1.0±4.6		44.3±4.1	-2.2±8.9
Ethyl acetate		31.52±0.91	-0.1±4.5		40.2±2.8	-6.3±8.4
Isopropanol		39.1±1.0	7.5±4.5		62.5±3.2	16.0±8.5

Calculated values of enthalpy and entropy of fusion (Table 5) were recalculated relative to a generally accepted temperature of 298 K according to Eqs. (5) and (6) [19].

$$\Delta_{fus}H_T = \Delta_{fus}H_{T_{fus}} + \Delta_{fus}Cp(T - T_{fus}) =$$

$$= \Delta_{fus}H_{T_{fus}}\left[1 + \frac{1}{a}\left(\frac{T - T_{fus}}{T_{fus}}\right)\right] \quad (5)$$

$$\Delta_{fus}S_T = \Delta_{fus}S_{T_{fus}} + \Delta_{fus}Cp\ln\frac{T}{T_{fus}} =$$

$$= \Delta_{fus}S_{T_{fus}}\left[1 + \frac{1}{a}\ln\frac{T}{T_{fus}}\right] \quad (6)$$

where $\left(\frac{\Delta_{fus}S^0}{\Delta_{fus}Cp^0}\right)_{T_{fus}} = \left(\frac{\Delta_{fus}H^0}{T_{fus}\cdot\Delta_{fus}Cp^0}\right)_{T_{fus}} = 1.35 \pm 0.11.$

According to Table 5, the mixing of saturated solutions of both investigated acids in ethyl acetate occurs with negative deviations from the ideal solution ($\Delta_{mix}H < 0$), and the mixing in isopropanol – with positive ones ($\Delta_{mix}H > 0$). Mixing in acetonitrile and methyl ketone occurs with different signs of deviation. The saturated solutions of 2-methyl-5-(2-chloro-5-trifluoromethyl-phenyl)-furan-3-carboxylic acid are mixed with negative, and saturated solutions of 2-methyl-5-(2,5-dichloro-phenyl)-furan-3-carboxylic acid – with positive deviations from the ideal solution.

We also managed to establish the compensatory effect of the mixing process for the acids (Eq. (8)) using organic solvents except acetonitrile (Fig. 2). A similar dependence was observed in our previous studies [13] for 2-methyl-5-phenylfuran-3-carboxylic acid (Eq. (9)) and 2-methyl-5-(4-methylphenyl)-furan-3-carboxylic acid (Eq. (10)).

The location of 1–4 points outside the straight lines can be explained by the formation of hydrogen bond of various types between acids and solvents. An intermolecular hydrogen bond with oxygen is formed between acids and dimethyl ketone, ethyl acetate and isopropanol due to the carbonyl and hydroxyl groups; in the acetonitrile molecules the hydrogen bond is formed between the hydrogen atoms of the hydroxyl group and nitrogen of the nitrile group.

$$\Delta_{mix}H_{298} = 0.350\cdot\Delta_{mix}S_{298} - 2.17 \quad (7)$$

$$\Delta_{mix}H_{298} = 0.346\cdot\Delta_{mix}S_{298} + 1.94 \quad (8)$$

$$\Delta_{mix}H_{298} = 0.414\cdot\Delta_{mix}S_{298} + 6.40 \quad (9)\ [13]$$

$$\Delta_{mix}H_{298} = 0.409\cdot\Delta_{mix}S_{298} + 1.59 \quad (10)\ [13]$$

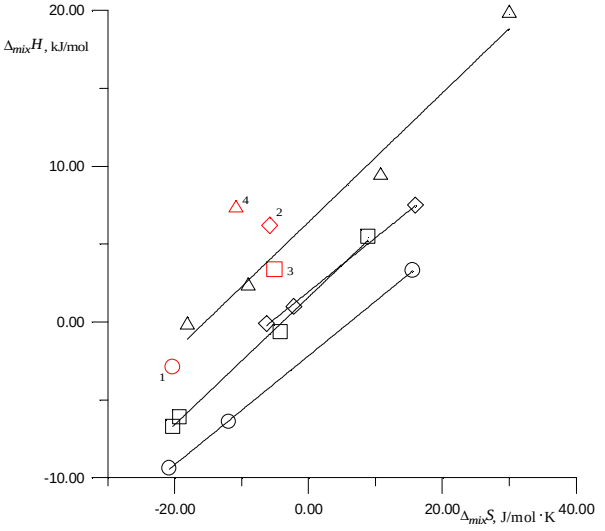

Fig. 2. Dependence between the enthalpy and the entropy of mixing for acids in organic solvents: 2-methyl-5-(2-chloro-5-trifluoromethylphenyl)-furan-3-carboxylic acid (○); 2-methyl-5-(2,5-dichlorophenyl)-furan-3-carboxylic acid (◊); 5-methyl-5-(4-methylphenyl)-furan-3-carboxylic acid [13] (□) and 5-phenyl-2-methyl-3-furancarboxylic acid [13] (Δ); points 1–4 refer to solutions of investigated compounds in acetonitrile

4. Conclusions

The thermodynamic properties of 2-methyl-5-(2-chloro-5-trifluoromethylphenyl)-furan-3-carboxylic acid and 2-methyl-5- (2,5-dichlorophenyl)-furan-3-carboxylic acids solubility in organic solvents were determined. The established compensatory effect of mixing acids with solvents shows the same type of their intermolecular interaction with the formation of a hydrogen bond with oxygen between the carbonyl and hydroxyl groups. The mixing of acids with acetonitrile occurs *via* another mechanism (without compensatory effect) to form a hydrogen bond between hydrogen atoms the hydroxyl group and nitrogen of the nitrile group. The obtained results may be used for optimization of synthesis and purification of investigated acids.

Acknowledgements

The authors express their gratitude to Nadia Tyshchenko, the scientific researcher of the Institute of Materials Science Problems named after I.M. Frantsevich, for derivatographic investigations.

References

[1] Gandini A., Belgacem M.: Prog. Polym. Sci., 1997, **22**, 1203. https://doi.org/10.1016/S0079-6700(97)00004-X
[2] Karateev A., Koryagin A., Litvinov D. *et al.*: Chem. Chem. Technol., 2008, **2**, 19.
[3] Shivarama Holla B., Akberali P., Shivananda M.: Farmaco. 2000, **55**, 256. https://doi.org/10.1016/S0014-827X(00)00030-6
[4] Subrahmanya K., Shivarama Holla B.: Heterocyc. Commun., 2003, **9**, 625. https://doi.org/10.1515/hc.2003.9.6.625
[5] Williams D., Lee M.-R., Song Y.-A. *et al.*: J. Am. Chem. Soc., 2007, **129**, 9258. https://doi.org/10.1021/ja072817z
[6] Moya-Garzón M., Higueras M., Peñalver C. *et al.*: J. Med. Chem., 2018, **61**, 7144. https://doi.org/10.1021/acs.jmedchem.8b00399
[7] Denton T., Srivastava P., Xia Z. *et al.*: J. Med. Chem., 2018, **61**, 7065. https://doi.org/10.1021/acs.jmedchem.8b00084
[8] Duffy J., Kirk B., Kevin N. *et al.*: Bioorg. Med. Chem. Lett., 2003, **13**, 3323. https://doi.org/10.1016/S0960-894X(03)00680-2
[9] Chen M., Yu Q., Sun H.: Int. J. Mol. Sci., 2013, **14**, 18488. https://doi.org/10.3390/ijms140918488
[10] Martins A., Facchi S., Follmann H. *et al.*: Int. J. Mol. Sci., 2014, **15**, 20800. https://doi.org/10.3390/ijms151120800
[11] Chethan P., Vishalakshia B., Sathish L. *et al.*: Int. J. Biol. Macromol., 2013, **59**, 158. https://doi.org/10.1016/j.ijbiomac.2013.04.045
[12] Sobechko I., Van-Chin-Syan Yu., Gorak Yu. *et al.*: Rus. J. Phys. Chem., 2015, **89**, 919. https://doi.org/10.1134/S003602441506028X
[13] Sobechko I., Dibrivnyi V., Horak Y. *et al.*: Chem. Chem. Technol., 2017, **11**, 397. https://doi/org/10.23939/chcht11.04.397
[14] Sobechko I.: Voprosy Khim. Khim. Technol., 2014, **5-6**, 48.
[15] Marshalek A., Sobecjko I., Gorak Yu. *et al.*: Voprosy Khim. Khim. Technol., 2017, **1**, 18.
[16] Sobechko I., Gorak Yu., Van-Chin-Syan Yu. *et al.*: Izv. Vysshikh Ucheb. Zaved., 2015, **58**, 45.
[17] Sobechko I., Chetverzhuk Y., Horak Y. *et al.*: Chem. Chem. Technol., 2017, **11**, 131. https://doi/org/10.23939/chcht11.02.131
[18] Chemistry Web-book. http://webbook.nist.gov (March 18th, 2015)
[19] Sobechko I., Prokop R., Gorak Yu. *et al.*: Vopr. Khim. Khim. Technol., 2013, **4**, 12.
[20] Kochubei V., Horak Yu., SObechko I. *et al.*: Visnyk Lviv. Univ., 2015, **56**, 301.

Received: April 13, 2018 / Revised: October 29, 2018 / Accepted: November 12, 2018

ТЕРМОДИНАМІЧНІ ВЛАСТИВОСТІ РОЗЧИНІВ ХЛОРПОХІДНИХ 2-МЕТИЛ-5-АРИЛФУРАН-3-КАРБОКСИЛЬНИХ КИСЛОТ В ОРГАНІЧНИХ РОЗЧИННИКАХ

Анотація. *Експериментально визначено температурні залежності розчинності 2-метил-5-(2-хлор-5-трифторметилфеніл)-фуран-3-карбонової та 2-метил-5-(2,5-дихлорфеніл)-фуран-3-карбонової кислот в ацетонітрилі, диметилкетоні, ізо-пропанолі та етилацетаті. Розраховані ентальпії плавлення досліджених речовин та їх ентальпії та ентропії змішування за 298 К. Встановлено рівняння зв'язку концентрації насиченого розчину з величинами ентальпії і ентропії розчинності за 298 К. Виявлений компенсаційний ефект змішування досліджених кислот зі всіма розчинниками, що містять карбонільну групу.*

Ключові слова: *ентальпія, ентропія розчинності, змішування і плавлення, 2-метил-5-(2-хлор-5-трифторметилфеніл)-фуран-3-карбонова кислота, 2-метил-5-(2,5-дихлорфеніл)-фуран-3-карбонова кислота.*

Chem. Chem. Technol., 2019,
Vol. 13, No. 3, pp. 288–295

Chemistry

THE SYNTHESIS AND THEORETICAL ANTI-TUMOR STUDIES OF SOME NEW MONOAZA-10*H*-PHENOTHIAZINE AND 10*H*-PHENOXAZINE HETEROCYCLES

Efeturi A. Onoabedje[1], Sunday N. Okafor[2], Kovo G. Akpomie[1], Uchechukwu C. Okoro[1,*]

https://doi.org/10.23939/chcht13.03.288

Abstract. The synthesis and anticancer activity of a series of new 3-amido derivatives of 3-chloro-10*H*-pyrido[3,2-b][1,4]benzoxazine and 3-chloro-10*H*-pyrido [3,2-b][1,4]benzothiazine is presented. The synthesized structures were characterized by UV-visible, FT-IR, ^{1}H NMR spectroscopy and elemental analytical data. The *in silico* physicochemical properties disclosed that neither 3-chloro-10*H*-pyrido[3,2-b][1,4]benzoxazine and 3-chloro-10*H*-pyrido[3,2-b][1,4]benzothiazine intermediates nor their carboxyamido derivatives violate Lipinski's rule of five. In addition, molecular docking studies showed that they exhibited good interaction with cancer receptors. 1,3-di-10*H*-Pyrido[3,2-b][1,4]benzothiazin-3-ylurea which showed a significant interaction with all the employed receptors possessed the highest anticancer activity.

Keywords: synthesis, phenoxazine, phenothiazine, carboxyamide, anticancer, docking.

1. Introduction

Anticancer activity of new phenothiazine derivatives was extensively studied over the last two decades [1]. A variety of benzo and dibenzophenothiazine was known to display a promising anticancer activity [2, 3]. Pluta *et al.* [4] have recently described a significant anticancer activity of azaphenothiazines tested on 55–60 *in vitro* cell lines such as leukemia, non-small cell lung, colon, CNS, melanoma, ovarian, renal, prostate and breast cancers. The anticancer activity of the azaphenothiazines was attributed in part to the thiazine nitrogen in the molecules [4]. Also in recent times various derivatives of phenoxazine have been reported to possess multidrug resistance (MDR) modulator in cancer cells [5, 6]. The presence of phenoxazine nucleus in the structure of naturally occurring Actinomycin D antibiotic and anticancer produced by *Streptomyces* suggests synthesized derivatives of phenoxazine to be potential chemotherapeutic agents [7]. Kato [8] reported that 2-amino-4,4α-dihydro-4α,7-methyl-3*H*-phenoxazin-3-one and 2-aminophenoxazin-3-one were effective in the treatment of pancreatic cancer. In another development, Kapadia [9] demonstrated that the modification of phenothiazine and phenoxazine ring afforded derivatives which possess significant inhibition of *in vitro* Epstein-Barvirus early antigen (EBV-EA). Our earlier work also disclosed phenoxazines as antibiotic leading agents because of their potent inhibition of penicillin binding proteins (PBP) [10]. The inability of anticancer chemotherapeutic agents to selectively discriminate normal cell from cancerous cells as well as serious side effects of administering anticancer drugs constitutes the greatest challenge in cancer treatments [11]. Another major issue in a cancer therapy is the multidrug resistance effect of cancerous cells to numerous chemotherapeutic drugs which often result in treatment failure [12]. Therefore, dedicated effort towards evaluation of potential anticancer agents by medicinal chemists in view to find solutions of the aforementioned problems continued unabatedly.

Recently, metal-catalyzed amidation reactions of aryl halides have become an attractive protocol for synthesizing *N*-arylamides [13-16] and this had been utilized in accessing various azaphenoxazine carboxamides [17]. In this study, similar protocols were applied in the synthesis of new azaphenothiazine carboxy-amides as potential anticancer agents. The *in-silico* physicochemical properties and molecular docking studies of azaphenoxazine and azaphenothiazine carboxamides for anticancer drugs likeness were also described.

[1] Department of Pure & Industrial Chemistry, University of Nigeria, Nsukka, Nigeria
[2] Department of Pharmaceutical and Medicinal Chemistry, University of Nigeria, Nsukka, Nigeria
[*] *uchechukwu.okoro@unn.edu.ng*

2. Experimental

2.1. General Information

All chemicals were purchased from Sigma-Aldrich Chemical Company and were used without further purification. Melting points were determined with a Fischer-Johns apparatus and were uncorrected. ^{1}H and ^{13}C NMR data were recorded with Brucker DPX 400 MHz spectrometers relative to TMS as an internal standard. All chemical shifts were reported in ppm (δ) and coupling constants (J) reported in Hz. Multiplicity are indicated using the following abbreviations: br, for broad; s, for singlet; d, for doublet; t, for triplet; dd, for doublet of doublets and; m, for multiplet. Elemental analysis was carried out at the Central Science Laboratory, University of Cairo, Egypt on a CE440 Elemental Analyzer. UV-Visible Spectra were recorded on Cecil 7500 Aquarius 7000 Series Spectrometer at Chemistry Advance Laboratory (CAL), Sheda Science & Technology Complex (Shestco) Abuja, Nigeria, using matched 1 cm quartz cells and methanol as a solvent. Infrared spectral data were obtained on FT-IR-8400s using KBr disc and reported in wave number (cm^{-1}). The physicochemical properties were studied using Molinspiration Chemoinformatics softwares (http://www.molinspiration.com). The drug-likeness was evaluated using Lipinski's rule of five. In order to gain more insight about the binding modes of compounds **1**–**12**, docking studies were performed. Five cancer target proteins were chosen for this study and the 3D structures of these proteins were downloaded from the Protein Data Bank. They are Signaling protein [18] (PDB code: 3kkp) at the resolution of 1.35 Å; Mitotic regulator for chromosomal alignment and segregation (PDB code: 2x9e) at the resolution of 3.10 Å [19]; Oncogene protein [20] (PDB code: 5P21) at the resolution of 1.35 Å; Androgen receptor [21] (PDB code: 1gs4) at the resolution of 1.95 Å and RAS-RAF-mitogen activated protein kinase/extracellular signal-regulated kinase [18] (PDB code: 3PP1) at the resolution of 1.35 Å.

Human androgen receptor activity has been clearly linked to a prostate cancer. Prostate cancer cells, similar to normal prostate cells, require androgens to grow and survive [21]. However, inhibition of androgen receptor activity will ultimately prevent the production of androgens, and subsequently inhibits prostate cancer growth. Human Mitogen-activated protein kinase is one of the activators that mediates pathways for proliferative and anti-apoptotic signaling from growth factors and oncogenic factors leading to a tumor growth, progression, and metastasis [22] This, therefore, provides a molecular target for discovery of new anti-cancer drugs. Human monopolar spindle 1 (MPS1) kinase (2x9e) is a key regulator of the spindle assembly checkpoint (SAC). SAC is required for proper chromosomal alignment and segregation. This kinase has been found in a wide range of human tumors and is necessary for tumoral cell proliferation [23]. The inhibition of SAC will reduce cancer cell proliferation or cancer cell death, making 2x93 a new approach to selectively target cancer cells. Ras family small GTPases/proteins are one of the focal points in a cancer research because of their role as "on/off switch" signaling pathways. They include 3kkp and 5p21. They control cellular signaling pathways responsible for growth, migration, adhesion, cytoskeletal integrity, survival and differentiation. As a result, multiple approaches are undertaken to develop tumor therapies efficiently targeting RAS and RAS effector pathways [24].

The initial preparation of the pdb files to select the needed chains, delete multiple ligands and non-protein parts were done using Discover Studio visualize [25] version 16. 1.0. 15350. The 2D and 3D structures of the ligands were drawn using ACD/ChemSketch 2015 version [26]. OpenBabel [27] GUI version 2.3.2 and AutoDock [28] were used to convert the pdb file to pdbqt format. AutoDock Tools 1.5.6 and AutoDock Vina version 1.1.2 (downloaded from http://autodock.scripps.edu) were used for molecular docking process [29]. Discover Studio visualize [26] version 16.1.0.15350 was used for analyzing docking results [30].

2.2. Synthesis of 3-Chloro-10*h*-pyrido[3,2-b][1,4]benzothiazine 7

In a 250 ml flask containing sodium hydroxide (1.79 g, 3 mmol) in 50 ml of water was added 2-aminothiophenol (2 g, 2 mmol) and entire mixture warmed until reagents dissolved. Thereafter, freshly prepared 2,3,5-trichloropyridine (2.92 g, 1.6 mmol) in 50 ml of DMF was added in drops within 15 min and the mixture boiled for 4 h. The reaction mixture at the end was filtered and the residue was washed with cold water. The obtained solid product was dried and recrystallized from ethanol to yield a yellow colored compound. Yield 7.90 g (65 %), m.p. 375–376 K. UV-Visible λ_{max} (ethanol): 280 (4.55), 310 (4.40), 350 (3.93). FT-IR (cm^{-1}) (KBr): 3438 (N-H), 3049 (Ar-H), 1615 (C=C), 1356–1315 (C-N). δ_H (400 MHz $CDCl_3$): 7.82 (1H, s, br, N-H), 7.6–6.8 (6H, m, Ar-H). δ_c (100 MHz $CDCl_3$): 144.19, 140.39, 138.98, 120.39, 118.20, 115.57, 110.33, 106.02. (Anal. calcd. for $C_{11}H_7ClN_2S$: C, 43.34; H, 2.42. Found: C, 43.10; H, 2.60).

2.3. General Procedure for Synthesis of Benzoxazine/Benzothiazine Carboxamides

A 250 ml two-necked flask containing $NiCl_2$ (0.3 g, 2.3 mmol) and PPh_3 (0.9 g, 3.4 mmol) was fitted with a teflon septum. The vessel was evacuated and backfilled with nitrogen (three times) before degassed water (1 ml) and *tert*-butanol (2 ml) were injected into the vessel and entire mixture heated for 1 min thereafter K_2CO_3 (1.38 g, 10 mmol), 3-chloro-1-azaphenoxazine (2.18 g, 9.90 mmol), and amides (10.0 mmol) were added to the solution and entire mixture heated at 383 K for 4 h under inert atmosphere until a limiting reactant was completely consumed. The reaction was cooled to room temperature, diluted with ethyl acetate and the crude product extracted from water 3 times. The combined organic extracts were dried with $MgSO_4$, and concentrated in vacuum. The crude product was purified by a silica-gel column chromatography to afford the desired product as a light yellow solid after recrystallization from the aqueous ethyl acetate.

2.4. *N*-(10*H*-Pyrido[3,2-b][1,4]benzothiazin-3-yl)acetamide 8

Compound **8** was obtained as a dark-grey solid after recrystallization from the aqueous ethyl acetate. Yield 43 %, m.p. 381–383 K (dec). UV-Visible λ_{max} (ethanol): 288 (4.55), 290 (4.40), 360 (3.93). FT-IR (cm^{-1}) (KBr): 3310–3250 (N-H), 3030 (Ar-H), 1708 (C=O), 1615 (C=C), 1464–1414 (C=N), 1356–1305 (C-N), 832, 754 (mono substituted benzene ring). δ_H (400 MHz $CDCl_3$): 8.78 (s, br, 1H, HNCO), 7.81 (1H, s, br, N-H), 7.6–6.8 (6H, m, Ar-H), 2.4 (3H, s, CH_3-). δ_c (100 MHz $CDCl_3$): 184.19 (C=O), 140.39, 138.98, 120.39, 118.20, 115.57, 110.33, 106.02, 32.00. (Anal. calcd. for $C_{13}H_{11}N_2OS$: C, 60.68; H, 4.31. Found: C, 60.49; H, 4.50).

2.5. *N*-(10*H*-Pyrido[3,2-b][1,4]benzothiazin-3-yl)benzamide 9

Compound **9** was obtained as a dark ash solid after recrystallization from the aqueous ethyl acetate. Yield 32 %, m.p. 361–363 K (dec). UV-Visible λ_{max} (ethanol): 216 (4.78), 254 (4.80), 309 (4.46), 475 (4.06). FT-IR (cm^{-1}) (KBr): 3350–3307 (N-H), 3161–3070 (Ar-H), 1660 (C=O), 1615 (C=C), 1484–1425 (C=N), 1356–1225 (C-N), 893 (monosubstituted aromatic ring). δ_H (400 MHz $CDCl_3$): 8.50 (1H, s, HNCO), 7.81 (1H, s, br, N-H), 7.60–6.85 (11H, Ar-H), 4.24 (s, 1H, -NH-). δ_c (100 MHz $CDCl_3$): 177 (C=O), 154.19, 148.39, 141.98, 130.59, 128.20, 122.34, 115.57, 110.33, 106.02. (Anal. calcd. for $C_{13}H_{11}N_2OS$: C, 60.68; H, 4.31. Found: C, 60.49; H, 4.50).

2.6. 4-Nitro-*N*-(10*H*-pyrido[3,2-b][1,4]benzothiazin-3-yl)benzamide 10

Compound **10** was obtained as a light yellow solid after recrystallization from the aqueous ethyl acetate. Yield 40 %, m.p. 375–377 K (dec). UV-Visible λ_{max}(ethanol): 212 (3.40), 251 (4.93), 306 (4.40), 404 (2.88). FT-IR (cm^{-1}) (KBr): 3400–3310 (N-H), 3040 (Ar-H), 1690 (C=O), 1610 (C=C), 1405 (C=N), 1356–1305 9 (C-N). δ_H (400 MHz $CDCl_3$): 10.2 (1H, s, HNCO), 8.22 (1H, s, br, N-H), 7.53–6.61 (10H, m, Ar-H). δ_c(100 MHz $CDCl_3$): 175.20 (C=O), 149.11, 143.30, 138.18, 132.39, 128.20, 120.34, 115.57, 110.33, 106.02. (Anal. calcd. for $C_{18}H_{12}N_4O_3S$: C, 59.33; H, 3.32. Found: C, 59.49; H, 3.30)

2.7. 2-(10*H*-Pyrido[3,2-b]benzothiazin-3-yl)-2,3-dihydroisoquinoline-1,4-dione 11

Compound **11** was obtained as a light yellow solid after recrystallization from the aqueous ethyl acetate. Yield 42 %, m.p. 379–381 K (dec). UV-Visible λ_{max}(ethanol): 201 (4.55), 251 (4.03), 320 (4.40), 424 (2.98). FT-IR (cm^{-1}) (KBr): 3450–3320 (N-H), 3040 (Ar-H), 1720, 1698 (C=O), 1610 (C=C), 1405 (C=N), 1356–1335 (C-N). δ_H (400 MHz $CDCl_3$): 8.72 (1H, s, br, N-H), 8.11–7.25 (8H, m, Ar-H), 2.18–2.32 (2H, s, -CH_2-). δ_c (100 MHz $CDCl_3$): 181.23, (C=O), 147.11, 145.30, 140.28, 135.30, 130.20, 125.14, 120.52, 115.03, 106.02, 40.34. (Anal. calcd. for $C_{20}H_{13}N_3O_2S$: C, 66.84; H, 3.65. Found: C, 66.79; H, 3.50).

2.8. 1,3-di-10*H*-Pyrido[3,2-b][1,4]benzothiazin-3-ylurea 12

Compound **12** was obtained as a light yellow solid after recrystallizatiom from the aqueous ethyl acetate. Yield 40 %, m.p. 369–371 K (dec). UV-Visible λ_{max} (ethanol): 247 (2.10), 351 (2.43), 451 (3.40), 520 (3.05). FT-IR (KBr, cm^{-1}): 3411–3355 (N-H), 3051 (Ar-H), 1684 (C=O), 1613 (C=C), 1474–1405 (C=N), 1356–1305 (C-N). δ_H (400 MHz $CDCl_3$): 10.4 (2H, s, br, HNCO), 8.22 (2H, s, NH), 7.5–6.8 (12H, m, Ar-H). δ_c(100 MHz $CDCl_3$): 171.20 (C=O), 150.21, 145.30, 138.10, 135.33, 130.20, 135.30, 125.97, 120.33, 116.12. (Anal. calcd. for $C_{23}H_{16}N_6OS_2$: C, 60.51; H, 3.53. Found: C, 60.40; H, 3.62).

Table 1

Amidation of 3-chloro-10*H*-pyrido[3,2-b]benzoxazine and 3-chloro-10*H*-pyrido[3,2-b]benzothiazine

Entry	Oxazine/thiazine	Amide	Product
1	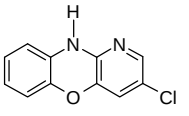 **1**	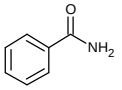	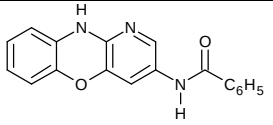 **2**
2	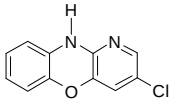	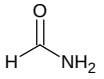	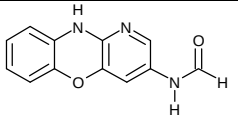 **3**
3	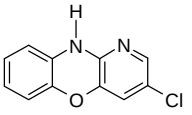	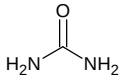	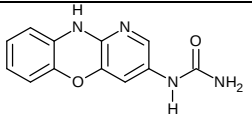 **4**
4	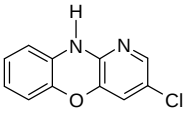	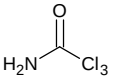	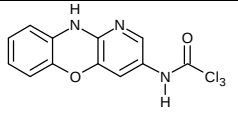 **5**
5	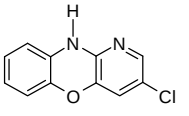	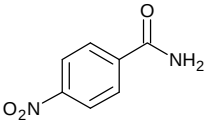	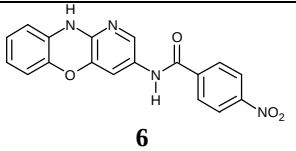 **6**
6	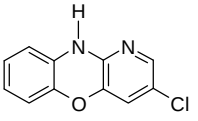		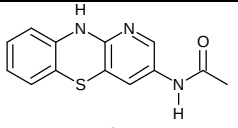 **8**
7	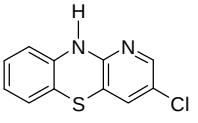 **7**	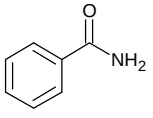	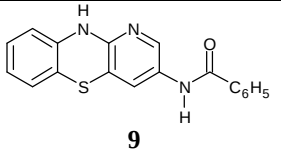 **9**
8	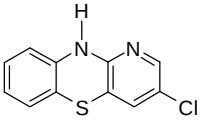	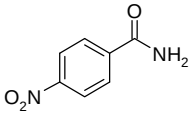	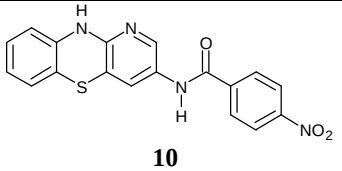 **10**
9	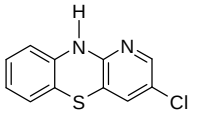	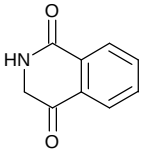	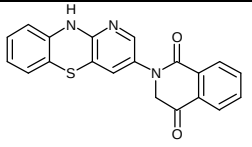 **11**
10	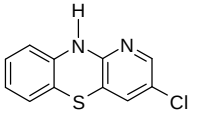	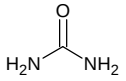	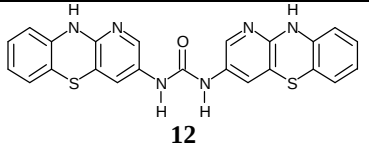 **12**

Reaction conditions: $NiCl_2$ (0.3 g, 2.3 mmol) and PPh_3 (0.9 g, 3.4 mmol), water (1 ml) and *tert*-butanol (2 ml), K_2CO_3 (1.38 g, 10 mmol), 3-chloro-1azaphenoxazine (9.90 mmol), and amides (10.0 mmol).

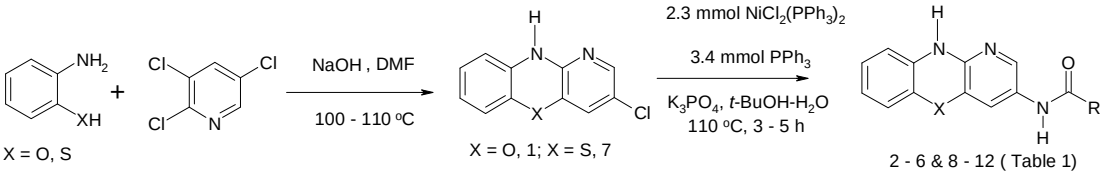

Fig. 1. Synthesis of 3-chlorophenoxazine and 3-chlorophenothiazine amido derivatives

3. Results and Discussion

3.1. Synthesis of Amido Derivatives of Phenoxazine and Phenothiazine

The intermediate compounds, 3-chloro-10*H*-pyrido[3,2-b]benzoxazine **1** and 3-chloro-10*H*-pyrido[3,2-b]benzothiazine **7** were prepared by the anhydrous base catalyzed reaction in DMF or dioxane of 2-aminophenol and 2-aminothiophenol with 2,3,5-trichloropyridine at 373 K respectively to afford yellowish powdered products in good yields after recrystallization from the aqueous ethanol (Fig. 1) [31, 32].

The cross-coupling of compounds **1** and **7** with a variety of amides *via* Ni-PPh_3 mediation afforded the 3-amido derivatives (**2-6** and **8-12)** (Fig. 1, Table 1). The synthesis and characterization of compounds **1** and **2-6** were earlier reported [17] while newly synthesized compounds **7-12** were obtained as yellowish solids in moderate isolated yields.The UV-visible data of compounds **9-12** showed bathochromic shifts as a result of extended conjugation in their molecular structures. The characteristic IR frequencies of N–H and C=O functionalities were found at 3400–3100 and 1700–1640 cm^{-1}, respectively for compounds **7-12**. The proton nuclear magnetic spectra gave broad singlet signals for N–H and HNCO protons correspondingly in such a way N–H protons were located at higher field than HNCO for all the derivatives. The assigned structures of the synthesized compounds were in agreement with other spectral and analytical data.

3.2. *In - Silico* Physicochemical Evaluation

Table 2 contains Lipinski properties such as molecular weight (MW), partition coefficient value (Log P), number of hydrogen bond donor (HBD), hydrogen bond acceptor (HBA) rotatable bonds (NoRB), total polar surface area (TPSA) and other parameters for 3-chloro-10*H*-pyrido[3,2-b]benzoxazine **1**, 3-chloro-10*H*-pyrido [3,2-b]benzothiazine **7** and their amido derivatives.

In accordance with Lipinski's rule of five, a drug must have a molecular weight value of ≤500, hydrogen bond donor ≤5, hydrogen bond acceptor ≤10 and partition coefficient (Log P) ≤5 [20]. Table 2 shows that the synthesized compounds passed the Lipinski's rule of five. The polar surface area (PSA) which is an indicator of the ligand hydrophilicity plays an important role in the protein-ligand interaction. Veber *et al.* [33] showed that 10 or fewer rotatable bonds and polar surface area, PSA ≤140 $Å^2$ would have a high probability of good oral bioavailability in rats. In addition, compounds **1, 3, 5, 7, 8, 9** and **11** were found to have PSA ≤90 $Å^2$ and so can cross the BBB and penetrate the CNS [25]. Pluta [1] noted that the biological activity of phenothiazine derivatives is a result of interaction of pharmacophoric substituents and multicyclic ring (pi-pi interaction, intercalation in DNA) as well as the penetration of biological membrane is a result of the lipophilic character of the molecule.

Table 2

***In-silico* physicochemical properties of the studied compounds**

Compound	MW	Log P	HBD	HBA	nViolation	TPSA	NoRB	Volume
1	218.64	3.29	1	3	0	41.82	0	175.38
2	303.32	3.51	2	5	0	70.92	2	264.64
3	227.22	1.86	2	5	0	70.92	1	193.23
4	242.24	1.75	4	6	0	96.94	1	204.51
5	344.58	3.64	2	5	0	70.92	2	250.34
6	348.32	3.46	2	8	0	116.75	3	287.97
7	234.71	3.94	1	2	0	28.68	0	184.52
8	257.32	2.48	2	4	0	57.78	1	218.93
9	319.39	4.15	2	4	0	57.78	2	273.78
10	364.39	4.11	2	7	0	103.61	3	297.11
11	359.41	3.73	1	5	0	66.06	1	299.10
12	456.56	5.78	4	7	1	98.49	2	373.12

Notes: MW – molecular weight; NoRB – number of rotatable bonds; P – partition coefficient; HBA – number of hydrogen bond acceptors; HBD – number of hydrogen bond donors, nViolation – number of violation; TPSA – total polar surface area.

3.3. Molecular Docking Calculations

The docking study was performed using the AutoDock Tools and AutoDock vina. 3-chloro-10*H*-pyrido [3,2-b]benzoxazine **1**, 3-chloro-10*H*-pyrido[3,2-b]benzothiazine **7** and their amido derivatives were docked into the active sites of the selected cancer target proteins.

All the compounds docked showed significant binding affinities with each of the five proteins. The interactions of compounds **11** and **12** with the receptors 3kkp, 5p21, 2x9e and 1gs4 elicited higher binding affinities than the standard drug. In addition, compounds **6** and **12** showed better interaction and higher binding affinities with the receptor 3pp1 than the standard drug (Table 3).

Compound **12,** 1,3-di-10*H*-pyrido[3,2-b][1,4]benzothiazin-3-ylurea showed the best interaction and the the highest anticancer activity with all the receptors than other derivatives. Particularly, compound **12** showed highest activity with 5p21 and 1gs4 (-11.5 and 11.2 kcal/mol, respectively). These binding energies were significantly high compared to the standard drug (methotrexate). Therefore, compound **12** with the highest binding affinity was selected to illustrate further their binding modes with 5p21 and 1gs4 (Figs. 2 and 3). A careful look at receptor-compound interaction of **12** shows the following interactions of amino acid residues of the receptors (1gs4 and 5p21**)** and the pharmacophoric atoms of the ligand **12:** hydrogen bond, aromatic pi-alkyl, aromatic pi-sulphur, Van der Waals, pi-lone pair and pi-donor hydrogen bond interactions (Figs. 4 and 5). The distances of their interactions in Å are also given.

Table 3

Binding affinity of different compounds with cancer target proteins

Compound	3kkp	Binding energy (Δ*G*), kcal/mol			
		2x9e	5p21	1gs4	3pp1
1	-6.9	-6.8	-7.3	-8.1	-7.2
2	-8.2	-7.7	-9.5	-8.5	-10.0
3	-7.1	-6.9	-8.2	-7.5	-7.6
4	-7.4	-6.9	-8.4	-8.2	-8.2
5	-7.7	-6.9	-8.5	-7.6	-8.3
6	-8.5	-8.0	-9.2	-8.5	-10.3
7	-6.5	-6.6	-6.9	-7.6	-7.1
8	-7.0	-6.7	-7.6	-7.6	-7.9
9	-7.9	-7.7	-8.3	-8.1	-8.7
10	-8.2	-8.0	-8.7	-8.0	-9.5
11	-8.8	-8.8	-9.8	-8.9	-9.7
12	-8.8	-10.0	-11.5	-11.2	-10.9
MTX	-8.2	-7.7	-9.4	-7.8	-8.7

Note: MTX – methotrexate

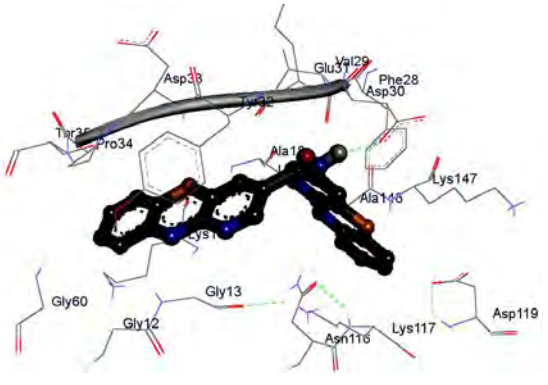

Fig. 2. Binding mode of **12** with amino acid residues of the 5p21

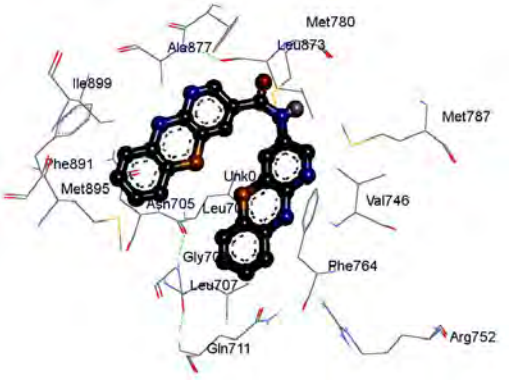

Fig. 3. Binding mode of **12** with amino acid residues of the 1gs4

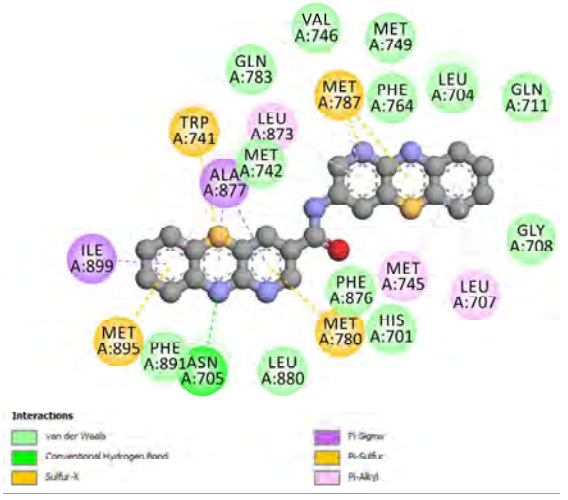

Fig. 4. Interactions of **12** with amino acid residues of the 1g4s

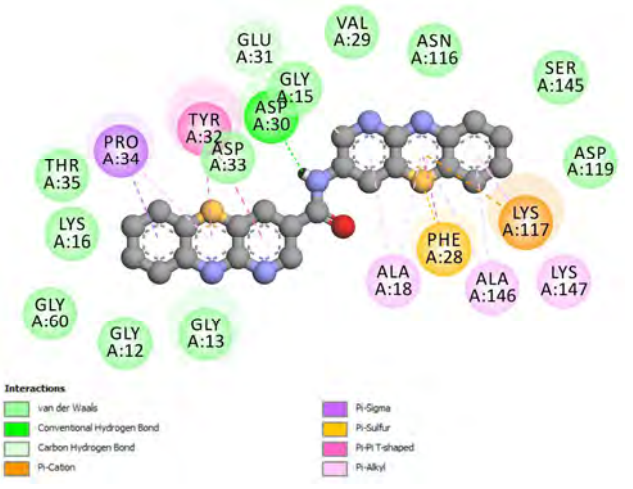

Fig. 5. Interactions of **12** with amino acid residues of the 5p21

It is worthy to note that each of the synthesized compounds was able to interact with each of the cancer target proteins, inhibiting their biochemical processes. This shows that the compounds can act as anticancer agents at different targets, interrupting essential biochemical pathways for the survival of the cancer cells, and ultimately lead to their deaths. In all the receptors used, it was observed that replacement of the chlorine atom in compound **1** and **7** with amido moieties gave rise to compounds with better binding affinities. Particularly, derivatives with benzamido group such as **2**, **6**, **9**, **10**, **11** and **12** possess higher binding affinities than other compounds without the aromatic ring in the amido group. This may be attributed to the ability of the aromatic ring to form pi interactions with sigma, alkyl and sulphur of the amino acid residues of the target proteins.

4. Conclusions

3-amido derivatives of 3-chloro-10*H*-pyrido[3,2-b][1,4]benzoxazine and 3-chloro-10*H*-pyrido[3,2-b][1,4]benzothiazine exhibited a good interaction with cancer receptors. 1,3-di-10*H*-Pyrido[3,2-b][1,4]benzo-thiazin-3-ylurea (compound **12**) possesses the highest anticancer activity, showing the significant interaction with all the receptors employed in the docking. The results from physicochemical and molecular docking studies of derivatives need to be validated by experimental data.

Acknowledgments

We thank Pharm U. S. Onoabedje for proof reading the manuscript.

References

[1] Pluta K., Morak-Mlodawska B., Jelen M.: Eur. J. Med. Chem., 2011, **46**, 3180. https://doi.org/10.1016/j.ejmech.2011.05.013
[2] Aaron J., Gaye Seye M., Trajkovska S. *et al.*: Top. Heterocycl. Chem., 2009, **16**, 202. https://doi.org/10.1007/7081_2008_125
[3] Motohashi N., Sakagami H., Kamata K., Yamamoto Y.: Anticancer Res., 1991, **11**, 1933.
[4] Pluta K., Jelen M., Morak-Mlodawska B. *et al.*: Pharmacology Rep., 2010, **62**, 319. https://doi.org/10.1016/S1734-1140(10)70272-3
[5] Miyano-Kurosaki N, Ikegami K., Kurosaki K. *et al.*: J. Pharmacol. Sci., 2009, **110**, 87. https://doi.org/10.1254/jphs.08347FP
[6] Thimmaiah K., Horton K., Seshadri R. *et al.*: J. Med. Chem., 1992, **35**, 3358. https://doi.org/10.1021/jm00096a009
[7] Shimizu S., Suzuki M., Tomoda A. *et al.*: Tohoku J. Exp. Med., 2004, **203**, 47.
[8] Kato S., Shirato K., Imaizumi K. *et al.*: Oncol. Rep., 2006, **15**, 843.
[9] Azuine M., Tokuda H., Takayasu J. *et al.*: Pharmacol. Res., 2004, **49**, 161. https://doi.org/10.1016/j.phrs.2003.07.014
[10] Onoabedje E., Ibezim A., Okafor S. *et al.*: PLoS ONE, 2016, **11**, e0163467. https://doi.org/10.1371/journal.pone.0163467
[11] Ghorab M., Alsaid M., Al-Dosary M. *et al.*: Chem. Cent. J., 2016, **10**, 1. https://doi.org/10.1186/s13065-016-0148-1
[12] Ullah M.: Asian Pacific J. Cancer Prev., 2008, **9**, 1.
[13] Fors B., Dooleweerdt K., Zeng Q. *et al.*: Tetrahedron, 2009, **65**, 6576. https://doi.org/10.1016/j.tet.2009.04.096
[14] Brett P., Philip K., Strieter F. *et al.*: Org. Lett., 2008, **10**, 3505. https://doi.org/10.1021/ol801285g
[15] Yin J., Buchwald S.: Org. Lett., 2000, **2**, 1101. https://doi.org/10.1021/ol005654r
[16] Buchwald S., Yin J.: Tetrahedron, 2009, **65**, 6576. https://doi.org/10.1016/j.tet.2009.04.096
[17] Agbo S., Anoh V., Okoro U.: J. Applicable Chem., 2014, **3**, 2526.
[18] Shima F., Ijiri Y., Muraoka S. *et al.*: J. Biol. Chem., 2010, **285**, 22696. https://doi.org/10.1074/jbc.M110.125161
[19] Colombo R., Caldarelli M., Mennecozzi M. *et al.*: J. Moll. Cancer Res., 2010, **70**, 10255. https://doi.org/10.1158/0008-5472.CAN-10-2101

[20] Pai E., Krengel U., Petsko G. *et al.*: EMBO J., 1990, **9**, 2351. https://doi.org/10.1002/j.1460-2075.1990.tb07409.x
[21] Matias P., Carrondo M., Coelho R. *et al.* J. Med. Chem., 2002, **45**, 1439. https://doi.org/10.1021/jm011072j
[22] Dong Q., Dougan D., Gong X. *et al.*: Bioorg. Med. Chem. Lett., 2011, **21**, 1315. https://doi.org/10.1016/j.bmcl.2011.01.071
[23] Colombo R., Caldarelli M., Mennecozzi M.: Cancer Res., 2010, **70**, 10255. https://doi.org/10.1158/0008-5472.CAN-10-2101
[24] Rajalingam K., Schreck R., Rapp U., Albert S.: Biochim. Biophys. Acta, 2007, **1773**, 1177. https://doi.org/10.1016/j.bbamcr.2007.01.012
[25] Dassault Systèmes BIOVIA, Discovery Studio Modeling Environment, Release 2017, San Diego: Dassault Systèmes, 2016.
[26] ACD/ChemSketch (Freeware), version 15.01, Advanced Chemistry Development, Inc., Toronto, ON, Canada, www.acdlabs.com, 2015.
[27] Boyle N., Banck M., James C. *et al.*: J. Chemoinform., 2011, **3**, 33. https://doi.org/10.1186/1758-2946-3-33
[28] Morris G., Huey R., Lindstrom W. *et al.*: J. Comput. Chem., 2009, **16**, 2785. https://doi.org/10.1002/jcc.21256
[29] Trott O., Olson A.: J. Comput. Chem., 2010, **31**, 455. https://doi.org/10.1002/jcc.21334
[30] The PyMOL Molecular Graphics System, Version 1.8 Schrödinger, LLC.
[31] Okafor C., Castle R., Wise Jr. D.: J. Heterocyclic Chem., 1983, **20**, 1047. https://doi.org/10.1002/jhet.5570200441
[32] Okafor C., Uche I., Akpanisi L.: J. Heterocyclic Chem., 1981, **18**, 1589. https://doi.org/10.1002/jhet.5570180820
[33] Veber D., Stephen R., Hung-Yuan C. *et al.*: J. Med. Chem., 2002, **45**, 2615. https://doi.org/10.1021/jm020017n

Received: February 02, 2018 / Revised: April 26, 2018 / Accepted: October 15, 2018

СИНТЕЗ І ТЕОРЕТИЧНІ ПРОТИПУХЛИННІ ДОСЛІДЖЕННЯ ДЕЯКИХ НОВИХ МОНОАЗА-10*Н*-ФЕНОТИАЗИНОВИХ ТА 10*Н*-ФЕНОКСАЗИНОВИХ ГЕТЕРОЦИКЛІВ

Анотація. *Синтезовано ряд нових 3-амінопохідних 3-хлор-10Н-піридо[3,2-b][1,4]бензоксазину та 3-хлор-10Н-піридо[3,2-b][1,4]бензотіазину та визначено їх протипухлинну активність. Синтезовані сполуки проаналізовані УФ-, 1Н ЯМР-спектроскопією, спектроскопією Фур'є та елементним аналізом. На основі фізико-хімічних властивостей за методом in silico виявлено, що проміжні продукти 3-хлор-10Н-піридо[3,2-b][1,4]бензоксазину і 3-хлор-10Н-піридо[3,2-b][1,4]бензотіазину, та їх карбоксиамідні похідні не порушують правила Ліпінського. За допомогою молекулярного докінгу показано, що синтезовані сполуки непогано взаємодіють з рецепторами раку. Визначено, що найвищу протипухлинну активність має 1,3-ді-10Н-піридо[3,2-b][1,4]бензотіазин-3-ілсечовина.*

Ключові слова: *синтез, феноксазин, фенотіазин, карбоксиамід, протипухлинні засоби, докінг.*

Chem. Chem. Technol., 2019,
Vol. 13, No. 3, pp. 296–302

Chemistry

SYNTHESIS AND ANTIPLATELET ACTIVITIES OF SOME DERIVATIVES OF *p*-COUMARIC ACID

Juni Ekowati[1, *], Nuzul W. Diyah[1], Achmad Syahrani[1]

https://doi.org/10.23939/chcht13.03.296

Abstract. The synthesis of new derivatives of *p*-coumaric acid was carried out through serial reactions, *i.e.* alkylating, base hydrolysis, catalytic hydrogenation, and Fisher esterification. All reactions except catalytic hydrogenation were conducted by utilizing microwave irradiation from a household microwave oven. The antiplatelet tests using clotting time showed that *p*-coumaric acid and its derivatives have antiplatelet activity which is related to the lipophilic nature of the compounds and its affinity with the selected target molecule, *i.e.* COX-1 enzyme (PDB ID 1CQE).

Keywords: *p*-coumaric acid, antiplatelet, COX-1, clotting time, catalytic hydrogenation.

1. Introduction

One of the leading causes of death from cardiovascular disease is thromboembolism. The accumulation of platelet formation plays an important role in the pathogenesis of thromboembolic disorders [1]. Many endogenous compounds, *e.g.* thromboxane A2, thrombin, von Willebrand factor, and ADP increase platelet aggregation on different routes. Platelets maintain a balance between anti-aggregator and pro-aggregator behavior under normal physiological conditions [2]. The main treatment for this disease is antithrombotic, including antiplatelet. Aspirin is a widely used antiplatelet with the inhibiting mechanism of cyclooxygenase-1 (COX-1) enzyme [3]. However, about 15–25 % of patients are known to be resistant to aspirin. In addition, there are side effects in the form of bleeding and neutropenia [4, 5].

One of the derivatives of the cinnamate compound, namely *p*-coumaric acid, [(E)-3-(4-hydroxyphenyl)acrylic acid] (**1**) has been reported to have antiplatelet activity [6, 7]. Zhao *et al.* [8] reported that compound **1** acts as an anti-inflammatory agent by reducing the expression of inducible nitric oxide synthase (iNOS), COX-2, IL-1β, and TNF-α at mRNA and/or protein levels in RAW264.7 cells stimulated by lipopolisacharide (LPS). Molecule **1** also decreases cytokine levels to reduce MAPK pathway activation, NF-κB, and decreases immune response [8].

One of the factors affecting antiplatelet activity is the drugs ability to penetrate cell membranes or lipophilicity of the compounds [7]. To improve the lipophilicity of **1**, methylation reaction was carried out with dimethyl sulphate in alkaline condition and Fisher esterification to modify carboxylic and OH-phenolic moieties of **1** thereby increasing the value of log*P* of its derivatives. The hydrogenation of vinyl double bond of **1** will also be performed to determine the effect of double bond against antiplatelet activity.

The antiplatelet test was implemented by the blood clotting time slide method. The prediction of antiplatelet mechanisms was studied in the *in silico* study with COX-1 enzyme [9]. The *in silico* study results were compared in terms of Rerank Score (RS) with aspirin.

2. Experimental

2.1. Materials

p-Coumaric acid (**1**) was bought from Aldrich; dimethyl sulphate, KOH, acetone, chloroform, potassium carbonate, HCl, H_2SO_4, NaOH, ether, ethanol, methanol, and Raney-Ni were purchased from Merck. Derivatives of compound **1** (*i.e.* **2-5**) were synthesized *via* several reactions (Fig. 1).

2.2. Methods

The synthesis reaction was monitored with TLC using UV lamp on l = 254 nm to spot detection. Some synthesis reactions were conducted by household microwave oven SHARP model R-230R(S). Melting points were measured by Fischer-John melting point apparatus without correction. UV spectra were obtained by Shimadzu HP 8452 UV-vis spectrophotometer. IR spectra were performed using a Jasco FT-IR 5300

[1] Department of Pharmaceutical Chemistry, Faculty of Pharmacy, Airlangga University,
Jalan Dharmawangsa Dalam, Surabaya 60286, Indonesia
[*] *juni-e@ff.unair.ac.id*

spectrophotometer. The ^{1}H and ^{13}C NMR spectra were obtained from the JEOL JNM-ECS 400 instrument (^{1}H NMR: 400 MHz, ^{13}C NMR: 100 MHz) using appropriate solvent (DMSO-d_6 for **2, 3**, **5**; Pyr-d_5 for **4)**. Physicochemical properties (log*P*, MR, E_{total}) were obtained by Chem Bio Ultra program.

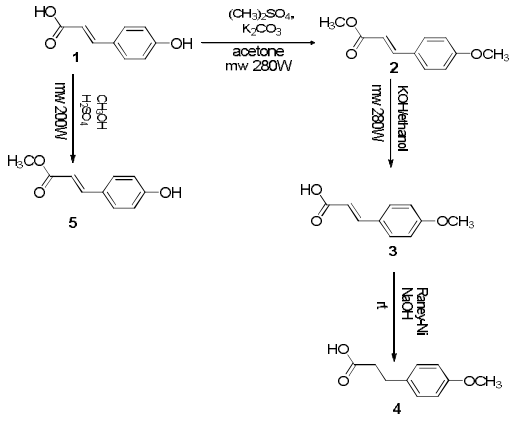

Fig. 1. Structure modification of *p*-coumaric acid (**1**)

2.2.1. (***E***)-Methyl 3-(4-methoxyphenyl)acrylate (2)

p-Coumaric acid (500 mg, 3.05 mmol) was dissolved in 10 ml of acetone. Potassium carbonate (1.25 g, 9.6 mmol) and dimethyl sulphate (2 ml, 21.9 mmol) were added to the mixture. The resulting mixture was irradiated in a microwave oven at 70 % power (280 W) for 10 min. (The mixture was tested by TLC, every 30 s). The crude product was poured into an Erlenmeyer flask containing distilled water and stirred at room temperature, after which it was washed several times and then recrystallized from ethanol.

Obtained product is white crystal; 75 % yield; m.p. 361 K. UV: λ_{max} (EtOH) 228 and 310 nm. IR (KBr; υ cm^{-1}): 2948, 1717, 1637, 1603, 1513, 1288, 1175, 823. ^{1}H NMR (DMSO-d_6, δ ppm): 7.63 (2H, d, *J*=8.4 Hz, -C<u>H</u>=CH-), 7.57 (1H, d, *J* = 15.8 Hz, Ar–CH=C<u>H</u>-C=O), 6.93 (2H, d, *J* = 8.4 Hz, -C<u>H</u>=CH-) 6.44 (1H, d, *J* = 15.8 Hz, Ar–C<u>H</u>=CH-C=O), 3.76 (3H, s, -OC<u>H</u>$_3$), 3.66 (3H, s, -OC<u>H</u>$_3$). ^{13}C NMR (DMSO-d_6, δ ppm): 167.5, 161.7, 144.9, 130.7, 130.7, 127.1, 115.6, 114.9, 114.9, 55.9, 51.8. All the spectral data are in agreement with the structure of the compound **2**.

2.2.2. (***E***) -3- (4-Methoxyphenyl)acrylic acid (3)

Compound **2** (500 mg; 2.60 mmol) was dissolved in 20 ml of 5 % KOH/ethanol solution. The mixture was irradiated into a microwave oven at 70 % power (280 W) until the reaction was complete (6 min). Thereafter, the resulting mixture was acidified with HCl to yield sediment of compound **3**. This crude product was purified by recrystallization using methanol.

Obtained product is white crystal; 85 % yield; m.p. 443 K. UV: λ_{max} (EtOH) 228 and 308 nm. IR (KBr; υ cm^{-1}): 2936, 2844, 2561, 1685, 1623, 1598, 1255, 1173, 827 cm^{-1}. ^{1}H NMR (DMSO-d_6) 3.78 (3H, s, -OC<u>H</u>$_3$), 6.60 (1H, d, *J* = 16Hz, Ar–C<u>H</u>=CH-C=O), 6.96 (2H, d, *J* = 5.0 Hz, -C<u>H</u>=CH-), 7.53 (1H, d, *J* = 16 Hz, Ar–CH=C<u>H</u>-C=O), 7.62 (2H, d, *J* = 5.0 Hz, -C<u>H</u>=CH-). ^{13}C NMR (DMSO-d_6, δ ppm): 55.5, 114.5, 116.7, 127.0, 130.1, 143.9, 161.1, 168.0. All the spectral data are in agreement with the structure of the compound **3**.

2.2.3. 3-(4-Methoxyphenyl)propanoic acid (4)

Compound **3** (500 mg; 2.77 mmol) was dissolved in25 ml of 5 % NaOH solution. The mixture was heated until the MCA was dissolved and then cooled to room temperature again. A catalytic compound of Raney-Ni (565 mg; 5 mmol) was added to the mixture and stirred at room temperature for 1 h. When the rate of gas release decreased, the mixture was heated until the entire hydrogen gas was exhausted (if the volume of the mixture was reduced during heating, sufficient water was added to the initial volume) then the mixture was filtered. The black precipitate of Ni residue on the filter paper was washed with 2×5 ml of 5 % hot NaOH solution, followed by 2×5 ml of hot water. The filtrate was collected and cooled at room temperature. Then, 5 ml of HCl concentrate was dripped slowly and the temperature was maintained within 353–358 K. The precipitate was extracted using 3×10 ml of ether. The ether phase was evaporated and the forming crystals were dissolved in acetone to separate from the remaining Al mixed with the crystals. The acetone phase was evaporated, then white precipitate **4** was obtained. This crude product was purified by recrystallization using ethanol [10].

Obtained product is white crystal; 85 % yield; m.p. 369 K. UV: λ_{max} (EtOH) 202 and 223 nm. IR (KBr; υ cm^{-1}): 2930, 2835, 2596, 1703, 1612, 1512, 1302, 1246, 1215, 821. ^{1}H NMR (Pyr-d_5; TMS; δ ppm): 6.88 (2H, d, *J* = 6.0 Hz, -C<u>H</u>=CH-), 7.15 (2H, d, *J* = 6.0 Hz, -CH=C<u>H</u>-), 3.82 (3H, s, -OC<u>H</u>$_3$), 2.88 (2H, t, *J*= 6.0 Hz, Ar-CH$_2$-C<u>H</u>$_2$-C=O), 2.54 (2H, t, *J*=9.0 Hz, Ar-C<u>H</u>$_2$-CH$_2$-). ^{13}C NMR (Pyr-d_5, TMS, δ ppm): 175.4, 158.7, 133.9, 130.3, 129.9, 114.9, 114.5, 55.3, 36.9, 30.9. All the spectral data are in agreement with the structure of the compound **4**.

2.2.4. (***E***)-Methyl-3-(4-hydroxyphenyl)acrylate (5)

Compound **1** (500 mg; 3.05 mmol) was dissolved in 5 ml of methanol, then 2 drops of concentrated H_2SO_4

were slowly added to the mixture. The mixture was introduced into a microwave oven and irradiated at 50 % power (200 W) until the reaction was completed. The excess of methanol was evaporated, and then the residue was neutralized with 5 % potassium carbonate solution. The crude product **5** was washed with cold water and then purified by recrystallization using an appropriate solvent.

Obtained product is white crystal; 75 % yield; m.p. 419 K. UV: λ_{max} (EtOH) 230 and 314 nm. IR (KBr; υ cm^{-1}): 3378, 1687, 1268, 1177, 1617, 823. ^{1}H NMR (DMSO-d_6; TMS; δ ppm) : 9.96 (1H,s, -OH), 6.75 (2H, d, J = 8.2 Hz, -CH=CH-), 7.50 (2H,d, J = 8.2 Hz, -CH=CH-), 3.65 (3H, s, -OCH_3), 7.52 (1H, d, J=15.8 Hz, Ar–CH=CH-C=O), 6.35 (1H, d, J=15.8 Hz, Ar–CH=CH-C=O). ^{13}C NMR (DMSO-d_6, TMS, δ ppm): 167.6, 160.4, 145.3, 130.8, 130.8, 125.6, 116.3, 116.3, 114.4, 51.7. All the spectral data are in agreement with the structure of the compound **5**.

2.2.5. Clotting Time Assay

White male adult mice in good health of age 8-12 weeks and weight of 20-22 g were adapted and fed for one week and then randomly divided into 5 groups, each consisting of 6 mice. Each mouse was fed with their usual food every day and was given drink of water *ad libitum*. All mice were tested for blood clotting time (day 0) and were put into the mounting. The blood clotting time was calculated by putting mice on an observation desk. The mice's tail was cleaned by 70 % alcohol and then pierced with a surgical knife as far as 2 cm from the tail edge for 2 mm puncture depth. The dripping blood were then dripped into the object glass and observed for every 15 s to determine the onset of fibrin formation. Afterwards, the scarred mice were treated using betadine solution according to their groups. Low dose of ASP (80 mg) was used as a positive control and 0.5 % CMC-Na solution was used as negative control, both administered orally. The test solutions were given orally with the same dose of aspirin for 7 days. On the 8th day, blood clotting time on the test animals were analyzed according to the procedure outlined above [1]. Antiplatelet assay was approved by the Ethical Commission of Airlangga University.

2.2.6. *In silico* study

The *in silico* study was performed on the crystal structure of the enzyme COX-1 (PDB ID 1CQE) with 2.90 Å resolution, which was downloaded from the RCSB Protein Data Bank (www.rcsb.org), in the form of binding ligand crystal COX-1 with FLP_1650 [A]. The complex 1CQE-FLP_1650 [A] crystal structure was downloaded to the active site and determined for its binding sites. The 3D molecular structure of test compounds was imported into the active site and placed in a cavity in accordance with FLP_1650 [A]. The *in silico* assay was conducted into an appropriate cavity of the SE algorithm using MolDock with the maximum of 1500 iterations. The affinity of the ligand was determined and the score expressed as Rerank Score (RS). The complex enzyme ligand with pose with the highest score showed the best interaction. The best docking result must fulfill the requirements, namely the lowest energy and the position of the molecule that is in the same bond with FLP_1650 [A], observed visually. Observation of enzyme-ligand interactions included hydrogen bonding, steric interactions (Van der Waals), as well as electrostatic performed to pose with the highest score of RS [10].

3. Results and Discussion

The structure modification of the *p*-coumaric acid (**1**) used the Fisher esterification reaction, alkylation, and catalytic dehydrogenation mentioned above, yielded the desired compounds, namely **2, 3, 4, 5** (Fig. 1).

In this research, syntheses of **2, 3,** and **5** were successfully conducted by microwave irradiation. The basic mechanism of microwave irradiation is caused by the agitation of polar or ionic molecules that move because of magnetic field movement. The occurrence of these magnetic movements causes the particles to try to orientate or parallelize with the field, limiting the movement of particles due to the interaction between particles and dielectric resistance. This will cause heat that centers on the magnetic plate. Microwave irradiation is different from the conventional heating method since in the conventional heating, oil bath or heating mantle is heated first followed by its solvent. This kind of heat distribution will cause heat differences between the mantle and the solvent [11, 12].

The alkylation reaction between the phenolic group of **1** with dimethyl sulfate was conducted, according to the principle of Williamson ether synthesis [13], to produce compound **2**. It was indicated by the loss of sharp peak the phenolic group of compound **1** at wavenumber of 3383 cm^{-1} and the appearance of a new peak of methoxy ether moiety of compound **2** at wavenumber of 1288 cm^{-1}. These changes were supported by three protons addition of the methoxy group (s, 3H) at 3.76 ppm of ^{1}H NMR spectrum. This methoxy group could also be observed in the ^{13}C NMR spectrum of compound **2** at a chemical shift of 51.8 ppm. The loss of phenolic groups had been confirmed by $FeCl_3$ reagent addition, which gave a positive purple color for the compound **1** as the result of complex formation between Fe^{3+} and the ligand, *i.e.* phenolic group. On the other hand, the compound **2** showed no purple color indicating that it had no phenolic groups. During process reaction, there should be no presence water that may affect hydrolysis of the dimethyl sulfate. Therefore, acetone was used as a solvent. The

methylation reaction using dimethyl sulfate on cynamate derivate, namely Azragel, that has activities as antiplatelet which inhibited thromboxane formation, was also reported by Baytas *et al.* [14].

Besides being able to alkylating the phenolic moiety of **1**, dimethyl sulfate can also be used for the alkylation of carboxylate moiety. Potassium carbonate was used to form the carboxylic ion of **1** so that its nucleophilic property increased to react with methyl group of dimethyl sulfate [15]. The alteration of carboxylic acid group of **1** into an ester group of **2** was shown by the loss peak at the wavenumber of 2836 cm^{-1}, which appears as a broadened peak because of the presence of the hydrogen bonds between –OH of carboxylic acid moiety of **1**. In addition, the C=O carbonyl group of **1** at wavenumber of 1672 cm^{-1} was replaced by the peak of C=O ester of **2** at wavenumber of 1717 cm^{-1}. The presence of methyl ester and methyl ether could be observed in the chemical shift of 3.76 and 3.66 ppm (s, 3H) of ^{1}H NMR spectra as well as at 55.9 and 51.8 ppm of ^{13}C NMR spectra of **2**. Interpretation of spectral data from structural characterization of **2** concludes that its chemical structure is identical to the structure of same compound that was reported by Sun *et al*. [16].

The hydrolysis of **2** into **3** was performed in the base condition using KOH as reagent with ethanol as a solvent according to our previous research [17]. This method was selected because it is an irreversible reaction with the formation of potassium *p*-methoxycoumarate salt, and that salt was reacted easily with HCl to obtain compound **3**. The alteration of ester moiety of **2** into carboxcylic acid group of **3** was displayed by the loss of –C=O carbonyl ester peak at wavenumber of 1717 cm^{-1} and the presence of –C=O carbonyl acid at 1685 cm^{-1}. The hydrogen bonding of –OH carcoxylic acid of **3** also showed at wave number 2844 cm^{-1}. This change was also clarified by the loss of three protons of the methyl ester group of **2** at the chemical shift 3.66 ppm (3H,s) of ^{1}H-NMR spectra and the loss of one carbon atom at 51.8 ppm of ^{13}C-NMR spectra. Hydrolysis of ethyl *p*-methoxycinnamate in alkaline condition, which employs conventional heating, may also produce compound **3** [17], but it will take a longer time than the microwave irradiation method that was used in this study.

The structure modification from **3** to **4** was conducted through the catalytic hydrogenation reaction with Raney-Ni as the metal catalyst. Raney-Ni metal works to reduce the double bond of **3** by these mechanisms: (i) adsorption of vinylic double bond of compound **3** on the surface of the hydrogenated metal catalyst, (ii) attachment of hydrogen by the β-carbon of compound **3** to form a σ-bond between the metal and α-C, and finally (iii) reductive elimination of the free alkane, compound **4** [10, 18]. The transformation of structure **3** to **4**, was characterized by the loss of proton vinylic double bond, which was visible on the chemical shift 6.60 ppm (1H,d, J = 16 Hz) and 7.53 ppm (1H,d, J = 16 Hz). This double bond was transformed into a single bond which was characterized by two triplet peaks at chemical shift 2.88 and 2.54 ppm of ^{1}H NMR spectra.

The alteration of compound **1** into **5** was characterized by the appearance of peaks at 3378 and 1687 cm^{-1} of ester moiety, replaced peaks at 2836 and 1672 cm^{-1} of carboxylic acid moiety. The methyl ester group also was observed at chemical shift 3.65 ppm (s, 3H) in ^{1}H NMR spectra and 51.7 ppm in ^{13}C NMR spectra. Vo *et al.* [19] reported anti-inflammatory activity of **5** by stimulation Akt signaling pathway on macrophage cells. This anti-inflammatory mechanism compound **5** is same as compound **1** [8].

Structural modification of **1** into **2-5** will cause changes in physicochemical properties of the molecules, including log*P*, MR and E_{total}. The change in molecular properties result in the difference in nature of their interactions with target molecules (receptors), that can be expressed in rerank score (RS). The physicochemical properties of the compound are shown in Table 2. Log*P* describes the ratio of molecular affinity of nonpolar solvents versus polar solvents representing lipophilic character of QSAR study [20]. MR is a molecular size influenced by its polarizability that classified as steric property, E_{total} is molecular free energy in the most stable conformation that is one of the electronic properties of a molecule, whereas RS is a free energy of ligand-protein binding that exhibits the affinity of the compound against a selected target molecule [21], *i.e.* COX-1 enzyme (PDB ID 1CQE).

3.5. Antiplatelet Activities Test Conducted with the Clotting Time Slide Method

Low dose of aspirin can be used as an antiplatelet and inhibitor of COX-1 [3, 21]. Based on this fact, the anti-platelet test was performed using mice with corresponding aspirin doses (20 mg/kg BW). The results of antiplatelet of each compound group with slide clotting time method are: CMC-Na (129.7±6.39); **1** (253.5±11.61); **2** (355.6±8.79); **3** (301.8±11.66); **4** (211.8±11.66), **5** (263.7±12.89); ASP (339.2±9.9) seconds as shown in Fig. 2.

Based on the ANOVA statistical test (Fig. 2) it can be seen that the blood clotting time of compound **1** and its derivates (**2-5**) have significant differences with the negative control group, namely the CMC-Na test group ($P < 0.05$). This suggests that compound **1** and its derivatives have antiplatelet effects. The clotting times of

compounds **2, 3,** and **5** show significant improvements compared to the compound **1**. While compound **4** has significantly different clotting time compared to all test groups ($P < 0.05$), it has a lower antiplatelet effect than other derivatives. All synthesized compounds give greater effect than negative control. Compounds **2** and **3** have clotting times that are not significantly different from the positive control of aspirin (ASP), which shows its potential as the same antiplatelet.

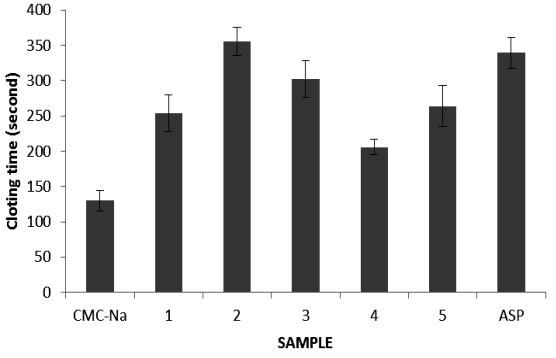

Fig. 2. Histogram of antiplatelet activity (mean ± SE) by slide clotting time method of compounds **1–5**, CMC-Na (control negative), and ASP (control positive)

This can be explained with the *in silico* study of COX-1, where the docking score in the form of rerank scores (RS) according to the MVD 5.5 program is shown in the Table. The RS of ASP is -287.4 kJ/mol. The RS value of *p*-coumaric acid is higher than those of its derivatives. It means that its derivatives are capable to construct more stable interactions with the receptor than *p*-coumaric acid. Meanwhile, the RS of **4** show similarly low interactions with COX-1 and thromboxane. The best docking poses of ASP and *p*-coumaric acid derivatives (**2-5**) are shown in Fig. 3. The interactions of the functional groups of each test compound with the COX-1 amino acid residue are shown in Fig. 4.

The COX-1 enzyme was constitutively expressed in most tissues, in which it controlled the synthesis of prostaglandins. COX-1 is the only form of enzyme present in mature thrombocyte and is also present in the blood vessels of endothelium, gastrointestinal epithelium, brain, spinal cord, and kidney [22].

In Fig. 4 it can be seen that all molecules of the test compound are in the same bonding place as FLP_1650 [A], namely cavity-5. RS FLP is -372.1964 kJ/mol. The RS data in the Table, which is free energy of enzyme-ligand interaction (ΔG, kJ/mol), shows the amount of energy of Van der Waals, electrostatic and hydrogen bonding interactions, and it can be used to predict how strong the ligand-enzyme bonds. The presence of methoxy groups in compounds **2** and **3** increases the strength of interaction with amino acid residues in compound **1** and all derivates having carboxylate groups form the hydrogen bond on the –COOH moiety with the amino acid residues of Arg 120 of COX-1 enzyme as in the ligand reference, namely flubiprofen (FLP_1650 [A]), as reported by Fauchier *et al.* [7]. The double bond change of vinylic in **3** into single bond in **4** converts the hybridization of the rigid sp2 bond into freely rotating sp3, resulting in weaker interactions with the residue.

Table

Physicochemical properties of *p*-coumaric acid (1) and its derivatives (2-5)

Compound	Chemical structure	RS, kJ/mol PDB 1CQE	log*P*	MR, cm^3/mol	E_{total}, kJ/mol
1	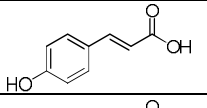	-289.8067	1.54	44.67	44.096
2	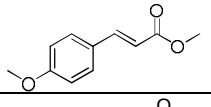	-318.2710	2.07	55.54	58.279
3	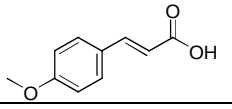	-301.9787	1.81	50.10	73.370
4	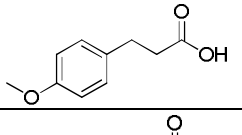	-275.7909	1.56	48.25	26.888
5	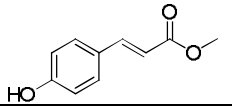	-308.7899	1.81	50.10	28.350

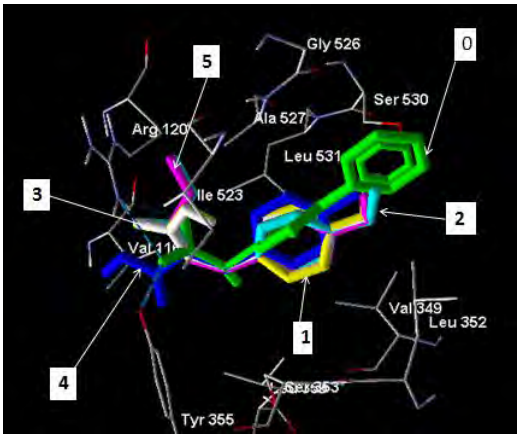

Fig. 3. Docking pose of FLP_1650 [A] (**0**), **1**, **2**, **3**, **4**, **5**
on cavity 5 (Vol 54.272) of COX-1 (PDB 1CQE)

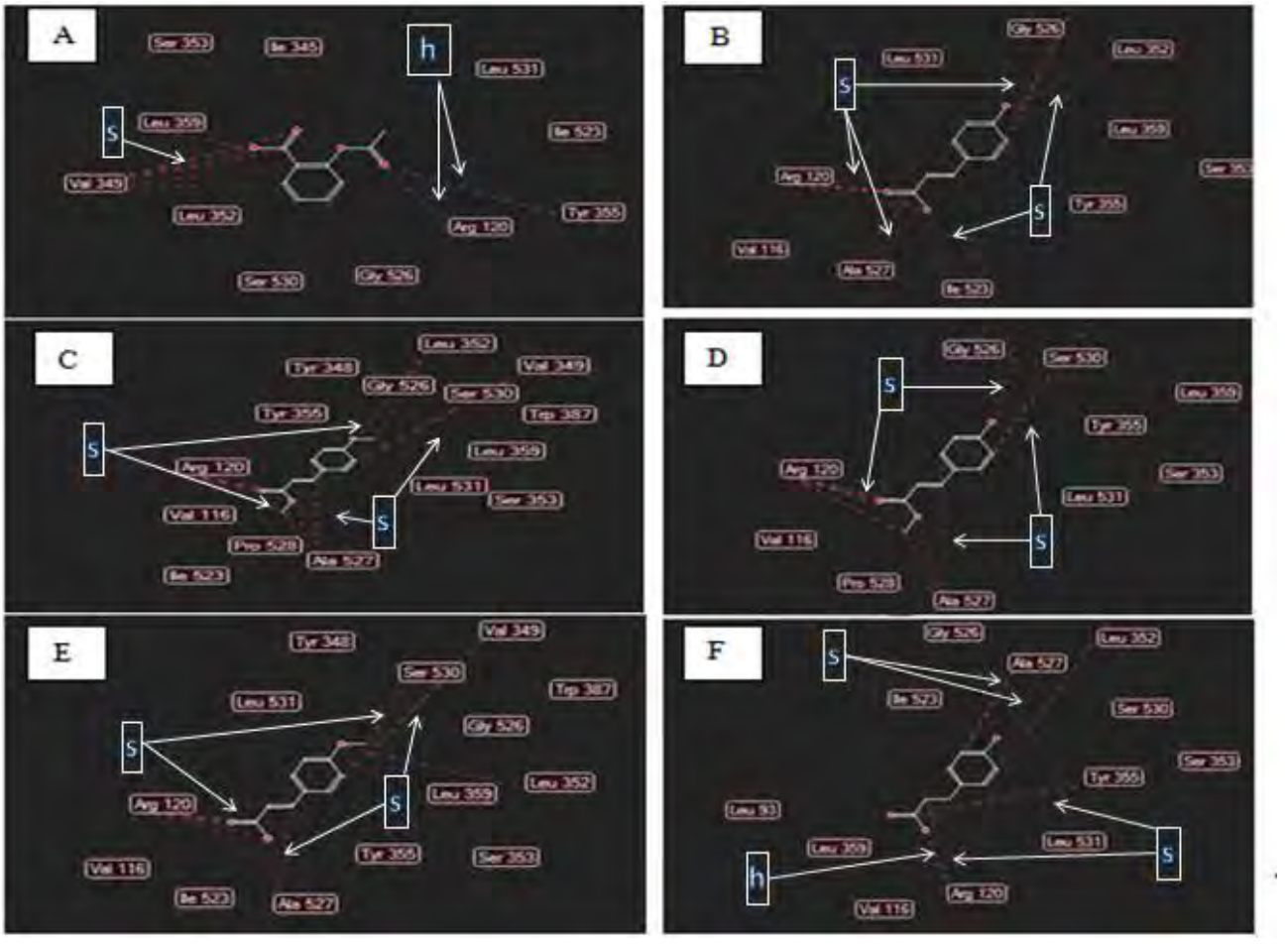

Fig. 4. 2D pictures showed interaction of ASP (4A), **1** (B), **2** (C), **5** (D),
3 (E), and **4** (F) with amino acid residues in cavity 5 of enzyme COX-1 (PDB 1CQE).
Hydrogen bonding interaction marked as **h**; steric interaction marked as **s**

As *in silico* study results, it appears that the molecule **1** and its derivatives inhibit COX-1 enzyme. COX-1 binding of compound **1** and its derivatives in blood platelets will prevent COX-1 pathway to produce thromboxane-A2 (TXA2) and afterward restrain platelet aggregation for the period of platelets lifecycle [20, 21].

3.6. The Relationship between Physico-Chemical Properties and Biological Activity

The statistical analysis was carried out by regression method between each dependent variable against antiplatelet activity, with one independent variable of physicochemical property. The result showed a linear relationship between physicochemical properties and antiplatelet activity among 5 tested compounds. The result is supported by the physicochemical properties, especially lipophilic (log*P*) and RS properties. It may occur because in the determination of antiplatelet activity, the tested compound is administered through oral route to experimental animals. By this route, the compound capability in penetrating membrane barrier directly to the site of action depends on their lipophilic character. In this case the lipophilic nature (log*P*) appears to indicate a significant role. There is a significant linear relationship ($P < 0.05$) between log*P* (partition coefficient) and antiplatelet activity (blood clotting time). The significant linear relationship ($P < 0.05$) also occurs between docking score (RS) and blood clotting time (CT) as indicated by the equations:

(1) $CT = 227.749 \log P - 123.102$

($n = 5$, adjust $R^2 = 0.785$, $F = 15.163$, $P = 0.030$)

(2) $CT = -13.228 RS - 666.662$

($n = 5$, adjust $R^2 = 0.713$, $F = 10.927$, $P = 0.046$)

Based on these equations it is known that antiplatelet activity is related to the lipophilic nature of the compound (log*P*) and its affinity (RS) with the selected target molecule, ***i.e***. COX-1 enzyme (PDB ID 1CQE). With the higher log*P* value, the antiplatelet activity will increase according to the coefficient of variable having a positive value. In terms of RS, with more negative free energy of the interaction between the compound and COX-1 the antiplatelet activity increases.

4. Conclusions

Four derivatives of *p*-coumaric acid (**2-5**) have been obtained through some reactions, ***i.e***. alkylation, hydrolysis, catalytic hydrogenation, and Fisher esterification. All of the derivatives have anti-platelet activities. The presence of methyl group increases the activity, whereas the change of double bond of vinylic into single bond in **4** decreases the interaction with COX-1, hence decreasing its antiplatelet potentials compared to those of other derivatives.

Acknowledgments

This research was funded by Research Publication Acceleration Grant of Faculty of Pharmacy Airlangga University in year 2016-2017.

References

[1] Sathyapriya E., Velpandian V., Anbu J., Anjana A.: Int. J. Life Sci. Pharma Res., 2012, **2**, 4.
[2] Ruggeri Z.: J. Thromb. Haemost., 2003, **1**, 1335. https://doi.org/10.1046/j.1538-7836.2003.00260.x
[3] Dudley A., Thomason J., Fritz S. *et al.*: J. Vet. Int. Med., 2013, **27**, 141. https://doi.org/10.1111/jvim.12022
[4] Hall R., Mazer C.: Anesth. Analg., 2011, **112**, 292. https://doi.org/10.1213/ANE.0b013e318203f38d
[5] Massimi I., Ciuffetta A., Temperilli F. *et al*.: Mediators Inflamm., 2015, **2015**, 1. https://doi.org/10.1155/2015/607957
[6] Ilavenil S., Da Kim H., Srigopalram S. *et al*.: Molecules, 2016, **21**, 1. https://doi.org/10.3390/molecules21080997
[7] Fauchier L., Greenlaw N., Ferrari R. *et al*.: PLoS One, 2015, **10**, 1. https://doi.org/10.1371/journal.pone.0125164
[8] Zhao Y., Liu J.: Med. Chem., 2016, **6**, 327. https://doi.org/10.4172/2161- 0444.1000365
[9] Bao J., Zhou N., Luo K. *et al.*: Int. J. Mol. Sci., 2014, **15**, 15994. https://doi.org/10.3390/ijms150915994
[10] Ekowati J., Chaulah N., Budiati T.: Berkala Ilmiah Kimia Farmasi, 2014, **3**, 44.
[11] Akomas S., Ijioma S.: Compr. J. Med. Sci., 2014, **2**, 9.
[12] Nerkar A., Pawale D., Ghante M. *et al*: Int. J. Pharm. Pharm. Sci., 2013, **5**(Suppl 3), 564.
[13] Selva M., Perosa A.: Green Chem., 2008, **10**, 457. https://doi.org/10.1039/b713985c
[14] Baytas S., Turan Dural N., Özkan Y. *et al*.: Turkish J. Chem., 2012, **36**, 367. https://doi.org/10.3906/kim-1110-8
[15] Lamoureux G.: Arkivoc, 2009, **2009**, 251.
[16] Sun P., Zhu Y., Yang H. *et al*.: Org. Biomol. Chem., 2012, **10**, 4512. https://doi.org/10.1039/c2ob25462j
[17] Ekowati J., Tejo B., Sasaki S. *et al*.: Int. J. Pharm. Pharm. Sci., 2012, **4**(Suppl 3), 528.
[18] Mattson B., Foster W. *et al*.: J. Chem. Ed., 2013, **90**, 613. https://doi.org/10.1021/ed300437k
[19] Vo V., Lee J., Shin S. *et al*.: Biomol. Ther., 2014, **22**, 10. https://doi.org/10.4062/biomolther.2013.095
[20] Agrawal V., Desai S.: J. Pharmacogn. Phytochem., 2015, **145**, 145.
[21] Kujawski J., Popielarska H., Myka A. *et al*.: Comput. Methods Sci. Technol., 2012, **18**, 81. https://doi.org/10.12921/cmst.2012.18.02.81-88
[22] White W.: Hypertension, 2007, **49**, 408. https://doi.org/10.1161/01.HYP.0000258106.74139.25

Received: March 05, 2018 / Revised: March 27, 2018 / Accepted: August 29, 2018

СИНТЕЗ І АНТИТРОМБОЦИТАРНА ДІЯ ДЕЯКИХ ПОХІДНИХ *p*-КУМАРОВОЇ КИСЛОТИ

Анотація. *Синтезовано нові похідні р-кумарової кислоти за участю реакцій алкілування, основного гідролізу, каталітичного гідрування та естерифікації Фішера. Всі реакції, за винятком каталітичного гідрування, проводились за допомогою мікрохвильового опромінення побутової мікрохвильової печі. За результатми аналізів на тромбоцити, враховуючи час згортання крові, показано, що р-кумарова кислота та її похідні мають антитромбоцитарну активність, яка пов'язана з ліпофільною природою сполук та їх спорідненістю з вибраною цільовою молекулою, тобто ферментом COX-1 (PDB ID 1CQE).*

Ключові слова: *р-кумарова кислота, антитромбоцитарний, COX-1, час згортання крові, каталітичне гідрування.*

Chem. Chem. Technol., 2019,
Vol. 13, No. 3, pp. 303–316

Chemistry

THE STUDY OF THE INTERACTION MECHANISM OF LINOLEIC ACID AND 1-LINOLEYL-2-OLEOYL-3-LINOLENOYL-GLYCEROL WITH FE_3O_4 NANOPARTICLES

Iryna Tsykhanovska[1]*, Victoria Evlash[2], Alexandr Alexandrov[1], Tatyana Gontar[1], Daniil Shmatkov[1]

https://doi.org/10.23939/chcht13.03.303

Abstract. The interaction mechanism of Fe_3O_4 nanoparticles with linoleic acid and 1-linoleyl-2-oleoyl-3-linolenoyl-glycerol represented by two-layer coordination model has been determined. By means of Fourier spectroscopy, scanning electron microscopy, energy dispersive X-ray spectroscopy, X-ray photoelectron spectroscopy, X-ray phase and thermal gravitational analysis, the interaction mechanism of lipids (linoleic acid and sunflower oil) with Fe_3O_4 nanoparticles has been studied.

Keywords: Fe_3O_4 nanoparticles, linoleic acid, 1-linoleyl-2-oleoyl-3-linolenoyl-glycerol, sunflower oil, chemisorption.

1. Introduction

One of the important operational and technological properties of the food raw materials and food ingredients that determines the technological processes course and the finished product quality is the fat holding capacity (FHC). FHC is the capacity to bind and hold fats which are triglycerides. Apart from triglycerides, the edible fats contain the higher fatty acids (oleinic, linoleic and linolneic acids in oils; palmitic and stearic acids in animal fats). Therefore, when studying the FHC mechanism, it is necessary to consider the physicochemical interactions of the food system ingredients with the main components of fats and oils – triglycerides and the higher fatty acids. Knowledge of the binding mechanisms will allow to rationally use the new types of food raw materials and additives, as well as to predict the behavior of ingredients in the food systems (dough and confectionery masses, minced meat, *etc*.) during processing and storage of the finished products.

[1] Ukrainian Engineering Pedagogic Academy,
16, Universitetskaya St., 61003 Kharkiv, Ukraine
[2] Kharkiv State University of Food Technology and Trade,
333, Klochkovskaya St., 61051, Kharkiv, Ukraine
* *cikhanovskaja@gmail.com*

The food fibers have the high fat binding capacity (FBC), the mechanism of which is not well studied. There is an opinion that FHC and FBC are determined by lignin presence and independent from its particles size [1, 2]. Some authors [3-6] showed the dependence of fat holding and binding capacities on the number and size of the raw material particles. This suggested that the mechanism of fat absorption by the food fibers can be determined not only by the lignin sorption activity, the efficiency of which increases when grinding, but also by the surface adsorption [3-6].

The numerous studies show that the structure peculiarities and the presence of hydrophobic groups contribute to the fat binding by the raw material components [3-8]. By the experimental studies the good FHC was found for citrus fibers Herbacel AQ Plus, type N and Citrifi; carrageenans; carob bean, guar and xanthan gums [7-9]; the egg powder, the milk powder and the dairy foods; wheat, soya, oatmeal and pea flour [7, 9, 10]; various functional ingredients derived from the industrial by-products (skin, hoof, feathers, by-products, *etc*.) [9, 11]; and the oil based functional gels [12, 13]. First grade flour binds and holds the fats better compared with top quality flour due to the higher content of proteins and food fibers in it. Carrageenans contain hydrophilic and hydrophobic groups providing their ability to bind and hold fats. FHC of milk powder and dairy foods is provided by the presence of casein, which has both the hydrophobic and hydrophilic sites [7]. Recently, various nanopowder food additives, in particular, silver, iron oxides, titanium dioxide, and silicon dioxide, have been used to improve FHC of the food systems [14-21]. This ability is associated with the high dispersion, which allows not only to bind free fats, but also to hold them on the nanoparticles surface while cooking, as well as with a good accessibility of numerous hydrophobic sites [14-17].

In the scientific works [18-20] a model of monolayer adsorption (chemisorption) of fatty acids on the nanoparticles surface of the metal oxides is proposed. A model of two-layer adsorption is also considered: the

first monolayer occurs on the nanoparticle surface due to the chemisorption of fatty acids and makes the particles superhydrophobic; the second layer occurs due to the interaction of hydrophobic sites of the first monolayer with the alkyl substituents of fatty acids [21]. However, these assumptions are controversial and require the additional experimental confirmation.

The analysis of literary sources [1-21] showed that there are insufficient data on the FHC mechanism by the nanopowder food additives, in particular, Fe_3O_4 nanoparticles. Fe_3O_4 nanopowder is a major component of Magnetofood food additive developed by the authors of this work.

The nanopowder based on Fe_3O_4 (Magnetofood) has the great potential and new operational and technological properties (emulsifying, water-binding, water-holding, fat-binding, fat-holding) and promising technological applications [16, 17, 22-25]. The interaction of Magnetofood nanoparticles with the biopolymers of the food systems (proteins, proteids, carbohydrates, lipids) is a system of complex chemical reactions. The supramolecular organization of Fe_3O_4 nanoparticles and the organic matrix structure play the important role. The result is the formation of spatial nanostructures which significantly affect the functional and technological properties of the raw materials and semi-finished products (confectionery and dough masses, minced meat, *etc*.) [16, 17, 23, 25].

Therefore, the works on the creation of the new operational and technological properties of the food systems with the help of the nanopowder food additives of the complex action are topical. At the same time, it is important to understand the mechanisms of main properties formation, including FHC. To explain the FHC mechanism by Fe_3O_4 nanoparticles of Magnetofood, it is necessary to understand the nature of Fe_3O_4 nanoparticles interaction with triglycerides and the higher fatty acids.

So, the purpose of this work is the study of the interaction mechanism of linoleic acid and triglyceride – 1-linoleyl-2-oleoyl-3-linolenoyl-glycerol with Fe_3O_4 nanoparticles.

2. Experimental

2.1. Materials

Five samples were used for the investigations.

Sample 1. High-dispersive black colored powder of Fe_3O_4 with the particles size of ~78 nm. The sample was obtained according to the technology developed by us [15] *via* the reaction of chemical co-precipitation of the iron salts in an alkaline medium.

Sample 2. Linoleic acid purchased from Reakhim, Ukraine.

Sample 3. Crude sunflower oil purchased from Vinnytska industrial company ViOil, Ukraine or 1-linoleyl-2-oleoyl-3-linolenoyl-glycerol obtained *via* the esterification reaction of glycerol with non-saturated fatty acids (linoleic, oleic and linolenic) laboratory of the Department of Chemical and Food Technologies of Ukrainian Engineering Pedagogics Academy.

Sample 4. Fe_3O_4 nanoparticles coated with linoleic acid. They were obtained by the dispersion of 1 g of Fe_3O_4 nanoparticles (sample 1) and 0.2 g of linoleic acid in 10 ml of dimethylformamide for 12 h at (323 ± 1) K under nitrogen stream blowing over the reaction mixture surface. After cooling the suspension to 293–298 K, Fe_3O_4 nanoparticles coated with linoleic acid were separated by magnetic filtration and washed with the water-ethanol mixture (1: 1) 5–7 times. The final product was dried in a vacuum at 333 ± 1 K for 24 h.

Sample 5. Fe_3O_4 nanoparticles coated with crude sunflower oil or 1-linoleyl-2-oleoyl-3-linolenoyl-glycerol. They were obtained by the procedure analogous to the previous one with the only difference that crude sunflower oil or 1-linoleyl-2-oleoyl-3-linolenoyl-glycerol was taken instead of linoleic acid.

2.2. Research Methods

2.2.1. IR-Fourier spectroscopy (FTIR)

A Tensor 37 Fourier spectrometer (Bruker, Germany), controlled by the OPUS software package with the standard graduated capabilities in the frequency range of 4000–400 cm^{-1} in the absorption format was used. Spectra of samples 1, 4, 5 were recorded in the KBr tablets; samples 2, 3 – in the "liquid film").

2.2.2. X-ray diffraction analysis (XRD)

XRD of the experimental samples 1, 4, 5 was performed using a powder diffractometer Siemens D500 (Germany) in the copper radiation with a graphite monochromator. The researches were carried out according to the well-known Bragg-Brenton technique [26]. The sample was dried at room temperature (293 K), thoroughly ground and mixed in a mortar. Then the sample was transferred to $2\times1\times0.1$ mm^3 glass cuvette to record the diffractogram. The angle range was $10° < 2\theta < 150°$ with the step of 0.02° and an accumulation time of 12 s at each point. The primary phase search was performed by using the PDF-4 card file [27], and then the roentgenogram was calculated using the Ritveld method.

2.2.3. Transmission electron microscopy (TEM)

For samples 1, 4 and 5 the particles size and morphology were determined by using a JSM-820

scanning electron microscope (JEOL, Japan) with the magnification of 150000. The obtained images in a planar geometry with the electron beam falling along the hexagonal axis and perpendicular to it were processed with the help of AutoCAD 2014 and MathCad 2014 programs. Based on the obtained results, the particle distribution was calculated relative to the diameter. To determine the average values the particles number in the sample was at least 500.

2.2.4. Energy dispersive X-ray spectroscopy (EDX)

To determine the elemental composition of the experimental samples 1, 4 and 5, a scanning electron microscope JSM-820 (JEOL, Japan) with an EDX connector was used. X-ray spectra were obtained by bombarding experimental samples with electrons using an acceleration voltage of 20 kV (corresponding to the lines of the characteristic spectra of Fe, C and O).

2.2.5. X-ray photoelectron spectroscopy (XPS)

The chemical composition of the surface layers and the chemical state of the elements on the surface of samples 4 and 5 were determined using a Kratos Axis Ultra DLD electron spectrometer (Kratos Analytical Ltd, UK). The exciting X-ray was the Al K_α line with photon energy $h\nu$ = 1486.6 eV, tube voltage was 15 kV, the emission current was 10 mA. General XPS-spectra were recorded under constant energy mode of 160 eV and spectra of the internal electronic levels of the main elements Fe 2p, O 1s, C 1s – of 40 eV. The scale of the binding energy (E_b) was pre-calibrated according to the position of the main levels peaks Au $4f_{5/2}$ (E_b = 83.96 eV), Ag $3d_{5/2}$ (E_b = 368.21 eV) and Cu $2p_{3/2}$ (E_b = 932.62 eV); calibration accuracy was ±0.03 eV. Samples charge was evaluated according to carbon C 1s spectra (284.5 eV).

The samples were prepared by embedding thin layer of the sample (~50.0 mg) into metallic indium, which is located directly in the holder of the measuring unit of the device.

For a detailed analysis of the atoms chemical states we used spectra decomposition by the individual components according to the program that takes into account the mixed Lorentz-Gaussian shape of the peaks and the area under the peaks with simultaneous optimization of the background parameters. At the same time the minimizing principle of the bands number needed to describe the experimental spectra was used.

The error in the peak position determining was ±0.01 eV. To analyze the atoms chemical state (Fe, O, C) on the samples surface the spectra of the electronic levels Fe 2p (705–740 eV), O 1s (525–554 eV) and C 1s (275–295 eV) were studied in detail and thus the phase composition of the samples surface was quantified.

2.2.6. Thermogravimetric analysis (TGA)

The thermogravimetric investigations of samples 4 and 5 (~5.0 mg) were carried out using a Q-1500D derivatograph (IOM, Hungary) within the temperature range of 293–1173 K) at a heating rate of 5 K/min. An aluminum oxide (T = 1473 K) was used as a standard.

3. Results and Discussion

3.1. Substantiation of the Interaction Mechanism of Linoleic Acid and 1-Linoleyl-2-Oleoyl-3-Linolenoyl-Glycerol with Fe_3O_4 Nanoparticles

Adsorption (chemisorption) of the higher fatty acids and triglycerides on the Fe_3O_4 nanoparticles surface is mainly determined by electrostatic – dipole-dipole (Van der Waals forces), ion-dipole and ionic interactions. The donor-acceptor (coordination) interactions are also involved in the adsorption of fats and oils. The interactions appear between the Fe_3O_4 nanoparticles surface and triglyceride and the adsorbed free fatty acids. It means that under the influence of Fe_3O_4 nanoparticles the fats and oils undergo the structural changes affecting the fat holding and binding processes.

The RHC mechanism of Fe_3O_4 nanoparticles can be presented by the two-layer coordination model. The first adsorption layer is formed on the nanoparticle surface due to the electrostatic interactions of polarized lipid groups with ionized Fe_3O_4 particles and the coordination bonds of Fe atoms of Fe_3O_4 nanoparticles with the carbonyl and hydroxyl O atoms of the carboxyl groups of the free fatty acids, as well as with O atoms of ester groups of triglycerides. The second adsorption layer occurs due to the electrostatic hydrophobic interactions of the hydrophobic centers of the first monolayer and the aliphatic side chains of the acyl residues of triglycerides and the alkyl components of the free fatty acids.

The Fe^{2+} and Fe^{3+} cations of Fe_3O_4 magnetic nanoparticles are the structure-forming ions. The high intensity of the electric field generated by iron ions of Fe_3O_4 enhances the polarization of the triglyceride molecules and free fatty acids, which contributes to the additional ordering of bond dipoles $C^{\delta+}=O^{\delta-}$ and $O^{\delta-}-H^{\delta+}$ outside the surface of Fe_3O_4 particles and lipid adsorption.

Fig. 1 shows the types of the ionized Fe_3O_4 nanoparticles (NP). There are opposite polarized areas (Fe "+" and O "–", Fig. 1a) on the surface of Fe_3O_4 NP. In the presence of H^+ protons, originating in the acidic media during the hydrolysis of edible fats and oils, the formation of the protonated Fe_3O_4 NP is possible (Fig. 1b). These

particles appear as a coordination bond (oxygen of Fe_3O_4 is a donor, H^+ proton of the medium is an acceptor). The energy of the coordination bond is 50–200 kJ/mol. The protonated Fe_3O_4 particles can form the bonds of ion-ion (energy ~100–400 kJ/mol) and ion-dipole (energy ~50–200 kJ/mol) types with ions and the polarized molecules of free lipids (fatty acids and triglycerides) [16, 17, 20].

The ionized Fe_3O_4 particles are capable of chemical and electrostatic interactions (Figs. 2, 3). In Fig. 2 the ionic interactions between the ionized Fe_3O_4 nanoparticles and the charged carboxyl group (COO^-) of the higher fatty acids are represented. They are characterized by the high binding energy (~500–1000 kJ/mol) [16, 17, 20].

Probable ion-dipole interactions of Fe_3O_4 nanoparticles with the ionic groups of triglycerides and free fatty acids are shown in Fig. 3. These interactions occur between the protonated NP ($Fe_3O_4H^+$) and oxygen of hydroxyl and carbonyl groups of free fatty acids carboxylate; alcohol and carbonyl oxygen of triglyceride ester group.

Fig. 4 shows the dipole-dipole interactions of Fe_3O_4 nanoparticles with the ionic groups of triglycerides and free fatty acids. The energy of the dipole-dipole (Van der Waals) interaction is small – about 5–50 kJ/mol [16, 17, 20]. The dipole-dipole interactions are possible between the polarized Fe_3O_4 nanoparticle ($^{+}Fe_3O_4^{-}$) and dipole of hydroxyl ($^{-\delta}O - H^{\delta+}$) and carbonyl ($^{-\delta}O = C^{\delta+}$) group of free fatty acids carboxylate; alcoholic ($^{-\delta}O - C^{\delta+}$) and carbonyl ($^{-\delta}O = C^{\delta+}$) dipoles of triglycerides ester group.

The interaction of Fe_3O_4 nanoparticles with the polarized carboxyl groups of free fatty acids and ester groups of triglyceride is also possible due to the coordination bonds.

Under the influence of Fe_3O_4 nanoparticles the fats and oils undergo the structural changes and form together stable complexes. Fig. 5 shows the process of nanoparticles self-organization in electrostatic complexes with linoleic acid and with 1-linoleyl-2-oleoyl-3-linolenoyl-glycerol, which are stabilized by the coordination (donor-acceptor) bonds of Fe and O atoms.

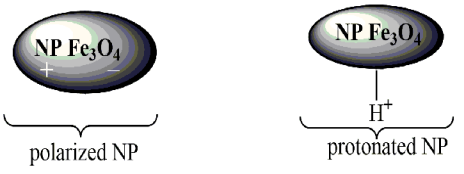

Fig. 1. Polarized (a) and protonated (b) Fe_3O_4 nanoparticles

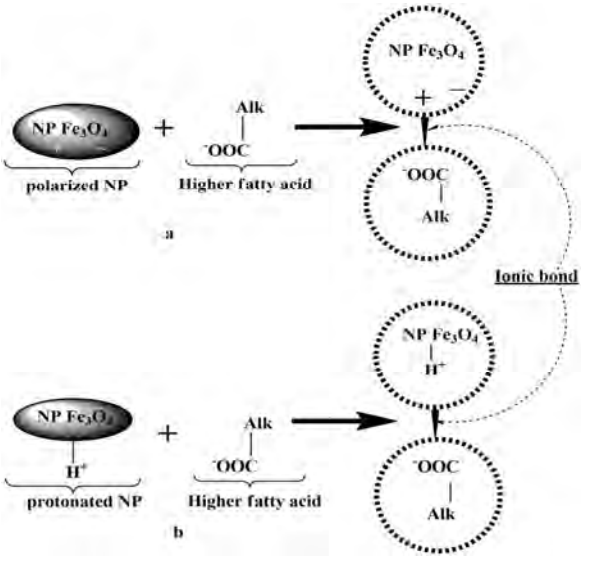

Fig. 2. The ionic interactions between the polarized (a) and protonated (b) Fe_3O_4 nanoparticles and COO^- group of the higher fatty acids

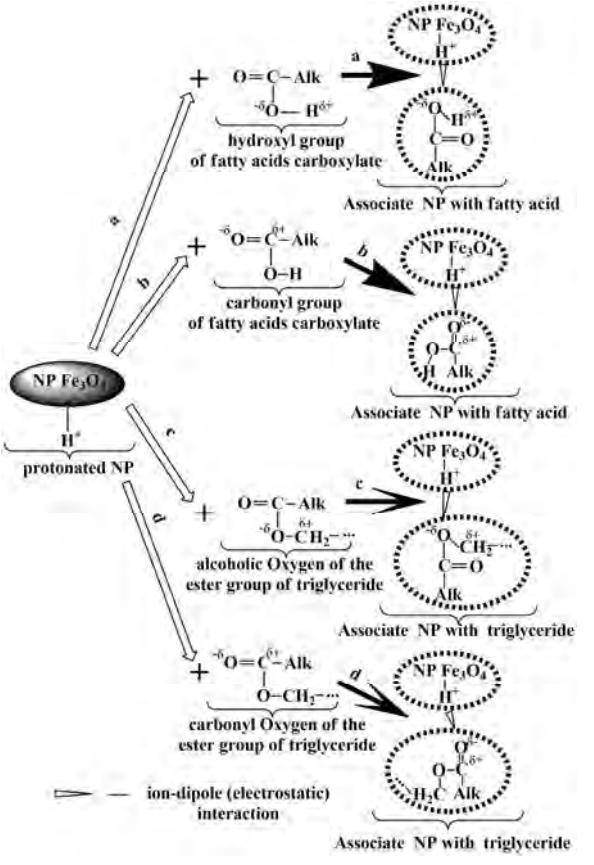

Fig. 3. The ion-dipole interaction between protonated Fe_3O_4 nanoparticle ($Fe_3O_4H^+$) and oxygen of carboxylate hydroxyl group of free fatty acids (a); oxygen of carboxylate carbonyl group of free fatty acids (b); alcoholic oxygen of triglyceride ester group (c) and carbonyl oxygen of triglyceride ester group (d)

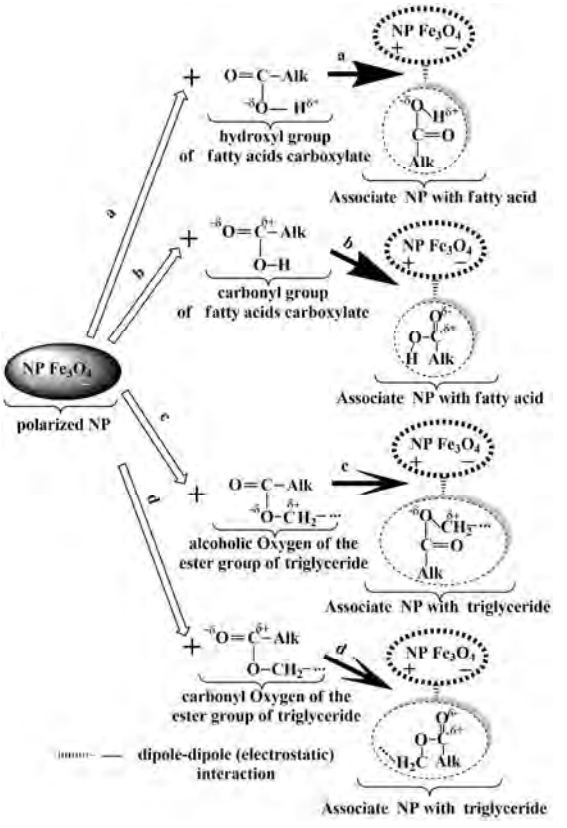

Fig. 4. The dipole-dipole interaction between the polarized Fe_3O_4 nanoparticles ($^{+}Fe_3O_4^{-}$) and dipole of the hydroxyl group ($^{-\delta}O - H^{\delta+}$) of free fatty acids carboxylate (a); dipole of the carbonyl group ($^{-\delta}O = C^{\delta+}$) of free fatty acids carboxylate (b); alcohol dipole ($^{-\delta}O - C^{\delta+}$) of triglyceride ester group (c) and carbonyl dipole ($^{-\delta}O = C^{\delta+}$) of triglyceride ester group (d)

From data of Fig. 5 it should be noted that Fe_3O_4 nanoparticles form the electrostatic complexes due to the coordination bonds with the oxygen atoms of carboxylate (the interaction with linoleic acid) and ester (the interaction with triglyceride – 1-linoleyl-2-oleoyl-3-linolenoyl-glycerol) groups.

The ability of Fe_3O_4 nanoparticles to enter into the electrostatic (Figs. 2-4) and coordination (Fig. 5) interaction with the hydrophilic centers of free fatty acids and triglycerides causes the chemisorption of the ionized Fe_3O_4 NP on the reactive surface. As a result, the first adsorption layer is formed on the particles surface. Taking into account all mentioned above and previous studies regarding the chemical reactions of the metal oxides nanoparticles and carboxylates of the higher fatty acids, the model of interaction between the hydrophilic centers of triglycerides and fatty acids with Fe_3O_4 NP can be represented by four types: ionic (Fig. 2), monodentate (Fig. 6), bidentate (chelate) (Fig. 7), and bidentate (bridge) (Fig. 8) [16, 17, 20].

It is obvious from Fig. 6 that due to the complex interaction (electrostatic and coordination) one Fe cation of Fe_3O_4 binds to one carboxylic oxygen atom of fatty (linoleic) acid (Fig. 6a) or to one esteric oxygen atom of triglyceride (1-linoleyl-2-oleoyl-3-linolenoylg-lycerol) (Fig. 6b). As a result, the monodirectional electrostatic complex is formed.

The bidentate electrostatic complex (Fig. 7) in which one Fe cation of Fe_3O_4 is bound with two oxygen atoms of the linoleic acid carboxyl group or the ester group of 1-linoleyl-2-oleoyl-3-linolenoyl-glycerol is formed due to the complex interaction (electrostatic and coordination).

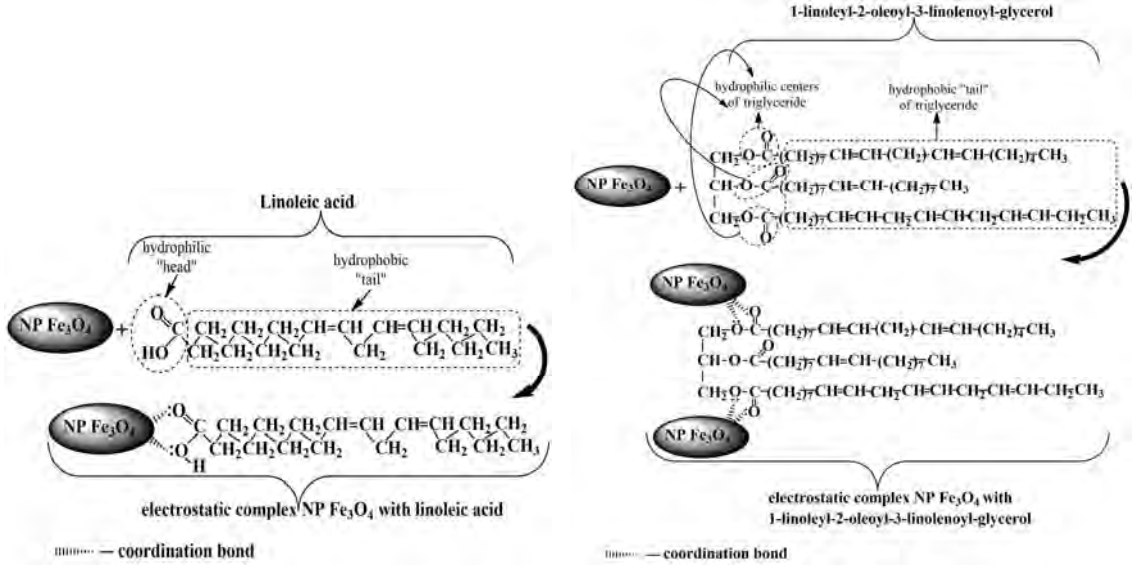

a) b)

Fig. 5. The formation of electrostatic complex Fe_3O_4 nanoparticles with linoleic acid (a) and 1-linoleyl-2-oleoyl-3-linolenoyl-glycerol (b)

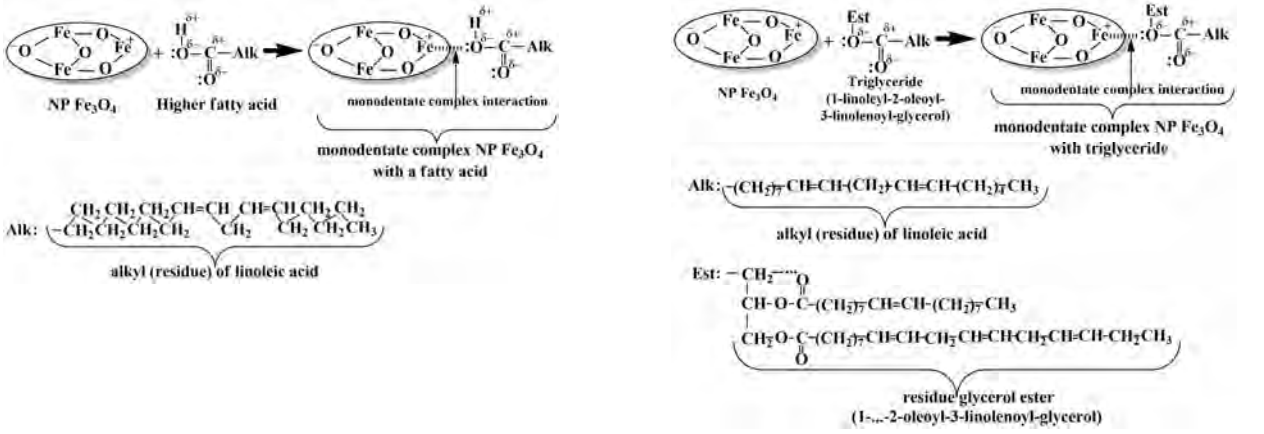

a) b)

Fig. 6. The formation of monodentate complex Fe_3O_4 nanoparticles with fatty (linoleic) acid (a) and triglyceride (1-linoleyl-2-oleoyl-3-linolenoylglycerol) (b)

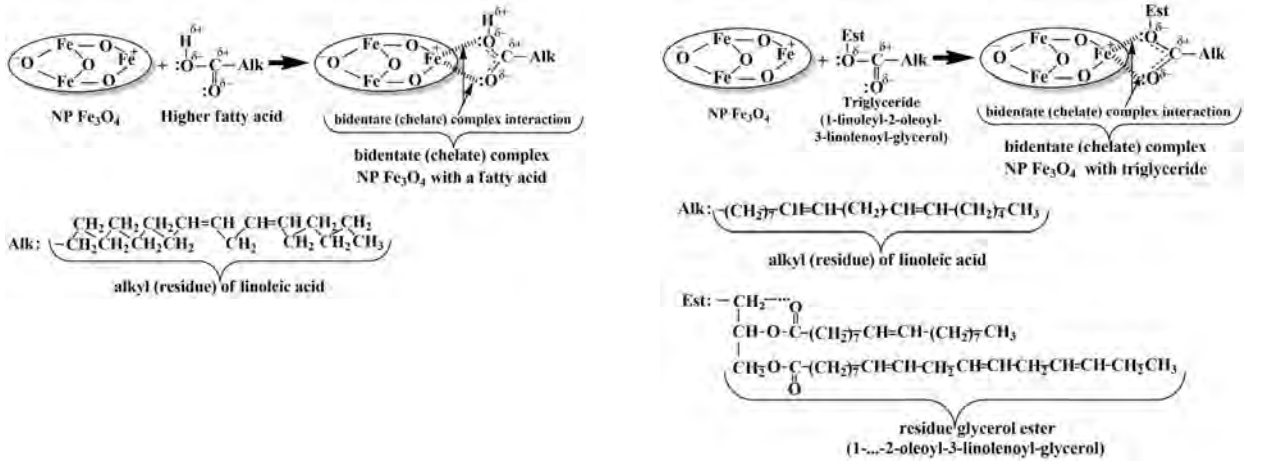

a) b)

Fig. 7. The formation of bidentate (chelate) complex Fe_3O_4 nanoparticles with fatty (linoleic) acid (a) and triglyceride (1-linoleyl-2-oleoyl-3-linolenoylglycerol) (b)

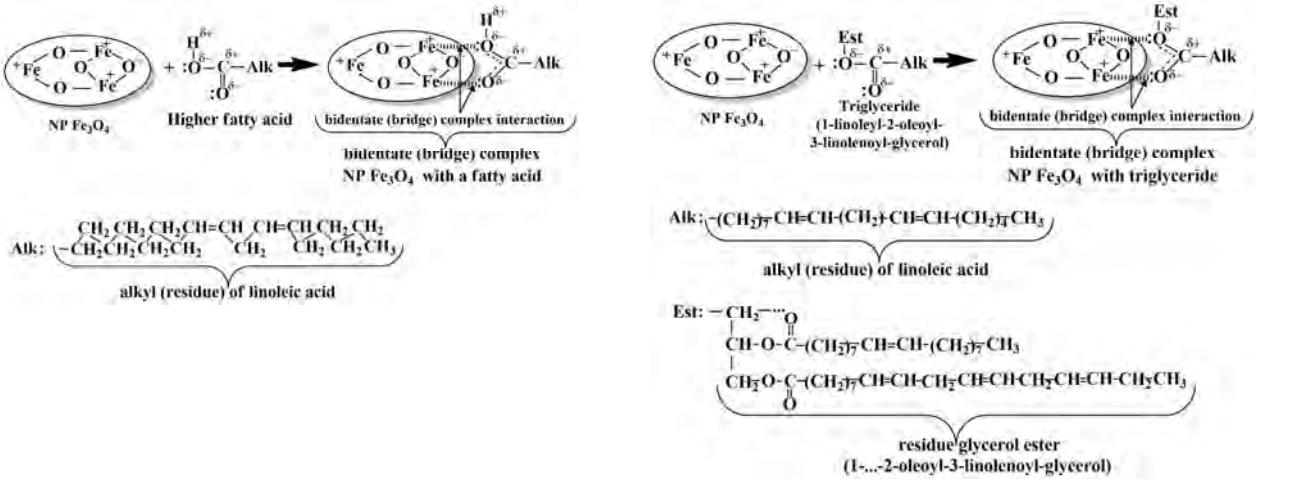

a) b)

Fig. 8. The formation of bidentate (bridge) complex Fe_3O_4 nanoparticles with fatty (linoleic) acid (a) and triglyceride (1-linoleyl-2-oleoyl-3-linolenoylglycerol) (b)

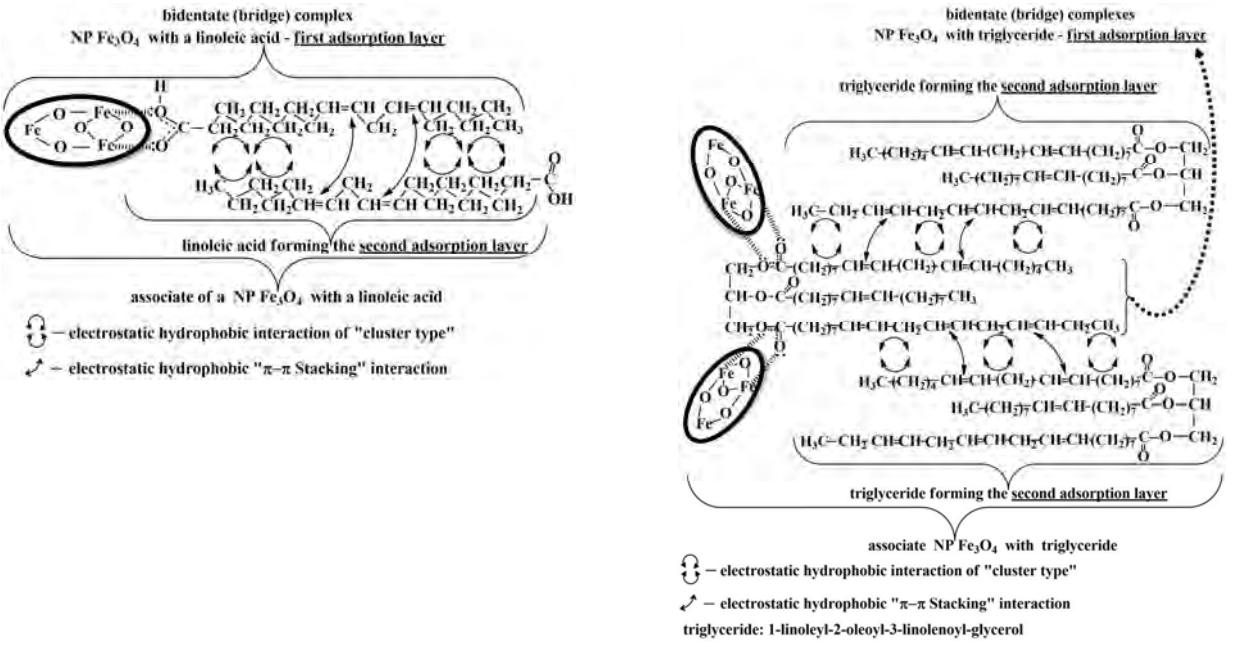

a) b)

Fig. 9. The formation of Fe_3O_4 nanoparticles lipid associate with linoleic acid (a) and 1-linoleyl-2-oleoyl-3-linolenoylglycerol (b)

The formation mechanism of the bidentate (bridge) complex Fe_3O_4 nanoparticles with linoleic acid and 1-linoleyl-2-oleoyl-3-linolenoylglycerol is shown in Fig. 8. In this model two Fe cations of Fe_3O_4 are bound with two oxygen atoms (carboxyl group of linoleic acid or ester group of 1-linoleyl-2-oleoyl-3-linolenoylglycerol) due to the complex interaction.

The first adsorption layer, which is formed as a result of electrostatic and coordination interactions (Figs. 2-8), is hydrophobic due to alkyl hydrophobic residues ("tails") of the fatty acids (in particular, linoleic acid) and triglycerides (in particular, 1-linoleyl-2-oleoyl-3-linolenoyl-glycerol).

Then, the second adsorption layer is formed owing to the electrostatic hydrophobic interaction. The hydrophobic matrix of the first adsorption layer enters into the electrostatic hydrophobic interaction with hydrophobic aliphatic "tails" of fatty acids and triglycerides.

The Fe_3O_4 NP-lipid associate is formed due to the hydrophobic interactions. The formation mechanism is represented in Fig. 9. Long molecules of the higher fatty acids and triglycerides give the possibility for multicentered dispersion interaction. As a result, the lipid alkyl matrix is structured according to Van der Waals complexes. The matrix forms the second adsorption layer and the associate of Fe_3O_4 NP with lipids.

3.2. Experimental Studies of the Lipid interaction with Fe_3O_4 Nanoparticles

3.2.1. IR- Fourier Spectroscopy (FTIR)

To establish the adsorption interaction mechanism of the lipid molecules (in particular, linoleic acid and sunflower oil) with Fe_3O_4 nanoparticles, the IR-spectroscopic studies of samples 1-5 were conducted in the range of 400–4000 cm^{-1}. To analyze the experimental data (Fig. 10) we compared the characteristic bands of samples 4 and 5 with the bands of the initial substances (samples 1-3).

The molecules of linoleic acid and sunflower oil on the solid surface of Fe_3O_4 nanoparticles are under its influence. As a result, new absorption bands appear in the spectra (Fig. 10) and some characteristic absorption bands shift to the region of lower frequencies. This means the chemisorption of lipids, namely, linoleic acid and sunflower oil triglycerides on Fe_3O_4 NP surface.The absorption band of Fe–O bond with the maximum at ~532 cm^{-1} is observed in the spectrum of pure Fe_3O_4 (sample 1, Fig. 10a), which is in a good agreement with literature data (lit. ~530 cm^{-1}) [16, 17, 20, 28, 29]. The shift of this band maximum to ~584 cm^{-1} (samples 4 and 5, Figs. 10d and 10e) can be explained by the introduction of linoleic acid and sunflower oil surface molecules in the near-surface layer of Fe_3O_4 nanoparticles and their chemical interaction with iron cations (Figs. 2-8).

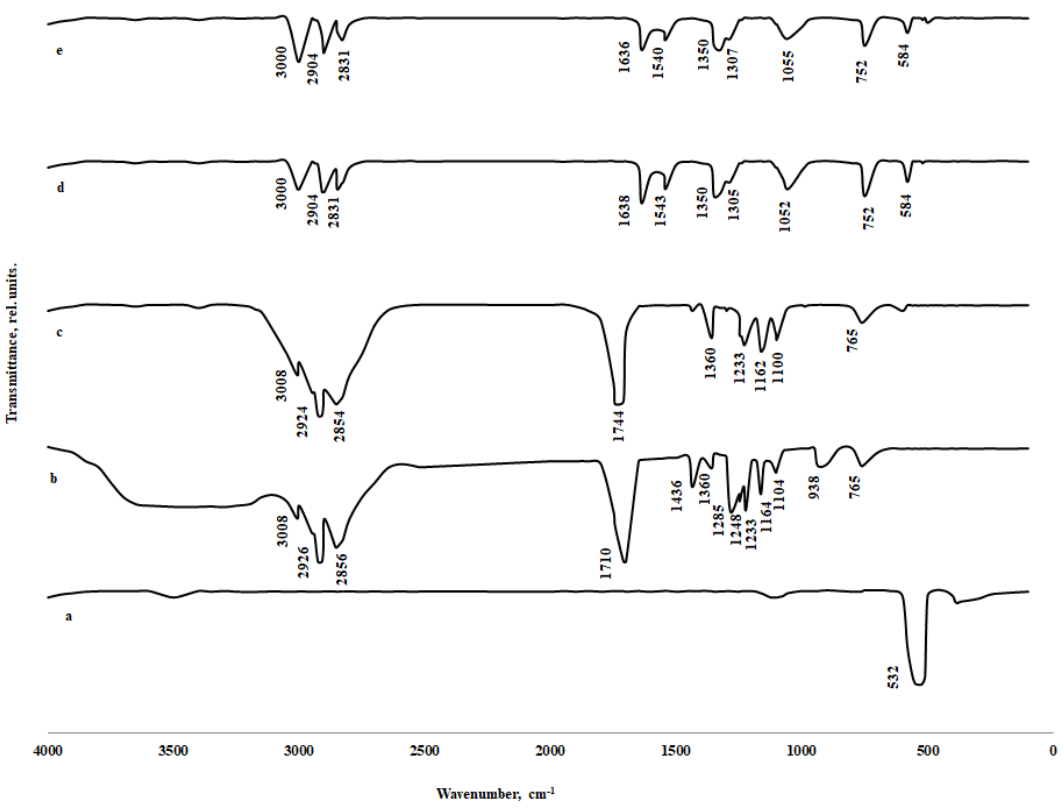

Fig. 10. FTIR spectra of the experimental samples: high-dispersive powder of Fe_3O_4 (a); linoleic acid (b); sunflower oil (c); Fe_3O_4 nanoparticles coated with linoleic acid (d)б and Fe_3O_4 nanoparticles coated with sunflower oil (e)

For lipid-Fe_3O_4 NP compositions the stretching vibration of C=O group have the greatest significance. The absorption band at 1710 cm^{-1} corresponds to an unexcited state of mentioned vibrations (Fig. 10b). For sunflower oil (Fig. 10c) we observe an intense peak of C=O vibrations in the area of 1744 cm^{-1} but this band disappears in the spectra of Fe_3O_4 nanoparticles coated with lipides (Fig. 10d, e). Moreover, the new bands appear at 1543 cm^{-1} (Fig. 10d), 1540 cm^{-1} (Fig. 10e), 1638 cm^{-1} (Fig. 10d), and 1636 cm^{-1} (Fig. 10e), which are typical of the stretching asymmetric (ν_{as}) and symmetric (ν_s) vibrations of the carboxylate group (COO^-). In other words, the lipids (carboxylic acids or triglycerides) are chemisorbed on the surface of Fe_3O_4 nanoparticles in carboxylate form (Figs. 7, 8, 10d, 10e) with the help of two oxygen atoms, which are symmetrically coordinated with the surface due to the electrostatic coordination interactions with Fe atoms. The result is the formation of chemically adsorbed lipid monomolecular layer (the first adsorption layer) on the NP surface (Figs. 2-8) [16, 17, 30, 31].

In the spectra of linoleic acid and sunflower oil, the intense bands with the maxima at 2926 and 2856 cm^{-1} (Fig. 10b); 2924 cm^{-1} and 2854 cm^{-1} (Fig. 10c) are observed. These peaks can be attributed to the asymmetric and symmetric vibrations of the C–H bond in CH_2 group. Also, there is a band of deformation vibrations (δ) of $–CH_3$ group at ~1360 cm^{-1}; for linoleic acid this band is very weak [28-32].

The shift of absorption bands toward a lower field is observed in Figs. 10d and 10e (ν_{as} = 2904 cm^{-1}; ν_s = 2831 cm^{-1} and δ = 1350 cm^{-1}, respectively). The reasons are: (i) the hydrocarbon chains of linoleic acid and sunflower oil triglycerides in the monolayer (the first adsorption layer) surrounding the nanoparticles are under the influence of the near-surface layer of Fe_3O_4 NP and chemical interaction with Fe cations; (ii) the hydrophobic interaction of hydrophobic centers of the first adsorption layer with the hydrocarbon chains of linoleic acid and sunflower oil triglycerides occurred due to the dispersion forces contributes to the formation of the second adsorption layer on the surface of Fe_3O_4 nanoparticles [31, 32].

The unsaturated hydrocarbon chains in the structure of linoleic acid and sunflower oil triglycerides are represented by the stretching vibrations of–CH=CH– group at ~3008 cm^{-1} and deformation vibrations of C–H bond at ~765 cm^{-1} (Fig. 10b, c). For the structured Fe_3O_4 nanoparticles (Fig. 10d, e), there is a shift of these absorption bands toward ν = 3000 cm^{-1} and δ = 752 cm^{-1}, respectively [28]. The reasons are: (i) the effect of Fe_3O_4 NP on the hydrocarbon chains of linoleic acid and

sunflower oil triglycerides in the formation of the first adsorption layer; (ii) the electrostatic interactions of the hydrophobic centers of the first adsorption layer with the alkyl matrix of triglycerides and the alkaline "tail" of the linoleic acid modeled on Van der Waals complexes. This contributes to the structuring of the "hydrophobic matrix" of the lipid-Fe_3O_4 NP complex and the formation of the second adsorption layer on the surface of Fe_3O_4 nanoparticles on which lipids (linoleic acid or sunflower oil) have already been adsorbed in the first adsorption layer [31, 32].

Three absorption bands corresponding to C□O group are observed in each of linoleic acid and sunflower oil spectra: the intense band at 1164 and 1162 cm^{-1} (Figs. 10b and 10c, respectively) and two less intensive bands at 1236 and 1233 cm^{-1} (Figs. 10b and 10c, respectively); 1104 and 1100 cm^{-1} (Figs. 10b and 10c, respectively). A doublet with the first peak at 1285 cm^{-1} and the second one at 1248 cm^{-1} is visible in the spectrum of linoleic acid (Fig. 10b). The first peak appears due to the combination of plane deformation ($\delta_{pd.}$) vibrations of O–H and C–O bonds. The second peak refers to the symmetric stretching vibrations of C–O bond. The asymmetric stretching vibrations typical of C–O bond of the linoleic acid carboxyl group appear on the doublet as the peak at 1436 cm^{-1} [30-32].

The mentioned bands are absent in the spectra of Fe_3O_4 NP coated with lipids (Fig. 10d, e). At the same time, there are two new ones: at 1052 and 1305 cm^{-1} (Fig. 10d); 1055 and 1307 cm^{-1} (Fig. 10e), which are typical of plane deformation and stretching vibrations of C–O which interacts with polarized Fe_3O_4 nanoparticles (Figs. 4-6) [16, 17, 30-32].

The presence of the broad absorption band of average intensity in the spectrum of linoleic acid (Fig. 10b) in the range of 3200–3600 cm^{-1} is associated with the characteristic vibrations of the surface OH^- groups. Out-of-plane deformation vibrations of O–H bond of the linoleic acid carboxyl group are observed at 938 cm^{-1} but this band disappeared in the spectra of samples 3-5 (Fig. 10c, d, e). It is the confirmation of free hydroxyl groups absence on the surface of the lipid-Fe_3O_4 NP complex, as well as chemisorption of oleic acid and sunflower oil triglycerides on the surface of Fe_3O_4 nanoparticles (Figs. 2-8).

The results of IR spectroscopy and previous studies [16, 17, 30-32] confirm the formation mechanism of the first lipid adsorption layer on Fe_3O_4 nanparticles represented by four types: monodentate, bidentate (bridge), bidentate (chelate), and ionic interaction (Figs. 2-8) [16, 17, 20].

The difference in the wavenumber values ($\Delta\nu_o$) between the asymmetric and symmetric stretching vibrations of the carboxylate group (Fig. 10d, e) can be used to identify the type of interaction between COO^- group of lipid and Fe atom of Fe_3O_4 nanoparticles. The largest value $\Delta\nu_o$ = (200–320) cm^{-1} corresponds to the monodentate interaction, and the smallest one $\Delta\nu_o$ < 110 cm^{-1} – to bidentate (chelate). The value of 140–190 cm^{-1} is characteristic of the bidentate (bridge) interaction. In this work, the $\Delta\nu_o$ value of ~100 cm^{-1} (1638 – 1543 = 95 cm^{-1} for the sample d and 1636 – 1540 = = 96 cm^{-1} for the sample (e)) indicates the bidentate structure, where two oxygen atoms of the lipid carboxyl group is coordinately bound with Fe atoms of Fe_3O_4 nanoparticles (Figs. 7, 8).

Thus, *the formation scheme of the first adsorption layer* on the nanoparticles surface is the chemisorption of lipid molecules on the Fe_3O_4 NP surface due to the electrostatic interactions of lipid polarized groups with the ionized particles and the coordination bonds of Fe atoms with oxygen of COO^- group. Moreover, the first adsorption layer is a combination of the symmetrically bound lipid molecules at an angle to the particles surface. Free hydrocarbon chains of sunflower oil and linoleic acid triglycerides bound with NP are perpendicular to the particles surface. These chains are superhydrophobic and they are a matrix for electrostatic hydrophobic interaction with hydrophobic "tails" of lipids.

The formation scheme of the second adsorption layer on the surface of Fe_3O_4 nanoparticles is the electrostatic interaction (due to dispersion forces) of the hydrophobic centers of the first adsorption layer with hydrophobic hydrocarbon "tails" of lipids (linoleic acid or sunflower oil triglycerides).

Thus, the mechanism of fat holding and fat binding capacity of Fe_3O_4 NP is the chemisorption of fats on the particles surface and can be represented by the two-layer coordination model.

3.2.2. X-ray diffraction analysis (XRD)

The crystal phases of Fe_3O_4 nanoparticles (sample 1) and nanoparticles coated with linoleic acid and sunflower oil (samples 4 and 5) were examined by X-ray diffraction analysis (Fig. 11).

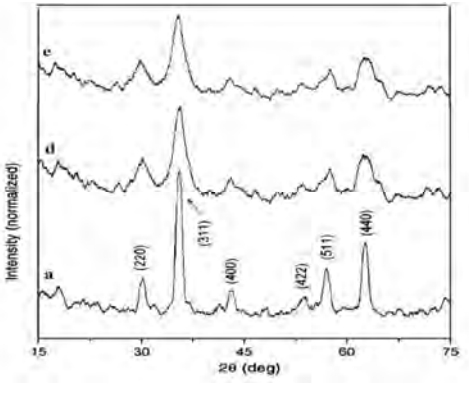

Fig. 11. X-ray diagrams of high-dispersive powder of Fe_3O_4 (a); Fe_3O_4 nanoparticles coated with linoleic acid (d) and Fe_3O_4 nanoparticles coated with sunflower oil (e)

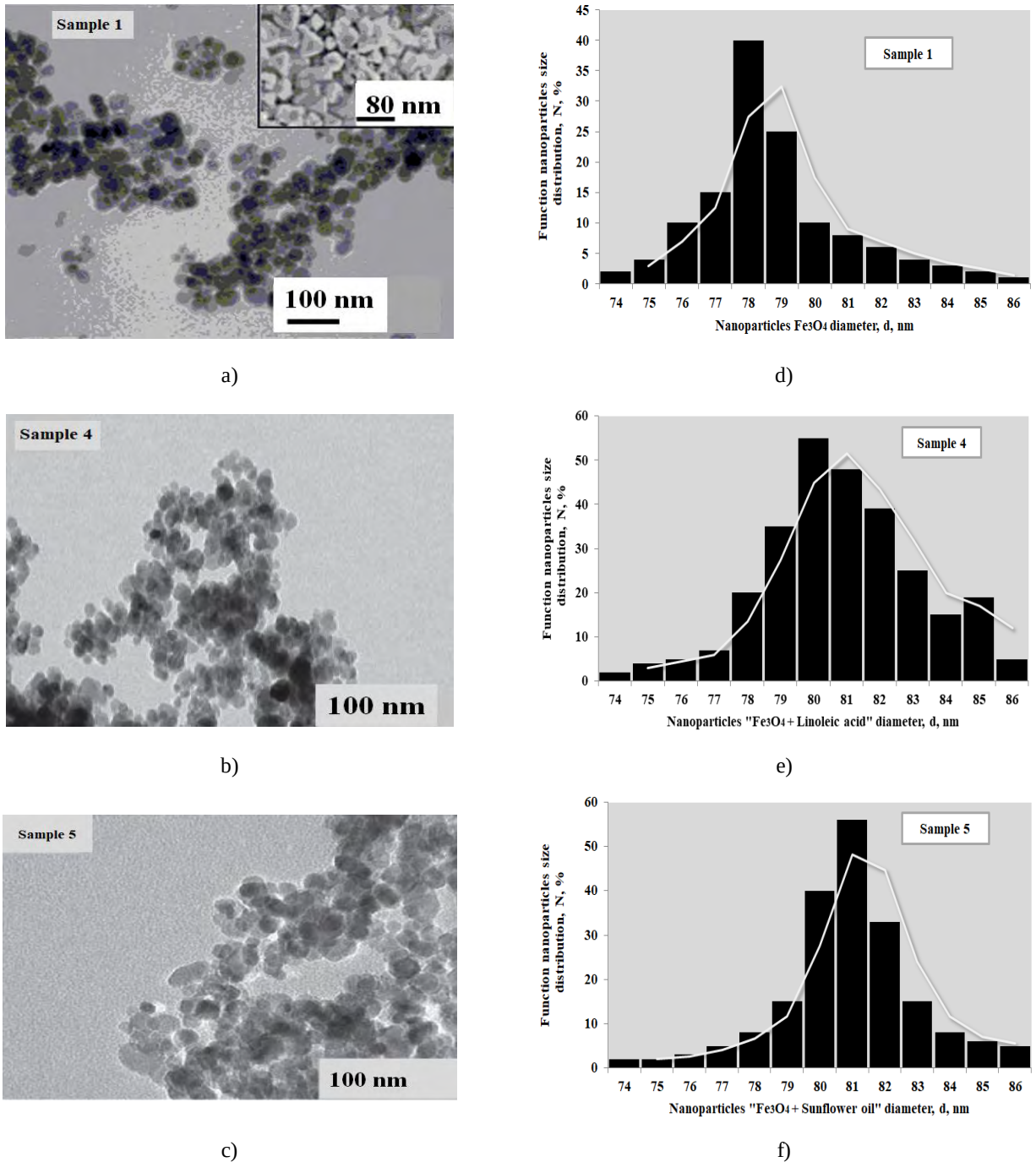

Fig. 12. TEM images (a, b, c) and nanoparticles size distribution (d, e, f) of Fe_3O_4 high-dispersive powder (a, d); Fe_3O_4 nanoparticles coated with linoleic acid (b, e) and Fe_3O_4 nanoparticles coated with sunflower oil (c, f)

The main bands of sample 1 (Fig. 11a) at $2\theta = 9.6°$; 30.42°; 35.59°; 43.42°; 54.58°; 57.60°, and 63.60° correspond to the diffraction of 220°; 311°; 400°; 422°; 511°, and 440°. They are typical of magnetite with a spinel structure and crystal lattice parameters of 0.83716(4) nm, while for an ordered and stoichiometric magnetite the suitable parameter is 0.83952(2) nm [26, 27, 33, 34]. The sharp peaks also suggest a good crystalline structure of Fe_3O_4 nanoparticles. Generally, sample 1 can be attributed to a highly dispersed spinel system.

There is also a widening of the bands in Fig. 11a, indicating a small size (nanosize) of particles and a slight tension of the crystalline structure. This affects the physico-chemical properties of Fe_3O_4 NP, in particular, by increasing their surface activity and reactivity, *e.g.*, the ability to interact with lipids of the food systems, namely, the higher fatty acids and triglycerides of fats. The established effect is associated with a small deficit of Fe^{3+} and Fe^{2+} cations both in tetrahedral and octahedral positions, which can be approximately evaluated as 5 %. But in general, this effect can be quite important and valuable for the modification of biopolymer matrices and stabilization of lipid-Fe_3O_4 systems.

Similar diffraction peaks are observed in the spectra of sample 4 (Fig. 11d) and sample 5 (Fig. 11e), *i.e.* the structure of cubic spinel remains unchanged for Fe_3O_4 coated with lipids. However, there is a widening of the diffraction peaks and a decrease in the signals intensity. These facts provide chemisorption of lipids on the NP surface and the effect of the surface molecules of linoleic acid and sunflower oil triglycerides due to their introduction in the near-surface layer of Fe_3O_4 nanoparticles and chemical interaction with Fe cations.

3.2.3. Morphological analysis of the experimental samples. Transmission electron microscopy (TEM)

The size of the particles and the morphology of the experimental samples 1, 4 and 5 (Fig. 12) were studied using a transmission electron microscopy (TEM).

It is evident that all particles in experimental samples are nanosized, spherical in shape and have a uniform size distribution. Based on the obtained results, the particle distribution was calculated relative to the diameter. To determine the average values the particles number in the sample was at least 500. The established distribution function is rather narrow and symmetric, which validates the investigated systems as homogeneous ones with a low degree of polydispersity. The determined average sizes are: for sample 1 <d> ~78 ± 2.36 nm; for sample 4 <d> ~80 ± 2.57 nm; for sample 5 <d> ~81 ± 2.93 nm.The increase in the size of Fe_3O_4 particles of samples 4 and 5 compared with pure Fe_3O_4 (sample 1) is caused by adsorption of linoleic acid and sunflower oil on Fe_3O_4 NP surface and additionally confirms the proposed two-layer coordination model, the essence of which is the formation of two monomolecular layers on Fe_3O_4 NP surface. The total thickness ($2d$) is equal to two diameters of lipid molecules, *i.e.* for sample 4 $2d$ = 2.2–2.5 nm; for sample 5 $2d$ = 2.8–3.2 nm.

3.2.4. Elemental analysis of the experimental samples. Energy dispersive X-ray spectroscopy (EDX)

To confirm the chemisorption of lipids (linoleic acid and sunflower oil triglycerides) on particles surface the energy dispersive X-ray spectroscopy (EDX) was used. Using the EDX-spectra the elemental composition of the complex lipid-Fe_3O_4 NP was determined (Fig. 13).

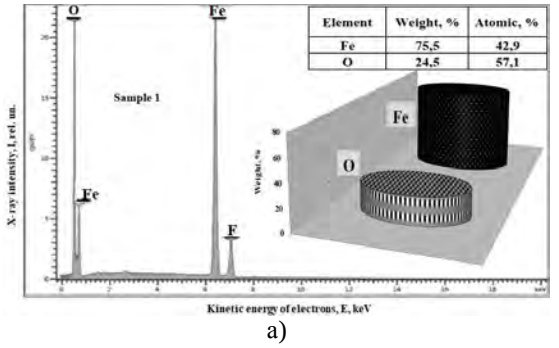

a)

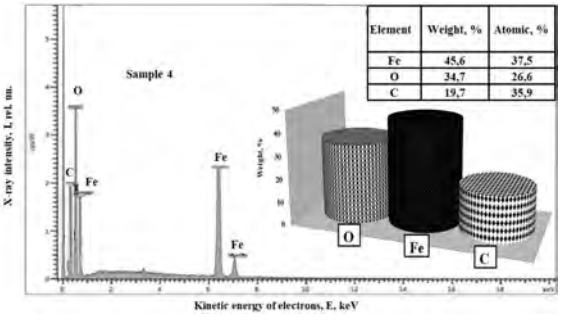

b)

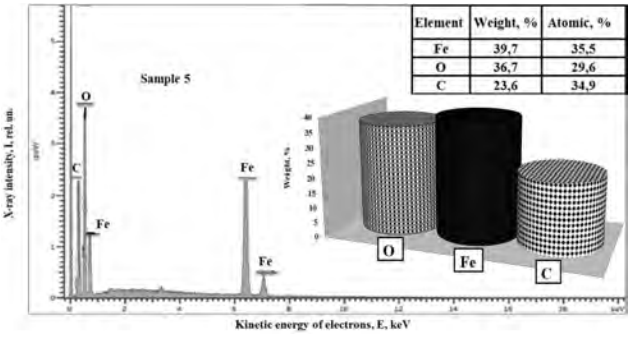

c)

Fig. 13. EDX spectra and the percentage of Fe, O, C of Fe_3O_4 high-dispersive powder (a); Fe_3O_4 nanoparticles coated with linoleic acid (b) and Fe_3O_4 nanoparticles coated with sunflower oil (c)

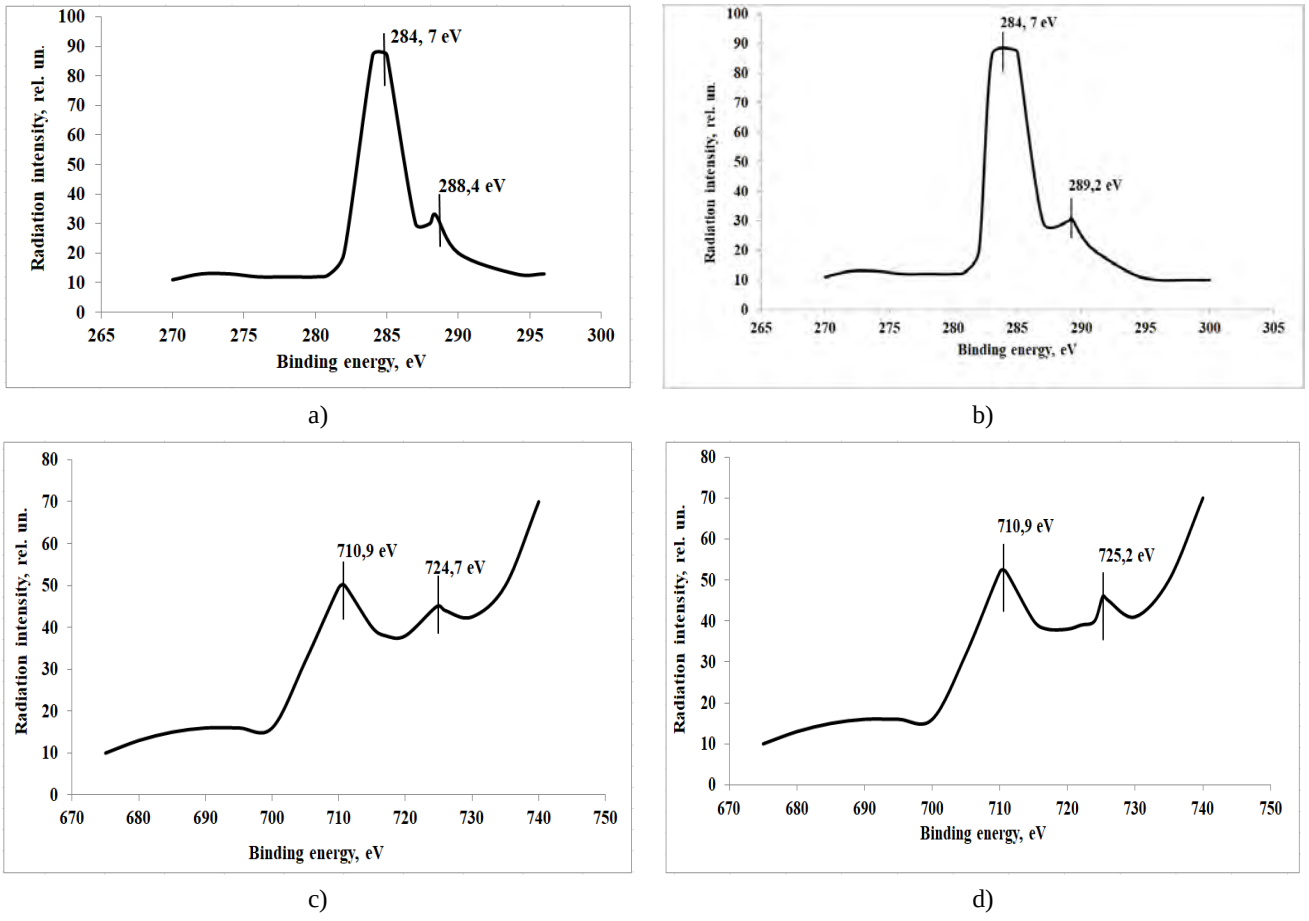

Fig. 14. XPS images of C 1s and Fe 2p internal electronic levels: C 1s level of Fe_3O_4 nanoparticles coated with linoleic acid (a); C 1s level of Fe_3O_4 nanoparticles coated with sunflower oil (b); Fe 2p level of Fe_3O_4 nanoparticles coated with linoleic acid (c) and Fe 2p level of Fe_3O_4 nanoparticles coated with sunflower oil (d)

In the spectra (Fig. 14a, b), there is no absorption band C 1s at 290 eV corresponding to carbon of carboxylic group (–COOH) [20]. This indicates the absence of free carboxylic acid or ester group of triglyceride on Fe_3O_4 nanoparticles coated with lipids. The peak at 284.7 eV (Fig. 14a, b) is attributed to the carbon atoms in the aliphatic chain (C–C); and the peaks at 288.4 eV (Fig. 14a) and 289.2 eV (Fig. 14b) are related to carboxylate (–COO–), which is in agreement with the received data from the literature [20, 35, 36].

The characteristic peak of oxides and iron hydroxides at 710.9 eV is not observed in the spectra (Fig. 14c, d). The peak characterizes the binding energy at basic level Fe $2p_{3/2}$ [20]. However, for samples 4 and 5 we observe the appearance of absorption band in the area of higher binding energies: 724.7 eV (Fig. 14c) and 725.2 eV (Fig. 14d). This absorption band is related to Fe carboxylate [20, 35, 36].

The obtained data give one more confirmation of the chemical structure of the experimental samples and indicate the formation of the chemical bonds between Fe atoms of Fe_3O_4 NP and oxygen atoms of lipids.

3.2.6. Thermogravimetric analysis (TGA)

The character of possible high-temperature transformations in samples 4 and 5 was investigated by using the thermogravimetric analysis [18, 20, 37, 38]. The results are represented in Fig. 15 in the form of thermogravimetric (TG) and the differential-thermogravimetric (DTG) curves.

Within the temperature range of 273–1173 K there are five temperature transformations:

– the first peak at 503 K (sample 4) and 500 K (sample 5) is accompanied by weight loss of 19.9 and 19.7 wt %, respectively. This peak is observed at the temperatures equal to the boiling points of linoleic acid (T_b = 503 K) and sunflower oil (T_b = 500 K). The weight loss is associated with the removal of free lipids (linoleic acid and sunflower oil) from the surface of Fe_3O_4 nanoparticles;

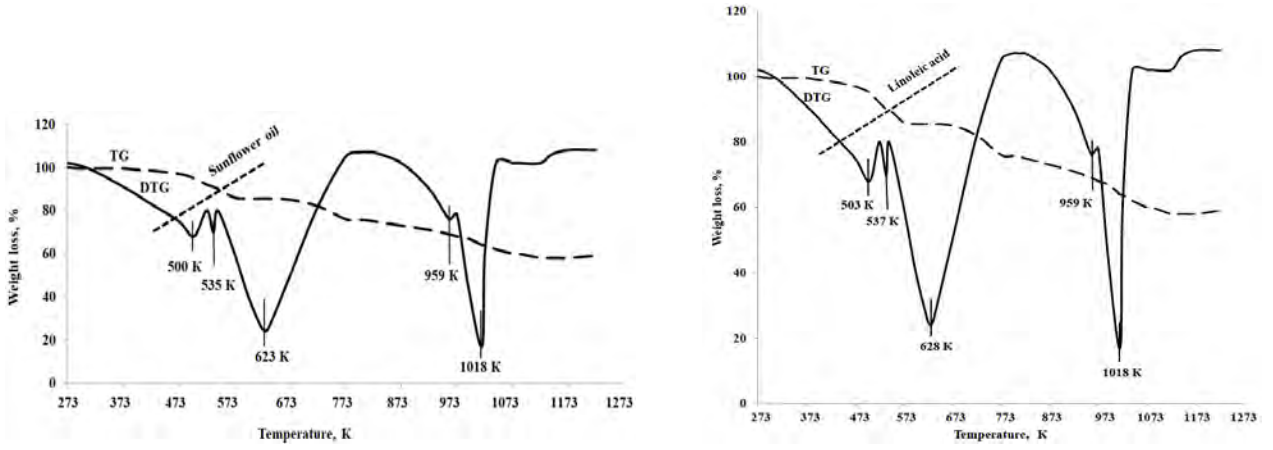

a) b)

Fig. 15. Derivatograms of Fe_3O_4 nanoparticles coated with linoleic acid (a) and Fe_3O_4 nanoparticles coated with sunflower oil (b)

– the second peak at 537 K (sample 4) and 535 K (sample 5) with weight loss of 12.2 and 12.0 wt %, respectively, may be associated with the desorption of the second adsorption layer formed due to the electrostatic interactions of the hydrophobic centers of the first adsorption layer and the hydrocarbon "tails" of the higher fatty acids (in particular, linoleic) and triglycerides of free fat (in particular, sunflower oil). This fact coincides with the models of two-layer modification of nanoparticles by the various chemical reagents [19, 20, 40-42];

– the third peak at 628 K (sample 4) and 623 K (sample 5) is accompanied by weight loss of 22.3 and 21.6 wt %, respectively. The mass loss is connected with the desorption of the first adsorption layer, which is formed due to the stronger (compared with the hydrophobic interaction in the second layer) electrostatic interactions of lipid polarized groups with ionized Fe_3O_4 NP and the coordination bonds of Fe atoms of Fe_3O_4 nanoparticles with oxygen of COO^- group of "hydrophilic heads" of fat (in particular, sunflower oil triglycerides) and the higher fatty acids (in particular, linoleic acid). This is in agreement with literature data [19, 20, 40-42] and additionally confirms the proposed two-layer coordination model;

– the fourth peak at 959 K (samples 4, 5) is accompanied by the insignificant weight loss of 2.6 wt % related to the phase conversion of double Fe(II) and Fe(III) oxide (Fe_3O_4) into metastable Fe(III) oxide γ-Fe_3O_4 with the cubic structure. Further heating provides the transformation of γ–modification into diamagnetic rhombohedral structure (hematite). This is in good agreement with literature data [41, 42];

– the fifth peak at 1015 K (samples 4, 5) is associated with weight loss of 14 wt %, due to the possible deoxidation of FeO of Fe_3O_4 NP.

Thus, the TGA method, along with other investigation methods regarding the mechanism of lipids chemisorption on the surface of Fe_3O_4 nanoparticles, confirms the proposed two-layer coordination model.

4. Conclusions

The interaction mechanism of Fe_3O_4 nanoparticles with linoleic acid and 1-linoleyl-2-oleoyl-3-linolenoyl-glycerol has been grounded. The mechanism is presented by the two-layer coordination model. The first adsorption layer is formed on the nanoparticle surface due to the electrostatic interactions of polarized lipid groups with ionized Fe_3O_4 particles and the coordination bonds of Fe atoms of Fe_3O_4 nanoparticles with the carbonyl and hydroxyl oxygen atoms of the carboxyl groups of free fatty acids, as well as with oxygen atoms of ester groups of triglycerides. The second adsorption layer occurs due to the electrostatic hydrophobic interactions of the hydrophobic centers of the first monolayer and the aliphatic side chains of the acyl residues of triglycerides and the alkyl components of the free fatty acids.

Different methods of analysis (FTIR, XRD, TEM, EDX, XPS, TGA) regarding the mechanism of lipids chemisorption on the surface of Fe_3O_4 nanoparticles, confirmed the proposed two-layer coordination model.

The obtained results will allow to simulate the processes of fat holding and fat binding capacity in various technological and food systems, as well as to improve the functional and technological characteristics of fat-containing compositions and the quality of finished products.

Further investigations concerning chemisorption of the higher fatty acids, fats, and oils of various origin and chemical composition on the surface of Fe_3O_4 nanoparticles are of great interest.

References

[1] Rogov I., Tokaev Eh., Kovalev Yu.: Ispolzovanie Syria s Vysokim Soderzhaniem Pishchevykh Volokon v Tekhnologii Dieticheskikh Miasnykh Produktov. Agroniitehimmp, Moskva 1988.
[2] Citrusovye volokna Herbacel AQ Plus – tip N: Specifikacii dlya pishchevyh dobavok i receptury, 2013. http://specin.ru/kletchatka/109.htm
[3] Pavlovich-Abril A., Rouzaud-Sández O., Romer-Baranzini A. L. *et al.*: J. Food Quality, 2015, **38,** 30. https://doi.org/10.1111/jfq.12103
[4] Varastegani B., Zzaman W., Yang T.: J. Food Quality, 2015, **38**, 175. https://doi.org/10.1111/jfq.12129
[5] Http://www.pischevie-volokna.ru
[6] Rodríguez R., Jiménez A., Fernández-Bolaños J. *et al.*: Trends Food Sci. Tech., 2006, **17**, 3. https://doi.org/10.1016/j.tifs.2005.10.002
[7] Chang T., Wang S., Wang C., Shi L. *et al.*: J. Food Quality, 2014, **37**, 339. https://doi.org/10.1111/jfq.12096
[8] https://www.ingredientsnetwork.com/Herbacel_AQ_Plus_Citrus_manu_vegan_Cleanlabel_emulsions-file072775.pdf
[9] Beriain M., Gómez I., Ibáñez F. *et al.*: Improvement of the Functional and Healthy Properties of Meat Products [in:] Holban A.-M., Grumezescu A.-M. (Eds.), Food Quality: Balancing Health and Disease. Academic Press, NY 2018, 1-74. https://doi.org/10.1016/B978-0-12-811442-1.00001-8
[10] Domoroshchenkova M., Demyanenko L., Kamysheva T.: Maslozhyrovaya Prom., 2007, **4**, 24.
[11] Lai W., Khong N., Lim S. *et al.*: Trends Food Sci. Tech.., 2017, **59**, 148. https://doi.org/10.1016/j.tifs.2016.11.014
[12] Heymans R., Tavernier I., Dewettinck K., Van der Meeren P.: Trends Food Sci. Tech., 2017, **69A**, 13. https://doi.org/10.1016/j.tifs.2017.08.015
[13] Paglarini C., Furtado G., Biachi J. *et al.*: J. Food Eng., 2018, **222**, 29. https://doi.org/10.1016/j.jfoodeng.2017.10.026
[14] Ramachandraiah K., M.-J. Choi, G.-P. Hong: Trends Food Sci. Tech., 2018, **71**, 25. https://doi.org/10.1016/j.tifs.2017.10.017
[15] Ilyuha N., Barsova V., Kovalenko V., Tsyhanovska I.: Vost. Evr. Zh. PeredovyhTekhnol., 2010, **6**, 32.
[16] Tsykhanovska I., Alexandrov A., Evlash V. *et al.*: East. Eur. J. Adv. Technol., 2018, **2**, 70. https://doi.org/10.15587/1729-4061.2018.126358
[17] Tsykhanovska I., Alexandrov A., Evlash V. *et al.*: East. Eur. J. Adv. Technol., 2018, **4**, 61. https://doi.org/10.15587/1729-4061.2018.140048
[18] Drmota A., Kosak A., Znidarsik A.: Mater. Technol., 2008, **42**, 79.
[19] Mahdavi M., Ahmad M., Haron M. *et al.*: Molecules, 2013, **18**, 7533. https://doi.org/10.3390/molecules18077533
[20] Zhang L., He R., Gu H.-C.: Appl. Surf. Sci., 2006, **253**, 2611. https://doi.org/10.1016/j.apsusc.2006.05.023
[21] Chernyshova I., Ponnurangam S., Somasundaran P.: Langmuir, 2011, **27**, 10007. https://doi.org/10.1021/la2017374
[22] Alexandrov A., Tsykhanovska I., Evlash V. *et al.*: East. Eur. J. Adv. Technol., 2017, **5**, 61. https://doi.org/10.15587/1729-4061.2017.111522
[23] Tsykhanovska I., Skurikhina L., Evlash V. *et al.*: Ukr. Food J., 2018, **7**, 379. https://doi.org/10.24263/2304-974X-2018-7-3-4
[24] Tsykhanovska I., Alexandrov A., Evlash V. *et al.*: Eureka: Life Sci., 2018, **4**, 63. https://doi.org/10.21303/2504-5695.2017.00511
[25] Tsykhanovska I., Alexandrov A., Evlash V. *et al.*: Eureka: Life Sci., 2018, **2**, 67. https://doi.org/10.21303/2504-5695.2018.00611
[26] Russ J.: Fundamentals of Energy Dispersive X-Ray Analysis. Butterworth-Heinemann 1984.
[27] ICCD: The International Centre For Diffraction Data. http://www.icdd.com/
[28] Wang L.: Advances in nanocomposites, 2008, 34, 289.
[29] Hajdu A., Illes E., Tombacz E., Borbath I.: Colloid. Surf., 2009, **347**, 104. https://doi.org/10.1016/j.colsurfa.2008.12.039
[30] Shen Y., Tang J., Nie Z. *et al.*: Sep. Purif. Technol., 2009, **68**, 312. https://doi.org/10.1016/j.seppur.2009.05.020
[31] Skopenko V., Civadze A., Savranskij L., Garnovskij A.: Koordinacionnaya Khimia. Akademkniga, Moskva 2007.
[32] Steed J., Atwood J.: Supramolecular Chemistry. John Wiley & Sons, Ltd., Chichester 2009.
[33] Andrade F. R. D. *et al.*: Geol. USP, Sér. cient., 2016, **16**, 19. https://doi.org/10.11606/issn.2316-9095.v16i2p19-24
[34] Kazeminezhad I., Mosivand S.: Acta Phys. Polonica A., 2014, **125**, 1210. https://doi.org/10.12693/APhysPolA.125.1210
[35] Yamashita T., Hayes P.: Appl. Surf. Sci., 2008, **254**, 2441. https://doi.org/10.1016/j.apsusc.2007.09.063
[36] Poulin S., França R., Moreau-Bélanger L.: J. Phys. Chem. C, 2010, **114**, 10711. https://doi.org/10.1021/jp100964x
[37] Levitin E., Vedernikova I., Onoprienko T., Tsykhanovska I.: Farmakom, 2007, **1**, 61.
[38] Sahoo Y., Pizem H., Fried T. *et al.*: Langmuir, 2001, **17**, 7907. https://doi.org/10.1021/la010703+
[39] Shen L., Laibinis P., Hatton T., Langmuir, 1999, **15**, 447. https://doi.org/10.1021/la9807661
[40] Yee C., Kataby G., Ulman A. *et al.*: Langmuir, 1999, **15**, 7111. https://doi.org/10.1021/la990663y
[41] Bozort R: Ferromagnetism. Izd-vo standartov, Moskva 1986.
[42] Goss C.: Phys. Chem. Minerals, 1988, **16**, 164. https://doi.org/10.1007/BF00203200

Received: November 08, 2018 / Revised: January 22, 2019 / Accepted: April 23, 2019

ДОСЛІДЖЕННЯ МЕХАНІЗМУ ВЗАЄМОДІЇ ЛІНОЛЕВОЇ КИСЛОТИ ТА 1-ЛІНОЛЕЇЛ-2-ОЛЕОЇЛ-3-ЛІНОЛЕНОЇЛГЛІЦЕРИНУ З НАНОЧАСТИНКАМИ Fe_3O_4

Анотація. *Обгрунтовано механізм взаємодії наночастинок Fe_3O_4 з лінолевої кислотою та з 1-лінолеїл-2-олеоїл-3-ліноленоїлгліцерином, який представлений моделлю «двошарової координації». Методами ІЧ-Фур'є спектроскопії, трансмісійної електронної мікроскопії, енергодисперсійної рентгенівської спектроскопії, рентгенівської фотоелектронної спектроскопії, рентгенофазового і термогравіметричного аналізу вивчений механізм взаємодії лінолевої кислоти і соняшникової олії з наночастинками Fe_3O_4.*

Ключові слова: *наночастинки Fe_3O_4, лінолева кислота, 1-лінолеїл-2-олеоїл-3-ліноленоїлгліцерин, соняшникова олія, хемосорбція.*

Chem. Chem. Technol., 2019,
Vol. 13, No. 3, pp. 317–325

Chemistry

LOW-PRESSURE DISCHARGE PLASMA TREATMENT OF AQUEOUS SOLUTIONS WITH Mn, Cr AND Fe

Oleksandr Pivovarov[1], Tetiana Derkach[2, *], Margarita Skiba[1]

https://doi.org/10.23939/chcht13.03.317

Abstract. The effect of low-pressure glow discharge on the formation of peroxide and the degree of oxidation of Mn, Cr and Fe was studied in the aqueous solutions of different compounds. The plasma treatment causes the reduction of Mn(VII) through Mn(IV) to Mn(II), Cr(VI) to Cr(III) and oxidation of Fe(II) to Fe(III). Among other reactive species, peroxide formed under the action of plasma treatment takes an active part in redox reactions. The concentration of peroxide usually increases with treatment time, but its presence is detected only after completion of active redox processes.

Keywords: low-pressure glow discharge plasma treatment, redox reactions, peroxide formation, reduction, oxidation.

1. Introduction

The application of plasma discharge to treat liquid solutions is characterised by high diversity. In particular, in mining and metallurgy, plasma technologies are used for material processing [1], intensification of leaching of noble metals from ore concentrates [2], obtaining fullerenes and nanopowders [3], *etc*. In analytical chemistry, plasma discharges are utilised in the course of sample preparation, as microsized sources of emission for analysis of water solutions, as ionisation sources for mass spectrometry, as well as for enhancement of an analytical signal [4-6]. In the chemical industry, there are known examples of modification of polymer surfaces, cellulose bleaching and chemical synthesis. Plasma-aided blood coagulation, tissue ablation, wound healing and sterilisation are among typical medical applications of the plasma discharge [7].

Environmental remediation and wastewater treatment are reckoned among the most critical applications of plasma technologies [8]. The wastewater releasing from industrial plants or households often contains harmful elements and compounds, in many cases of organic origin. So, it is vital to remove them from the Earth biosphere.

Various methods of water treatment, such as physical, biological and chemical, have been developed during centuries. Physical and biological processes are usually low cost but, in some cases, they do not efficiently remove some kinds of pollutants, especially organic compounds. Also, the biological treatment is typically much slower than other processes. Chemical methods are based on direct oxidation *via* reactants with high oxidation potential such as chlorine, ozone, potassium permanganate, *etc*. However, the use of such reagents is limited due to the formation of potentially hazardous by-products (for example halogenated in case of chlorine treatment). The ozonation is very efficient but the most expensive method of water treatment.

Plasma treatment realised in various forms of plasma discharge is a very effective attractive alternative to the methods of solution treatment mentioned above. Plasma discharge was successfully used to treat wastewaters contaminated with herbicides/pesticides, decompose pharmaceuticals, surfactants, sulfonol, phenol and textile dyes [9-12]. Many of the researches have focused on the decomposition of organic compounds which are key contaminants in source water. Another critical application is to remove ions of heavy metals contained in wastewaters [13].

The discharge releases high energy into a liquid phase and generates highly reactive species. Plasma in liquids can be produced in devices with different electrode configurations (a corona discharge over the surface solution, a contact glow discharge, a pulsed streamer discharge in or above solution, dielectric barrier discharge, gliding arc) and voltage regimes (DC pulsed, DC non-pulsed, AC, HF, *etc*.) [14]. A diversity of configurations promotes a variety of applications.

The plasma discharge causes various physical and chemical effects in the treated medium. Among physical phenomena, diffusion and advection, local heating, surface tension, secondary emission and charge deposition, sputtering and evaporation can be listed as

[1] Department of Inorganic Substances and Ecology, Ukrainian State University of Chemical Technology,
8, Gagarina Ave., 49005 Dnipro, Ukraine
[2] Department of Industrial Pharmacy, Kyiv National University of Technologies and Design,
2, Nemirovicha-Danchenko St., 01011 Kyiv, Ukraine
[*] *derkach.tm@knutd.edu.ua*

typical for plasma discharges in solutions. Processes of surface electrolysis, hydrolysis, charge transfer, electron-ion and ion-ion recombinations, reduction-oxidation (redox) reactions, and collision relaxation take simultaneously place in gas-plasma and liquid regions, as well as the gas-liquid interface, that determines the complexity of chemical effects.

As was classified in [15], three different species of particles take part in the processes of plasma treatment. The gaseous parent species are determined by the ambient gas. For a plasma reactor operated in air, for example, these species are molecules of O_2, N_2, and H_2O. The primary species are being directly formed in the burning discharge. They include various highly reactive particles, such as radicals, high energetic electrons, excited ions, molecules, and photons. Further, the secondary species result from reactions which are not directly formed in the discharge but involve either primary species or primary and parent species. The primary species quickly appear but are not stable. The secondary species result from chemical reactions and, at least, some of them are more stable and thus are of interest for practical applications.

The chemical effects induced by the discharge and concerning the solutes depend on the formed species. Essential reactive species are hydroxyl radicals which are characterised by a high oxidation potential. Other strong oxidation reagents produced by plasma are oxygen radicals, ozone and hydrogen peroxide. A synergic effect of more oxidation reagents is possible as was discussed in [16] where simultaneous reduction of Cr(VI) and oxidation of As(III) were observed in wastewaters under plasma treatment.

The formation of peroxide in water and aqueous solution has been observed in many works [17-19]. There is a consensus that peroxide results from various reactions between chemically reactive particles produced by a plasma discharge and thus is a secondary species of plasma treatment. However, observations of its behaviour are less definite. In some cases, the peroxide concentration is a linear function of plasma treatment time. Sometimes, a clear time-delay is observed in the peroxide emergence. In other cases, the peroxide concentration remains depressive over the observation time.

It is well known that peroxide can participate in redox reactions and affect the oxidation state of metallic elements in various compounds. Therefore, it is of practical interest to study the rates of peroxide formation and consumption in the course of redox reactions in different aqueous solutions. The paper goal is to research the concentrations of peroxide and ions that contain metals (Fe, Cr and Mn) as a function of plasma treatment time in correlations with different pH and to reveal any relationships between peroxide and oxidation level of metallic elements.

2. Experimental

A barrel-type glass reactor with inside diameter of 30 mm and 180 mm in height was used for plasma treatment. Stainless steel electrodes were made of the wire rod of 4 mm in diameter. The plasma discharge used is reckoned in a low-pressure glow discharge type. One of the electrodes (cathode), being immersed in the studied solution, was placed in the lower part of the reactor. Another electrode (anode) was set at an adjustable distance of 5–7 mm above the solution surface. Air pressure in the reactor was held constant by a vacuum pump at a level of 12–15 kPa. The discharge was generated by applying a DC high voltage (~500–700 V) between the metal anode and water solution. The discharge current varied between 10 and 100 mA. Optimal values of the discharge current and air pressure were determined and applied to each treated solution.

The volume of the solution in the reactor was 50 ml. The time of plasma treatment varied from 0.1 to 30 min. Continuous circulation of cold water was maintained in an outer jacket to cool down the reaction mixture. The initial temperature of the solution was 293 K; it elevated to 303–308 K in the course of plasma treatment. Evaporation of the solution was observed during the discharge process. However, the lowering in solution level was negligible at the time of the experiment. The compositions of as-treated solutions, as well as crucial treatment regimes, are shown in Table 1.

The method of flame atomic absorption spectroscopy (FAAS) was used to measure the total content of metals (Cr, Fe or Mn) in filtered solutions. The quantification of FAAS was performed with the use of certified reference materials produced by O. V. Bogatsky Physics and Chemistry Institute (Odessa, Ukraine). The concentration of Mn^{2+} ions in solutions was measured by the Volhard method.

The solute concentrations of Fe(III), Cr(VI) and Mn(VII) were determined by spectrophotometry. Chemical methods controlled the Mn(IV) level. The completeness of Mn(VII)-to-Mn(II), Cr(VI)-to-Cr(III) and Fe(II)-to-Fe(III) transformations was estimated by a combination of FAAS and spectrophotometry.

The total content of oxidisers, including peroxide, was measured in the plasma-treated solutions by an iodometric titration method. Also, the content of hydrogen peroxide was separately determined by either permanganatometry or spectrophotometry using the reaction of H_2O_2 with ions that contain Ti(IV) by the analysis of the maximum absorbance of the yellow $[TiO{\cdot}H_2O_2]^{2+}$

complex at the wavelength of 410 nm. The difference between the total oxidiser content and peroxide content studied by different methods was used to consider the influence of particles of different types on the reaction course.

3. Results and Discussion

3.1. Solutions with Mn

The results of plasma treatment of solutions that contain Mn in different oxidation states are shown in Fig. 1. A pronounced decrease of the total Mn concentration is observed in two more concentrated solutions after 2–4 min of treatment (Fig. 1a). This effect is accompanied by intense precipitation. With increasing treatment time, the precipitates interact with active reducers accumulated in the solution and start to dissolve increasing the Mn concentration.

The total Mn concentration in two diluted solutions is less changeable (Fig. 1a). A small amount of precipitates is observed in these two solutions after more prolonged plasma treatment.

All changes of pH with treatment time also depend on the Mn concentration (Fig. 1c). A clear local maximum on the pH curves with simultaneous decolouration of the solutions is observed in diluted solutions with 37 and 58 μmol/l Mn after 1–3 min of treatment. With a further increase of treatment time, the pH values start to decrease from 8.7 to 3.1 with concurrent precipitation.

For more concentrated solutions, such as 173 and 335 μmol/l, initial pH growth and its follow-up reduction are more temperate and peaks on the pH curves are less pronounced.

Peroxide H_2O_2 appears in the solution in the course of plasma treatment (Fig. 1b). For diluted solutions, this process starts very quickly, just after some seconds of plasma treatment. For concentrated solutions, there is a noticeable time delay in H_2O_2 formation. The value of such a delay usually increases with Mn concentration.

The comparison of Mn (Fig. 1a) and H_2O_2 (Fig. 1b) curves allows one to conclude that peroxide starts to accumulate actively in the solution only after completion of the process of Mn(VII) reduction. Evidently, this time depends on the initial Mn concentration. It is tiny in diluted samples and varies between 6 and 10 min in concentrated solutions.

Table 1

Plasma treatment regimes of aqueous solutions that contain Mn, Cr and Fe in different oxidation states

Soluted compound	Metal	Initial valence	Metal concentration, μmol/l	Discharge current, mA	Air pressure, kPa	Treatment time, min
$KMnO_4$	Mn	VII	37–336	15–25	15	0–15
$K_2Cr_2O_7$	Cr	VI	250	25	12	0–20
K_2CrO_4	Cr	VI	250–700	25	12	0–20
$KCr(SO_4)_2{\cdot}6H_2O$	Cr	III	280	25	12	0–20
$FeSO_4$	Fe	II	2850	25	13	0–12
$Fe_3(SO_4)_2$	Fe	III	2500	25	13	0–12

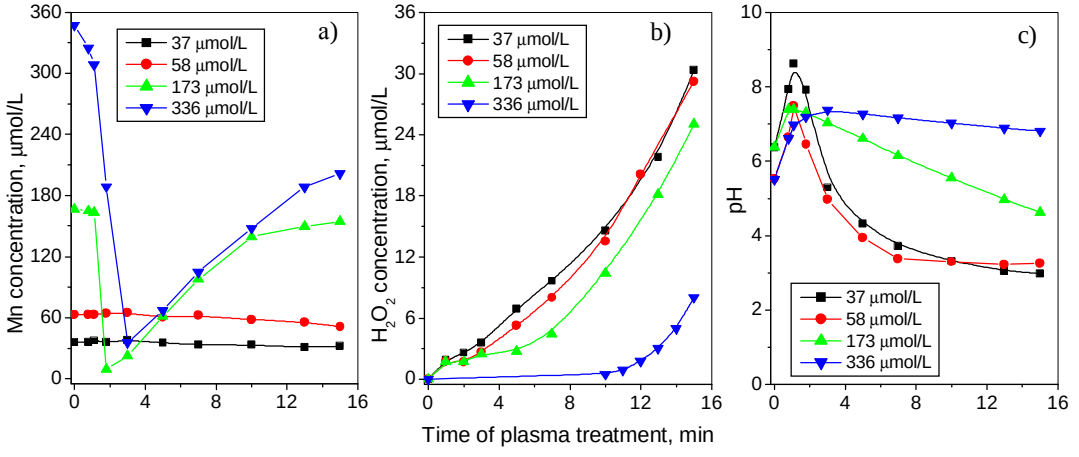

Fig. 1. Concentrations of Mn (a), H_2O_2 (b), and pH (c) in aqueous solutions of $KMnO_4$ with different Mn concentrations as a function of plasma treatment time

3.2. Solutions with Cr

Redox effects under plasma treatment become apparent in changes of the oxidation level of Cr in compounds. Aqueous solutions of potassium dichromate and bichromate were treated with a low-pressure plasma discharge and the results obtained are shown in Fig. 2. Approximately half of the Cr(VI)-containing ions in chromate solutionis reduced to Cr(III) for 2 min while the reduction process is completed for approx. 18 min of the plasma treatment (Fig. 2a). The formation of peroxide in chromate and dichromate solutions accelerates after completing the Cr(VI) reduction process (Fig. 2b). In particular, the delay in H_2O_2 formation for the most concentrated 700 μmol/l K_2CrO_4 is observed for more than 16 min.

When a solution of chromic potassium alum was treated, no visible changes in the solution and the oxidation level of Cr(III) were observed. The formation of H_2O_2 proceeds with a high rate without any delay (Fig. 2b). Therefore, ions with Cr(VI) seem to react actively with peroxide while Cr(III) ions remain inactive in plasma-treated solutions.

The plasma treatment of solutions with fixed started concentrations of Cr(VI) and Cr(III) for 5–10 min lead to decreasing hydrogen index by at least four units to pH = 2.8 (Fig. 2c). The shapes of pH(*t*) were almost independent of the initial Cr concentrations. Evidently, the observed decrease of pH is mainly caused by an interaction of plasma with water molecules as follows from the shape of the pH(*t*) curve for distilled water. Plasma discharge, interacting with a liquid phase, generates particles with strong acid properties. As a result of further recombination processes, peroxide, which is detected in all studied solutions, is formed.

3.3. Solutions with Fe

Taking in mind different behaviour of ions containing Cr(VI) and Cr(III) in plasma treated solutions, both Fe(III) and Fe(II) sulphates were studied in experiments with Fe-containing solutions. The concentration of Fe(III) ions quickly increases in $FeSO_4$ within the first minute of plasma treatment but remains unchanged in $Fe_3(SO_4)_2$ during the whole period of observation (Fig. 3a). Simultaneously the concentration of Fe(II) ions drops to zero in $FeSO_4$ solutions, and this ion is never observed in plasma-treated $Fe_3(SO_4)_2$.

The form into which Fe(II) is transformed under the plasma action depends on the initial pH of a $FeSO_4$ solution. The quantitative transition of Fe(II)↔Fe(III) without the formation of a solid phase is carried out at pH = 1.6. The oxidation rate of Fe(II) slightly increases with increasing pH from 1.6 to 2.9. However, at pH > 2.2, precipitation of $Fe(OH)_3$ occurs. Due to partial deposition, the total concentration of Fe begins to decrease after 1–3 min treatment of solutions with pH > 2.2.

The peroxide concentration generated by the plasma discharge (Fig. 3b) behaves similarly as in solutions of manganese compounds (Fig. 1b) and Cr (Fig. 2b) ions. The H_2O_2 concentration in general increases with treatment time. In $FeSO_4$ solutions, some time-delay is observed in the peroxide formation which correlates well with the time of active oxidation of Fe(II)-to-Fe(III). On the contrary, no delay is detected in $Fe_3(SO_4)_2$ solutions where no plasma-induced redox processes occur.

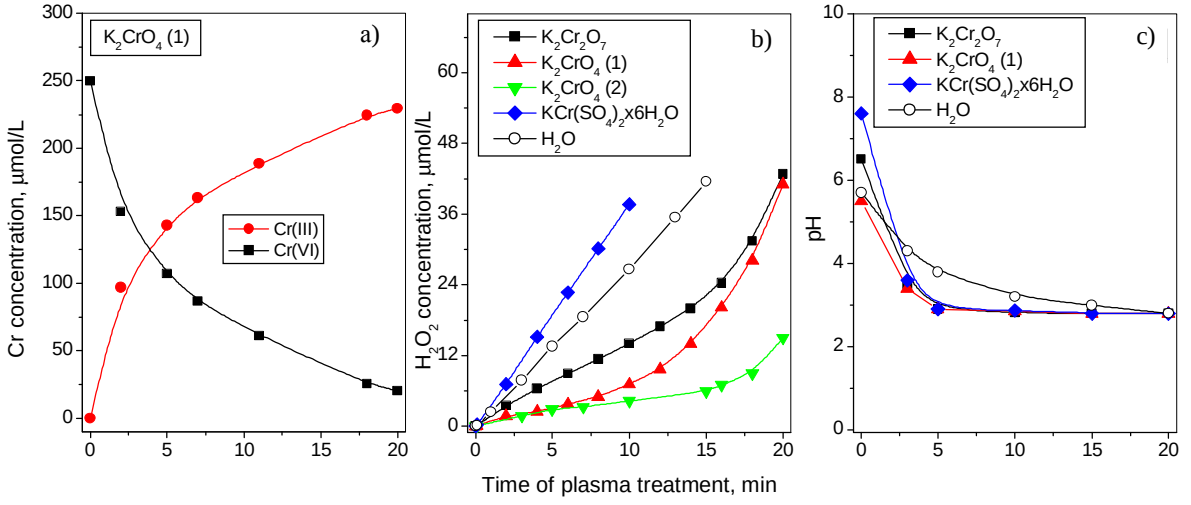

Fig. 2. Concentrations of Cr (a), H_2O_2 (b), and pH (c) in aqueous solutions of $K_2Cr_2O_7$ (250 μmol/l Cr), K_2CrO_4 (1 – 250 μmol/l Cr, 2 – 700 μmol/l Cr) and $KCr(SO_4)_2 \cdot 6H_2O$ (280 μmol/l Cr) as a function of time of plasma treatment

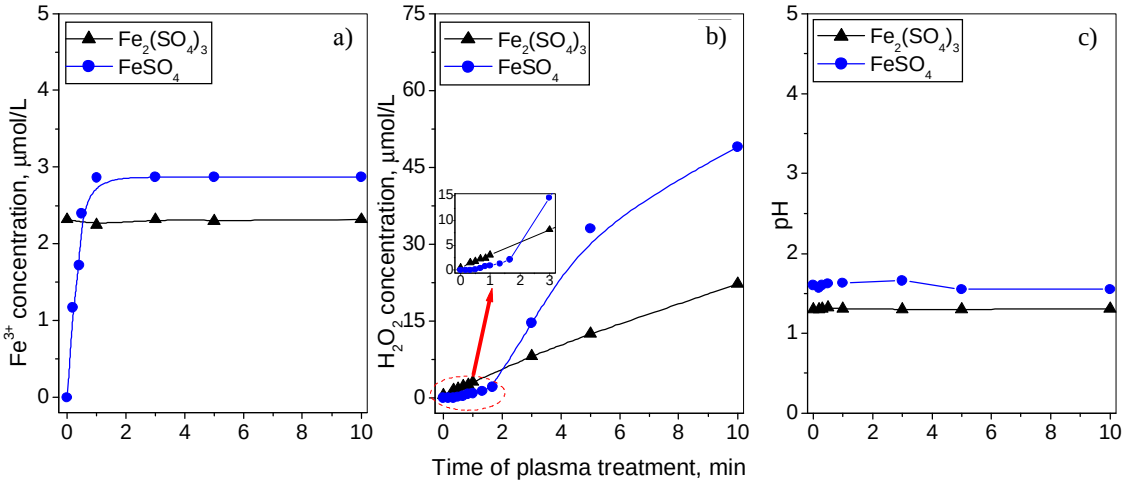

Fig. 3. Concentrations of Fe(III) (a), H_2O_2 (b) and pH (c) in aqueous solutions of $FeSO_4$ (pH = 1.3) and $Fe_2(SO4)_3$ (pH = 1.6) with 2.85 mmol/l Fe and 2.5 mmol/l Fe, respectively, as a function of time of plasma treatment

3.4. Peroxide Formation

Peroxide plays an essential role in plasma-induced redox reactions. While OH radicals have higher oxidation potential, however, they are unstable and easily decay in reactions with one another or hydrogen atoms. There is a consensus that peroxide is formed in plasma-treated solutions due to secondary reactions occurring with the participation of plasma-induced primary species. The basic processes of formation of primary active particles begin in the gas phase [20]. After discharge ignition, collisions of charged particles and gas molecules lead to the formation of several radicals and active species like solvated electrons (e_{eq}), OH, H, O, O_3 in the gas phase. These radicals may then react with themselves in a gas phase and with other particles in a thin subsurface layer of a liquid. The charged-particle bombardment of the solution surface causes the transfer of neutral particles to the plasma zone. Therefore, the reaction types and rates are dependent on gas medium and characteristics of a liquid phase, such as pH.

Reactions with the participation of $OH^{\bullet}$ radicals are usually considered as the main source of H_2O_2 formation [18]:

$$OH^{\bullet} + {}^{\bullet}OH \rightarrow H_2O_2 \quad (1)$$

On the other hand, $OH^{\bullet}$-radicals, as well as solvated electrons e_{eq} can simultaneously react with the hydrogen peroxide and thus decrease its concentration in the solution:

$$OH^{\bullet} + H_2O_2 \rightarrow HO_2^{\bullet} + H_2O \quad (2)$$
$$OH^{\bullet} + H_2O_2 \rightarrow O_2 + H_2O \quad (3)$$
$$e_{eq} + H_2O_2 \rightarrow OH^{\bullet} + OH^{-} \quad (4)$$

Therefore, the relationship between the rates of reactions (1) and (2-4) can determine the behaviour of peroxide concentration [12]. Such a course of events seems to describe the simplest situation, but it does not always fit the experimental observations. For examples, sometimes the measured rate of formation of $OH^{\bullet}$ radicals was much lower than the rate of formation of H_2O_2 [18]. As found in [21], $OH^{\bullet}$ radicals play an important role in the H_2O_2 formation under nitrogen and helium atmosphere where the reaction of $OH^{\bullet}$-radicals dimerisation dominates.

In air with water vapour, $OH^{\bullet}$-radicals have a limited direct effect, and the most probable mechanisms include hydrogen atoms reacting with HO_2 and process of HO_2 dimerisation:

$$H^{\bullet} + HO_2^{\bullet} \rightarrow H_2O_2 \quad (5)$$
$$HO_2^{\bullet} + HO_2^{\bullet} \rightarrow H_2O_2 + O_2 \quad (6)$$

Also, excited oxygen molecules can contribute to the formation of H_2O_2 in the solution in an air discharge by the following reactions [21, 30]:

$$H + O_2 \rightarrow HO_2 \quad (7)$$
$$O_2 + e \rightarrow O_2^{-} \quad (8)$$
$$O_2^{-} + H^{+} \leftrightarrow HO_2 \quad (9)$$
$$HO_2 + e \rightarrow HO_2^{-} \quad (10)$$
$$HO_2^{-} + H^{+} \rightarrow H_2O_2 \quad (11)$$
$$HO_2 + H \rightarrow H_2O_2 \quad (12)$$

When accumulating in the course of chemical transformations, hydrogen peroxide tends to polymerise forming hydrogen polyoxides [22]. In general, this process can be described as follows:

$$(n-1)H_2O_2 \rightarrow HO_nH + (n-2)H_2O \quad (13)$$

The action of plasma on electrolyte solutions initiates oxidation and reduction processes. Since both H^{+} and OH^{-} ions participate in plasma-initiated redox reactions, their concentration in the solution changes with treatment time [23]. Therefore, the acidity of the as-

treated solution, as well as redox potentials, will also change with treatment time. The plasma treatment of distilled water reduces its pH to a level 2–3 that can be explained by the accumulation of hydrogen polyoxides which have acidic properties [23].

Also, the plasma forms nitric oxides (NO_x) in nitrogen/oxygen-rich environments, such as air. They dissolve in the solution to form nitrous (HNO_2) and nitric (HNO_3) acid which also lowers pH [24].

In the solution with different pH, different ways of peroxide formation are operative [22] and, thus, the rate of H_2O_2 formation is sensitive to the pH index. In alkaline solutions, the H_2O_2 yield is usually much lower than that in neutral or acidic mediums [25]. Being a weak acid, H_2O_2 is intensively consumed by reacting with OH^- to form HO_2^- that causes a rather low H_2O_2 yield:

$$H_2O_2 + OH^- \rightarrow HO_2^- + H_2O \quad (14)$$

3.5. Effect of the Discharge Current of Peroxide Formation

Depending on discharge type, the yield of $H^\bullet$ and $OH^\bullet$ radicals fluctuates in a rather narrow range 3–8 [20] or 7.6–10 mol/F [18]. The initial yield of peroxide was estimated to be close to ~1.5 mol/F [20]. However, the concentrations of peroxide vary in a rather broad range. That indicated that the rate of peroxide degradation is sensitive to the solution type and may differ by almost two orders of magnitude even for similar types of the discharge.

The analysis of experimental and literature data [13, 18, 26, 27] suggests that the rate of formation of peroxide depends on the type of discharge, its polarity, and, as a rule, increases with increasing discharge current. There is also some evidence that the material of cathode influences the chemical reactions in the solution via catalytic effects of emitted ions [28]. Such dependencies are easily observed by treating distilled water when the presence of solute compounds does not affect the rate of peroxide release.

During first minutes of plasma treatment, the peroxide concentration (C_{H2O2}) exhibits a linear dependence of treatment time *t*. Therefore, the slope angle dC_{H2O2}/dt in coordinates $C_{H2O2} = f(t)$ can be used as a measure of the rate of peroxide formation. The dependences of dC_{H2O2}/dt on the discharge current are shown in Fig. 4 for different plasma types and configurations. As is seen, the experimental curves are divided into three clusters and thus clearly illustrate the effectiveness of one or another type of discharge relative to the formation of peroxide.

The glow discharge exhibits the highest peroxide formation rates and the most pronounced dependence on the current while the frontal discharge is the least effective in both parameters. Similar results were discussed in [29]. Discharge with water as a cathode is usually much more efficient for H_2O_2 production as is seen from Fig. 4 and reported in many researches [30, 31]. When liquid acts as an anode, the cathode voltage fall is formed on the metallic electrode, and the charged particles are electrons entering the anodic solution [25]. Thus, no sputtering and field-induced ion emission takes place at the liquid surface. Evaporation is the only way to transfer water molecules from the liquid phase into the gaseous plasma resulting in a low H_2O_2 yield. Higher energy of $OH^\bullet$-radicals excited by an intensive electron flux in the configuration with a liquid anode may also cause their quicker decay and thus suppress the rate of peroxide production.

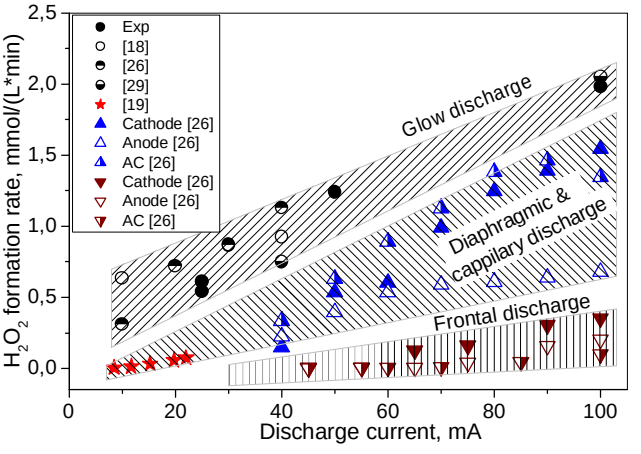

Fig. 4. The rate of H_2O_2 formation (dC_{H2O2}/dt) as a function of discharge current for different plasma configurations: dots – glow discharge by various authors, triangles up – diaphragmic discharge in cathode, anode and AC configurations, triangles down – frontal discharge in cathode, anode and AC configurations, stars – AC capillary discharge

3.6. Plasma-Induced Redox Reactions

The experimental results obtained, in particular, changing the oxidation state of metals, show that the plasma treatment initiates both oxidation and reduction processes with participation of ions that contain Fe, Mn and Cr. Some redox processes observed in the given paper and other reports are listed in Table 2. Both oxidation and reduction reactions are possible in the considered solution under the action of plasma discharge, as follows from Table 2. Their direction, as well as intensity, depend on many factors, including pH, the concentration of components, discharge type and modes. Evidently, an essential stage of technological applications is the optimisation of the modes and type of discharge. Optimal conditions are dependent on application field.

As was stated before, peroxide molecules formed in the course of plasma treatment in the solution play an important role in redox processes. This statement is evidenced by the correlations observed between concentrations of peroxide (Fig. 5) and Mn-containing ions (Fig. 1a). As is seen the peroxide appears in the solution after a certain time-delay which increases from approximately 4 to 10 min with increasing Mn concentration from 150 to 336 μmol/l.

The anticipated sequence of chemical transformations is as follows:

$$Mn(VII) \rightarrow Mn(VI) \rightarrow Mn(IV) \rightarrow Mn^{2+}. \quad (15)$$

Several methods, namely: titrimetric (permanganatometric and iodometric) and spectrophotometric (formation of complex compounds with titanium) have been used to determine the content of hydrogen peroxide. For solutions containing $KMnO_4$, the use of both titrimetric methods yields different curves for the H_2O_2 concentration as a function of plasma treatment time (Fig. 5). The possible explanation for this fact is that both titrimetric methods may not be selective for H_2O_2 in the presence of other oxidising and reducing particles in the system. Then, the curve obtained from the results of iodometric titration can show the presence of other oxidising particles that are formed both under the influence of the plasma and in the process of redox reactions with hydrogen peroxide. The H_2O_2 curves obtained by spectrophotometry and permanganatometric titration coincide. Therefore, these two methods more adequately characterise the presence of H_2O_2 in the system.

Reducing particles enter into a reaction with Mn(VII)-containing ions, and they cannot be detected until all Mn(VII) have reacted. The curves in Fig. 5 support this conclusion: an apparent time delay is observed at both parmanganatometric and spectrophotometric curves, and the duration of the delay increases with the Mn concentration.

Table 2

Redox processes in aqueous solutions with Mn, Cr and Fe caused by plasma treatment

Process	Transformations	Medium	Reference
Oxidation	$Mn^{2+} \rightarrow MnO_2$	Neutral, acid	Experiment, [32]
Reduction	$MnO_4^- \rightarrow MnO_2$	Neutral, acid	[32]
Reduction	$MnO_4^- \rightarrow MnO_2$	Alkaline	[33]
Reduction	$MnO_4^- \rightarrow MnO_2 \rightarrow Mn^{2+}$	Neutral, acid	Experiment
Oxidation	$Fe^{2+} \rightarrow Fe^{3+}$	Acid	Experiment, [32]
Oxidation	$Fe^{2+} \rightarrow Fe(OH)_3$	Neutral	Experiment,
Oxidation of the central ion	$[Fe(CN)_6]^{3-} \rightarrow Fe[Fe(CN)_6]$	Neutral	[32]
Reduction	$Cr_2O_7^{2-} \rightarrow Cr_2O_3$	Neutral	[32]
Oxidation	$Cr^{3+} \rightarrow Cr_2O_6^{2-}$	Neutral, acid	[32]
Reduction	$Cr_2O_7^{2-} \rightarrow Cr^{3+}$	Neutral, acid	Experiment
Reduction	$CrO_4^{2-} \rightarrow Cr^{3+}$	Neutral, acid	Experiment

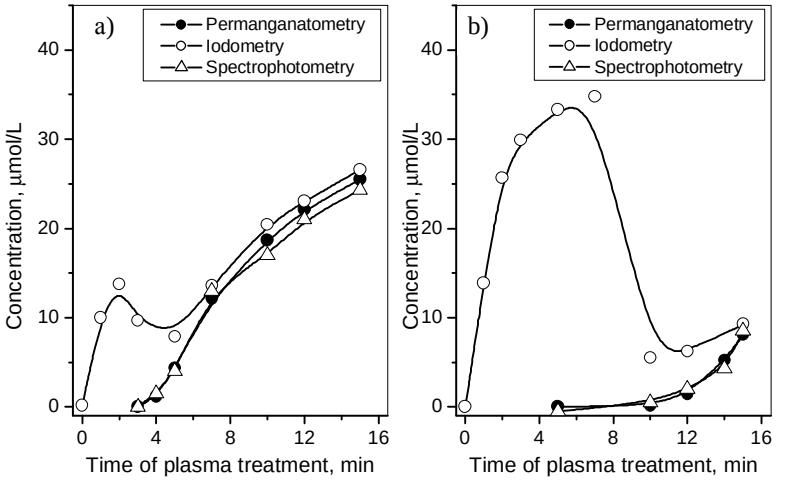

Fig. 5. Concentrations of oxidising compounds and peroxide, determined by permanganatometry (black dots), iodometry (open dots) and spectrophotometry (triangles), in aqueous solutions of $KMnO_4$ with 150 μmol/l Mn (a) and 336 μmol/l Mn (b) as a function of plasma treatment time

After reduction of manganese to Mn^{2+}, an excess of reducing particles reacts with oxidising particles. Such a reaction results in a temporal decrease of the total concentration of oxidising compounds at a particular stage of plasma treatment as is illustrated by the iodometric curves in Fig. 5.

Later, redox processes tend to their completion, and the rate of consumption of both reducing and oxidising particles diminishes. As a result, accumulation of these particles is resumed in the solution. Hydrogen peroxide is then determined both iodometrically and permanganatometrically/spectrophotometrically. At this stage, all the above methods give close values of the peroxide concentration.

4. Conclusions

Aqueous solutions of various compounds containing Mn, Fe and Cr were treated by a low-pressure glow discharge. The discharge conditions, such as polarity, discharge current and air pressure, were preliminary optimised regarding increasing the effectiveness of its influence on the redox processes. The concentration of peroxide, as well as the concentration and oxidation level of metals in the as-treated solutions, were studied as a function of treatment time.

The effect of plasma treatment of manganese permanganate solutions consists in the reduction of Mn(VII) first to Mn(IV) and then to Mn(II). Hydrogen peroxide is generated under the plasma action but is initially expended in reducing the Mn-containing ions. When the redox processes diminish, H_2O_2 molecules accumulate in the solution.

In ferrous solutions, the oxidation of Fe(II) to Fe(III) ions occurs under the action of plasma. If pH of the solution is less than 2 (strong-acidic medium), the transformation of Fe(II) to Fe(III) is almost complete, and the total content of iron ions does not change in the solution. If pH is higher than the value mentioned above, the oxidation process is also completed, but the total concentration of Fe in solution is reduced because of partial precipitation. In solutions with Fe(III), the plasma discharge does not change the oxidation level of Fe.

In solutions of chromium compounds, the reduction of Cr(VI) to Cr(III) is observed in an acidic medium. The value of pH index reduces from 6–8 to 2.8 concurrently with the Cr reduction. The oxidation level of metal does not change under the plasma action in solutions that contain Cr(III).

The action of a plasma discharge results in the acidification of the treated medium. Such a phenomenon was observed in all Cr- and Mn-containing solutions and was less-pronounced in solutions of Fe compounds.

The concentration of hydrogen peroxide formed under the plasma discharge was measured by titrimetric (permanganatometric and iodometric) and spectrophotometric methods. The permanganatometry and spectrophotometry allowed to estimate the amount of hydrogen peroxide molecules which act as reducing agents. The results of iodometric measurements described the total concentration of all oxidisers.

The concentration of hydrogen peroxide usually increases with treatment time, but it is not detected during active redox interaction with metal-containing ions. In general, the curves characterising the change in the ion concentrations with metals of different oxidation level correlate well with the curves describing the hydrogen peroxide formation.

References

[1] Ishijima T., Nosaka K., Tanaka Y. *et al.*: Appl. Phys. Lett., 2013, **103**, 142101. https://doi.org/10.1063/1.4823530
[2] Vorobyova M., Pivovarov O.: Voprosy Khim. Khim. Tekhnol., 2014, **3**, 19.
[3] Mariotti D., Sankaran R. *et al.*: J. Phys. D, 2011, **44**, 174023. https://doi.org/10.1063/1.4823530
[4] Smoluch M., Mielczarek P., Silberring J.: Mass Spectrom. Rev., 2016, **35**, 22. https://doi.org/10.1002/mas.21460
[5] Chmilenko F., Derkach T., Smityuk A.: J. Anal. Chem., 2000, **55**, 327. https://doi.org/10.1007/BF02757765
[6] Chmilenko F., Pivovarov A., Derkach T. *et al.*: J. Anal. Chem., 1997, **52**, 311.
[7] Fridman G., Friedman G., Gutsol A. *et al.*: Plasma Proc. Polym., 2008, **5**, 503. https://doi.org/10.1002/ppap.200700154
[8] Jiang B., Zheng J., Qiu S. *et al.*: Chem. Eng. J., 2014, **236**, 348. https://doi.org/10.1016/j.cej.2013.09.090
[9] Misra N.: Trends Food Sci. Tech., 2015, **45**, 229. https://doi.org/10.1016/j.tifs.2015.06.005
[10] Magureanu M., Piroi D., Mandache N. *et al.*: Water Research, 2010, **44**, 3445. https://doi.org/10.1016/j.watres.2010.03.020
[11] Shutov D., Isakina A., Konovalov A. *et al.*: High Energ. Chem., 2013, **47**, 201. https://doi.org/10.1134/S0018143913040115
[12] Bobkova E., Krasnov D., Sungurova A. *et al.*: Korean J. Chem. Eng., 2016, **33**, 1620. https://doi.org/10.1007/s11814-015-0292-7
[13] Choukourov A., Manukyan A., Shutov D. *et al.*: Izv. Vyssh. Uchebn. Zaved. Khim. Khim. Tekhnol., 2016, **59**, 4. https://doi.org/10.6060/tcct.20165912.5413
[14] Ramli N., Zaaba S., Mustaffa M. *et al.*: AIP Conf. Proc., 2017, **1824**, 030015-1. https://doi.org/10.1063/1.4978833
[15] Brisset J.-L., Moussa D., Doubla A. *et al.*: Ind. Eng. Chem. Res., 2008, **47**, 5761. https://doi.org/10.1021/ie701759y
[16] Jiang B., Guo J., Wang Z. *et al.*: Chem. Eng. J., 2015, **262**, 1144. https://doi.org/10.1016/j.cej.2014.10.064
[17] Pivovarov O., Zakharov R., Nikolenko M.: Chem. Chem. Technol., 2015, **9**, 95. https://doi.org/10.23939/chcht09.01.095
[18] Bobkova E., Shikova T., Grinevich V. *et al.*: High Energ. Chem., 2012, **46**, 56. https://doi.org/10.1134/S0018143912010079
[19] De Baerdemaeker F., Simek M., Leys C.: J. Phys. D, 2007, **40**, 2801. https://doi.org/10.1088/0022-3727/40/9/021
[20] Maksimov A., Khlyustova A.: High Energ. Chem., 2009, **43**, 149. https://doi.org/10.1134/S0018143909030011

[21] Zhao Y., Wang T., Wilson M. *et al.*: IEEE Transact. Plasma Sci., 2016, **44**, 2084. https://doi.org/10.1109/TPS.2016.2547841
[22] Pivovarov A., Kravchenko A., Tishchenko A. *et al.*: Russ. J. Gen. Chem., 2015, **85**, 1339. https://doi.org/10.1134/S1070363215050497
[23] Pivovarov A., Nikolenko N., Zakharov R. *et al.*: Voprosy Khim. Khim. Tekhnol., 2012, **3**, 127.
[24] Go D.: J. Phys. Conf. Series, 2015, **646**, 012052. https://doi.org/10.1088/1742-6596/646/1/012052
[25] Liu J., He B., Chen Q. *et al.*: Sci. Rep., 2016, **6**, 38454. https://doi.org/10.1038/srep38454
[26] Silkin S.: Elektronnaya Obrabotka Mater., 2014, **50**, 106.
[27] Pivovarov A., Zakharov R., Nikolenko N.: Voprosy Khim. Khim. Tekhnol., 2013, **3**, 174.
[28] Kuz'micheva L., Titova Yu., Maksimova A. *et al.*: Surf. Eng. Appl. Electrochem., 2013, **49**, 485. https://doi.org/10.3103/S1068375513060100
[29] Kuz'micheva L., Titova Yu., Maksimova A.: Elektronnaya Obrabotka Mater., 2007, **2**, 20.
[30] Xiong R., Nikiforov A., Vanraes P. *et al.*: J. Adv. Oxid. Technol., 2012, **15**, 197. http://hdl.handle.net/1854/LU-2125069
[31] Miyahara T., Oizumi M., Nakatani T. *et al.:* AIP Adv., 2014, **4**, 047115. https://doi.org/10.1063/1.4871475
[32] Kutepov A., Zakharov A., Maksimov A., Titov V.: High Energ. Chem., 2003, **37**, 317. https://doi.org/10.1023/A:1025704930260
[33] Kuz'micheva L., Maksimova A., Titova Yu.: Elektronnaya Obrabotka Mater., 2005, **5**, 47.

Received: February 24, 2018 / Revised: March 31, 2018 / Accepted: June 12, 2018

ОБРОБЛЕННЯ ПЛАЗМОВИМ РОЗРЯДОМ ПОНИЖЕНОГО ТИСКУ ВОДНИХ РОЗЧИНІВ, ЩО МІСТЯТЬ Mn, Cr ТА Fe

Анотація. *Досліджено вплив тліючого розряду пониженого тиску на утворення гідроген пероксиду та зміну ступеню окиснення металів у водних розчинах сполук Mn, Cr та Fe. Показано, що плазмове оброблення спричиняє відновлення Mn(VII) через Mn(IV) до Mn(II), Cr(VI) до Cr(III) та окиснення Fe(II) до Fe(III). Гідроген пероксид, що утворюється під дією плазмового оброблення, активно бере участь в окисно-відновних реакціях. Концентрація гідроген пероксиду зазвичай збільшується з часом оброблення, однак виявити його наявність стає можливим тільки після закінчення перебігу активних окисно-відновних процесів.*

Ключові слова: *оброблення плазмовим розрядом пониженого тиску, окисно-відновні реакції, утворення гідроген пероксиду, відновлення, окиснення.*

Chem. Chem. Technol., 2019,
Vol. 13, No. 3, pp. 326–333

Chemistry

KINETICS OF Os(VIII) CATALYZED OXIDATION OF 2-PYRROLIDINE CARBOXYLIC ACID IN ALKALINE MEDIUM USING SODIUM PERIODATE AS OXIDANT: A MECHANISTIC APPROACH

Madhu Gupta[1], Amrita Srivastava[1], Sheila Srivastava[2, *], Ashish Verma[1]

https://doi.org/10.23939/chcht13.03.326

Abstract. The present paper deals with the kinetic and mechanistic investigation of Os(VIII) catalyzed oxidation of 2-pyrrolidinecarboxylic acid by sodium periodate ($NaIO_4$) in alkaline medium in the temperature range of 303–318 K. The experimental result shows a first order kinetics with respect to Os(VIII) and periodate while positive effect with respect to substrate *i.e.*, 2-pyrrolidinecarboxylic acid was observed. The reaction showed negative effect for [OH^-]. Negligible effect of $Hg(OAc)_2$ and ionic strength of the medium was observed. The reaction is carried out in the presence of mercuric acetate as a scavenger. The reaction of sodium periodate and 2-pyrrolidinecarboxylic acid in alkaline medium shows 2:1 stoichiometry. The values of rate constants observed at different temperatures were utilized to calculate the activation parameters. A mechanism involving the complex formation between a catalyst, substrate and oxidant has been proposed. L-glutamic acid has been identified as the main oxidation product of the reaction using chromatography and spectroscopy. Based on kinetic data, the reaction stoichiometry and product analysis of the reaction a feasible mechanism has been proposed. The rate law has been derived from obtained kinetic data.

Keywords: kinetics, Os(VIII), oxidation, 2-pyrrolidine-carboxylic acid, sodium periodate, alkaline medium.

1. Introduction

Amino acids are the derivatives of protein in the diet or degradation of intracellular proteins is the final class of biomolecules and their oxidation makes a significant role in production of metabolic energy. Based upon the number of carbon atoms in the α-amino acids species, they get oxidized to α-keto glutamate, succinates, fumerate, oxaloacetate, *etc*. 2-Pyrrolidinecarboxylic acid (L-pro) is one among 20 α-amino acids with five-carbon atoms in pyrrolidine skeleton. This pyrrolidine ring is opened [1] by oxidation at the carbon atom most distant from the carboxylic group to produce a Schiff's base and hydrolysis of this Schiff's base produces a linear glutamic semi-aldehyde, which is further oxidized at the same carbon atom leading to glutamic acid. However, the earlier reports [2] reveal that L-pro undergoes oxidation with the cleavage of pyrrolidine ring at the nearest carbon atom from the carboxylic acid group followed by decarboxylation to produce 4-amino butanol or 4-amino butyric acid, whereas D-proline leads to keto acid. Since L-pro has a cyclic structure with an imino [3] group attached at one end by $–CH_2$ and at the other end by >CH–COOH, the cleavage at the closest carbon atom from carboxylic group is unusual. This may also be due to the less reactivity of α-carbon/hydrogen. Hence, the ring opening takes place at a carbon atom of far end from a carboxylic group. Moreover, when $–NH_2$ group is not present at α-carbon atom, there is no other driving force remaining for decarboxylation to produce butaraldehyde, butyric acid or keto acids. Some reports about the oxidation of L-pro claimed that the ring cleavage took place between N and C, by retaining the $–NH_2$ group with the main moiety without liberating ammonia, and the decarboxylation was proposed as a mechanism for the oxidation [4].

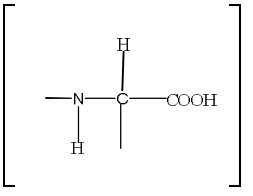

L-proline is one among non-essential amino acids and is an important component of collagen. According to [3], L-proline is considered to be the world's smallest natural enzyme and it plays an important role in catalysing the aldol condensation of acetone to various aldehydes with high stereo-specificity.

[1] Department of Chemistry, University of Lucknow, Lucknow, U.P., India
[2] Chemical Laboratories Feroze Gandhi College, Raebareli, U.P., India
[*] *She_ila72@yahoo.com*

Many transition and non-transition metal ions in their complex form are good oxidants in acidic, basic or neutral medium. However, oxidation capacity depends upon their redox potential. It is also known that the redox potential of the couple depends on the medium pH. In recent years, the use of transition metal ion such as osmium, ruthenium and iridium as a catalyst in various redox processes has attracted considerable interest [5-6]. The mechanism of the catalysis is quite complicated because of the formation of different intermediate complexes, free radicals and different oxidation states of osmium. Although, both osmium and ruthenium belong to the same group, their compounds are stable in different oxidation states. Osmium compounds are highly stable in +8 oxidation state whereas ruthenium compounds are in +3 or +4. Hence, their catalytic role varies to a large extent; in most of the oxidations [6, 7] of organic compounds, the reaction was independent upon substrate concentration in Ru(III) catalysis and unity or fractional order in Os(VIII) catalysis. This may be due to the large difference in their redox potentials. The redox potentials of Ru(IV)/Ru(III) is +1.3 V which is unexpectedly higher than that of Os(VIII)/Os(VI) equal to +0.85 V.

Periodate is a clean and relatively selective reagent for the oxidative cleavage of organic compounds containing -hydroxy, -oxo, -amino, or -carboxyl groups. There is extensive literature on the kinetics of the periodic acid oxidation of glycols [8-9] but the kinetics of the periodate oxidation of amino alcohols [10], dicarbonyl compounds [11], and amino acids [12], has received much less attention. Oxidation with periodate has been shown to cause denaturation of proteins and inactivation of enzymes and these findings have been interpreted on the basis of periodate attack on essential amino acids. Periodate (Per) is a two electron oxidant with a redox potential of +0.70 V in alkaline medium and is a more suitable reagent for the study of oxidation reactions of both organic and inorganic substrates [13]. Further we have isolated the oxidized products in a way to arrive at a suitable mechanism on the basis of kinetic and spectral results and to compute the thermodynamic quantities of various steps. An understanding of the mechanism allows the chemistry to be interpreted, understood and predicted.

2. Experimental

2.1. Materials

Reagent grade chemicals and double-distilled water (from alkaline $KMnO_4$ in all-glass apparatus) were used. An aqueous solution of $NaIO_4$ was prepared by dissolving $NaIO_4$ (BDH) in water and was standardized iodometrically [14]. L-proline, a colorless crystalline compound (E-Merck) was used without further purification for the preparation of aqueous stock solution. The stock solution of Os(VIII) was obtained by dissolving osmic acid (OsO_4) (Johnson-Matthey) in 0.5 mol·dm^{-3} sodium hydroxide solution and its concentration was ascertained [15] against standard ceric ammonium sulfate solution in acid medium. Aqueous solutions of NaOH and NaCl were used to maintain the [OH^-] and ionic strength, respectively. In the present investigation, the effect of concentration of [$NaIO_4$] was studied from $0.8\cdot10^{-3}$ to $5.0\cdot10^{-3}$ and [L-proline] was studied between $2.0\cdot10^{-4}$ to $1.3\cdot10^{-3}$. The reaction stills were blackened from outside to prevent photochemical effects.

2.2. Kinetic Procedure

Appropriate volumes of the solutions of substrate, NaOH, $Hg(OAc)_2$, OsO_4 and the requisite volume of doubly distilled H_2O were placed in the reaction vessel, which was located in an electrically operated thermostatic water bath maintained at the desired temperature within the ±0.1 K. When the mixture attained the bath temperature, the reaction was initiated by adding the required volume of $NaIO_4$ solution, which was also placed separately in the same bath in another vessel. The kinetics of the reaction was followed by estimating the quantity of unconsumed $NaIO_4$. An aliquot (5 ml) of the reaction mixture was withdrawn at regular time intervals and was monitored by iodometric determination of the remaining $NaIO_4$ up to two half lives of the reaction. The reaction rate (dc/dt) in each kinetic run was determined by the slope of the tangent drawn at fixed concentrations of $NaIO_4$ in the plots of unconsumed $NaIO_4$ *versus* time. The order of the reaction with respect to each reactant was determined with the help of (dc/dt) values calculated for various concentrations of each reactant. The moderately higher concentration of NaOH was used to maintain the OH^- concentration in the reaction. Hence, the effect of dissolved CO_2 on the rate was examined by carrying out the kinetics in the presence of CO_2 and N_2. It was found that there was no variation of rate constants which indicates that dissolved CO_2 had any effect on the reaction rate.

3. Results and Discussion

3.1. Determination of Stoichiometry and Product Analysis

The stoichiometric analysis of oxidation reaction of proline with sodium periodate indicates that two moles of the oxidant react with one mole of a substrate. This result

showed 1:2 stoichiometry according to the equation. Varying [$NaIO_4$]:[proline] ratios were equilibrated at 313 K for 72 h under the experimental conditions [$NaIO_4$] >> [proline]. Estimation of unconsumed [$NaIO_4$] in different sets showed that two moles of $NaIO_4$ were consumed in order to oxidise one mole of proline. Accordingly, the following stoichiometry equation can be formulated.

The main oxidative product of L-proline was identified as L-glutamic acid by its spot test in which the intense blue color was obtained by adding ninhydrin [16]. It supports the results from the earlier work [17]. It is also estimated quantitatively as a ninhydrin derivative by spectrophotometric methods [18]. It was found that L-proline is oxidized to L-glutamic acid. Other plausible products like glutamic semialdehyde and R-keto acid were not found.

Further, L-glutamic acid was separated from the reaction mixture by an ether extract which was concentrated by evaporation and mixed with concentrated hydrochloric acid (2 ml). The residue was then evaporated several times with water (ca. 5 ml portions) to remove the excess of hydrochloric acid and finally with methanol (10 ml). The white needles produced were collected, dried, and analyzed for C, H, N, and Cl contents. The elemental analysis was consistent with that of L-glutamate hydrochloride ($C_{10}H_{17}N_2O_8Cl$). (Found: C, 40.5; H, 7.5; N, 8.6; Cl, 16.6. Calcd: C, 41.9; H, 7.3; N, 9.8; Cl, 17.2 %). Further it was subjected to IR scanning. The stretching frequencies of –NH2, –COOH and carbonyl were found to be 3430, 3060, and 1684 cm^{-1}, respectively, and C–N vibration frequencies at 1124 cm^{-1} were also observed (Fig. 1). The product was also confirmed by UV spectrum (Fig. 2). This clearly indicates that the oxidative product of L-proline was found to be L-glutamic acid which is formed by reacting with 2 moles of [$NaIO_4$] as shown by Eq. (1).

3.2. Reaction Orders

Reaction order and the order with respect to each reactant were determined by varying the concentrations of oxidant, reductant, catalyst and alkali in turn, while keeping the other constants.

3.3. Effect of [L-Proline]

The dependence of reaction rate on L-proline concentration was examined over concentrations in the range of $(0.13–2.00)\cdot10^{-3}$ mol·dm^{-3} at different temperatures in the range of 303–318 K. The results in Table 1 showed that the rate constant increased with the increase in [L-proline]. It was confirmed by a plot of log[L-Pro] *vs.* log*dc*/*dt* (Fig. 3). Further the plot of *dc*/*dt* *versus* [L-proline] was linear (Fig. 4), passing through the origin according to Eq. (2). The zero intercept revealed that the self decomposition of $NaIO_4$ did not take place under the experimental conditions employed in this study.

$$k_{obs} = k_2[\text{proline}] \quad (2)$$

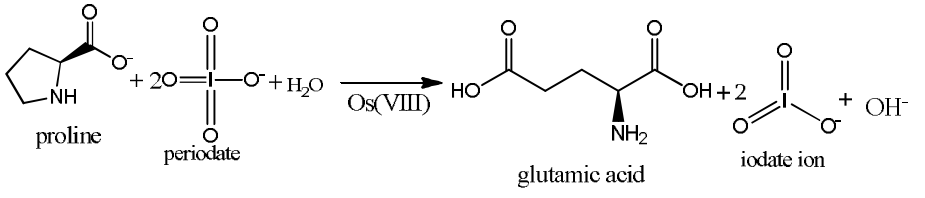

(1)

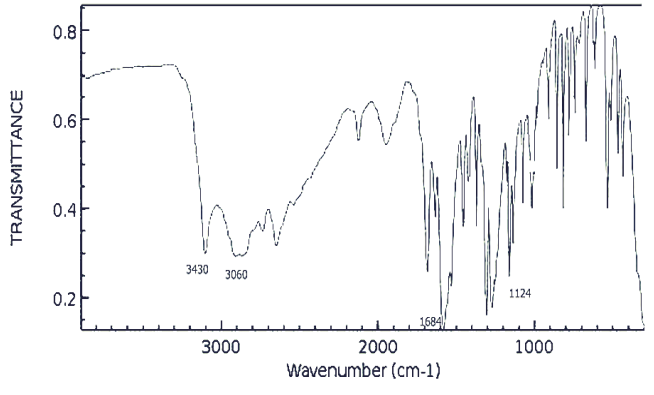

Fig. 1. IR-spectrum of the main product

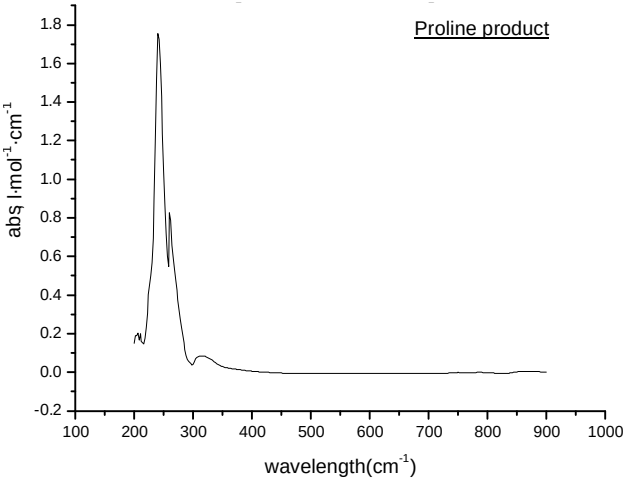

Fig. 2. UV spectrum of the main product

Table 1

Effect of [$NaIO_4$], [L-Proline], [$Hg(OAc)_2$] [NaOH] and Os(VIII) on oxidation of L-proline by $NaIO_4$ catalyzed by Os(VIII) in alkaline medium at 303 K

$[NaIO_4]\cdot10^3$, mol·dm^{-3}	$[S]\cdot10^2$, mol·dm^{-3}	$[Hg(OAc)_2]\cdot10^3$, mol·dm^{-3}	$[NaOH]\cdot10^3$, mol·dm^{-3}	$(-dc/dt)$, mol·dm^{-3}·s^{-1}	$K_1\cdot10^2$
0.83	1.00	1.25	1.00	0.40	1.87
1.00	1.00	1.25	1.00	0.48	2.10
1.25	1.00	1.25	1.00	0.53	2.91
1.67	1.00	1.25	1.00	0.78	3.64
2.50	1.00	1.25	1.00	1.00	3.30
5.00	1.00	1.25	1.00	1.84	6.10
1.00	0.13	1.25	1.00	0.20	1.04
1.00	0.17	1.25	1.00	0.21	1.08
1.00	0.25	1.25	1.00	0.23	1.26
1.00	0.50	1.25	1.00	0.24	1.40
1.00	2.00	1.25	1.00	0.26	1.69
1.00	1.00	0.83	1.00	0.33	1.85
1.00	1.00	1.00	1.00	0.29	1.73
1.00	1.00	1.67	1.00	0.27	1.86
1.00	1.00	2.50	1.00	0.28	1.10
1.00	1.00	5.00	1.00	0.30	1.03
1.00	1.00	1.25	0.83	0.28	1.42
1.00	1.00	1.25	1.25	0.23	1.34
1.00	1.00	1.25	1.67	0.21	1.19
1.00	1.00	1.25	2.50	0.20	1.03
1.00	1.00	1.25	5.00	0.19	0.84

Notes: Os(VIII) = $2.63\cdot10^{-6}$ M, $[NaIO_4] = 1.00\cdot10^{-3}$ M, [L-proline] = $1.00\cdot10^{-2}$ M, $[Hg(OAc)_2] = 1.25\cdot10^{-3}$ M, [NaOH] = $1.00\cdot10^{-3}$ M

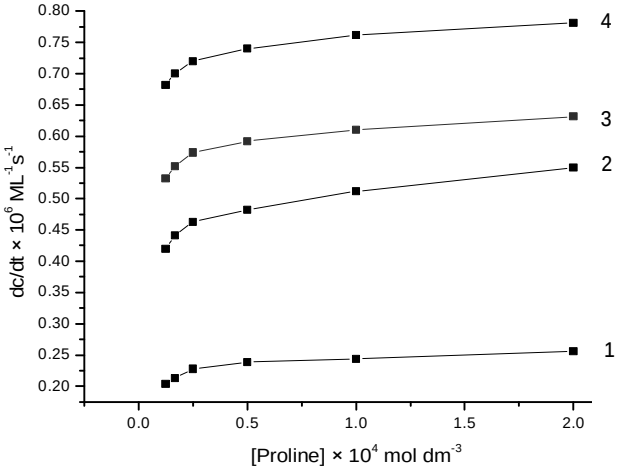

Fig. 3. Plot between rate of reaction $(-dc/dt)\cdot10^6$ *vs.* $[\text{L-proline}]\cdot10^4$ on the reaction rate at different temperatures (K): 303 (1), 308 (2), 313 (3) and 318 (4). [Os(VIII)] = $26.25\cdot10^{-5}$ M, $[Hg(OAc)_2] = 1.25\cdot10^{-3}$ M, [Oxidant ($NaIO_4$)] = $1.00\cdot10^{-3}$ M, [NaOH] = $1.00\cdot10^3$ M

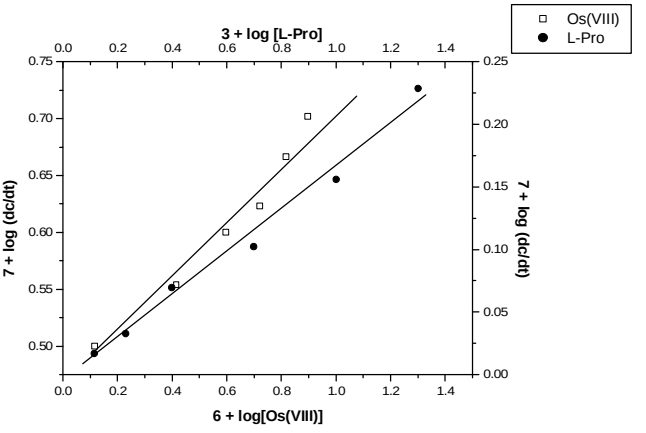

Fig. 4. Plot between rate log[Os(VIII)] *vs.* log(dc/dt) and log[L-Pro] *vs.* log(dc/dt) for oxidation of L-Pro at 308 K

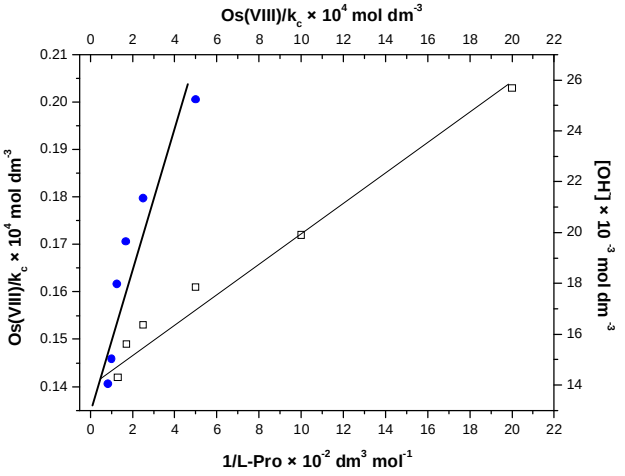

Fig. 5. Verification of rate law (5) in form of (6) for Os(VIII) catalyzed oxidation of L-proline by sodium periodate at 298 K

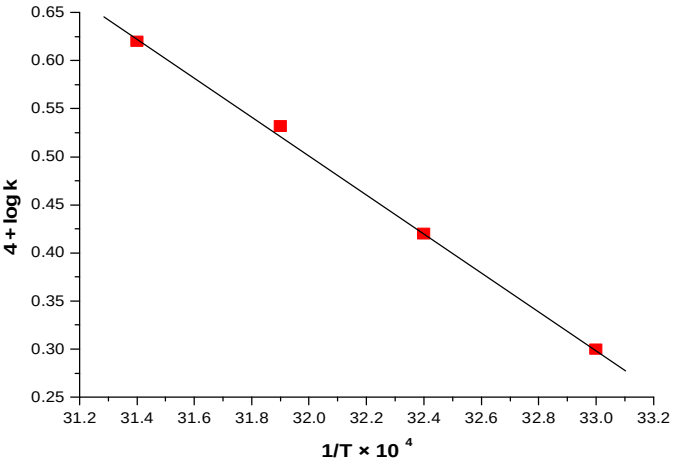

Fig. 6. Effect of temperature on rate constant for oxidation of L-Pro at 308 K. $[NaIO_4] = 1.0 \cdot 10^{-3}$ mol·dm^{-3}; [L-Pro] = $1.0 \cdot 10^{-2}$ mol·dm^{-3}; Os(VIII) = $2.6 \cdot 10^{-6}$ mol·dm^{-3}; [NaOH] = $1.0 \cdot 10^{-3}$ mol·dm^{-3}; $[Hg(OAc)_2] = 1.25 \cdot 10^{-3}$ mol·dm^{-3}

Table 2

Activation parameters for Os(VIII) catalyzed oxidation of L-Proline by $NaIO_4$ in alkaline medium at 303–318 K

Parameters	Temperature, K	L-Proline
$k_1 \cdot 10^4$ s^{-1}	303	1.96
$k_1 \cdot 10^4$ s^{-1}	308	2.44
$k_1 \cdot 104$ s^{-1}	313	3.90
$k_1 \cdot 10^4$ s^{-1}	318	3.56
log*A*	–	14.45
E_a*, kJ·mol^{-1}	308	82.93
Δ*G**, kJ·mol^{-1}	308	71.83
Δ*H**, kJ·mol^{-1}	308	80.35
Δ*S** , J·K^{-1}·mol^{-1}	308	-6.61

Notes: Os(VIII) = $2.63 \cdot 10^{-6}$ M, $[NaIO_4] = 1.00 \cdot 10^{-3}$ M, L-Proline = $1.00 \cdot 10^{-2}$M, $[Hg(OAc)_2] = 1.25 \cdot 10^{-3}$ M, [NaOH] = $1.00 \cdot 10^{-3}$M.

3.4. Effect of Alkali Concentration

At a fixed ionic strength of 0.5 mol·dm^{-3} and other conditions remaining constant, [OH$^-$] was varied from 0.083 to 0.50 mol·dm^{-3}. It was noticed that as [OH$^-$] decreases the rate of reaction was increased (Table 1). The plot of log[OH$^-$] *vs.* log*dc*/*dt* was linear (Fig. 5). Its decreasing effect on rate is due to the variation of concentration of hydroxide species of Os(VIII) at different [OH$^-$]. The various forms of hydroxide complexes in alkaline medium such as $[OsO_3(OH)_3]^-$, $[OsO_4(OH)_2]^{2-}$, and $[OsO_5(OH)]^{3-}$ are in equilibrium with each other.

3.5. Effect of Temperature

The effect of temperature on the reaction rate was studied within the range of 303–318 K and keeping all the other parameters at constant values. The *dc*/*dt* values increased with the increase in the temperature. Plots of 1/*T versus* [4+log*K*] at different temperatures were linear (Fig. 6). Thermodynamic activation parameters, associated with k_2K_1, were calculated using a least-squares fit to the transition state theory equation as, $\Delta H^* = 69.0$ kJ·mol^{-1} and, $\Delta S^* = -21.42$ J·K^{-1}·mol^{-1} (Table 2). Both ΔH^* and ΔS^* are composite values that include formation of the precursor intermediate complex and the intramolecular electron transfer step. The reaction was endothermic as indicated from the positive value of ΔH^*, and the intermediate was rigid as indicated from the negative value of the entropy of activation (ΔS^*).

3.6. Catalytic Activity

The variation of concentration of Os(VIII) with alkali (as shown in Fig. 2) indicates that $[OsO_4(OH)_2]^{2-}$ is the reactive species; its concentration was varied linearly

with [OH-]. The concentrations of the other two species, $[OsO_5(OH)]^{3-}$ and $[OsO_3(OH)_3]^-$ are either decreased or increased drastically with various $[OH^-]$ and are not varied parallel to the variation of *dc*/*dt* for different $[OH^-]$. Hence, they are not considered as reactive species. The formation of $[OsO_4(OH)_2]^{2-}$ is important in this study as reported earlier [19]. Each fractional order in [OH-] and [L-proline] is an implicit fact to support the expectation of the pre-equilibrium before rate determining step. First-order in oxidant and catalyst can also be accommodated in the mechanism as shown in Scheme 1. Hence, the scheme is written in accordance with the above facts and the consideration of active species of Os(VIII) in alkali as $[OsO_4(OH)_2]^{2-}$ in the first equilibrium step.

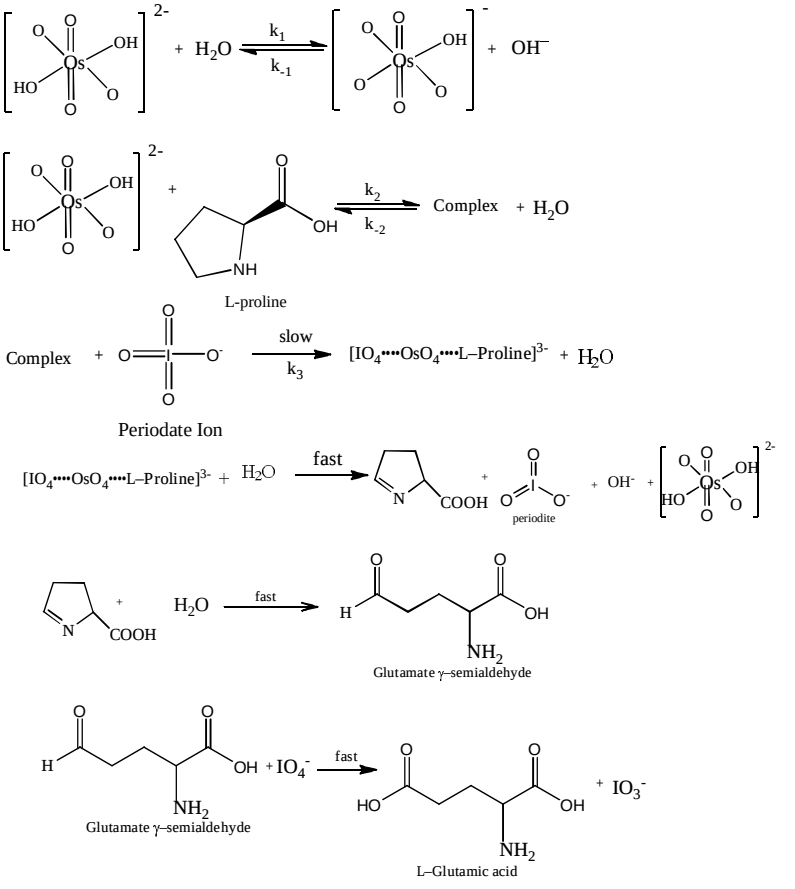

Scheme 1

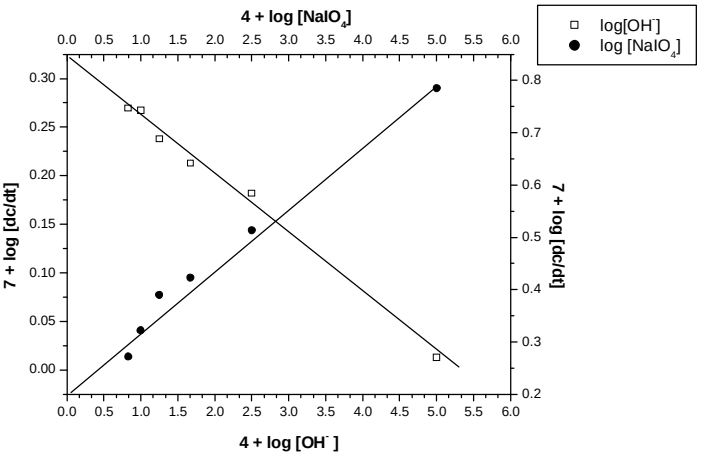

Fig. 7. Plot between log $[OH^-]$ *vs*. log(*dc*/*dt*) and log$[NaIO_4]$ *vs*. log(*dc*/*dt*) for oxidation of L-Pro at 308 K

The Lineweaver-Burk plot proved the complex formation between Os(VIII) and L-Pro, which explains fractional order in [L-Pro]. The rate law for Scheme 1 is derived as,

$$Rate = \frac{d[IO_4^-]}{dt} \quad (3)$$

$$Rate = \left\{ \frac{k_3 K_2 [IO_4^-][Os(VIII)_T] \cdot [L-pro]}{1 + K_1[OH^-] + K_2[L-pro]} \right\} \quad (4)$$

$$k = \frac{Rate}{[IO_4^-]} = \left\{ \frac{k_3 K_2 [Os(VIII)_T] \cdot [L-pro]}{1 + K_1[OH^-] + K_2[L-pro]} \right\} \quad (5)$$

$$\frac{[Os(VIII)_T}{k} = \frac{1}{k_3 K_2 [L-pro]} + \frac{K_2[OH^-]}{k_3 K_2 [L-pro]} + \frac{1}{k_3} \quad (6)$$

The rate law (5) can be rearranged to Eq. (6), which is suitable for verification.

Eq. (6) proves that, the plots of [Os(VIII)]/*k vs.* 1/[L-pro] and [Os(VIII)]/*k vs.* [OH^-] were linear (Fig. 7). L-proline has two donor atoms, namely N from imino moiety and O from the carboxylic group, having a lone pair of electrons. It is a known [20] fact that N is a small potent atom and can donate a pair of electrons to the central metal ion of Os(VIII) to form an adducts. The presence of two $–CH_2$ groups on either side of the N atom favours the positive charge on the N atom and makes it easy to form the complex. Thus, formation of a complex between Os(VIII) and O atom of carboxylic group can be ruled out. The adduct formed in this way with N might be very reactive and undergoes oxidation easily by $NaIO_4$. This is evidenced by the fact that in the absence of Os(VIII), the reaction between L-proline and $NaIO_4$ was not observed. Therefore, the intermediate as shown in the second step of Scheme 1 reacts with $NaIO_4$ in the rate-determining step to give an intermediate from L-proline. This justifies the unit order each in oxidant and catalyst. The mechanism as in Scheme 1 and rate law are verified by plotting the graphs of log[OH-] and log[L-proline] *vs.* log*dc*/*dt* which should be linear (Figs. 4, 5). From the slopes and intercepts of such plots, the values of *k*, K_1, and K_2 are calculated. The K_1 found in this study is in close agreement with the reported value [19]. This justifies the formation of $[OsO_4(OH)_2]^{2-}$.

A negative value of ΔS^* (-6.61 $J \cdot K^{-1} \cdot mol^{-1}$) suggests that the two ionic species combine in rate determining step to give a single intermediate complex which is more ordered than the reactants [21, 22]. The smaller rate constant of the slow step of the mechanism indicates that the oxidation presumably occurs through an inner-sphere mechanism. This conclusion was supported by earlier reports [23-25].

4. Conclusions

Thus, in the oxidation of L-proline by $NaIO_4$ in alkaline media, it has been found that $NaIO_4$ itself is the main oxidizing species, and the conjugate base of L-proline is the main reducing species and the reaction was first-order dependent on both [proline] and [$NaIO_4$]. L-glutamic acid was identified as the final oxidation product. Oxidation of L-proline was set-up to mimic the biological path. The reaction product was found to be L-glutamic acid. However, earlier studies reveal that the products were 4-amino butyric acid [3], 4-amino butaraldehyde [26], and keto acids [27]. The 4-amino butaraldehyde is the most unpredictable product, as L-proline oxidizes through a pyrrolidine ring cleavage without decarboxylation. If aldehyde is formed at all, it would be glutamic semialdehyde. In the absence of Os(VIII), the reaction between L-proline and $NaIO_4$ is almost imperceptible, whereas the addition of a small amount of Os(VIII) favours the spontaneity of the reaction. This might be the reactive species of adduct, which is formed by interacting L-proline with Os(VIII).Though Os(VIII) is used as a catalyst it did not undergo reduction to Os(VI), but it catalyzes through the formation of active adduct and regenerates in the rate determining step by reacting with NaOH.

Appendix: Derivation of Rate Law for Scheme 1

$[Os(VIII)]_T$ is equal to the sum of concentrations:

$$\frac{d[IO_4^-]}{dt} = Rate = k_3[IO_4^-][Complex] \quad (1)$$

$$Os(VIII)_T = [C_1] + [C_2] + [Complex] \quad (2)$$

$$\frac{d[C_1]}{dt} = -k_1[C_1][OH^-] + k_{-1}[C_2] - $$

$$- k_2[C_1][L-pro] + k_{-2}[Complex] \quad (3)$$

On applying steady state approximation to Eq. (3) we get:

$$-k_1 C_1[OH^-] + k_{-1}[C_2] -$$

$$- k_2[C_1][L-pro] + k_{-2}[Complex] = 0 \quad (4)$$

Similarly we have the rate of formation of [C_2]:

$$\frac{d[C_2]}{dt} = k_1[C_1][OH^-] - k_{-1}[C_2] \quad (5)$$

On applying steady state approximation to the above equation we get:

$$k_1[C_1][OH^-] - k_{-1}[C_2] = 0 \quad (6)$$

$$[C_2] = \frac{k_1[C_1][OH^-]}{k_{-1}} \quad (7)$$

From Eqs. (4) and (6) we get:

$$[C_1] = \frac{k_{-2}[Complex]}{k_2[L-pro]} \quad (8)$$

Putting the value of $[C_1]$ in Eq. (7) we get:

$$[C_2] = \frac{k_1 k_{-2}[OH^-][Complex]}{k_{-1}k_2[L-pro]}$$

$$[C_2] = \frac{K_1[OH^-][Complex]}{K_2[L-pro]} \quad \left\{\mathbf{Q}\, K_1 = \frac{k_1}{k_{-1}};\ K_2 = \frac{k_2}{k_{-2}}\right\} \quad (9)$$

Thus from Eqs. (2), (8) and (9) we get total concentration of the catalyst, *i.e.*

$$Os(VIII)_T = \frac{[Complex]}{K_2[L-pro]} + \frac{K_1[OH^-][Complex]}{K_2[L-pro]} +$$

$$+[Complex] = \quad (10)$$

$$= [Complex]\left\{\frac{1+K_1[OH^-]+K_2[L-pro]}{K_2[L-pro]}\right\}$$

$$[Complex] = \left\{\frac{K_2[L-pro][Os(VIII)_T]}{1+K_1[OH^-]+K_2[L-pro]}\right\} \quad (11)$$

$$Rate = \left\{\frac{k_3 K_2[HIO_4^-][Os(VIII)_T][L-pro]}{1+K_1[OH^-]+K_2[L-pro]}\right\} \quad (12)$$

The rate law is in agreement with all observed kinetics.

References

[1] Nelson D., Cox M.: Lehninger Principles of Biochemistry, 4th edn. W.H. Freeman and Co., New York 2007.
[2] Hiremath C., Kiran T., Nandibewoor S.: J. Mol. Catal. A., 2006, **248**, 163. https://doi.org/10.1016/j.molcata.2005.12.018
[3] Seregar V., Hiremath C., Nandibewoor S.: J. Phys. Chem., 2006, **220**, 615. https://doi.org/10.1524/zpch.2006.220.5.615
[4] List B., Lerner R., Barbes C.: J. Am. Chem. Soc., 2000, **122**, 2395. https://doi.org/10.1021/ja994280y
[5] Das A.: Coord Chem., 2001, **213**, 307. https://doi.org/10.1016/S0010-8545(00)00376-3
[6] Srivastava S., Patel R.: World J. Pharm. Pharm. Sci., 2014, **3**, 365.
[7] Gupta M., Srivastava S.: Bull. Catal. Soc. India, 2015, **14**, 1.
[8] Vijayasri K., Rajaram J., Kuriacose J.: J. Chem. Sci., 1985, **95**, 573.
[9] Duk F.: J. Am. Chem. Soc., 1947, **69**, 3054. https://doi.org/10.1021/ja01204a038
[10] Buistc G., Bunton A., Hipperson W.: J. Chem. Soc. B, 1971, 2128. https://doi.org/10.1039/J29710002128
[11] Maros L., Molnar-Perel I., Schissel E., Szerdahelyi V.: J. Chem. Soc. Perkin Trans., 1980, **11**, 39. https://doi.org/10.1039/P29800000039
[12] Dahlgre G., Reed K.: J. Am. Chem. Soc., 1967, **89**, 1380. https://doi.org/10.1021/ja00982a018
[13] Rao M., Sethuram B., RaoN.: J. Indian Chem. Soc., 1980, **57**, 149.
[14] Rao D., Sridevi M., Vani P.: Indian J. Appl. Res., 2013, **3**, 585.
[15] Mendham J., Denney R., Barnes J., Thomas M.: Vogel's Text Book of Quantitative Chemical Analysis, 6th edn. Pearson Education, Delhi 2003.
[16] Tuwar S., Nandibewoor S., Raju J.: Trans. Met. Chem., 1991, **16**, 430. https://doi.org/10.1007/BF01129458
[17] Feigl F.: Spot Tests in Organic Analysis. Elsevier, New York 1975.
[18] Nelson D., Cox M.: Lehningers, Principles of Biochemistry, 4th edn. Freeman and Co., New York 2007.
[19] Wilson K., Walker J.: Practical Biochemistry, 5th edn. Cambridge University Press, Cambridge 2005.
[20] Devendra M., Gupta Y.: J. Chem. Soc., Dalton Trans., 1977, 1085. https://doi.org/10.1039/DT9770001085
[21] Sethuram B.: Some Aspects of Electron Transfer Reactions Involving Organic Molecules. Allied Publ. Ltd., Mumbai 2003.
[22] Laidler J.: Chemical Kinetics, 3rd edn. Pearson Education Ptc. Ltd., New Delhi 2004.
[23] Upadhyay S., Agrawal M.: Indian J. Chem., 1977, **15A**, 709.
[24] Sutin N.: Annu. Rev. Phys. Chem., 1966, **17**, 119. https://doi.org/10.1146/annurev.pc.17.100166.001003
[25] Lancaster M., Murray R.: J. Chem. Soc. A, 1971, 2755. https://doi.org/10.1039/J19710002755
[26] Martinez M., Pitarque M., Eldik R.: J. Chem. Soc., Dalton Trans., 1996, 2665. https://doi.org/10.1039/dt9960002665
[27] Shettar R., Hiremath M., Nandibewoor S.: Electron. J. Chem., 2005, **9**, 91.
[28] Upadhyay S.: Int. J. Chem. Kinet., 1983, **15**, 669. https://doi.org/10.1002/kin.550150708

Received: March 05, 2018 / Revised: March 28, 2018 / Accepted: August 30, 2018

КІНЕТИКА ОКИСНЕННЯ 2-ПІРОЛІДИНКАРБОНОВОЇ КИСЛОТИ В ПРИСУТНОСТІ КАТАЛІЗАТОРА Os(VIII) В ЛУЖНОМУ СЕРЕДОВИЩІ З ВИКОРИСТАННЯМ ПЕРІОДАТУ НАТРІЮ: МЕХАНІСТИЧНИЙ ПІДХІД

Анотація. *Проведено кінетичні та механічні дослідження окиснення 2-піролідинкарбонової кислоти, періодатом натрію (NaIO4) в лужному середовищі в діапазоні температур 303–318 K в присутності каталізатора Os(VIII). Визначено, що реакція є першого порядку відносно Os(VIII) та періодату. Спостерігається позитивний ефект відносно субстрату, тобто 2-піролідинкарбонової кислоти, негативний вплив на $[OH^-]$ і незначний вплив $Hg(OAc)^2$ та йонної сили середовища. Встановлено стехіометрію реакції між періодатом натрію та 2-піролідинкарбоновою кислотою в лужному середовищі (2:1). З використанням констант швидкості за різних температур розраховано енергію активації. Запропоновано механізм, що передбачає утворення комплексу між каталізатором, субстратом та оксидантом. Хроматографічними та спектроскопічними методами визначено, що основним продуктом окиснення є L-глутамінова кислота. На підставі кінетичних даних, стехіометрії та аналізу продуктів реакції запропоновано можливий механізм реакції. На основі отриманих кінетичних даних виведені кінетичні рівняння.*

Ключові слова: *кінетика, Os(VIII), окиснення, 2-піролідинкарбонова кислота, періодат натрію, лужне середовище.*

Chem. Chem. Technol., 2019,
Vol. 13, No. 3, pp. 334–340

Chemistry

MOLECULAR MODELLING OF ACRIDINE OXIDATION BY PEROXYACIDS

Volodymyr Dutka[1, *], Yaroslav Kovalskyi[1], Olena Aksimentyeva[1], Nadia Tkachyk[1], Nataliia Oshchapovska[1], Halyna Halechko[1]

https://doi.org/10.23939/chcht13.03.334

Abstract. The optimal geometric structure and reactivity of some peroxyacids, acridine and products of their interaction were calculated by quantum-chemical methods. It was found that the heat of formation of peroxyacids (PA) and carboxylic acids (CA) grow with increasing length of a hydrocarbon radical. The dependencies of the area of PA and molecules of CA on the number of carbon atoms in the molecules are linear. The potentials of ionization of all studied PA are close and lie within the range of 11.22–11.39 eV depending on the calculation methods. The theoretically calculated dipole moments of acids, acridine, peroxyacids, and *N*-oxide of acridine are in good accordance with experimental values, which indicate the correctness of our calculations. Theoretical calculated values of the heats of formation (ΔH_f^0) of peroxyacids and acridine are in good accordance with the values obtained by thermo-chemical methods. Calculations indicate that the size of the hydrocarbon radical practically does not affect the value of ΔH^0_{exp}. The results of quantum chemical calculations for the oxidation reaction of acridine may be useful for prediction of other mechanisms of oxidative processes.

Keywords: peroxyacids, quantum-chemical calculations, oxidation, acridine, heat of formation.

1. Introduction

Organic peroxy-compounds are widely used as a source of free radicals, oxidizing agents, intermediates in organic synthesis, disinfectant agent, *etc*. [1-3]. Peroxyacids interact with sulfides, amines, ethylene hydrocarbons, demonstrate mild oxidative effect, and give valuable products.

The information about the structure and electronic properties of molecules is important for successful application of peroxide compounds. Quantum-chemical calculations are used for this. We can predict the reactivity, calculate the thermodynamic parameters and the optimal structure of peroxide compounds using them [4, 5].

The aim of our work was quantum-chemical calculations for the reaction of acridine oxidation by peroxyacids. Often, these reactions are used to produce *N*-oxides. Oxidation reactions of nitrogen-containing compounds by different oxidants allow receiving different conducting polymers [6, 7], biologically active compounds [8, 9] and apply these processes to neutralize substances harmful to the environment [10].

2. Experimental

The results of the theoretical calculations using quantum chemical methods are shown in this work. These are standard heats of formation (ΔH_f^0), ionization potential (I_X), energy of higher occupied molecular orbital (HOMO) and a lower unoccupied molecular orbital (LUMO), dipole moments (D), volume (V) and area (S) of molecules of certain peroxyacids (PA), carboxylic acids (CA), acridine and its *N*-oxides.

Chemical potential (μ) and rigidity of the molecule (η) were calculated by the energy of higher occupied molecular orbital (E_{HOMO}) and a lower unoccupied molecular orbital (E_{LUMO}):

$$\mu = (E_{\text{HOMO}} + E_{\text{LUMO}})/2; \text{ and } \eta = (E_{\text{HOMO}} - E_{\text{LUMO}})$$

As is known, the frontier orbitals method, proposed by Fukui, identifies the relative reactive activity of the compounds by the energy of the molecular orbitals of E_{HOMO} and E_{LUMO} [11, 12]. The E_{HOMO} causes the interaction of the molecule with the electron acceptors, and the E_{LUMO} – electron donors. The positive energy of E_{LUMO} causes the nucleophile properties of the molecules, and the negative – the electrophilic ones.

All quantum-chemical calculations were carried out using semi-empirical methods implemented in the program MOPAC2016 [13] and using the graphical interface Winmostar [14]. The calculations were carried out using the methods AM1, PM3, PM6, PM7, MNDO, and RM1. All calculations were conducted for the gas phase. Based on the performed calculations, the heats of the reaction were obtained, and the possible mechanism of the reaction was predicted.

[1] Ivan Franko National University of Lviv,
6, Kyryla&Mefodia St., 79005 Lviv, Ukraine
[*] *vdutka@ukr.net*

3. Results and Discussion

Calculations for peroxyacids (PA) of the general formula:

R–C(O)–O–O–H

were carried out, were R is equal to: CH_3– (**I**); CH_3–CH_2– (**II**); CH_3–$(CH_2)_2$– (**III**); CH_3 –$(CH_2)_4$– (**IV**); CH_3–$(CH_2)_5$– (**V**); CH_3–$(CH_2)_6$– (**VI**); CH_3–$(CH_2)_7$– (**VII**); CH_3–$(CH_2)_8$– (**VIII**); C_6H_5– (**IX**).

Physico-chemical parameters were calculated for the studied peroxyacids using semiempirical method AM1. They are presented in Table 1.

The heats of formation of peroxyacids coincide with the results of thermo-chemical data. Quantum-chemical calculations for peroxybenzoic acid (PBA) and benzoic acid (BA) were different from the corresponding values for aliphatic peroxyacids and their corresponding carboxylic acids.

The heat of formation of peroxyacids (PA) and carboxylic acids (CA) grow with increasing length of a hydrocarbon radical. The numerical values of the heat of formation and dipole moments of the PA and CA, with different number of carbon atoms in molecules (*N*) are given in Tables 2 and 3.

Table 1

Physico-chemical parameters of peroxyacids. Calculation method - AM1

Parameters	Peroxyacids								
	I	**II**	**III**	**IV**	**V**	**VI**	**VII**	**VIII**	**IX**
$-\Delta H_f^0$, kJ/mol	298.69	324.48	352.91	410.16	436.30	462.32	496.69	516.70	152.26
D, Debye	2.443	2.515	2.573	2.607	2.658	2.396	2.675	2.567	3.241
E_{HOMO}, eV	-11.383	-11.258	-11.274	-11.247	-11.236	-11.089	-11.022	-10.999	-10.239
E_{LUMO}, eV	0.589	0.640	0.635	0.637	0.649	0.941	0.648	0.657	-0.671
μ, eV	-5.986	-5.307	-5.319	-5.303	-5.294	-5.074	-5.187	-5.171	-5.455
η, eV	11.997	11.898	11.872	11.873	11.885	12.030	11.670	11.674	9.568
S, Å^2	102.9	121.7	141.6	181.9	201.7	217.1	241.8	255.6	162.2
V, Å^3	85.51	106.7	128.7	173.0	195.2	215.2	238.9	259.5	155.8

Table 2

The dependence of the heats of formation of aliphatic peroxyacids (ΔH_f^0, kJ/mol) and dipole moments (*D*) on number of carbon atoms (*N*) in a molecule, calculated using various semi-empirical methods

N	2	3	4	5	6	7	8	9	10
$-\Delta H_f^0$, AM1	298,69	324.48	352.91	381.92	410.16	439.30	462.32	496.69	516.72
$-\Delta H_f^0$, PM3	325.72	344.51	369.16	389.78	414.45	435.17	454.76	480.60	498.71
$-\Delta H_f^0$, PM6	283,39	300.12	322.06	342.73	362.91	384.45	403.94	426.21	–
$-\Delta H_f^0$, PM7	307.06	325.51	347.05	368.08	389.06	410.85	430.58	453.58	471.66
$-\Delta H_f^0$, RM1	321.03	342.19	363.88	384.66	403.48	426.44	441.90	468.21	479.92
$-\Delta H_f^0$, MNDO	309.67	331.44	351.29	371.05	390.90	410.55	424.66	450.07	460.83
$-\Delta H_f^0$, exp.	–	–	–	–	428.3	448.9	469.5	490.1	510.7
D, RM1	2.55	2.53	2.59	2.58	2.53	2.60	2.43	2.61	2.42
D, exp.	–	–	–	–	–	–	–	2.37	2.27

Table 3

The dependence of the heats of formation of aliphatic acids (ΔH_f^0, kJ/mol) and dipole moments (*D*) on the number of carbon atoms (*N*) in a molecule, calculated using various semi-empirical methods

N	2	3	4	5	6	7	8	9	10
$-\Delta H_f^0$, AM1	431.24	456.69	485.55	514.09	542.79	571.35	594.53	628.86	–
$-\Delta H_f^0$, PM3	426.51	445.32	467.94	490.48	513.27	535.96	555.43	581.35	–
$-\Delta H_f^0$, PM6	423.67	440.22	452.31	482.85	503.80	524.65	544.28	566.48	–
$-\Delta H_f^0$, PM7	427.79	445.53	468.51	489.35	510.95	532.28	550.68	575.01	596.36
$-\Delta H_f^0$, RM1	423.51	443.44	466.93	487.69	508.62	529.48	544.71	571.26	591.15
$-\Delta H_f^0$, MNDO	422.62	445.06	461.61	481.36	501.08	520.84	538.16	560.36	580.13
$-\Delta H_f^0$, exp.	433.0	455.8	475.9	491	512	536.5	554.5	575.6	624.2
D, RM1	1.766	1.766	1.755	1.72	1.75	1.73	1.86	1.73	1.954
D, exp.	1.77	1.75	1.58	1.74	–	–	–	–	–

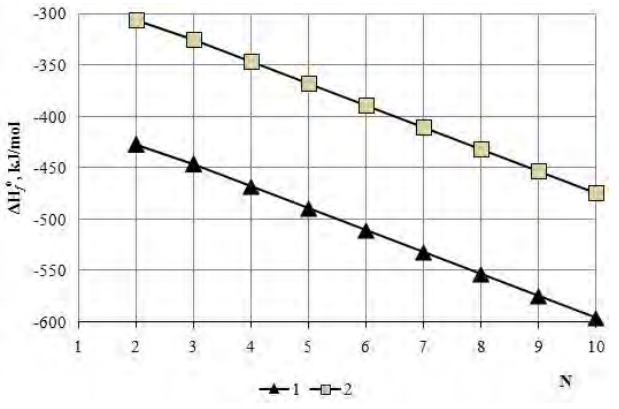

Fig. 1. The dependence of the heat of formation (ΔH_f^0) for carboxylic acids (1) and peroxyacids (2) on the number of carbon atoms (N) in molecules. Method of Calculation PM7

The dependencies of the heat of formation on the number of carbon atoms in molecule of peroxyacids or carboxylic acid calculated by different semiempirical methods are linear (Fig. 1). The numerical values of the heat of formation of peroxyacids or carboxylic acids with different values of N can be predicted with these dependencies.

The E_{HOMO} and E_{LUMO} are similar. Those characterize the oxidation-reducing properties of PA for compounds **I-VIII**. For peroxybenzoic acid, those differ slightly from the parameters for aliphatic peroxyacids. The parameters μ and η for peroxyacids **I-VIII** are almost the same (Table 1).

The numerical values of the areas and volumes of the compounds depend on their structure. The dependencies of the molecule area S of PA and CA on the number of carbon atoms in the molecules are linear. The difference between the areas of molecules of peroxyacid and carboxylic acid with the identical number of N calculated by various methods is within the range of 11.03–11.97 Å^2. This numerical value corresponds to the area of the oxygen atom in PA. Dependencies of volumes of molecules of PA and CA on the number of carbon atoms in molecules are linear too. The values of the volume of oxygen atom determined by the differences of PA and CA volumes are within the limits of 11.01–11.87 Å^3. The difference between the areas of PA containing N and N-1 atoms of carbon in the molecule will give the area of the CH_2 group in the investigated compounds. The numerical values of the CH_2 group area, depending on the calculation method, are within the range of 18.71–19.51 Å^2. The volumes of the CH_2 group are 21.25–22.04 Å^3. The potentials of ionization of all studied PA are close, and they are within the range of 11.220–11.389 eV depending on the calculation methods. Numerical values of I_X for carboxylic acids are similar to the values of PA and are changing within the limits of 11.054–11.492 eV.

The dipole moments of all studied PA and the structures of molecules of peroxyacids are similar. All PA in gas phase or in "inert" solvents form a compound with an intramolecular hydrogen bond (Fig. 2). Moreover, the hydrogen atom H(1) is bounding with oxygen of the carboxylic group O(5). The energy of hydrogen bond found based on the conformational analysis at the rotation of the OH group is 12.9 kJ/mol [15].

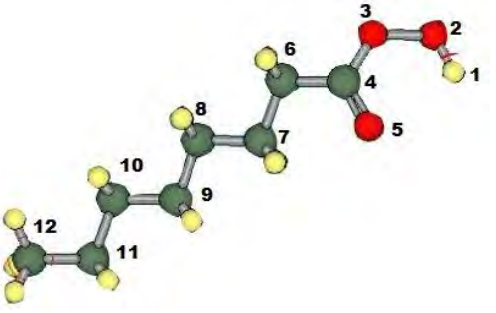

Fig. 2. The optimal molecular structure of peroxyacid **VI**

The length of O–O bond, according to the quantum-chemical calculations, is 1.399 Å. The length of this bond determined from X-ray diffraction data of peroxynonanic acid is equal to 1.442 Å [16]. The length of bond of the carbonyl group is 1.231 Å and the results of the theoretical calculations provide the value of 1.229 Å. The C–O–O angle obtained as a result of X-ray diffraction is 112.0^o, whereas according to the quantum-chemical calculations it is 129.5^o. Thus, experimental values and results of theoretical studies are in agreement. Small differences can be explained by the fact that X-ray diffraction was conducted for crystalline specimens in a solid state, while quantum-chemical calculations were performed for a molecule in the gas phase.

Valuable information can be obtained by investigating the partial charges on the atoms of PA. Partial charges on atoms calculated by semiempirical quantum-chemical methods AM1 are presented in the Table 4.

The atom H(1) has a deficiency of electron density, which indicates its "acid" character. The acidity of PA is less than for the corresponding carboxylic acids. The values of pKa for peroxyacids are within the limits of 7.01–8.7 [17]. The partial charges are almost identical at atoms of oxygen in peroxide group. It should be noted that the partial charges on the oxygen atoms of O(2) and O(3) in molecules of hydroperoxide are different, unlike molecules of PA [18].

The attack on the reaction center in the reactions of electrophilic oxidation is performed by an oxygen atom O(2). This statement is true for reactions involving hydroperoxides [2]. The attack on a multiple bond or a nitrogen atom in the case of peroxyacids can be carried out by O(2) and O(3) atom. The carbonyl group in molecules of PA is strongly polarized (Table 6). A partial charge on all other atoms for the investigated PA does not change with the radical change near the peroxide group of the PA. The partial charges for the molecule of peroxybenzoic acid are different from the parameters calculated for all aliphatic PA.

The infrared spectra of the PA calculation allowed detecting the bands characteristic of these compounds. The characteristic band in the IR spectrum of the PA is the absorption at 3280 cm^{-1}, which corresponds to the absorption frequency of the OH group, bound by the intra-molecular hydrogen bond. In addition, the absorption band at 2000 cm^{-1} is observed in the spectrum. This corresponds to the oscillation of the group C=O of PA. The absorption band of the O–O bond in the theoretically calculated spectrum is observed at 1500 cm^{-1}. In the spectrum of the PDA solution in carbon tetrachloride, the absorption band of the peroxide bond is observed at the wavelength of 865 cm^{-1}. The absorption band at 3280 cm^{-1} corresponds to the absorption frequency of the OH-group associated with the intramolecular hydrogen bond, which coincides with the value theoretically calculated. The absorption band at 1760 cm^{-1} corresponds to the absorption of the carbonyl group C=O, whereas, for the calculated spectrum, the quantum-chemical absorption method is observed at 2000 cm^{-1}.

In our opinion, some discrepancy between theoretically calculated and experimentally calculated wavelengths in IR spectra can be explained by the fact that those theoretical calculations of IR spectra are carried out for an individual molecule in a vacuum, while experimental measurements were carried out in a solution of carbon tetrachloride. It should be noted that according to the obtained data; the intra-molecular hydrogen bond is characterized by considerable strength. Spectroscopic studies in the wavelength range from 4000 to 2500 cm^{-1} for solutions of PDA with different concentrations practically do not change the position and nature of absorption bands. The change in the PDA concentration from 0.0125 to 0.2 mol/l in a solution of carbon tetrachloride gives a proportional increase in the optical density of the 3280 cm^{-1} band. This suggests that at the moderate concentrations of the peroxyacid molecules exist in a monomer state with intramolecular hydrogen bonds [19, 20].

Quantum-chemical calculations for acridine (AN) and acridine *N*-oxide (OAN) were carried out by semi-empirical methods. Optimal geometric structures of acridine and acridine *N*-oxide are given in Fig. 3.

According to quantum-chemical calculations, the acridine and acridine-10-oxide molecules are flat. All flat angles in both molecules are 120°. The heat of formation of acridine and acridine-10-oxide and other parameters calculated by semiempirical methods AM1, PM3, PM7, RM1, and MNDO are given in Tables 5 and 6.

The calculated heats of formation of acridine are within the range from -213.17 to -299.61 kJ/mol. The value of ΔH_f^0 which was found *via* thermo-chemical method, is equal to -273.9±2.0 kJ/mol, and corresponds well to the values calculated theoretically. The theoretically calculated dipole moments of acids, acridine, peroxyacids, and *N*-oxide of acridine are in good agreement with experimental values [21], which may indicate the correctness of our calculations. The values of partial charges on atoms can give important information about the reactivity of the molecules. The results of such calculations are presented in Table 7.

Table 4

Partial charges on the peroxyacids atoms (by Mulliken)

Peroxyacid	Atom label						
	H(1)	O(2)	O(3)	C(4)	O(5)	C(6)	C(7)
I	0.203	-0.156	-0.166	0.335	-0.317	-0.223	–
II	0.202	-0.156	-0.170	0.322	-0.316	-0.158	-0.214
III	0.202	-0.157	-0.165	0.321	-0.317	-0.158	-0.159
IV	0.203	-0.156	-0.161	0.365	-0.325	-0.158	-0.158
V	0.201	-0.156	-0.168	0.325	-0.318	-0.159	-0.158
VI	0.202	-0.156	-0.170	0.323	-0.318	-0.157	-0.152
VII	0.202	-0.157	-0.165	0.321	-0.317	-0.158	-0.158
VIII	0.211	-0.137	-0.168	0.269	-0.325	-0.157	-0.156
IX	0.213	-0.166	-0.132	0.316	-0.330	-0.123	-0.067

Notes: Atom labels correspond to the numbers in Fig. 2. Calculation method AM1.

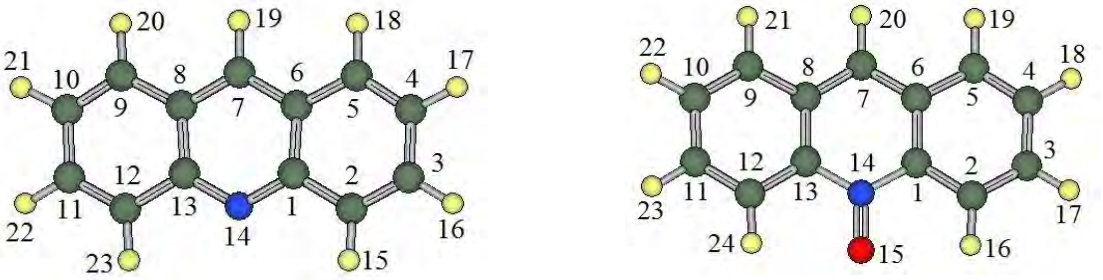

a) b)

Fig. 3. Optimal geometric structure of acridine (a) and its oxidation product – acridine-*N*-oxide (b)

Table 5

Physico-chemical parameters for acridine calculated using various semi-empirical methods

Parameter	Method of calculation				
	AM1	PM3	PM7	RM1	MNDO
$-\Delta H_f^0$, kJ/mol	297.59	268.91	299.61	260.96	213.72
D, Debye	1.681	1.681	1.456	1.871	1.595
E_{HOMO}, eV	-8.949	-8.974	-8.854	-8.719	-9.102
E_{LUMO}, eV	-0.604	-0.807	-1.232	-0.175	-0.394
μ, eV	-4.777	-4.891	-5.044	-4.447	-4.748
η, eV	8.345	8.167	7.622	8.532	8.708
S, Å^2	209.32	208.90	209.38	208.67	212.04
V, Å^3	215.07	214.44	215.51	214.10	218.76
I_X, eV	8.949	8.974	8.854	8.719	9.102

Table 6

Physico-chemical parameters for acridine-*N*-oxide calculated using various semi-empirical methods

Parameter	Method of calculation				
	AM1	PM3	PM7	RM1	MNDO
$-\Delta H_f^0$, kJ/mol	288.64	242.73	251.31	217.48	240.36
D, Debye	3.149	3.376	2.82	3.092	2.955
E_{HOMO}, eV	-8.751	-8.882	-8.516	-8.489	-8.898
E_{LUMO}, eV	-0.115	-0.365	-0.796	-0.049	-0.022
μ, eV	-4.433	-4.259	-4.656	-4.369	-4.460
η, eV	8.636	8.517	7.49	8.440	8.876
S, Å^2	215.96	215.43	215.40	215.12	219.15
V, Å^3	225.82	225.49	225.39	225.04	230.08
I_X, eV	8.75	8.593	8.516	8.489	8.898

Table 7

Partial charges on the atoms (by Mulliken) of the studied molecules of acridine and acridine *N*-oxide

Atom label	Acridine	Acridine-*N*-oxide	Atom label	Acridine	Acridine-*N*-oxide
1C	0.003	-0.026	8C	-0.066	-0.026
2C	-0.099	-0.105	9C	-0.116	-0.116
3C	-0.127	-0.123	10C	-0.123	-0.123
4C	-0.123	-0.123	11C	-0.127	-0.123
5C	-0.116	-0.116	12C	-0.099	-0.105
6C	-0.066	-0.026	13C	0.003	-0.026
7C	-0.095	-0.126	14N	-0.105	0.200
			15O	–	-0.350

Notes: The numbers of the atoms correspond to the numbers in Fig. 3. Method of calculation AM1.

Partial charges in the molecules of acridine and *N*-oxide of acridine for carbon atoms, which are in the identical positions, are almost identical. At the atom of nitrogen in the molecule of acridine, the partial charge is -0.105, and in the *N*-oxide of acridine, the corresponding value becomes positive and equal to 0.200. The oxygen atom in the *N*-oxide of acridine has a partial charge of -0.350, which indicates the polarization of the N–C bond.

The thermal effects of the reaction based on the quantum-chemical calculations were obtained. The scheme of oxidation reaction of acridine:

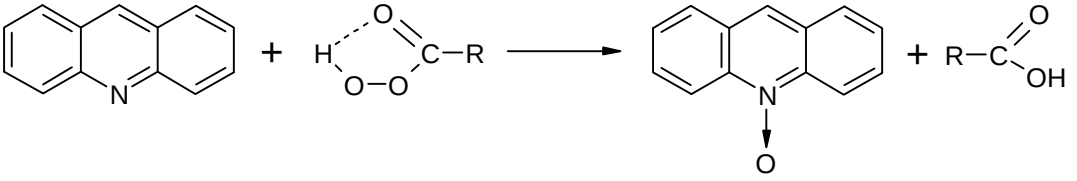

Table 8

The heat of formation of molecules and thermal effect of acridine oxidation by peroxydecanoic acid, calculated using different semiempirical methods

Method of calculation	The heat of formation of molecules ΔH_f^0, kJ/mol				Thermal effect of acridine oxidation ΔH_{exp}, kJ/mol
	Acridine	Peroxydecanoic acid	Decanoic acid	Acridine-*N*-oxide	
AM1	297.5	-516.7	-657.4	288.6	-149.6
PM3	268.9	-498.7	-604.2	242.7	-131.7
PM7	299.6	-471.6	-587.4	251.3	-164.1
RM1	260.9	-479.9	-587.4	217.4	-150.7
MNDO	213.7	-460.8	-592.2	240.3	-102.8
Thermo-chemical data	273.9±2	-509.4±2.2	-680.5	–	–

Table 9

Thermal effect of acridine oxidation by various peroxyacids, calculated using different semiempirical methods

Method of calculation	Thermal effect of acridine oxidation by various peroxyacids, $-\Delta H^0_{exp}$, kJ/mol								
	I	**II**	**III**	**IV**	**V**	**VI**	**VII**	**VIII**	**IX**
AM1	141.14	141.15	141.58	140.95	140.99	141.15	141.11	–	141.44
PM3	126.06	126.99	124.97	125.01	126.97	126.86	126.93	–	125.60
PM7	169.03	169.32	168.30	170.19	169.72	168.40	169.79	164.10	169.00
RM1	145.95	144.74	146.53	148.61	146.51	146.28	146.52	–	146.28

The heat of reaction of acridine by peroxydecanoic acid (PDA) using various methods calculated by the Hess equation is given in Table 8.

The numerical values of the heat of formation of PDA, decanoic acid and acridine well coincide with the corresponding values of ΔH_f^0 found thermo-chemically [22, 23]. The thermo-chemical data for *N*-oxide of acridine are absent in literature. According to quantum-chemical calculations, the numerical values of ΔH_f^0 are within the range of 217.4–288.6 kJ/mol. The reaction of oxidation of acridine is exothermic.

The thermal effect was calculated by different semiempirical methods. For this reaction, it is from -102.8 to -164.1 kJ/mol. The data on the thermal effects of the acridine oxidation by various peroxyacids, calculated using different semiempirical methods are presented in Table 9. Calculations indicate that the size of the hydrocarbon radical practically does not affect the value of ΔH^0_{exp}. Using the AM1 method, the numerical values of ΔH^0_{exp} are equal to 140.95–141.44 kJ/mol. In the case of use of peroxybenzoic acid as an oxidant, the thermal effect of the process is also -141.44 kJ/mol.

4. Conclusions

Quantum-chemical calculations allow to find the optimal geometric structure of molecules and predict the reactivity of peroxyacids. In our work, optimal geometric structures, the heats of formation of the starting compounds and the products of the reaction of acridine oxidation by peroxyacids were calculated. The obtained results can be considered reliable due to the good correspondence between the theoretical and calculated

values. The results of quantum chemical calculations for the oxidation reaction of acridine may be useful for prediction of other mechanisms of oxidative processes.

References

[1] Prylezhaeva E. (Ed.): Reaktsiya Prilezhaeva. Electrophil'noe Okislenie. Nauka, Moskva 1974.
[2] Tolstikov G. (Ed): Reaktsii Hydroperoksidnogo Okisleniya. Nauka, Moskva 1976.
[3] Antonovsky V., Khursan S. (Eds.): Phisicheskaya Khimiya Organicheskich Peroksidov. ICC "Akademkniga", Moskva 2003.
[4] Soloviev M., Soloviev M. (Eds.): Computernaya Khimiya. , Solon. Press, Moskva 2005.
[5] Clark T. (Ed.): A Handbook of Computational Chemistry. Wiley-Interscience, New York 1985.
[6] Blinova N., Stejkal J., Trchova M. *et al*.: Polymer, 2009, **50**, 50. https://doi.org/10.1016/j.polymer.2008.10.040
[7] Stejskal J., Gilbert R.: Pure Appl. Chem., 2002, **74**, 857. https://doi.org/10.1351/pac200274050857
[8] Dutka V., Matsyuk N., Dutka Yu.: Russ. J. Phys. Chem. A, 2011, **85**, 45. https://doi.org/ 10.1134/S0036024411010079
[9] Haynes A. (Ed.): Methods of Oxidation of Organic Compounds. Academic Press Inc., London 1985.
[10] Thomsen A.: Water Res., 1998, **32**, 136. https://doi.org/10.1016/S0043-1354(97)00200-5
[11] Parr R., Yang W.: Density-functional theory of atoms and molecules. Oxford University Press, New York 1989.
[12] Jasinski R., Baranski A.: J. Mol. Struc.-THEOCHEM, 2010, **949**, 8. https://doi.org/10.1016/j.theochem.2010.02.023
[13] Stewart J. (Ed.): Program Package MOPAC2016. http://www.openmopac.net
[14] Senda N. (Ed.): Program Package Winmostar. http://winmostar.com
[15] Dutka V., Derkach Y Savitska O. and Kovalsky Y.: Visnuk Lviv Nats. Univ., 2007, **48**, 166.
[16] Kitaigorodskii A., Zorkii P., Belskii V.: Stroenie Organicheskogo Veshchestva. Dannye Strukturnych Issledovanii 1929–1970. Nauka, Moskva 1980.
[17] Antonovsky V. (Ed.): Organicheskie Peroksidnye Initsiatory. Khimiya, Moskva 1972.
[18] Dutka V., Shchedry V., Gritselyak T., Kovalskyi Ya.: Visnuk Lviv Nats. Univ., 2013, **54**, 358.
[19] Shriner R., Fuson R., Curtin D. *et al*.: The Systematic Identification of Organic Compounds. A Laboratory Manual. John Wiley & Sons, NY-Toronto 1980.
[20] Zhukovskii V.: Russ. J. Phys. Chem., 1983, **57**, 2353.
[21] Osipov O., Minkin V. (Eds.): Spravochnik po Dipolnym Momentam. Vyschaja schkola, Moskva 1965.
[22] Lebedeva N.: Russ. J. Phys. Chem., 1964, **38**, 1435.
[23] Van-Chin-San Yu. *et al*. (Eds.): Thermodynamichni Vlactivosti Kysenvmisnykh Organichnykh Spoluk. Dovidnyk. NULP, Lviv 2012.

Received: March 19, 2018 / Revised: June 07, 2018 / Accepted: September 11, 2018

МОЛЕКУЛЯРНЕ МОДЕЛЮВАННЯ ОКИСНЮВАЛЬНОЇ РЕАКЦІЇ АКРИДИНУ ПЕРОКСИКИСЛОТАМИ

Анотація. *Квантово-хімічними методами розраховано оптимальну геометричну будову та реакційну здатність деяких пероксикислот, акридину та продуктів їхньої взаємодії. Встановлено, що теплота утворення пероксикислот (ПК) і карбонових кислот (КК) збільшується із підвищенням довжини вуглеводневого радикалу. Залежності площ молекул ПК та молекул КК від кількості атомів карбону в молекулах є лінійними. Потенціали йонізації всіх досліджених ПК близькі і знаходяться в діапазоні 11.22–11.39 еВ, залежно від методів розрахунку. Теоретично обчислені дипольні моменти кислот, акридинів, пероксикислот та N-оксидів акридину непогано узгоджуються з експериментальними значеннями, що вказує на правильність розрахунків. Теоретично обчислені значення теплоти утворення (ΔH_f^0) пероксикислот та акридину непогано узгоджуються зі значеннями, отриманими термохімічними методами. Розрахунки показують, що розмір вуглеводневого радикалу практично не впливає на величину ΔH^0_{exp}. Результати квантово-хімічних розрахунків для реакції окиснення акридину можуть бути корисними для прогнозування інших механізмів окиснювальних процесів.*

Ключові слова: *пероксикислоти, квантово-хімічні розрахунки, реакційна здатність окиснення, акридин, теплоти утворення.*

Chem. Chem. Technol., 2019,
Vol. 13, No. 3, pp. 341–346

Chemistry

STUDY OF IODINE OXIDE PARTICLES AT THE AIR/SEA INTERFACE IN THE PRESENCE OF SURFACTANTS AND HUMIC ACID

Salah Eddine Sbai [1, 2, *], ***Bentayeb Farida***[1]

https://doi.org/10.23939/chcht13.03.341

Abstract. In the present study, the formation procedure of iodine oxide particle (IOP) has been investigated in the presence of surfactants (nonanoic and stearic acids NA-SA) and humic acid (HA). It was established that iodine oxide which was mixed with the organic compounds (HA, NA and SA), and then irradiated with a xenon lamp leads to the formation of IOP. The evolution of formed particles number was followed by a scanning mobility particle sizer. Results obtained show that the number of particles decreases strongly in the presence of HA, NA and SA, this behavior is explained by the formation of organoiodine compounds.

Keywords: photochemistry, surfactants, iodine, particle, organoiodine.

1. Introduction

Photochemistry at the air/sea interface of halogens affects the chemical composition of the troposphere. Atmospheric chemistry of halogens is dominated by reactions between gas and aqueous phases species on ocean surfaces and marine aerosols [1]. It influences the oxidation capacity of the atmosphere by removing the great variety of organic and inorganic species, which are emitted by natural and anthropogenic sources, this occurs by the catalytic destruction of ozone and reactions with the important radical species (in particular the hydroxyl OH) which control the oxidation chemistry [2, 3]. The reactivity of iodine in the atmosphere and at sea level leads to the production of nanoparticles of iodine oxide (IOP). The production process of IOP involves the recombination reactions of the radicals IO and OIO to form oxides which then spontaneously condense forming particles [4, 5]. In the presence of moisture, these particles develop into clouds condensation nuclei (CCN), which would have an impact on the radiative balance of the atmosphere and therefore on the climate [6-11].

Some studies [12, 13] indicate the presence of a significant fraction of iodine soluble in marine aerosol in an organic form. The reaction mechanism between the dissolved organic matter (DOM) and the species aqueous HIO (hypoidic acid), which would recycle I^- in aerosols and also increase the release of I_2, in the gaseous phase and at the air/sea interface has already been studied [14]. This mechanism is highly dependent on pH. Humic acid (HA) is a diverse group of multifunctional organic compounds that are soluble in water at pH values above 4. It contains chromophores that participate in photosensitized chemical reactions in the presence of organic surfactants such as nonanouique acid (NA). The adsorption of the soluble reagents, such as O_3 and H_2O_2, of the gas phase on the aerosol surfaces will potentially lead to the oxidation of I^- directly to the aerosol of the seawater [15]. The release of these species into the atmosphere allows the recycling of iode to iodine I^- and iodine monoxide IO, which reacts actively with ozone and leads to the formation of iodine oxide particles (IOP) [16, 17]. The iodine oxide species IO_3^- is converted by a photochemical reaction with HA to the aqueous ionic form (I^-); this reaction is also showing the binding of the iodinated species to the humic acid, which influences the formation of marine particles. The spectroscopic analysis of iodate reactions with a number of compounds substituted with functional groups identified with structures of HA, were used to identify the chemical pathways and major species involved in the formation of non-volatile organic species containing iodine [15]. The reaction mechanism is likely to occur in the fixation of iodate on the HA and was, first of all, the absorption of visible light by the organic chromophores of HA, which leads to the generation of the solvated electrons, which are then captured by the iodate ion IO_3^-, which is considered as the species of the most active iodine in the formation of particles in the atmosphere. It is reduced to HOI which will produce the molecular iodine I_2 which reduces the number of IOP [15]. Iodate is accumulated in the marine aerosol by the adsorption of the species I_2O_3, I_2O_4 and I_2O_5 of the gas phase [18]. Most of the active chemistry of iodine in the gas phase takes place in the first 30 meters of the boundary

[1] Department of physics, Mohammed V University of Rabat,
4, Ave. Ibn Battouta B.P. 1014 RP, Rabat, Morocco
[2] University Lyon, University Claude Bernard Lyon 1, CNRS, IRCELYON,
2, Albert Einstein Ave., 69100 Villeurbanne, France
[*] *salaheddinechimie@gmail.com.*

layer [19]. Natural compounds containing bromine and iodine significantly reduce regional and global tropospheric ozone levels [20, 21]. These halogenated gases reduce the effects of global warming of ozone and hydrocarbons such as methane in the troposphere. Organic iodine compounds have been considered as the main source of oceanic iodine emissions. The reaction of ozone with iodide on the sea surface could represent about 75 % of the rates of iodine oxide observed in the tropical Atlantic Ocean [22].

According to several studies, the reaction of molecular iodine I_2 with DOM and the hypoiodic acid (HOI) with Cl^- and Br- leads to the decrease of the particle concentration in the atmosphere. Organic surfactants cause a decrease in I_2 gas emissions and reduce gas-air transfer rates which directly influence the number of particles emitted [23, 24]. Dissolved organic matter such as humic acid present on the surface of the sea [27], can be highly concentrated in the marine microlayer [26-28]. The presence of these complex and potentially photoactive compounds affects the mechanism of marine aerosols formation. Some researches [29-32] have studied organic enrichment in the marine microlayer in different regions of the ocean (subtropical, temperate, polar). They observed a much larger coverage than before and showed that the part of the oceans can be assumed to be completely covered by an organic layer of thickness 100 μm [33], especially C_9 carboxylic acids like NA during the autumn. The presence of these compounds affects the production mechanism of IOP. For this we decided to study the formation of IOP in the presence of DOM in the form of HA which is also considered as a photosensitizer, and in the presence of organic surfactants (NA, SA) which are ubiquitous in the marine environment. A very recent study [34] shows that photochemical halogenation of DOM may represent an important abiotic source of natural organoiodine compounds (OICs) in surface waters. The OICs were mainly in the region rich in alicyclic carboxylic molecules consisting of esterified phenolic compounds. The OICs could potentially have adverse health effects due to their relatively high cytotoxicity and genotoxicity [37]. Currently about 200 of natural OICs have been identified [38], most of them are produced in the marine environment.

The objective of this study is to highlight the effect of photosensitized organic films photochemistry at the air/sea interface on iodine oxide particles IOP, using fatty acids ubiquitous in the marine environment (NA, SA) as surfactants and HA as DOM and photosensitizer.

2. Experimental

Freshly prepared aqueous solutions of NaI (Sigma-Aldrich, purity ≥99.5 %) in ultrapure water (18 MΩ·cm) were used. HA solutions were prepared using a commercially available untreated form (Fluka). A small amount of solid was stirred in ultrapure water for 2–3 h, and then any undissolved material was filtered. The surfactant monolayer was prepared by adding a known concentration of either nonanoic acid or stearic acid to the solution by a micropipette. The pH value of the solution was raised to about 8 using sodium hydroxide solution. Humic acid was fully soluble under the slightly acidic conditions used in this study (pH > 4). We can assume that HA was evenly distributed in the reactor. The chemistry products used were: nonanoic acid (Alfa Aesar, 97 %) and humic acid (Fluka, technical grade, 97 %). Oxygen used for the generation of ozone was purchased from Linde (99.9991 %).

Solutions of iodate and HA were mixed and placed in the reactors (volume of 132 cm^3). The irradiation was carried out by a 1000 W xenon arc lamp (Oriel "Solar Simulator" without ozone). The lamp beam was optically filtered using a water filter to eliminate IR wavelengths and prevent heating of the solution. A mass of solar air filters the spectrum of the lamp in order to replicate the solar spectrum in the near UV-visible and a cut-off filter to eliminate one of the small outputs of the lamp at $\lambda < 310$ nm. The solution was continuously exposed to the filtered lamp beam during all experiments at room temperature (293 ± 1 K).

A flow of a carrier gas of 100 ml/min at atmospheric pressure was used during the experiments, which gave a residence time equal to 100 s. The reactor was washed twice with acetone and ethanol to remove all traces of organic compounds, thus avoiding any possible contamination.

Ozone was added directly to the reactor to facilitate oxidation of I to IO and formation of iodinated oxides. The production of iodine oxide particles (IOP) was initiated by the nucleation of these oxides in the gas phase, the size distribution of these nanoparticles was then measured using a scanning mobility particle sizer (SMPS) composed of a differential mobility analyzer (DMA, model 3081) coupled with a condensation particle counter (CPC, model 3776). Fig. 1 shows the diagram of our manipulation.

3. Results and Discussion

The photochemistry of surfactants (as NA) in the presence of a photosensitizer (HA) leads to the formation of unsaturated volatile organic compounds (VOCs) [39, 40] and the chemical transformation of NA, which leads to the formation of double bonds (*i.e*, removal of water). It also shows that the reaction is produced at the level of the surface microlayer (SML), which is defined as the tens to

hundreds of microns of the surface of the ocean from the surface of the Earth [41], it is enriched by DOM substances including HA that absorbs UV. According to several studies [40-42] photosensitized reactions initiated by a substance capable of absorbing the light (HA) and of transferring the energy towards the desired reagents (for example NA) at the air/sea interface, constitute a predominant process for the formation of VOC in the marine environment, that can react with ozone in the atmosphere and at the air/sea interface and produce secondary organic aerosols (SOA). However in the marine environment the presence of marine salts such as iodine, (NaI, 1 μM), which is considered as the key species that leads to the production of marine aerosols, interactions between iodine and fatty acids (HA, NA and SA) may affect the formation of marine aerosols. For this we studied the formation of IOPs in the presence of the humic acid (HA) as a photosensilizer and the nonanoic acid (NA) and the stearic acid (SA) as surfactants, we have noticed that the concentration of IOP iodine particles always decreases in the presence of these organic acids, moreover our experiments of these acids in the absence of iodine showed that the number of SOA particles does not exceed 200 #/cc (particles/cm^3) (Fig. 2).

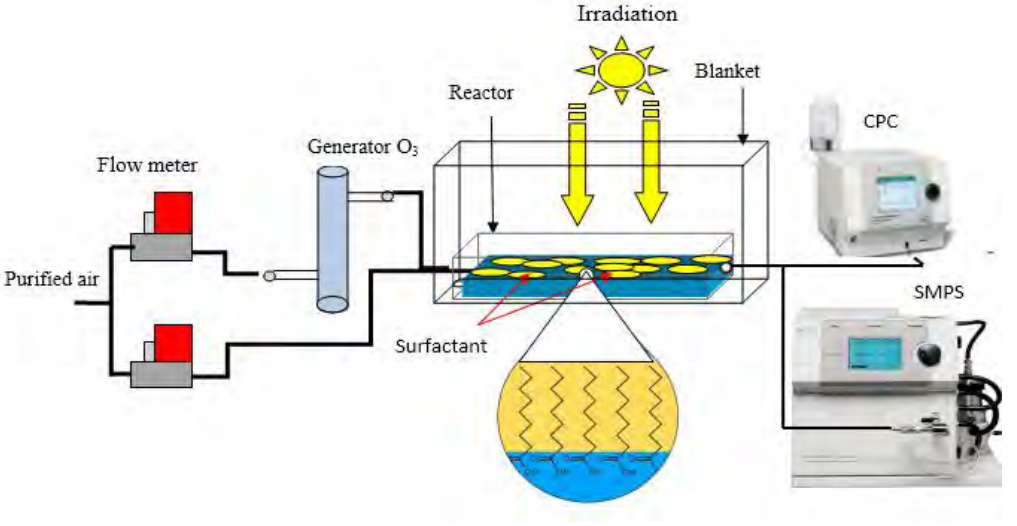

Fig. 1. Scheme of the multiphase atmospheric simulation reactor used for the investigation of photochemical processes at the air-sea interface

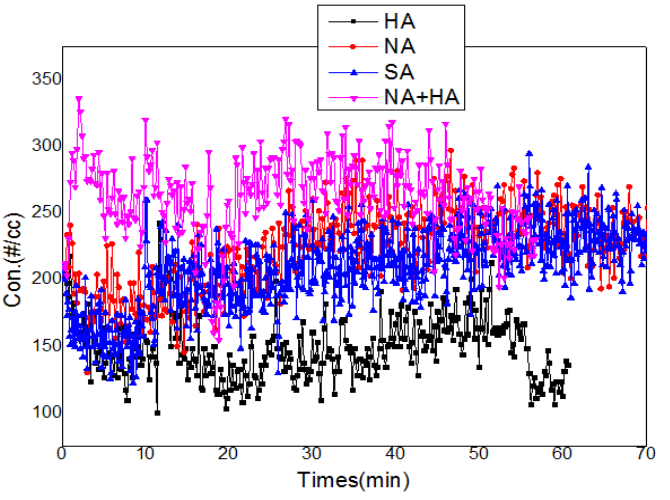

Fig. 2. Variation of the particles secondary organic aerosol (SOA) of HA, SA, NA and (HA+NA), in the presence of 20 ppb of ozone and under the effect of irradiation

The concentrations of SOA after the irradiation period were found in the range of 120–320 #/cc, they remain stable indicating that the presence of SOA as a background level will not affect our observations on the concentration of IOP.

Photolysis of NA in the presence of HA leads to the formation of VOCs such as saturated aldehydes (C_7-C_9), unsaturated aldehydes (C_6-C_9), alkanes (C_7-C_9), alkenes (C_5-C_9), and dienes (C_6-C_9). The reaction of these VOCs with ozone and OH radicals leads to the formation of SOAs. The mechanisms leading to the gas phase products observed in the presence of HA and NA have been described in detail by several studies [33]. They lead to the formation of saturated acids, unsaturated and saturated aldehydes which are very soluble in water. According to Henry's law, the solubility of non-oxygenated compounds is very low compared to that of oxygenates. A recent study was carried out in a simulation chamber in the presence of high concentrations of ozone (250–850 ppb), compared to those in the atmosphere (20–50 ppb) [33]. These fairly high ozone levels were used to compensate the low light intensity of UV lamps compared to solar radiation and the possible loss of reactive VOC on the chamber wall. However, the use of a high concentration of ozone can modify the reaction mechanism and leads to the ozonolysis and decarboxylation of organic acids by OH• radicals, producing a high number of SOA which is not our objective.

These problems make the work in the simulation chamber difficult under atmospheric conditions, and for this we used this reactor. The advantage of this reactor compared to the simulation chamber is that it is widely used for studying the aging phenomenon at the air/sea interface, has very short residence time (100 s) and background that does not exceed 20 #/cc.

The concentration of SOA found by photochemistry of NA in the absence of HA was almost similar to that found with the system NA-HA. The results obtained show that the photochemical processes of the NA-HA system are not a significant source of particles under these experimental conditions. When comparing these results with those obtained in the simulation chamber which shows the production of a high number of SOA particles (3060 #/cc) [33], we have checked whether they are particles that come from the reaction of VOCs produced by the system photochemistry (NA+HA) or by reactions of these with ozone and OH radicals. For this purpose we conducted a series of experiments with these organic compounds (NA, SA and HA) under the same conditions as those carried out in the simulation chamber [33]. For all the experiments the formation of particles started only after irradiation and addition of ozone (Fig. 3). The results obtained using NA (1 mM) alone with 800 ppb of ozone show that the number of IOP increases strongly after the irradiation from 10^2 to 810^3 #/cc, however the photochemistry of NA photosensitized by HA produces almost 10^6 #/cc. The difference between these results and those obtained by the surfactant alone is due to the reactions of VOCs produced by the system (NA-HA) with OH radicals and ozone.

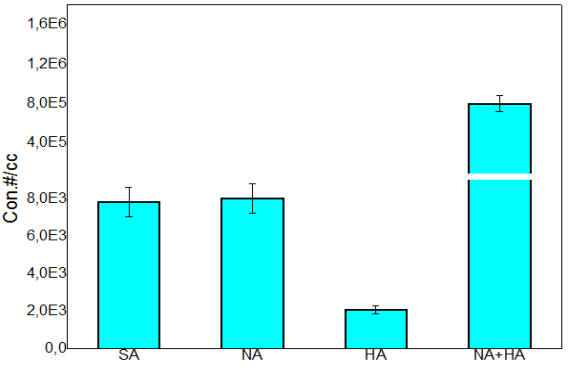

Fig. 3. Evolution of SOA concentration of in the presence of 800 ppb of ozone

It is well established that the OH radicals in an aqueous phase are generated by the absorption of light from humic substances but especially by the ozone photolysis [28-30]. Particle formation was only observed after irradiation and addition of ozone (Fig. 3). The results obtained using NA alone (1 mM) with 800 ppb of ozone shows that the number of IOPs after the irradiation strongly increases from 10^2 to 810^3 #/cc; NA photosensitized by HA produced nearly 10^6 #/cc. This difference is due to the reactions of the VOCs produced by the system (NA-HA) and OH radicals. NA is an effective sensor of OH radicals, and acting as an inhibitor of any secondary reaction of OH. These results show that the photochemistry of these organic acids under atmospheric conditions does not lead to the production of particles.

To study the effect of surfactants (NA, 1 mM) and organic matter (HA, 10 mg/l) on the mechanism of IOP formation we conducted a series of experiments with iodine (NaI, 1 mM) in the absence and in the presence of organic acids (NA, SA, HA) separated and mixed under atmospheric conditions (20 ppb O_3, 295 K, 1 atm), we noticed that the concentration of IOP decreased in the presence of surfactants (NA, SA) and the photosensitizer (HA). This shows that the concentration of the surface film, as well as the concentration of DOM in the volume, affect the formation of IOP (Fig. 4).

The concentration of IOP (iodine alone) decreased from $1.2 \cdot 10^6$ to $2 \cdot 10^3$ #/cc in the presence of organic matter (HA). This decrease is explained by the formation of organoiodines compounds (OIC_S) via halogenation reactions of iodine with humic acid and involves the important iodine gases such as CH_3I, CH_2I_2, $CHClI_2$ and CHI_3, which damage the atmospheric ozone layer. These gases are produced by abiotic mechanisms in natural environments [43,44]. Organoiodines compounds can also come from biotic pathways, in particular by nonspecific halogenation of dissolved organic matter, considering the covalent binding capacity of iodine to DOM [45].

The halogenation of DOM by photochemically generated reactive halogen species (RHS) contribute significantly to the formation of a much wider variety of OIC. Their molar masses vary between 178.916 ($C_7H_4IO_4$) and 713.1933 ($C_{30}H_{51}I_2O_3$), their structures depend on the type of reaction involved and the type of irradiation, as well as the water used (artificial fresh water or seawater) [34].

The mechanisms of the main reactions involved are as follows: firstly, the absorption of sunlight by DOM leads to the generation of reactive oxygen species (ROS) comprising the hydroxyl radical (OH), hydrogen peroxide (H_2O_2) and DOM triplet state (3DOM*) [46]. Then, iodide or IO_3^- were oxidized/reduced by DOM induced ROS to form reactive halogen species (RHS) [47, 48]. After that, RHS would react with DOM to form OCIs by addition to the unsaturated C=C bond, and recombination with carbon radicals and/or electrophilic substitution [49, 50]. The compounds formed are grouped into three categories according to the type of reaction: (i) substitution reaction (SR) between the reactive halogen species (RHS) and the organic matter (DOM); (ii) addition reaction (AR) between RHS and DOM; (iii) SR or AR accompanied by other reactions such as photooxidation (SAOR).

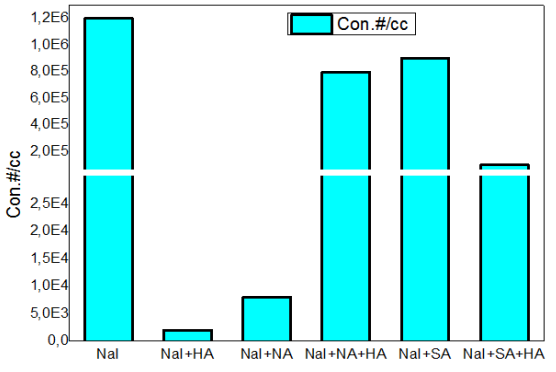

Fig. 4. Evolution of the IOP concentration in the presence and absence of surfactants (NA+SA) and the photososibilser HA

Effect of organic surfactants (NA, SA) on the formation of IOPs in the absence of DOM.

In the presence of NA as a surfactant, the number of IOP particles decreases from $1.2 \cdot 10^6$ to $8 \cdot 10^3$ #/cc even if the latter always remains on the surface. Such behavior is explained by the reaction of the VOCs produced by the photochemistry of surfactant NA with the iodinated species at the air/water interface and gas phase, whereas SA showed no effect. To explain these results, we have studied photochemistry of SA by TOF-PTR-MS. The results obtained show that there is no formation of VOCs, therefore the presence of SA did not affect the formation of IOP in contrast to NA which produces VOCs.

Effect of NA and SA organic surfactants on the formation of IOPs in the presence of DOM.

The addition of HA to the system (NA + NaI) led to a particle increase from $8 \cdot 10^3$ to $8 \cdot 10^5$ #/cc, which is explained by the reactions to the surfactant air/water interface and the photosensitizer. The same behavior is recorded in the presence of SA as the surfactant. These results show that the presence of an organic surfactant in the medium reduces the yield of organoiodine formation OIC_S which increases the concentration of IOP.

4. Conclusions

In this work, the formation of iodine particles in the presence of ubiquitous surfactants at the air/sea interface was studied for the first time. We found that the number of IOP decreased in the presence of surfactants (NA, SA) and dissolved organic matter. This behavior was explained by the formations of OIC. A strong production of IOP was observed during the irradiation of the reactor in the absence of DOM and the surfactants, whereas the release of IOP in the presence of these organic compounds remained rather moderate. The PTR-ToF-MS data gas phase SA shows that there is no formation of VOCs, which explains the difference between the results obtained using SA and NA. It should be noted that up to now, the mechanisms of production of IOP has been studied taking into account only the processes directly related to the photochemistry of marine salts as iodine. However, the presence of organic compounds at bulk or at the interface strongly affects the process, since iodine is captured by the latter. On the other hand, the results obtained by the photochemistry of surfactants (NA, SA) which lead to the emission of VOCs in the atmosphere, shows that the number of SOA is very low (200 #/cc) under these conditions. The increase in the concentration of ozone (*e.g.* 800 ppb) leads to a strong increase of SOA, for that we have to work with the atmospheric conditions, by simulating the photochemical reactions that can take place in the atmosphere.

Acknowledgements

This study was supported by the European Research Council under the Horizon 2020 Research and Innovation Program Project of the European Union under Convention N° 690958 (MARSU). The authors thank University Claude Bernard for the technical and financial support provided by the Institute for Research on Catalysis and the Environment of Lyon (IRCELYON).

We thank Mr. Christian George who participated during all the stages of preparation of this paper except the redaction.

References

[1] Shinichi E., Michael R.: J. Phys. Chem. A., 2016, **120**, 3578. http://doi.org/10.1021/acs.jpca.6b01261
[2] Simpson W., Brown S., Saiz-Lopez A. *et al.*: Chem. Rev., 2015, **115**, 4035. https://doi.org/10.1021/cr5006638
[3] Sbai S., Farida B.: Environ. Sci. Pollut. Res., 2019, 1. https://doi.org/10.1007/s11356-019-05012-5
[4] Sakamoto Y., Yabushita A., Kawasaki M., Enami S.: J. Phys. Chem., 2009, **113**, 7707. https://doi.org/10.1021/jp903486u
[5] Hayase S., Yabushita A., Kawasaki M. *et al.*: J. Phys. Chem., 2010, **114**, 6016. https://doi.org/10.1021/jp101985f
[6] Sayaka H., Akihiro Y., Masahiro K.: J. Phys. Chem. A, 2012, **116**, 5779. https://pubs.acs.org/doi/abs/10.1021/jp2048234.
[7] Saiz-Lopez A., Plane J.: Geophys. Res. Lett., 2004, **31**, L04112. https://doi.org/10.1029/2003GL019215
[8] Read K., Mahajan A., Carpenter L. *et al.*: Nature, 2008, **453**, 1232. https://doi.org/10.1038/nature07035
[9] Saiz-Lopez A., Chance K., Liu X. *et al.*: Geophys. Res. Lett., 2007, **34**, L12812. https://doi.org//10.1029/.2007GL030111
[10] Saiz-Lopez A., Shillito J., Coe H., Plane J.: Atmos. Chem. Phys., 2006, **6**, 1513. https://doi.org/10.5194/acp-6-1513-2006
[11] Saiz-Lopez A., Mahajan A., Salmon R. *et al.*: Science, 2007, **317**, 348. https://doi.org/10.1126/science.1141408
[12] Baker A.: Environ. Chem., 2005, **2**, 295. https://doi.org/10.1071/EN05070
[13] Gilfedde B., Lai S., Petri M. *et al.*: Atmos. Chem. Phys., 2008, **20**, 6069. https://doi.org/10.5194/acp-8-6069-2008
[14] Baker A.: Environ. Chem., 2005, **2**, 295. https://doi.org/10.1071/EN05070
[15] Russell W., Saunders R., Samantha M., John M.: Environ. Sci. Technol., 2012, **46**, 11854. https://doi.org/10.1021/es3030935
[16] Saunders R., Plane J.: Environ. Chem., 2005, **2**, 299. https://doi.org/10.1071/EN05079
[17] Saunders R., Kumar R., Martin J. *et* al.: Phys. Chem., 2010, **224** ,1095. https://doi.org/10.1524/zpch.2010.6143
[18] Pechtl S., Schmitz G., Von Glasow R.: Atmos. Chem. Phys., 2007, **7**, 1381. https://doi.org/10.5194/acp-7-1381-2007
[19] Mahajan A., Plane J., Oetjen H. *et al.*: Atmos. Chem. Phys. 2010, **10**, 4611. https://doi.org/10.5194/acp-10-4611-2010
[20] Read K.: Nature, 2008, **453**, 1232. https://doi.org/10.1038/nature07035
[21] Jones C.: Geophys. Res. Lett., 2010, **37**, L18804. https://doi.org/10.1029/2010GL043990
[22] Carpenter L.: Chem. Rev., 2003, **103**, 4953. https://doi.org/10.1021/cr0206465
[23] Reeser D., Donaldson D.: Atmos. Environ., 2011, **45**, 6116. https://doi.org/10.1016/j.atmosenv.2011.08.042
[24] Frew N.: J. Geophys. Res., 2004, **109**, C08S17. https://doi.org/10.1029/2003JC002131
[25] Garabetian F., Romano J., Paul R., Sigoillot J.: Mar. Environ. Res., 1993, **35**, 323. https://doi.org/10.1016/0141-1136(93)90100-E
[26] Schneider J., Gagosian R.: J. Geophys. Res., 1985, **90**, 7889. https://doi.org/10.1029/JD090iD05p07889
[27] Facchini M., Rinaldi M., Decesari S. *et al.*: Geophys. Res. Lett., 2008, **35**, L17801. https://doi.org/10.1029/2008GL034250
[28] Kovac N., Bajt O., Faganeli J. *et al.*: Mar. Chem., 2002, **78** , 205. https://doi.org/10.1016/S0304-4203(02)00033-6
[29] Tervahattu H., Juhanoja J., Vaida V. *et al.*: J. Geophys. Res., 2005, **110,** D6. https://doi.org/10.1029/2004JD005400
[30] Tervahattu H., Juhanoja J., Kupiainen K.: J. Geophys. Res., 2002, **107,** D16. https://doi.org/10.1029/2001JD001403
[31] Tervahattu H., Hartonen K., Kerminen V. *et al.*: J. Geophys. Res., 2002, **107**, D7. https://doi.org/10.1029/2000JD000282
[32] Wurl O., Wurl E., Miller L. *et al.*: Biogeosciences, 2011, **8**, 121. https://doi.org/10.5194/bg-8-121-2011
[33] Bernard R., Ciuraru A., George C.: Environ. Sci. Technol., 2016, **50**, 8678. https://doi.org10.1021/acs.est.6b03520
[34] Zhinen H., Yongguang Y., Dong C., Jing-fu L.: Environ. Sci.Technol., 2017, **51**, 5464. https://doi.org/10.1021/acs.est.6b03887
35] Gallard H., Allard S., Nicolau R. *et al.*: Environ. Sci. Technol., 2009, **43**, 7003. https://doi.org/10.1021/es9010338
[36] Leri A., Hakala J., Marcus M. *et al.*: Biogeochem., 2010, **24**, GB4017. https://doi.org/10.1029/2010GB003794
[37] Komaki Y., Pals J., Wagner E. *et al.*: Environ. Sci. Technol., 2009, **43**, 8437. https://doi.org/10.1021/es901852z
[38] Wang L., Zhou X., Fredimoses M. *et al.*: RSC Adv., 2014, **422**, 57350. https://doi.org/10.1039/C4RA09833A
[39] Leri A., Ravel B.: Environ. Sci.Technol., 2015, **49**, 13350. https://doi.org/10.1021/acs.est.5b03937
[40] Ciuraru R., Fine L., Van Pinxteren M. *et al.*: Sci. Rep., 2015, **5**, 12741. https://doi.org/10.1038/srep12741
[41] Ciuraru R., Fine L., Van Pinxteren M. *et al.*: Environ. Sci. Technol., 2015, **49**, 13199. https://doi.org/10.1021/acs.est.5b02388
[42] Peter A., Ciuraru R., Stéphanie R. *et al.:* Sci. Rep.,2017, **7**,12693. https://doi.org/10.1038/s41598-017-12601-2
[43] Wang L., Zhou X., Fredimoses M. *et al.*: RSC Adv., 2014, **101**, 57350. https://doi.org/10.1039/C4RA10456K
[44] Gallard H., Allard S., Nicolau R. *et al.*: Environ. Sci. Technol., 2009, **43**, 7003. https://doi.org/10.1021/es9010338
[45] Leri A., Ravel B.: Environ. Sci. Technol., 2015, **49**, 13350. https://doi.org/10.1021/acs.est.5b03937
[46] Marchisio A., Minella M., Maurino V. *et al.*: Water Res., 2015, **73**, 145. https://doi.org/10.1016/j.watres.2015.01.016
[47] Laurentiis E., Minella M., Maurino V. *et al.*: Sci. Total. Environ., 2012, **439**, 299. https://doi.org/10.1016/j.scitotenv.2012.09.037
[48] Saunders R., Kumar R., MacDonald S., Plane J.: Environ. Sci. Technol., 2012, **46**, 11854. https://doi.org/10.1021/es3030935
[49] Zhang P., Sun D., Wen M. *et al.*: Adv. Synth. Catal., 2012, **354**, 720. https://doi.org/10.1002/adsc.201290006
[50] Heeb M., Criquet J., Zimmermann-Steffens S., von Gunten U.: Water Res., 2014, **48**, 15. https://doi.org/10.1016/j.watres.2013.08.030

Received: February 26, 2018 / Revised: March 21, 2018 / Accepted: August 23, 2018

ДОСЛІДЖЕННЯ ЧАСТИНОК ОКСИДУ ЙОДУ НА ПОВЕРХНІ РОЗДІЛУ ФАЗ ПОВІТРЯ/ВОДА У ПРИСУТНОСТІ ПОВЕРХНЕВО-АКТИВНИХ РЕЧОВИН ТА ГУМІНОВОЇ КИСЛОТИ

Анотація. *У присутності поверхнево-активних речовин (нонанової НК та стеаринової СК кислот) та гумінової кислоти (ГК) досліджено формування частинки оксиду йоду (ОЙЧ). Встановлено, що оксид йоду, який змішували з органічними сполуками (НК, СК, ГК), а потім опромінювали ксеноновою лампою, приводить до утворення ОЙЧ. Виділення утворених частинок визначалось за допомогою скануючого класифікатора рухомості частинок. Показано, що кількість часток суттєво зменшується в присутності НК, СК, ГК; така поведінка пояснюється утворенням йодоорганічних сполук.*

Ключові слова: *фотохімія, поверхнево-активні речовини, йод, частинка, йодоорганічний.*

Chem. Chem. Technol., 2019,
Vol. 13, No. 3, pp. 347–351

Chemistry

PHYSICO-CHEMICAL AND TECHNOLOGICAL REGULARITIES OF FOAM POLYSTYRENE DEGAZATION IN THE LIQUID MEDIUM

Volodymyr Moravskyi[1, *], Volodymyr Levytskyi[1,2], Mykhailo Bratychak, Jr.[1], Ulyana Khromyak[3], Marta Kuznetsova[1], Nataliia Chopyk[1]

https://doi.org/10.23939/chcht13.03.347

Abstract. The regularities of compaction process of foam polystyrene plastics in the liquid mediums have been discovered. The influence of medium nature, temperature and technological characteristics of foam polystyrene (imaginary density, shredding degree) on the kinetics of gas phase release in the conditions of polystyrene segmental mobility has been determined. The design and method of calculation of the reactor for the process of foam polystyrene degazation *via* the continuous scheme is offered.

Keywords: foam polystyrene, butanol, degazation, recycling, secondary use.

1. Introduction

Owing to the combination of high working properties with the processability by all methods known for polymers, the polystyrene is widely used in the production of goods of various applications, including the foamed ones. Foam polystyrene is being applied in modern construction, in buildings insulation systems [1, 2], as well as in thermal insulation of capacitive machines and pipelines. The combination of high hygienic indicators [3] and heat-insulating properties of foam polystyrene makes it an ideal material for packaging and storage of food products. Another field of foamed polystyrene application, in which it practically does not have competitors, is the packaging of consumer electronics products [4, 5]. Such wide application of foam polystyrene in various industries causes the availability of a large amount of wastes. The above-mentioned wastes are mainly agglomerated in the form of utilized packaging and industrial waste.

Secondary processing of foamed polymers by the traditional methods [6], such as injection molding and extrusion requires elevated attention through the presence of gas inclusions, which during the melting of polymer materials adversely affect the melt homogeneity and, certainly, the quality of finished products with comparatively low productivity of equipment. In this regard, it is necessary to develop methods of raw materials preparation that would make it possible to minimize this negative impact. Among the methods of preparing of foamed poly-materials for recycling the most effective in economic and technological aspects are the methods based on the complete or partial removal of gas inclusions without pressure, in particular, by heating of foam plastic wastes in the air or in the liquid phase [7].

Such prepared wastes can be applied as additives to the primary polymer raw materials with the purpose of their utilization, as well as improvement and regulation of some properties of primary raw materials [8]. Furthermore, such secondary raw materials can be used to create completely new composite materials with predetermined technological properties [9-11].

The primary aim of the work was to determine the influence of medium nature on the regularities of foam polystyrene degazation and develop the design and methodology for calculating the reactor for degazation process.

2. Experimental

The household and industrial wastes of foam polystyrene with imaginary density of 10–60 kg/m^3 have been applied for the research. The gas phase release from the foam polystyrene samples was carried out in a liquid medium in a reactor equipped with mixing device in the air within a wide range of temperatures and pressures. The kinetics of degazation was studied by changing the volume of foam polystyrene samples in different mediums. The volume change (%) has been determined applying the spherical samples obtained by the grinding of waste products on a gear crusher with different diameter of holes, which provided the constant size of polystyrene

[1] Lviv Polytechnic National University,
12, S.Bandery St., 79013 Lviv, Ukraine
[2] The John Paul II Catholic University of Lublin,
14, Al. Racławickie, 20-950 Lublin, Poland
[3] Lviv State University of Life Safety,
35, Kleparivska St., 79000 Lviv, Ukraine
[*] *vmoravsky@gmail.com*

particles (degree of grinding). The initial imaginary density of foam polystyrene was determined according to ISO 845:2006.

In order to calculate the geometric dimensions of the apparatus for conducting degazation in a liquid medium there has been used a method describing the particle sedimentation under the action of gravity force [12] applying the following similarity criteria: Archimedes (Ar), Lyashenko (Ly) and Reynolds (Re).

To determine the particle sedimentation velocity, the Archimedes criteria were calculated at first:

$$\mathrm{Ar} = \frac{d^3(r - r_m)r_m g}{m_m^2} \quad (1)$$

where ρ and ρ_m are densities of the particle and medium, respectively, kg/m^3; g is the gravitational force equivalent, m/s^2; μ_m is the dynamic viscosity coefficient of the medium, Pa s.

By the determined above described value, applying the dependences of Re and Ly criteria on the Ar criterion for the sedimentation of single particle [12], the Ly or Re criteria were defined:

$$\mathrm{Ly} = \frac{\mathrm{Re}^3}{\mathrm{Ar}} = \frac{w_S^3 r_m^2}{m_m(r - r_m)g} \quad (2)$$

From where, the sedimentation velocity of the degassed particle was calculated by the formula:

$$w_S = \frac{\mathrm{Re}\, m_m}{r_m d_{sf}} \quad (3)$$

where d_{sf} is the diameter of a spherical particle, m.

Since the precipitated degassed foam polystyrene particles, as usually, have an irregular shape, instead of the d_{sf} value the d_e value of equivalent diameter of the irregular shape particle was used. It is calculated as the diameter of the conditional sphere, which volume V is equal to the volume of the body of irregular shape:

$$d_e = \sqrt[3]{\frac{6V}{p}} = 1.24\sqrt[3]{\frac{m}{r}} \quad (4)$$

where m is the particle weight, kg.

3. Results and Discussion

To determine the rational parameters of compaction of foam polystyrene (FPS) the kinetic regularities of the volume change of the investigated samples at different temperatures and in different mediums were researched. It has been determined that in the case of heating FPS in the air (Fig. 1) the temperature and pressure significantly influence on the velocity of gas phase release. The temperature rise and rarefaction accelerate the velocity of gas phase release; therefrom the degazation degree is increasing. However, it should be noted that the process is quite continued (1.5–2 h) and complete release of the gas phase from the polymer cannot be achieved even at a sufficiently high temperature and rarefaction. The process of degazation stops when the content of the gas phase is 10–15 %. This is caused by the formation of a sufficiently dense surface crust that prevents the gas phase to be transported from the middle of the sample.

Compaction of samples in water (Fig. 2) occurs slower than in the air. That is probably due to the hydrophobic nature of the gas phase containing isopentane, which is applied for the polystyrene foaming. The above-mentioned is confirmed by a slightly higher degazation degree of FPS in aqueous solution of PVP, where the presence of surface-active polymer, in some measure, increases the affinity between gas phase and medium. Butanol, which is related to isopentane, has the highest velocity and degazation degree. It can be assumed that the compaction of foam polystyrene during heating is caused by the stress relaxation that came up in the polymer during its foaming. This process can be realized only in the case of the segmental mobility of macromolecules and occurs at the temperatures exceeding the glass transition temperature of the polymer. It should be noted that the segmental mobility of macromolecules may also occur at lower temperatures in the presence of liquid phase [13, 14].

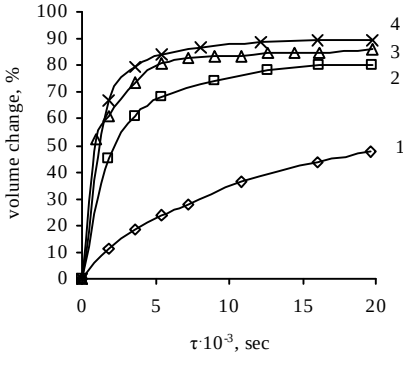

Fig. 1. Kinetics of FPS volume change in air depending on temperature, K: 343 (1); 373 (2, 4); 393 (3). Pressure, kPa: 101.3 (1-3) and 5.33 (4)

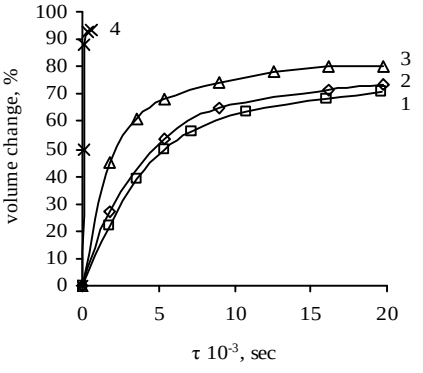

Fig. 2. Kinetics of FPS volume change at 373 K depending on the medium nature: water (1); 5% aqueous solution of PVP (2); air (3); butanol (4)

Obtained regularities of FPS degazation in different mediums can be explained by the following. In the case of degazation in air, the formation of a dense surface crust prevents the gas phase transportation from the middle of the sample. Volume reduction is primarily due to the compaction of the surface layers while the structure of the internal layers remains virtually unchanged owing to the pressure created by heated gases, which thereby counteract the relaxation of stress in the polymer. During degazation in water, the gas output even from the surface layers is impossible due to the locking of hydrophobic gas phase by water, which leads to the decrease in the degazation degree. At the same, butanol related to the isopentane fraction does not interfere with the release of the gas phase from the polymer. In addition, owing to the partial swelling of the polystyrene, the surface crust does not form, and the relaxation is accelerated. In this regard, the velocity of degazation is constant and high almost until the end of the compaction process. At the same time, the velocity and compaction degree can be regulated directly through the temperature of medium.

The researches concerning the release of the gas phase in butanol depending on the temperature have shown (Fig. 3) that the effect of temperature is displayed in increasing the velocity and degree of degazation with the temperature increasing. It should also be noted that at degazation in butanol the higher velocity and the degree of the process depth are achieved considerably more. Compared to other media, the FPS compaction process in butanol appears to be the most rational from the technological point of view. It can be explained by high productivity of the above-mentioned process and due to achievement of higher values of the density of FPS compared with the density of heated butanol the FPS compaction process in butanol can be carried out in a counter-current vertical continuous reactor.

While using butanol, the high temperature of approximately 363–383 K is required for the complete release of gas inclusions. One way to reduce the temperature is to apply the solvent which is more related to polystyrene. Such a solvent was blend of butanol-toluene. Thus, the temperature of the process has significantly reduced while holding high velocity and degree of degazation (Figs 4, 5). Application of toluene, which is a good solvent for polystyrene, may lead to dissolving of the latter, thus the concentration of toluene was limited up to 10 %. The dissolution of polystyrene at such content of toluene did not occur.

Significant intensification of the FPS compaction at increased toluene content can be explained by the greater movability of segments of polystyrene macromolecules in the presence of a good solvent for polystyrene in degassing environment. More significant segmental movability of polystyrene macromolecules with increasing temperature also leads to the increase in velocity of degazation.

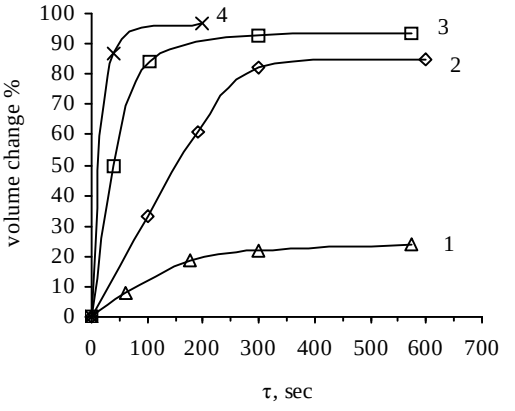

Fig. 3. Kinetics of FPS volume change in butanol depending on temperature, K: 328 (1); 343 (2); 363 (3) and 383 (4)

Since such technological characteristics of the raw material as shredding degree and the initial imaginary density of FPS can have a significant effect on the degassing process, as well as to determine the optimal technological parameters of the process, the degazation kinetics studies were conducted depending on the equivalent radius of the sample (r_{eq}) and the apparent density of the FPS (r_i) (Figs. 6, 7).

The time of achieving FPS maximum density is almost unchanged for samples with an equivalent radius of $(3–5)\cdot10^{-3}$ m, and at a greater radius it increases substantially and can be described by Eq. (5):

$$t_m = 11.94r_{eq}^3 - 136.32r_{eq}^2 + 509.56r_{eq} - 534.3 \qquad (5)$$

In this manner, the optimal equivalent radius of samples after grinding for degazation is $(3–5)\cdot10^{-3}$ m. It should also be noted that such technological characteristic of FPS as the imaginary density within 10–50 kg/m^3 does not significantly affect the time of achievement of the maximum density, which is 90–100 s and can be described by the following dependence:

$$\tau_m = 0.0064\rho_i^2 - 0.1357\rho_i + 90.6 \qquad (6)$$

The studies concerning the release of gas phase from FPS were conducted and the mathematical dependencies of maximum density achievement time on equivalent radius of the samples and the initial imaginary density of FPS were defined. The aforesaid can be used to determine the rational technological parameters of the compaction process depending on the raw material characteristics, and, thus, to obtain a secondary degassed FPS of a given degree of compaction which can be applied for further recycling.

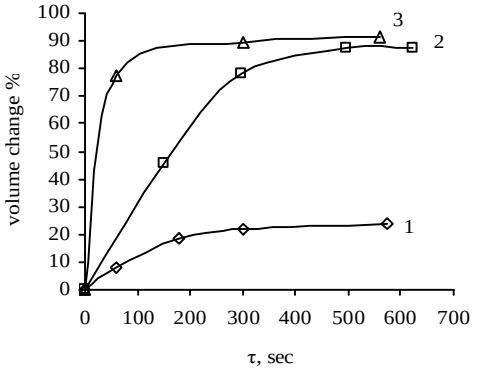

Fig. 4. Kinetics of FPS volume change at 333 K depending on the solvent nature: butanol (1); butanol 95% + toluene 5% (2) and butanol 90% + toluene 10% (3)

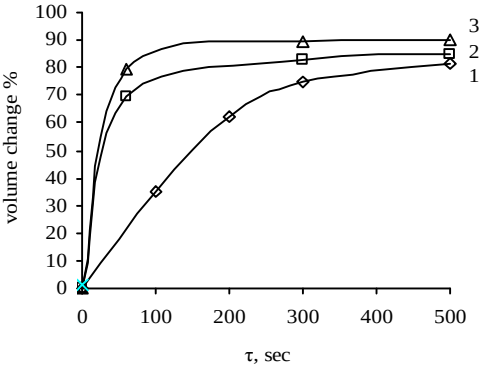

Fig. 5. Kinetics of FPS volume change in the solvent (butanol 90% + toluene 10%) depending on temperature, K: 313 (1); 323 (2) and 333 (3)

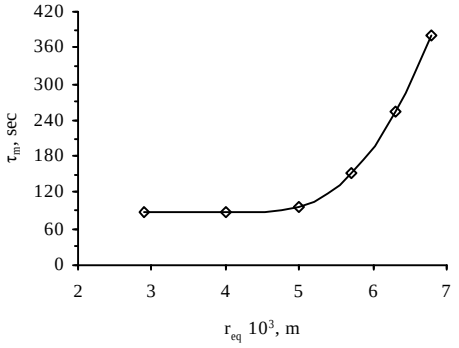

Fig. 6. Effect of equivalent radius of the sample on time of achieving FPS maximum density (t_m) in butanol at 363 K

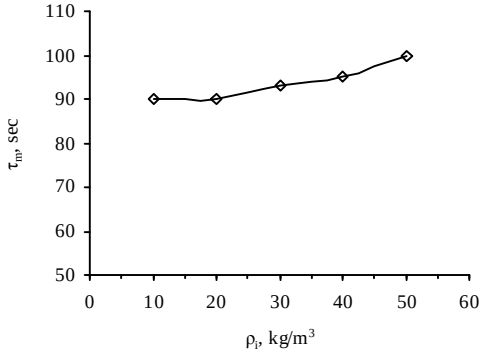

Fig. 7. Influence of apparent density of the sample on time of achieving FPS maximum density in butanol at 363 K

Table

Influence of medium and temperature on foam polystyrene degazation

Technological parameters				Properties of FPS	
Medium	*P*, MPa	*T*, K	τ, min	*r*, kg/m^3	Δ*V*, %
Air	0.1 0.005	373–393 353–363	10–12 5–7	950	87
Water	0.1	363–373	20–30	780	73
Water + butanol 10%	0.1	363–373	10–15	930	84
Butanol	0.1	363–373	2–3	1020	93
Butanol	0.1	378–388	1–2	1040	96
Butanol + toluene 5–10%	0.1	323–333	1–1.5	1040	96

The obtained results of the research concerning the gas phase release from FSP allowed determining the optimal technological parameters of the process by applying different mediums (Table).

The conducted researches also allow to propose a constructive design of the degazation process. To ensure the high efficiency and productivity of the process *via* the continuous scheme a cylindrical apparatus has been proposed, the specificity of which is a system of continuous unloading of the degassed FPS. The mentioned system consists of a screw conveyor and scraper providing the gathering and delivery to the screw of the degassed FPS.

In order to obtain a compacted FPS of the required quality the height of the apparatus should be sufficient to provide the necessary time for FPS staying in the reactor. The time, as was shown by the research relating to the regularities of FPS degazation in butanol solutions, is 1–1.5 min depending on the technological characteristics of the secondary raw material.

Obviously, the main parameter for calculating the geometric dimensions of the apparatus is the sedimentation velocity of the particle during the degazation. Using the proposed calculation method and substituting Eq. (4) into (3) we obtain the equation for calculating the sedimentation velocity of the FPS particle of irregular shape:

$$\omega_S = \frac{\mathrm{Re}\mu_m}{\rho_m\left(1.24\sqrt[3]{\frac{m}{\rho}}\right)} \quad (7)$$

Since the density of the FPS is changed during the degassing process, it is necessary to determine a number of assumptions allowing to calculate the sedimentation start time and the velocity at which the particle of the degassed FPS precipitates in the butanol solution. A separate FPS particle begins to precipitate when achieving the density of the butanol solution heated to the required temperature. The butanol density at 363 K is 758 kg/m^3, foam polystyrene (initial apparent density is 20 kg/m^3) reaches this density after 40 s. At the same time, the sedimentation velocity of PS particle with an initial volume of about 1 cm^3 is 0.087 m/s. Thus, the height of the working part of the reactor can be considered as the track passed by the particle for 50 s (the time of reaching the maximum density (90 s) minus the start time of the sedimentation (40 s)). In this case the apparatus height will be 4.35 m.

When using the apparatus of the proposed design its productivity will depend on the area of contact FPS with a butanol solution, *i.e.*, on the apparatus cross section, and can be calculated by Eq. (8):

$$F = \frac{V}{w'_s} \quad (8)$$

where V is a volumetric flow rate of granulated foam polystyrene, m^3/s; ω'_S is an average calculated sedimentation velocity, $w'_S = 0.5w_S$.

For example, with the apparatus productivity at an initial FPS of 10 m^3/h, the cross-sectional area of the apparatus will be 0.056 m^2, which corresponds to the diameter of 0.134 m.

Thus, the proposed design of the apparatus can be applied for the process of degassing. The subsequent improvement of the apparatus design can be achieved by reducing the geometric dimensions, in particular, by reducing its height. This can be achieved by the increasing of hydraulic resistance acting on the settling particle as a result of the counter current of the solution in the direction the particle sedimentation. It will make possible to decrease the velocity of its sedimentation and thus reduce the height of the device.

4. Conclusions

Based on this research it was determined that the optimum medium for the degassing process of secondary FPS are the butanol mediums, in which high compaction degree (at the level of 94–97 %) can be achieved, with high velocity. It makes the proposed technology of secondary FPS utilization attractive from an economic standpoint.

Acknowledgements

The work was carried out within the framework of the project Physico-chemical fundamentals of the synthesis and modification of selective sorption polymer inorganic (nano) composite materials (state registration number 0118U000263).

References

[1] Al-Homoud M.S.: Building and Environment, 2005, **40**, 353. https://doi.org/10.1016/j.buildenv.2004.05.013
[2] Aditya L., Mahlia T., Rismanchi B. *et al.*: Renew. Sustain. Energ. Rev., 2017, **73**, 1352. https://doi.org/10.1016/j.rser.2017.02.034
[3] Lickly T., Lehr K., Welsh G.: Food Chem. Toxicol., 1995, **33**, 475. https://doi.org/10.1016/0278-6915(95)00009-Q
[4] Ozturk U., Anlas G.: Mater. Design, 2011, **32**, 773. https://doi.org/10.1016/j.matdes.2010.07.025
[5] Di Landro L., Sala G., Olivieri D.: Polym. Test., 2002, **21**, 217. https://doi.org/10.1016/S0142-9418(01)00073-3
[6] Sikora J., Gerlach H., Levytskyi V., Moravskyi V.: J. Polym. Eng., 2013, **33**, 501. https://doi.org/10.1515/polyeng-2013-0006
[7] Kan A., Demirboğa R.: J. Mater. Process. Techn., 2009, **209**, 2994. https://doi.org/10.1016/j.jmatprotec.2008.07.017
[8] Levytskyj V., Laruk Yu., Huminetsky T., Sikora J.: Chem. Chem. Technol., 2015, **2**, 199. https://doi.org/10.23939/chcht09.02.199
[9] Moravskyi V., Dziaman I., Suberliak S. *et al.*: East.-Eur. J. Enterpr. Techn., 2017, **4**, 50. https://doi.org/10.15587/1729-4061.2017.108462
[10] Moravskyi V., Dziaman I., Suberliak S. *et al.*: 7th Int. Conf. on Nanomaterials: Applications and Properties, Ukraine, Zatoka 2017, 03NNSA18. 10.1109/NAP.2017.8190265
[11] Moravskyi V., Kucherenko A., Kuznetsova M. *et al.*: East.-Eur. J. Enterpr. Techn.., 2018, **3**, 40. https://doi.org/10.15587/1729-4061.2018.131446
[12] Kasatkin A.: Osnovnye Protsessy i Apparaty Khimicheskoy Tekhnologii. Goskhimizdat, Moskva 1961.
[13] Levytskyi V., Katruk D., Shybanova A. *et al.*: Mater. Sci., 2017, **52**, 559. https://doi.org/10.1007/s11003-017-9990-0
[14] Levyts'kyi V., Katruk D., Kochubei V. *et al.*: Mater. Sci., 2017, **53**, 385. https://doi.org/10.1007/s11003-017-0086-7

Received: November 30, 2018 / Revised: December 03, 2018 / Accepted: March 28, 2019

ФІЗИКО-ХІМІЧНІ ТА ТЕХНОЛОГІЧНІ ЗАКОНОМІРНОСТІ ДЕГАЗАЦІЇ ПІНОПОЛІСТИРОЛУ В РІДКОМУ СЕРЕДОВИЩІ

Анотація. *Виявлені закономірності процесу ущільнення пінополістирольних пластиків в рідинних середовищах, встановлено вплив природи середовища, температури і технологічних характеристик пінополістиролу (уявна густина, ступінь подрібнення) на кінетику вивільнення газової фази в умовах сегментальної рухливості полістиролу. Запропонована конструкція і методику розрахунку реактора для проведення процесу дегазації пінополістиролу за безперервною схемою.*

Ключові слова: *пінополістирол, бутанол, дегазація, утилізація, вторинне використання.*

Chem. Chem. Technol., 2019,
Vol. 13, No. 3, pp. 352–359

Chemistry

RECEIVING ELASTOVISCOUS SYSTEMS ON THE BASIS OF AQUEOUS SOLUTION OF ACETATE AND SUCCINIMIDE OF CHITOSAN IN THE PRESENCE OF POLYHYDRIC ALCOHOLS

Roman Lazdin[1], Marina Bazunova[1], Valentina Chernova[1], Angela Shurshina[1], Vadim Zakharov[1], Elena Kulish[1,*]

https://doi.org/10.23939/chcht13.03.352

Abstract. The rheological behavior of acetate and succinimide of chitosan in mixed solvents was investigated. It is shown that the replacement of a part of the solvent by two- or three-atom alcohols is accompanied by an increase in the relative and dynamic viscosity of the succinimide chitosan solution, an earlier formation of the net of links, a transition from viscoelastic systems to elastoviscous ones at lower polymer concentration values and an increase in the relaxation time.

Keywords: chitosan, succinimide chitosan, rheological behavior, mixed solvent, gel.

1. Introduction

Creation of new highly effective dosage forms is one of the top-priority directions in the development of modern chemistry, medicine and pharmacology [1-3]. The soft dosage forms which differ in high viscosity and thereof have a number of advantages compared to liquid dosage forms are highlighted [4, 5]. Physical and chemical processes proceeding in a viscous medium occur significantly more slowly and the viscous bases provide a prolonged release of drugs, which means high efficiency and minimum complexity of application. Moreover, at high viscosity, sedimentation processes practically do not occur, which means that the dispersed drug will be distributed in a viscous medium evenly.

Gels on the basis of bio- and haemocompatible biopolymers, for example, polysaccharides or proteins, occupy a specific place among various soft dosage forms. However, the direct dissolution of polymer does not always lead to high-viscosity solution. The use of co-solvents, which play the role of the modifying additives capable a forming of "bridge" connection between macromolecules, can become a solution in this situation. As a result of such "crosslinking", the macromolecules lose their kinetic independence, which in turn leads to an increase in viscosity. Some polyhydric alcohols – ethylene glycol, propylene glycol, and glycerin were used as co-solvents – polymer modifiers in our work. Polysaccharides, namely chitosan (ChT) and its water-soluble derivative – succinimide chitosan (SChT) were taken as gelling polymer. The choice of polymers was caused by a spectrum of unique properties, one of which is biocompatibility with body tissues, bacteriostaticity, ability to biodegradation, and much more [6-8].

The aim of the work was to study the rheological behavior of chitosan and succinimide chitosan in a mixed solvent to find conditions for formation of high-viscosity gels suitable for creation of soft dosage forms.

2. Experimental

SChT with M.M. = 207 kDa and the intrinsic viscosity [η] = 3.20 dl/g produced by Bioprogress (Shchelkovo, Russia) was used as the objects of the study. The degree of SChT substitution for the amino groups is 75 %. The degree of deacetylation of the initial sample of chitosan from which SChT was obtained was 82 %.

Bidistilled water and 1% acetic acid were used as the solvents for SChT and ChT, respectively. Glycerin, propylene glycol, and ethylene glycol was used as a modifier (co-solvent).

The intrinsic viscosities of the polymer were determined using a Ubellode viscometer at the temperature of 298±1 K and calculated using the Baranov method [9], which eliminates the effect of the polyelectrolyte swelling on the value of the intrinsic viscosity of the polymer [10].

Rheological investigations of solutions of polymers were carried out on a module dynamic rheometer Haake Mars III (THERMO Fisher, Germany) at 298 K in two modes: continuous shear deformation in the range of shear rates from 0.1 to 100 s^{-1} and oscillation mode. For creation of concentration curves and calculation of activation

[1] Bashkir State University, 32, Zaki Validi, 450076 Ufa, Russia
[*] *onlyalena@mail.ru*

energy we used the values η determined at shear rate equal to 0.1 s^{-1}. Since tests in the oscillation mode must be performed in the region of linear viscoelasticity, optimal values of the amplitude corresponding to the invariant values of the modules (linear viscoelasticity region) were initially determined on the basis of the dependences of the accumulation modules and losses on the amplitude of the stresses obtained at a constant oscillation frequency.

The activation energies of the viscous flow of the studied systems (ΔE_a) in the temperature range from 288 to 318 K were estimated by Arrenius-Frenkel-Airinga equation (1) and were calculated by the method of the least squares:

$$h = Ae^{\frac{\Delta E_a}{RT}} \quad (1)$$

where R is the universal gas constant, A is a constant.

3. Results and Discussion

It is known that the rheological behavior of solutions of polyelectrolytes (for example ChT and SChT) has its own characteristic features that distinguish them from solutions of non-ionic polymers. Manifestation of these features depends on concentration area in which the polymer is located. For example, in the field of the diluted solutions rheological behavior of both nonionic and ionic polymers is close to each other – macromolecular coils do not overlap and move independently of each other. Differences of solutions of polyelectrolyte from solutions of nonionic polymers begin to be shown at achievement of the critical concentration called by concentration of the crossover c^*, at which all volume of solution is filled with polymeric coils. In solutions of uncharged polymers the intermolecular association and formation of links net (at concentration of polymer in solution c_e) begin practically right after excess of polymer concentration above c^*, *i.e.* $c^* \approx c_e$ (Fig. 1). Existence of extended area of the semi-diluted solutions (at concentration bigger than c^*), in which coils already adjoin with each other but grids of gearings do not form yet, is characteristic of solutions of ionic polymers [11, 12].

The reason of such feature of rheological behavior of polyelectrolyte is connected with electrostatic repulsion of the same loaded chains interfering to penetration of one ball of polymer into another ball and with formation of a net of links. Earlier existence of such area of the semi-diluted solutions without formation of a net of links has been revealed for chitosan solutions in acetic acid.

The dependence of the greatest Newtonian viscosity η_0 on concentration of SChT in individual (water) and the mixed solvent (water-glycerin) is presented in Fig. 2.

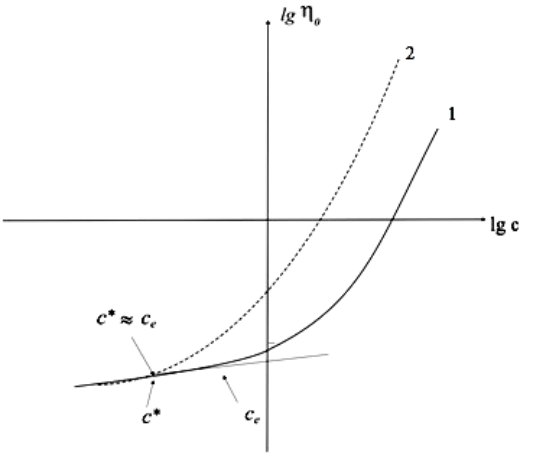

Fig. 1. Schematic representation of the dependence of the greatest Newtonian viscosity on concentration in double logarithmic coordinates for solutions of ionic (1) and nonionic (2) polymers

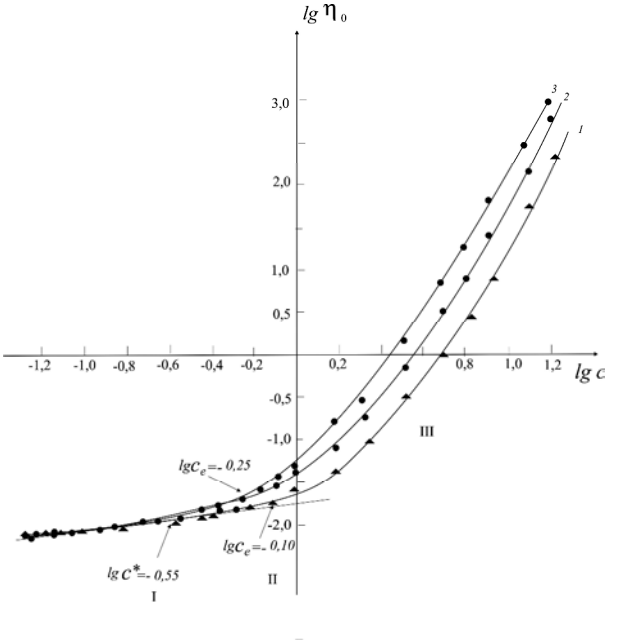

Fig. 2. Dependence of the dynamic viscosity measured at a shear rate of shift of 0.1 s^{-1} on the concentration of SChT in the individual (1) and mixed solvent water: glycerin with a components ratio (v/v) 80:20 (2) and 70:30 (3)

From the figure it is visible that the concentration dependence according to the standard approaches can be described by a power function of $C \sim C^n$ and broken into three sites. In the field of the diluted and concentrated solutions of polymer (site I and III on graphics, respectively) the viscosity actually linearly depends on concentration c (in double logarithmic coordinates) that corresponds to the area of the diluted solutions of the macromolecules, which are not interacting among themselves and the area of the concentrated solutions with

completely created net of links, characterized by the reptational mechanism of movement of macro chains, respectively. Intermediate site II is characteristic of the semi-diluted area in which macromolecules interact with each other and form a fluctuation network of links starting concentration $c_e \approx 0.8$ g/dl (value *lgc* = -0.1). On this site there is a continuous increase in an exponent of *n* testifying to the intermolecular association taking place. Considering that value of characteristic viscosity *[η]* for SChT was 3.20 dl/g, *i.e.* the crossover point ($c^* = 1/[\eta]$) corresponds to concentration of 0.3 g/dl, it is visible that achievement of a point of the crossover does not affect the mechanism of polymer solution flow. In this regard, and in case of solutions of SChT in water, it is possible to speak about existence of transitional area from site I to site II, in which macromolecules already adjoin each other, but net of links does not form yet.

Dissolution of SChT in the mixed solvent water-glycerin leads to some increase in dynamic viscosity (Fig. 2, *curves* 2-4). Several moments attract attention here. Firstly, increasing dynamic viscosity is followed by increase of relative viscosity (Fig. 3). It is important as it is worth remembering that the viscosity of glycerin is significantly higher than viscosity of water owing to what observed increase in dynamic viscosity upon transition from individual solvent of water to mixed – water-glycerin could be caused just by increase in viscosity of the mixed solvent.

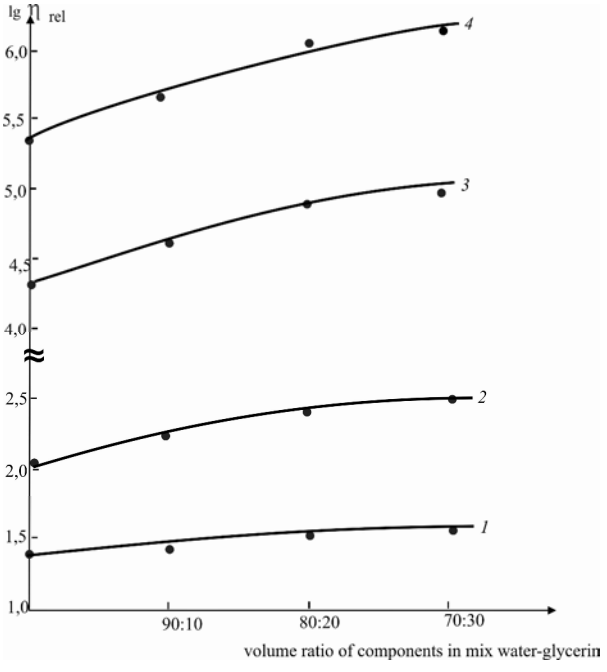

Fig. 3. Dependence of the relative viscosity of solutions of SChT of concentrations 1 (1), 2 (2), 10 (3) and 15 g/dl (4) on the volume ratio of components in mixture of water: glycerin in semi logarithmic coordinates

Secondly, addition of co-solvent to solution of SChT leads to reduction of values of concentration c_e that testifies to earlier formation of a net of links.

Similar regularities are observed in case of solutions of ChT in the mixed solvent of 1% acetic acid-glycerin (Fig. 4).

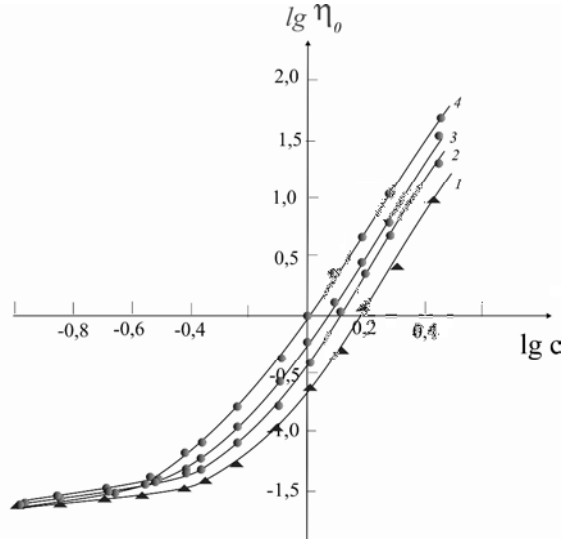

Fig. 4. Dependence of the dynamic viscosity measured at a share rate of 0.1 s^{-1} on the concentration of ChT in the individual (1) and the mixed solvent of 1% acetic acid: glycerin with a components ratio (v/v) 90:10 (2), 80:20 (3) and 70:30 (4)

There can be at least two reasons causing earlier formation of a net of links: physical "cross linking" of macromolecules by glycerin and enhanced aggregation of chains of ionic polymer in solvent with smaller dielectric permeability (relative dielectric permeability of water is 80 and glycerin – 47).

The strengthening of aggregation processes caused by reduction of extent of ionization of macromolecules at decrease in dielectric permeability of solvent is a more probable cause because the earlier formation of a net of links also takes place when ethyl alcohol is used as the modifying additive which is incapable to “cross-link” macromolecular chains.

The great values of an indicator of n in dependence $\eta_0 \sim C^n$ in the field of the concentration corresponding to concentration c_e also testify to more intensively proceeding aggregation processes in the presence of co-solvent (Figs. 2 and 4).

Thirdly, the viscosity of the studied systems of ChT and SChT in the mixed solvents measured at big rates of shift (about 100 s^{-1}), corresponding to completely destroyed net practically coincides with viscosity of solution of polymer in individual solvent of the corresponding concentration (Figs. 5 and 6).

It allows assuming that observed effects of increase in viscosity in systems polymer–mixed solvent in comparison with viscosity of solution of polymer in individual solvent are caused by formation or destruction of an additional network whose nodes are physical crosslink between the macromolecules.

Small values of energy of activation of a viscous current also testify to the physical nature of nodes of an additional network (Figs. 7 and 8).

It is important that the aggregation of macrochains forms system with elastic and viscous properties. The rheological measurements taken in the oscillation mode prove it.

Therefore, from Fig. 9 it is visible that for solutions of SChT in individual solvent the value of the module of accumulation becomes more than loss modulus only at achievement of concentration of SChT in solution C_{el} = 9 g/dl (value of lg$c$ = 0.95), that indicates the formation of elastic and viscous system and loss by the system of fluidity (see Fig. 10).

Replacement of a part of water by co-solvent (glycerin) leads to earlier transition of system from viscoelastic liquid to elastoviscous body. As can be seen from the data in Fig. 11, for the system SChT-water-glycerin with the ratio of components 80:20 (v/v) already in the field of concentration of SChT in solution of 6 g/dl a non-flowing elastoviscous system is formed.

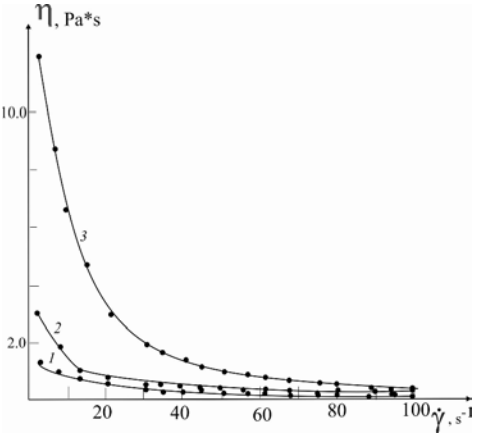

Fig. 5. Dependence of the dynamic viscosity on the shear rate for 5% solutions of SChT in the individual (1) and the mixed solvent (2, 3) with water:glycerin ratio (v/v) 90:10 (2) and 70:30 (3)

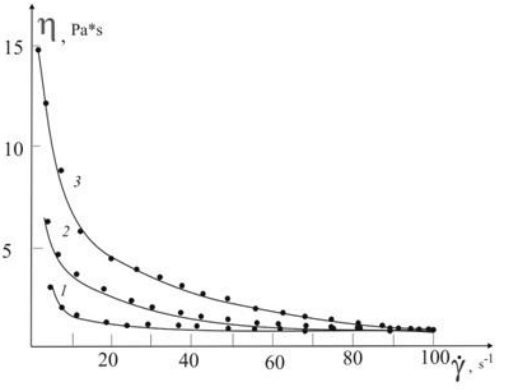

Fig. 6. Dependence of the dynamic viscosity on shift rate for 2% solutions of ChT in the individual (1) and the mixed solvent (2, 3) with 1% acetic acid:glycerin ratio (v/v) 90:10 (2) and 70:30 (3)

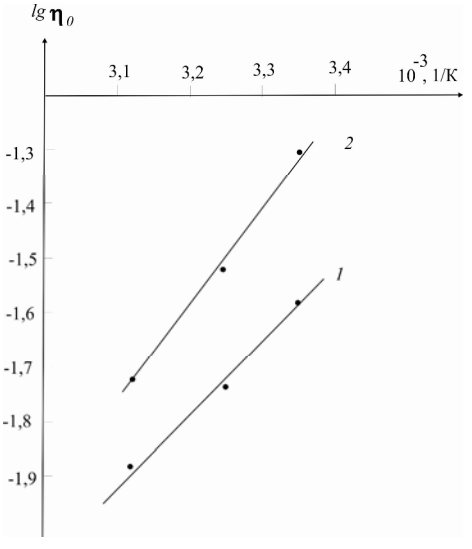

Fig. 7. Calculation of the energy of activation of viscous flow for solutions of SChT of concentration 1 g/dl in water (1) and in mixed solvent with water: glycerin ratio (v/v) 80:20 (2)

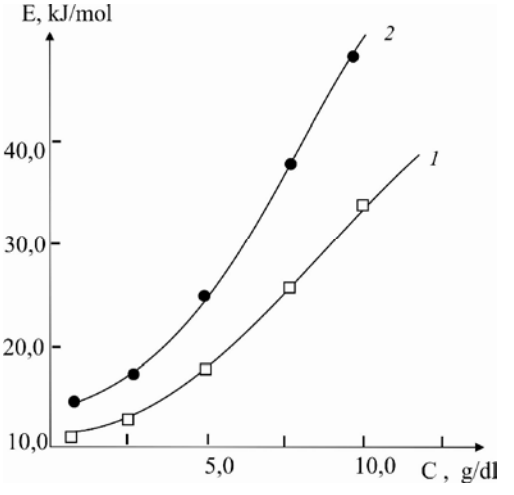

Fig. 8. Concentration dependence of activation energy of viscous flow of SChT solution in water (1) and mixed solvent with water: glycerin ratio (v/v) 80:20 (2)

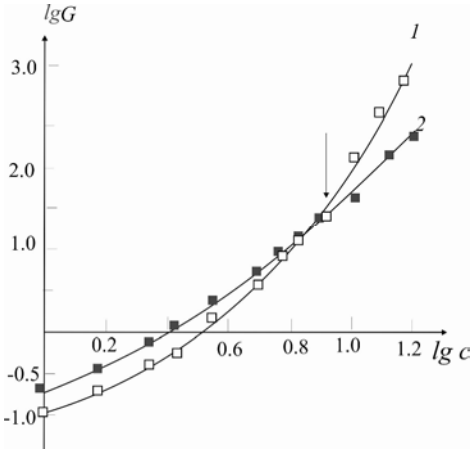

Fig. 9. Concentration dependence of the modulus of accumulations (1) and losses (2) for solutions of SChT in water in double logarithmic coordinates. The values of the module of accumulation and losses are determined in the field of linear viscoelasticity at the frequency of 1 s^{-1}. The arrow indicates the concentration at which the system acquires elastoviscous properties

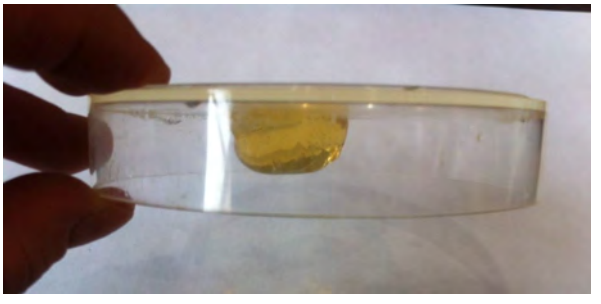

Fig. 10. 8% solution of SChT in water having elasticity properties

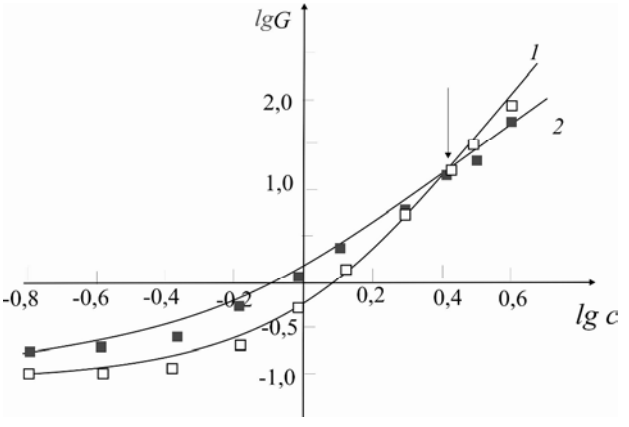

Fig. 12. Concentration dependence of the modulus of accumulations (1) and losses (2) for solutions of ChT in 1% acetic acid in double logarithmic coordinates. The values of the modulus of accumulations and losses are determined in the field of linear viscoelasticity at the frequency of 1 s^{-1}. The arrow indicates the concentration at which the system acquires elastoviscous properties

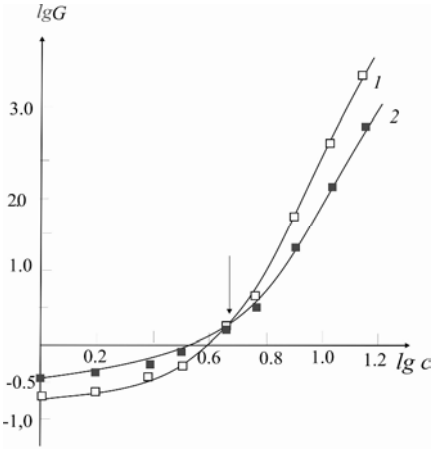

Fig. 11. Concentration dependence of the modulus of accumulations (1) and losses (2) for solutions of SChT in mixed solvent with water:glycerin ratio (v/v) 80:20 in double logarithmic coordinates. The values of the modulus of accumulations and losses are determined in the field of linear viscoelasticity at the frequency of 1 s^{-1}. The arrow indicates the concentration at which the system acquires elastoviscous properties

Similar regularities take place also for solutions of ChT in the mixed solvents. As can be seen from the data in Fig. 12, if for solutions of ChT in individual solvent the module of accumulation becomes more than loss modulus at concentration of polymer in solution more than 3 g/dl (lg3 = 0.47), then in the mixed solvent (for example, 80 % of 1% of acetic acid–20 % of glycerin) this transition happens in the field of much smaller concentration (Fig. 13).

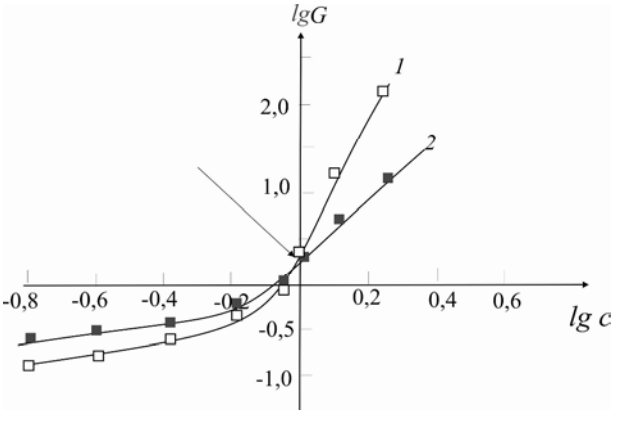

Fig. 13. Concentration dependence of the modulus of accumulations (1) and losses (2) for solutions of ChT in the mixed solvent with 1% acetic acid:glycerin ratio (v/v) 80:20 in double logarithmic coordinates. The values of the modulus of accumulations and losses are determined in the field of linear viscoelasticity at the frequency of 1 s^{-1}. The arrow indicates the concentration at which the system acquires elastoviscous properties

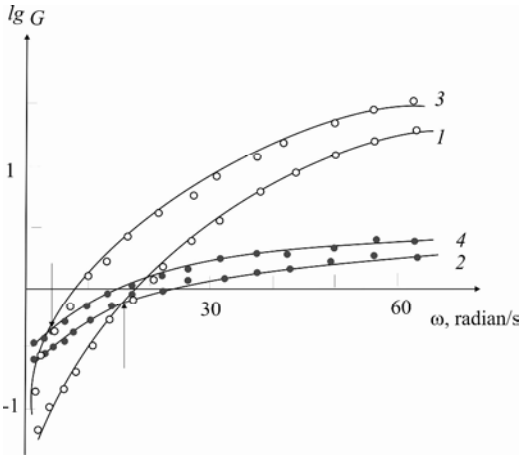

Fig. 14. Dependence of the modulus of accumulations (1, 3) and losses (2, 4) on the angular rate (frequency) of oscillations for solutions of SChT with the concentration of 2 g/dl in an individual (1, 2) and a mixed solvent with water:glycerin ratio (v/v) 80:20 (3, 4) in semi logarithmic coordinates. The arrow indicates the value of an angular rate at which $G' = G''$

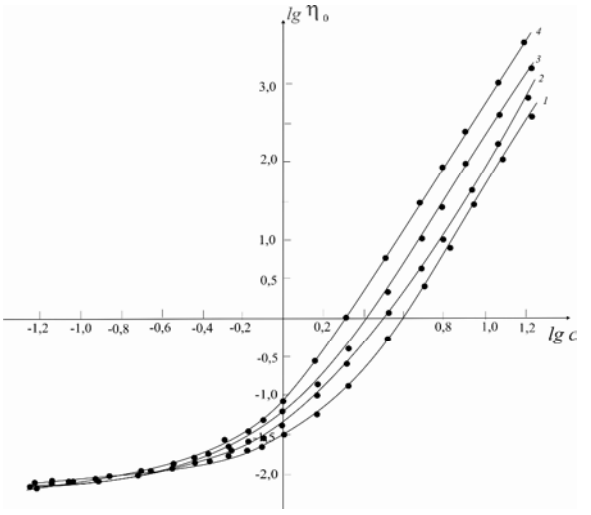

Fig. 15. Dependence of the dynamic viscosity measured at the shear rate of 0.1 s^{-1} on the concentration of SChT in the mixed solvent water:glycerin (1), water:propylene glycol (2), water:ethylene glycol (3), and water:ethanol (4) with the components ratio (v/v) 90:10

Table

The characteristics of elastoviscous properties of SChT received from rheological data

System	Volume ratio of components in mix water:co-solvent	c_e, g/dl	C_{el}, g/dl	$t^* \cdot 10^2$, s
SChT-water	100:0	0.80	9.0	6
SChT-water-glycerin	90:10	0.70	7.5	16
	80:20	0.60	6.0	25
	70:30	0.55	5.8	37
SChT-water-propylene glycol	90:10	0.68	7.4	20
	80:20	0.63	5.5	34
	70:30	0.60	5.2	42
SChT-water-ethylene glycol	90:10	0.60	5.5	35
	80:20	0.57	5.1	46
	70:30	0.48	4.8	68

Note: * the value of relaxation time is given for 2% solution of SChT

Reviewing the dependence of modules of accumulation and losses from the frequency (Fig. 14) allows to state that in the range of concentration of SChT in solution, corresponding to the area from $c_e \approx 0.8$ g/dl to $c_e \approx 3$ g/dl, the tangent of angle of the frequency dependence of the module of accumulation in double logarithmic coordinates is equal to 2, and the module of losses is 1. It testifies that the behavior of the system is well described by simple model of Maxwell for viscoelasticity liquid with time of relaxation τ, for which $G' = G''$. For solutions of ChT this field of intensive formation of a net of linkages corresponds to area of concentration from $c_e \approx 0.4$ g/dl to $c_e \approx 1$ g/dl.

From the data provided in the Table it is visible that replacement of a part of solvent by the modifying additive (glycerin) leads to increase in time of relaxation of the macromolecules τ that will be coordinated with the increased values of viscosity and the accelerated formation of a net of links. The data on values c_e and C_{el}, which undergo natural changes, are provided in the Table as well.

The observed regularities qualitatively coincide in case of use of propylene glycol and ethylene glycol as co-solvent. At the same time, for all studied structures (a water:co-solvent ratio (v/v) is equal to 90:10, 80:20 and 70:30) the increase in dynamic and relative viscosity, shift value c_e and C_{el} to the area of smaller values of

concentration and increase in time of relaxation in comparison with solution of SChT in individual solvent takes place (Table). The concentration dependence of the greatest Newtonian viscosity for solutions of SChT in the mixed solvent water:propylene glycols and water:ethylene glycol with the volume ratio of 90:10 is given in Fig. 15. As an example the dependence of viscosity on concentration for the system SChT-water-ethanol is given by *curve* 4.

The fact that rheological characteristics of the system SChT-mixed solvent correlate with value of dielectric permeability of the mixed solvent attracts attention.

Introduction of co-solvents in the system SChT-water, except increase in viscosity in system polymer-solvent and earlier formation of a net of links, allows solving some problems. The first problem concerns instability of solutions of chitosan, namely: as the solution of the polymer is maintained, its viscosity gradually decreases with time. Instability of solutions of ChT is a fact repeatedly noted in the literature. However, while for solutions of ChT in strong acids (*e.g.*, hydrochloric acid) reduction of viscosity is unambiguously connected with the course of acid hydrolysis, concerning the reasons of change of viscosity of polymer in solution of weak acetic acid, there was no uniform view point among researchers. Most of researchers see the reason of "inconstancy" of values of characteristic and relative viscosity in changes of a conformational condition of macromolecules, formation of intra chain and/or inter chain hydrogen communications, disintegration of units. In the earlier works of our department it has been proved too that the reason of decrease in viscosity of solutions of ChT is connected with the change of its supramolecular structure, owing to slow achievement in the course of dissolution of equilibrium structure [13]. The similar situation is observed in case of solutions of SChT in water. At the same time, as well as in case of ChT, on the nature of change of viscosity the basic value is rendered by concentration of polymer in initial solution. As can be seen from Fig. 16, in the case when SChT in solution has not created a net of links yet (solution with concentration $c < c_e$), or have created already rather developed net of links as a result of which the system has gained elastic and viscous properties (solution with concentration ($c > C_{el}$), values of dynamic viscosity practically do not change with hold time of solution. In the same case, when the solution of SChT in water is a typical viscoelasticity fluid with a formed net of links (solution with a concentration $c_e < c < C_{el}$), the dynamic viscosity decreases significantly when the solution is held. However, the presence of a co-solvent (glycerin, propylene glycol, ethylene glycol) in the system SChT-water leads to significant changes in the behavior of the systems under study. In this case, solutions with polymer concentration in solution over the whole range of concentrations are stable in all cases studied by us, apparently due to the "crosslinking" of macro-molecules taking place through interaction with a co-solvent (Fig. 17).

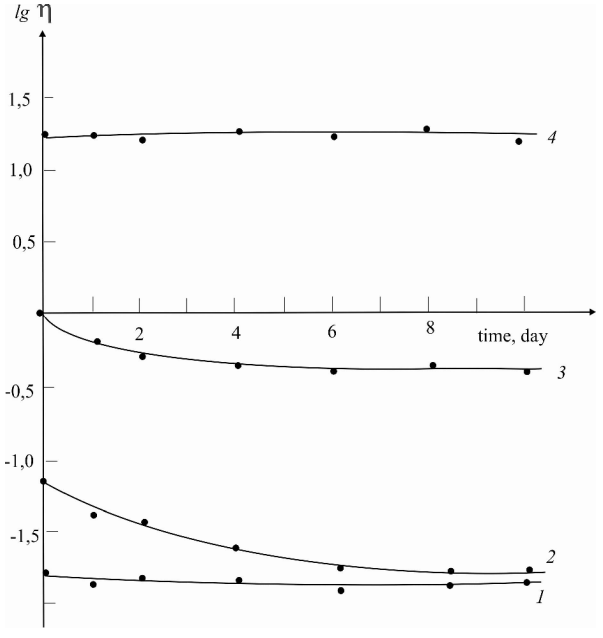

Fig. 16. Dependence of the greatest Newtonian viscosity on time of withstanding the solution of SChT in water of concentrations 0.5 (1), 2 (2), 5 (3), and 10 (4) g/dl

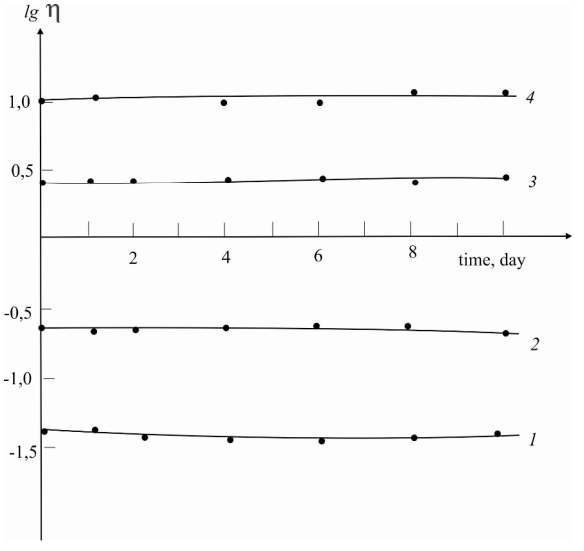

Fig. 17. Dependence of the greatest Newtonian viscosity on time with solution of SChT concentrations of 1 (1), 2 (2), and 5 (3, 4) g/dl in the mixed solvent water:propylene glycol (1, 2), water:glycerin (3) and water:ethylene glycol (4) with the ratio (v/v) 90:10

Stability of rheological characteristics of polymer in the system SChT-mixed solvent, certainly, has considerable advantages from the technological point of view at process of formation of polymeric materials in comparison with the system SChT-water.

The second problem is connected with solubility of ChT and its derivatives in water environments leading to essential reduction of service life of materials on the basis of these polymers. Several ways of ChT modification leading to the loss of solubility of chitosan materials in water is known. Thermal modification consisting in warming up of the created material at the temperature about 373–383 K within 30–60 min is the most widespread and convenient way of modification. After carrying out of this sort modification, a film of ChT loses solubility in water, but keeps the physico-mechanical and physico-chemical properties at the previous level. However, carrying out thermal modification of SChT does not lead to loss of solubility of materials in water. Even long (during 3–4 h) warming up of films at the temperature of 373–403 K is not followed by noticeable reduction of solubility. Introduction of co-solvent (glycerin) in amount of 20 vol % and more, allows to receive soft and elastic gel materials, well occluding water, but keeping at the same time the integrity and not capable to dissolution in water. At the same time, the effect of loss by material of ability to be dissolved in water takes place only when using as co-solvent of triatomic alcohol – glycerin. When using diatomic alcohols (propylene and ethylene of glycol) elastic gel materials at the long-lived contact with water pass into initial elastoviscous or viscoelastic gels.

Thus, the research of the rheological properties of SChT in the mixed solvent allows to draw a conclusion that replacement of a part of solvent by two- or triatomic alcohols is followed by growth of relative and dynamic viscosity of solution of SChT, earlier formation of a grid of gearings, transition from viscoelastic systems to elastic and viscous at smaller values of concentration of polymer and by the growth of relaxation time. The systems which are formed at the same time are characterized by stability of viscous characteristics in time and, in case of using glycerin, lead to receiving water non-soluble gel materials capable to become the main ones for creation of soft dosage forms.

4. Conclusions

It is established that increase of the dynamic viscosity of polymers (ChT and SChT) and earlier formation of the fluctuation grid of links occurs in the presence of co-solvents – glycerin, ethylene glycol and propylene glycol. According to the nature of the flow curves, it is established that the fluctuation grid has a physical character. It is shown that the addition of a co-solvent is followed by a decrease in the value of the polymer concentration in the solution, at which the transition from viscous-elastic liquids to elastoviscous systems occurs, and the increase in relaxation. It is shown that the introduction of a co-solvent into a solution of SChT and ChT leads to the formation of solutions with stable viscous characteristics and, in the case of using glycerin as a co-solvent, allows to receive elastic materials that are not capable of dissolving in water.

Acknowledgements

This study was supported by the Ministry of Education and Science of the Russian Federation (grant no. 4.5032.2017/BCh within the framework of the basic part of state assignment in the field of research activities).

References

[1] Jenkins M. (Ed.): Biomedical Polymers. 1st edn., Woodhead Publishing, Cambridge 2007.
[2] Uhrich K., Cannizzaro S., Langer R., Shakesheff K.: Chem.Rev., 1999, **10**, 3181. https://doi.org/10.1021/cr940351u
[3] Soppimath K., Aminabhavi T., Kulkarni A., Rudzinski W.: J. Control. Release, 2001, **70**, 1. https://doi.org/10.1016/S0168-3659(00)00339-4
[4] Muraviev I.: Tekhnologiya Lekarstv. Medicina, Moskva 1980.
[5] Rusak A., Marchenko L., Smehova I.: Tehnologiya Myagkih Lekarstvennykh Form. SpecLit, SpB 2004.
[6] Yin Y., Yang Y., Xu H.: J. Appl. Polym. Sci., 2002, **83**, 2835. https://doi.org/10.1002/app.10259
[7] Rabea E., Badawy M., Stevens C.: Biomacromolecules, 2003, **4**, 1457. https://doi.org/10.1021/bm034130m
[8] Bell C., Peppas N.: Adv. Polym. Sci., 1995, **122**, 125. https://doi.org/10.1007/3540587888_15
[9] Baranov V., Frenkel S., Agranova S. *et* al.: Vysokomol. Soed., 1987, **29**, 745.
[10] Chernova V., Tuktarova I., Kulish E.: Butlerovskie Soobsch., 2013, **34**, 102.
[11] Bazunova M., Shurshina A., Chernova V., Kulish E.: Rus. J. Phys. Chem. B, 2016, **10**, 1014. https://doi.org/10.1134/S1990793116060178
[12] Bazunova M., Valiev D., Chernova V., Kulish E.: Polym. Sci. A., 2015, **5**, 675. https://doi.org/10.1134/S0965545X15050041
[13] Kulish E., Chernova V., Volodina V., Kolesov S.: Polym. Sci. A., 2015, **5**, 508. https://doi.org/10.1134/S0965545X15050120

Received: January 24, 2018 / Revised: March 14, 2018 / Accepted: July 02, 2018

ОДЕРЖАННЯ ПРУЖНО-В'ЯЗКИХ СИСТЕМ НА ОСНОВІ ВОДНИХ РОЗЧИНІВ АЦЕТАТУ І СУКЦИНІМІДУ ХІТОЗАНУ У ПРИСУТНОСТІ БАГАТОАТОМНИХ СПИРТІВ

Анотація. *Досліджено реологічну поведінку ацетату та сукцинімідy хітозану в змішаних розчинниках. Показано, що заміна частини розчинника на дво- або триатомні спирти супроводжується збільшенням відносної та динамічної в'язкості розчину сукцинімідy хітозану, більш раннім формуванням сітки, переходом від в'язкісно-пружних систем до пружно-в'язких за менших значень концентрацій полімера і більшого часу релаксації.*

Ключові слова: *хітозан, сукцинімід хітозану, реологічна поведінка, змішаний розчинник, гель.*

Chem. Chem. Technol., 2019,
Vol. 13, No. 3, pp. 360–364

Chemistry

EPOXY COMPOSITES FILLED WITH NATURAL CALCIUM CARBONATE. 1. EPOXY COMPOSITES OBTAINED IN THE PRESENCE OF MONOPEROXY DERIVATIVE OF EPIDIAN-6 EPOXY RESIN

Michael Bratychak[1,*], Olena Astakhova[1], Olena Shyshchak[1], Olha Zubal[1], Maciej Sienkiewicz[2], Ostap Ivashkiv[1]

https://doi.org/10.23939/chcht13.03.360

Abstract. Physico-mechanical properties of the products based on filled epoxy-oligomeric mixtures composed of Epidian-5 epoxy resin, oligoesteracrylate TGM-3 and monoperoxide derivative of Epidian-6 epoxy resin (PO) have been investigated. $CaCO_3$ was used as a filler and polyethylene polyamine was a curing agent. The effect of PO and $CaCO_3$ on the gel-fraction content and physico-mechanical properties was examined. Using a scanning electron microscopy (SEM) the morphology of the samples has been studied.

Keywords: epoxy resin, oligoesteracrylate, peroxide, $CaCO_3$, gel-fraction, physico-mechanical properties, SEM.

1. Introduction

One of the main tasks of modern material science is to obtain composition polymer materials with predefined operational characteristics [1]. This is achieved by the directed control of polymer matrix structural network formation, as well as thermodynamic, kinetic and mechanical compatibility of the system components [2]. The choice of polymer component is important too. To date the composites based on epoxy resin are of great scientific and practical interest [3]. Epoxy resins provide high adhesion on the boundary polymer-filler and possess necessary technological properties during products formation. Moreover, they are compatible with other polymer materials and improve the properties of the resulting products [4].

Previously we showed the possibility of obtaining polymer materials based on Epidian-5 with functional derivatives of epoxy resins as a polymer additive [5]. These derivatives contain, apart from epoxy group, unsaturated methacrylate fragment [5], free carboxy group [6], primary hydroxy group [7] or fluorine atoms [8]. The introduction of epoxy resin functional derivative into the polymer mixture based on Epidian-5 resin and TGM-3 oligoesteracrylate improves the operational characteristics of the products due to the binding of all components [5-8].

On the other hand, the simultaneous improvement of operational characteristics and the reduction of products price are achieved by the introduction of mineral fillers into the polymer mixture [9]. The used fillers are TiO_2 [10, 11], silver [12], nano Si_3N_4 [13], graphite oxide [14], carbon black [15], natural zeolite [16], $CaCO_3$ [17-21] and others [22, 23]. $CaCO_3$ is the most available, and thus the most often used filler. Apart from its using for the production of epoxy resins based materials, it is applied to produce composites on the basis of polyvinyl chloride, polypropylene and polyesters [17-24].

The aim of this work was to study Epidian-5 based polymer mixture filled with calcium carbonate. The mixture contains TGM-3 oligoesteracrylate as a plasticizer, polyethylene polyamine as a curing agent and monoperoxy derivative of Epidian-6 resin (PO) of the formula:

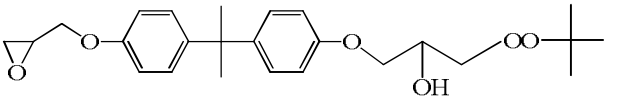

PO has a free epoxy group allowing to a introduce it into the polymer matrix which is formed by hardener. The peroxy group of PO contributes to the formation of free radicals during heating. Free radicals of the formed polymer matrix allows to graft TGM-3 molecules.

2. Experimental

2.1. Materials

The materials used for the experiments were:

Epidian-5 epoxy resin (Sarzyna-Ciech, Poland) of the formula, where n = 0–2:

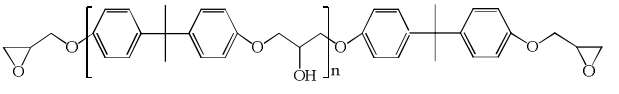

with a molecular weight of 390 g/mol and epoxy groups content (e.n.) of 20.0 %.

[1] Lviv Polytechnic National University
12, S.Bandery St., 79013 Lviv, Ukraine
[2] Gdansk University of Technology,
11/12 G. Narutowicza St., 80233 Gdansk, Poland
[*] *mbratychak@gmail.com*

Monoperoxy derivative of Epidian-6 epoxy resin (PO) was synthesized according to the procedure described in [25]. It was found for PO: molecular weight of 430 g/mol; active oxygen content of 2.8 % and e.n. of 9.5 %.

TGM-3 oligoesteracrylate is an esterification product of methacrylic acid and triethylene glycol in the solvent medium with M_n 286 g/mol. Its formula:

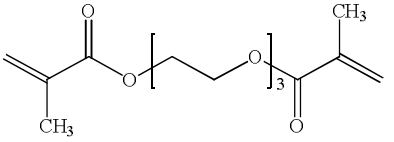

Polyethylenepolyamine (PEPA, Ukraine) of the formula

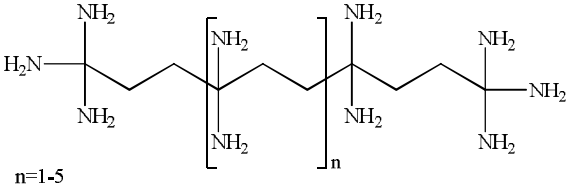

was the curing agent and was used as received without additional purification.

Calcium carbonate ($CaCO_3$, Sigma Aldrich) is a white odorless powder or colorless crystals.

2.2. Preparation of filled epoxy-oligomeric mixtures

Epidian-5, TGM-3, PO and $CaCO_3$ were mixed till the homogeneous mixture was obtained. Then it was degassed under vacuum to eliminate air bubbles. After PEPA addition the mixture was again mixed and degassed.

Fig. 1. General view of the moulds.
Sizes (mm) for dumbbell-shaped samples: length 165, width 10 and thickness 4.5; for bar: length 8, width 10 and thickness 4.5

To determine the film hardness and gel-fraction content the samples were poured over the standard glass plates. To determine physico-mechanical properties the samples were poured into special moulds in the form of dumbbell-shaped samples and bars (Fig. 1).

The dumbbell-shaped samples and bars were formed stepwise: first at room temperature for 24 h and then when heated to 423 K for 75 min.

2.3. Investigation Methods

Films hardness (*H*, rel.units) was determined according to the standard procedure [26] using M-3 pendulum device at room temperature. Gel-fraction content (*G*, %) was determined after extraction of grinded samples with acetone in Soxhlet apparatus for 12 h [26].

Tensile properties (ISO 527-21A), Charpy impact strength (ISO 179-1:2010), flexural properties (ISO 178:2010) and Shore D hardness (ISO 868) were determined with a Zwick/Roell device (Germany) in Gdansk University of Technology (Poland). Tensile tests were performed with a Zwick type Z020 tensile tester equipped with a 20 kN load cell. The tests were performed on molded samples having the dimensions of 75×4×2 mm. A grip-to-grip separation of 50 mm was used. The samples were pre-stressed to 3 N, then loaded with a constant cross-head speed of 50 mm/min. The average values reported were derived from at least five specimens.

SEM analysis of the freeze fractured samples was performed using HITACHI SU8010 apparatus equipped with a cold cathode field-emission source. The samples were sputter coated using Cressington Sputter Coater 108Auto with Au.

3. Results and Discussion

The described in the literature [17-21] epoxy resin based compositions with $CaCO_3$ do not contain monoperoxy derivative of Epidian-6 (PO). Therefore the plasticizer TGM-3 does not enter the three-dimensional cross-linked structure of the resulting product. This leads to the partial "sweating" of oligoesteracrylate during operational process and deterioration of the product properties. So, in this work it was important to determine the effect of PO and its amount on gel-fraction content and physico-mechanical properties of the product. The effect of $CaCO_3$ amount on the above mentioned characteristics should be determined as well.

The composition of the investigated mixtures is given in Table 1.

Mixture I is a standard mixture without mineral filler and PO. Mixture II additionally contains the mineral filler $CaCO_3$. In mixtures III-VIII the part of Epidian-5 resin is substituted for PO. $CaCO_3$ is absent in mixture III. For mixtures with PO the amount of filler varies from 10 to 60 mass parts.

3.1. Gel-Fraction Content and Hardness of Polymer Films

Gel-fraction content and hardness of polymer films were determined according to the procedures described in subsection 2.3. The experimental results are represented in Table 2.

Table 1

Composition of the mixtures

Component	Components content, mass parts							
	I	II	III	IV	V	VI	VII	VIII
Epidian-5	100	100	90	90	80	70	90	90
PO	0	0	10	10	20	30	10	10
TGM-3	10	10	10	10	10	10	10	10
PEPA	14	14	13.2	13.2	12.5	11.7	13.2	13.2
$CaCO_3$	0	30	0	30	30	30	10	60

Table 2

Gel-fraction content and hardness of polymer films

Mixture number according to Table 1	Gel-fraction content, %	Hardness, rel.units
I	93.6	0.57
II	94.1	0.72
III	93.2	0.74
IV	96.0	0.80
V	94.7	0.74
VI	93.5	0.72
VII	93.7	0.67
VIII	95.9	0.80

The least hardness is observed for the films without $CaCO_3$ and PO (mixture I). The introduction of $CaCO_3$ (mixture II) allows to considerably increase the films hardness with a slight increase in gel-fraction content. The partial substitution of Epidian-5 for PO also increases hardness (0.57 rel.units for mixture I *vs.* 0.74 rel.units for mixture III). This phenomenon may be explained by PO participation in the formation of film structure due to the binding of TGM-3 molecules. In the presence of PEPA, at room temperature, PO with epoxy group and labile peroxy bond in its structure enters the cross-linked matrix based on Epidian-5; –O–O– bonds are preserved. When heated, labile –O–O– bonds decompose and form free radicals which cause grafted polymerization of TGM-3 molecules to already cross-linked structure formed by Epidian-5 and PO molecules. The additional introduction of mineral filler to the mixture contributes to the increase in gel-fraction content and hardness of the films (mixture IV).

The decrease in $CaCO_3$ amount to 10 mass parts when PO amount is constant (mixture VII), decreases both gel-fraction and hardness. If we compare mixtures VIII and IV ($CaCO_3$ amount is 60 and 30 mass parts, respectively), we do not observe essential changes in the mentioned values.

The increase in PO amount from 10 to 20 and 30 mass parts (mixtures IV, V and VI, respectively) decreases gel-fraction content and hardness. The reason is possible reactions between PO molecules (at constant amount of TGM-3) leading to the formation not cross-linked structures but linear ones, which are soluble in organic solvents.

Thus, the introduction of $CaCO_3$ into the structure of polymer mixture considerably increases hardness of polymer films. The same results may be achieved by partial substitution of Epidian-5 for PO molecules. The simultaneous introduction of $CaCO_3$ in the amount of 30-60 mass parts abd PO in the amount of 10 mass parts (mixtures IV and VIII) increases both gel-fraction content and hardness of the films if compared with standard mixture I.

3.2. Physico-Mechanical Properties

Physico-mechanical properties of the mixtures were studied according to the procedure described in subsection 2.3. The experimental results are given in Table 3.

The comparison of mixtures without PO (mixtures I and II) shows that the introduction of mineral filler in the amount of 30 mass parts decreases the values of maximum tensile strength (TS_b), elongation at break (E_b), Charpy impact strength, maximum flexural strength (F_{max}) and break deformation (e-break) but increases Young's modulus (E_{Mod}) and Shore D hardness. It means that $CaCO_3$ increases hardness of the product but makes it brittle. Virtually the same results are obtained when 10 mass parts of PO were introduced (mixture III). The results are in agreement with those of Table 2 and once again indicate the participation of PO molecules in the formation of three-dimensional cross-linked structure based on Epidian-5 and TGM-3. The resulting product becomes hardener and less flexible. Simultaneous introduction of PO and $CaCO_3$ (mixture IV) decreases break deformation and impact strength by three times.

At the constant value of $CaCO_3$ amount in the mixture the PO increase from 10 to 20 and 30 mass parts (mixtures IV, V and VI, respectively) results in the

decrease of hardness and impact strength but increases the product flexibility. These data are also in agreement with the results from Table 2 and confirm the assumption that a great amount of PO leads to the less cross-link density of the mixture components.

The increase in $CaCO_3$ amount (mixtures VII, IV and VIII) increases hardness, Young's modulus, tensile strength and flexural strength but decreases impact strength.

Fig. 2 represents SEM images of some investigated mixtures.

Table 2

Mixture number according to Table 1	Tensile tests			Charpy impact strength, kJ/m^2	Flexural properties		Shore D hardness
	TS_b, mPa	E_b, %	E_{Mod}, GPa		F_{max}, MPa	e-break, %	
I	58.3	1.74	3.02	14.75	119.6	4.29	82.6
II	28.1	0.82	3.77	3.45	41.7	1.20	85.2
III	21.3	0.62	1.67	9.71	39.2	1.86	84.5
IV	21.2	0.61	3.79	3.31	39.2	1.13	85.0
V	29.3	0.90	3.16	3.01	49.2	1.48	84.0
VI	37.9	1.03	3.84	2.18	64.1	1.88	83.3
VII	24.6	0.88	2.99	5.15	47.1	1.36	85.7
VIII	34.8	0.77	4.70	2.80	53.5	1.21	86.6

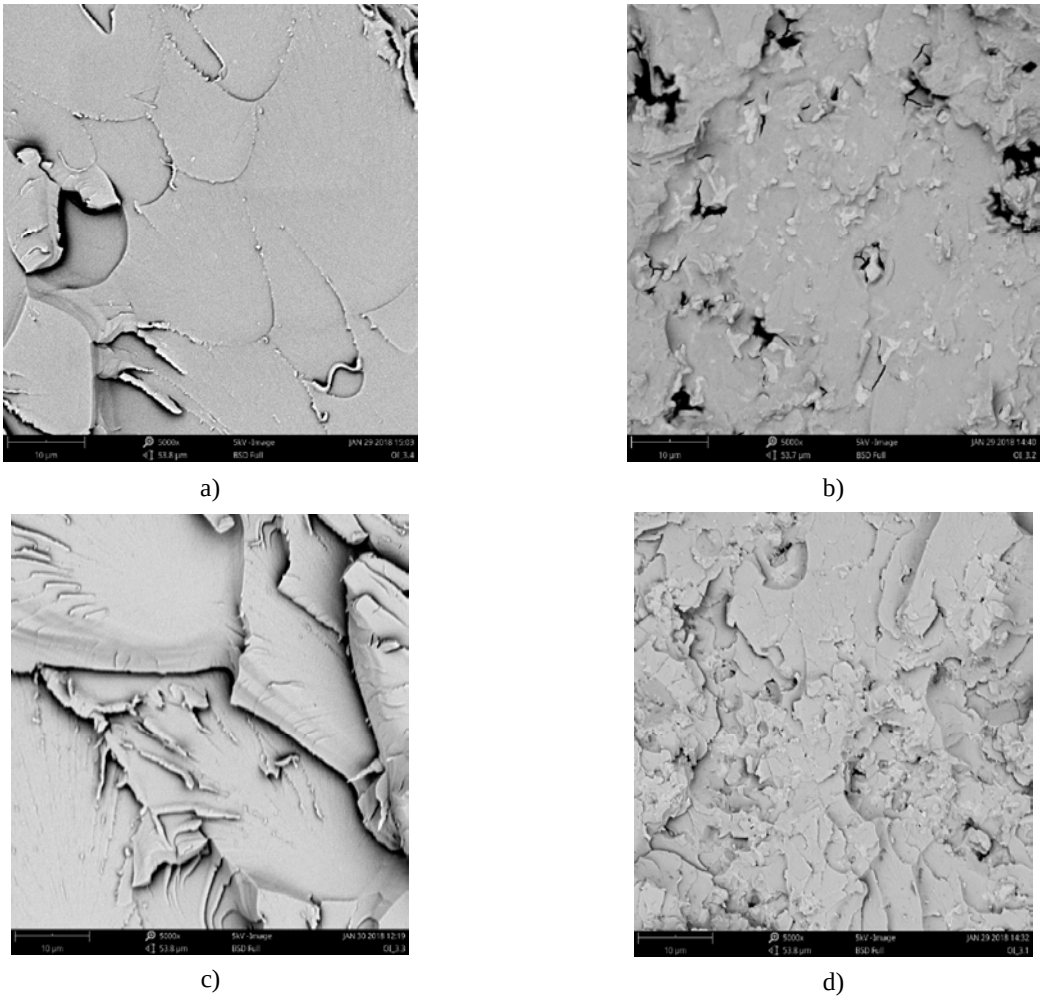

a) b) c) d)

Fig. 2. SEM images of mixture I (a), mixture II (b), mixture III (c) and mixture IV (d)

The introduction of PO into the mixture virtually does not affect the morphology of the samples (Figs. 2a and 2c). Large pores are not observed when PO and $CaCO_3$ are introduced simultaneously (cf. mixture IV, Fig. 2d and mixture II, Fig. 2b). It means that PO acts as a compatibilizer and binds all components of the mixture into unified three-dimensional cross-linked structure. This assumption correlates with the results represented in Tables 2 and 3.

4. Conclusions

Physico-mechanical properties of the samples formed on the basis of epoxy-oligoesteric mixtures have been investigated. The mixtures composed of Epidian-5 epoxy resin, TGM-3 oligoesteracrylate, monoperoxy derivative of Epidian-6 resin and calcium carbonate were cross-linked by polyethylene polyamine. The introduction of $CaCO_3$ considerably increases the films hardness. Similar results were obtained when Epidian-5 molecules were partially substituted for PO. Simultaneous introduction of $CaCO_3$ in the amount of 30–60 mass parts and PO (10 mass parts) increases both gel-fraction content and hardness if compared with mixtures without these components.

Mixtures without PO and with 30 mass parts of $CaCO_3$ are characterized by less values of maximum tensile strength, elongation at break, Charpy impact strength, maximum flexural strength and maximum deflection but higher values of Young's modulus and Shore D hardness. The analogous results are obtained when 10 mass parts of PO were introduced. The results indicate the participation of PO molecules in the formation of three-dimensional cross-linked structure. The resulting product becomes hardener and less flexible.

The increase in PO amount from 10 to 30 mass parts results in the decrease of hardness and increase in product flexibility. These data are also in agreement with the results from Table 2 and confirm the assumption that a great amount of PO leads to the less cross-link density of the mixture components. The increase in $CaCO_3$ amount increases hardness, tensile strength and flexural strength but decreases maximum deflection and impact strength.

SEM analysis confirms the improvement of product structure due to the simultaneous introduction of PO and $CaCO_3$.

References

[1] Hetmanchuk Yu., Bratychak M.: Khimiya Vysokomoleculiarnykh Spoluk. Vyd-vo Lviv Polytechnic, Lviv 2008.
[2] Hetmanchuk Yu., Bratychak M.: Khimiya i Technologiya Oligomeriv. Vyd-vo Kyiv Univ., Kyiv 2008.
[3] Bratychak M., Bratychak Mykh.: Peroksydni Pohidni Epoksydnykh Smol. Vyd-vo Lviv Polytechnic, Lviv 2003.
[4] Ellis B.: Chemistry and Technology of Epoxy Resins. Blackie Academic and Professional, London 1993.
[5] Iatsyshyn O., Astakhova O., Shyshchak O. *et al.*: Chem. Chem. Technol., 2013, **7**, 73. https://doi.org/10.23939/chcht07.01.073
[6] Bashta B., Astakhova O., Shyshchak O., Bratychak M..: Chem. Chem. Technol., 2014, **8**, 309. https://doi.org/10.23939/chcht08.03.309
[7] Bratychak M., Ivashkiv O., Bruzdziak P. *et al.*: Polimery, 2016, **61**, 316. https://doi.org/10.14314/polimery.2016.316
[8] Bratychak M., Kochubei V., Shust O. *et al.*: Chem. Chem. Technol., 2011, **5**, 41.
[9] Poh C., Mariatti M., Ahmad M. *et al.*: J. Mater. Sci. Mater. Electron., 2014, **25**, 2111. https://doi.org/10.1007/s10854-014-1847-9
[10] Ng C., Ash B., Schadler L. *et al.*: Adv. Compos. Lett., 2001, **10**, 101. https://doi.org/10.1177/096369350101000301
[11] Ng C., Schadler L., Siegel R.: Nanostruct. Mater., 1999, **12**, 507. https://doi.org/10.1016/S0965-9773(99)00170-1
[12] Tee D., Mariatti M., Azizan A. *et al.*: Compos. Sci. Technol., 2007, **67**, 2584. https://doi.org/10.1016/j.compscitech.2006.12.007
[13] Shi G., Zhang M.-Q., Rong M.-Z. *et al.*: Wear, 2003, **254**, 784. https://doi.org/10.1016/S0043-1648(03)00190-X
[14] Tang L.-C., Wan Y.-J., Yan D *et al.*: Carbon, 2013, **60**, 16. https://doi.org/10.1016/j.carbon.2013.03.050
[15] Schueler R., Petermann J., Schulte K. *et al.*: J. Appl. Polym. Sci., 1997, **63**, 1741. https://doi.org/10.1002/(SICI)1097-4628(19970328)63:13<1741::AID-APP5>3.0.CO;2-G
[16] Lee J.-Y., Shim M.-J., Kim S.-W.: Mater. Chem. Phys., 1997, **48**, 36. https://doi.org/10.1016/S0254-0584(97)80073-9
[17] Leong Y., Abu Bakar M., Mohd Oshak Z. *et al.*: J. Appl. Polym. Sci., 2004, **91**, 3315. https://doi.org/10.1002/app.13542
[18] Shi Q., Wang L., Yu H. *et al.*: Macromol. Mater. Eng., 2006, **291**, 53. https://doi.org/10.1002/mame.200500223
[19] Mustata F., Tudirachi N., Rosu D.: Compos. Part B-Eng., 2012, **43**, 702. https://doi.org/10.1016/j.compositesb.2011.11.047
[20] Yu H., Wang L., Shi Q. *et al.*: Prog. Org. Coat., 2006, **55**, 296. https://doi.org/10.1016/j.porgcoat.2006.01.007
[21] He H., Li K., Wang J. *et al.*: Mater. Design, 2011, **32**, 4521. https://doi.org/10.1016/j.matdes.2011.03.026
[22] Mohan T., Kanny K.: Compos. Part A-Appl. S., 2011, **42**, 385. https://doi.org/10.1016/j.compositesa.2010.12.010
[23] Yung K., Zhu B., Yue T. *et al.*: Compos. Sci. Technol., 2009, **69**, 260. https://doi.org/10.1016/j.compscitech.2008.10.014
[24] Yilmar M., Unal H., Mimaroglu A.: Express Polym. Lett., 2008, **2**, 890. https://doi.org/10.3144/expresspolymlett.2008.104
[25] Astakhova O., Shved M., Zubal O. *et al.*: Chem. Chem. Technol., 2019, **13**, 112. https://doi.org/10.23939/chcht13.01.112
[26] Ivanov V.: Rukovodstvo k Prakticheskim Rabotam po Khimii Polimerov. Izd-vo Leningrad. Univ., Leningrad 1982.

Received: October 23, 2018 / Revised: November 21, 2018 / Accepted: December 15, 2018

ЕПОКСИДНІ КОМПОЗИТИ З НАТУРАЛЬНИМ НАПОВНЮВАЧЕМ КАРБОНАТОМ КАЛЬЦІЮ. 1. ОДЕРЖАННЯ ЕПОКСИДНИХ КОМПОЗИТІВ У ПРИСУТНОСТІ МОНОПЕРОКСИДНОЇ ПОХІДНОЇ ЕПОКСИДНОЇ СМОЛИ EPIDIAN-6

Анотація. *Вивчені фізико-механічні властивості зразків на основі наповнених епокси-олігоестерних сумішей, що складаються із промислової епоксидної смоли Epidian-5 та олігоестеракрилату TGM-3 і містять монопероксидну похідну епоксидної смоли Epidian-6 (PO. Як мінеральний наповнювач використано $CaCO_3$, затвердни ком сумішей слугував поліетиленполіамін. Встановлено вплив PO і $CaCO_3$ на вміст гель-фракцій та фізико-механічні властивості виробу. З використанням скануючої електронної мікроскопії показана морфологія отриманих зразків.*

Ключові слова: *епоксидна смола, олігоестеракрилат, пероксид, $CaCO_3$, гель-фракція, фізико-механічні властивості, СЕМ.*

Chem. Chem. Technol., 2019,
Vol. 13, No. 3, pp. 365–371

Chemical
Technology

REMOVAL OF METHYLENE BLUE BY ADSORPTION ONTO ACTIVATED CARBONS PRODUCED FROM AGRICULTURAL WASTES BY MICROWAVE INDUCED KOH ACTIVATION

Ibtissem Kahoul[1, 2, *], Nabil Bougdah[1], Faycal Djazi[1, 2], Chahrazed Djilani[2], Pierre Magri[3], Mohamed Salah Medjram[1, 4]

https://doi.org/10.23939/chcht13.03.365

Abstract. The present study aims to describe new low cost activated carbons which were prepared from bean peel (BP), acorn peel (AP) and *Pistacia lentiscus* (PL) under microwave induced KOH chemical activation for the removal of methylene blue dye from aqueous solutions. Activated carbons were characterized using, thermogravimetric analysis, and scanning electron microscopy. The adsorption properties were examined considering several parameters including the effect of pH, contact time, adsorbent dosage and initial concentration. Activated carbons powders prepared from BP, AP and PL can be used as an eco-efficient and low-cost adsorbent for removing methylene blue dye from aqueous solution by adsorption process.

Keywords: activated carbon, agricultural wastes, adsorption, methylene blue, microwave.

1. Introduction

Wastewater effluents released from different industries such as textile, paper, rubber, leather, plastics, cosmetic, and printing contain several classes of synthetic dyestuffs [1].

Dyes are mainly used in the textile industry, although substantial quantities are consumed for coloring different materials, such as paper, leather, plastics, petroleum products, and food [2].

Methylene blue is the most common dye used in the dyeing of wood, cotton, and silk. It can cause eye injury to humans and animals. Its inhalation may lead to breathing difficulties while mouth ingestion induces burning, nausea, vomiting, sweating, and abundant cold sweats [3]. The treatment of industrial waste containing this type of dye is of a great interest.

A wide variety of physical, chemical and biological techniques have been developed and tested for the sake of treatment of effluents loaded with dyes. These processes include flocculation, precipitation, ion exchange, membrane filtration, irradiation, and ozonation. However, these methods are expensive and result in generation of large quantities of formed derivatives [4].

Among the processes of treatment of the liquid rejections, adsorption remains a technique relatively used and easy to implement. Adsorption is usually used to treat wastewater due to the efficient elimination of organic micropollutants and owing to economic considerations [5, 6].

The objective of this work was to test the efficiency of new activated carbons obtained from agricultural wastes, namely bean peel, acorn peel and *Pistacia lentiscus* under microwave induced KOH chemical activation for removing of cationic dye which is methylene blue from aqueous solutions by adsorption process.

2. Experimental

2.1. Preparation of Adsorbate

Methylene blue (MB), a basic dye having a molecular structure as C16H18N3SCl (with a molecular weight of 319.85 g/mol, and l_{max} 665 nm) was used in this work. The stock dye solution was prepared by dissolving accurately weighed dye in the deionized water to the concentration of 100 mg/l and subsequently, the experimental solutions of various initial concentrations (C_0) were prepared by diluting stock solution to the desired concentrations.

[1] Department of Petrochemistry and Process Engineering, Faculty of Technology,
University 20 August 1955-Skikda, Algeria
[2] Laboratory LRPCSI, University 20 August 1955-Skikda, Algeria
[3] LCP-A2MC, University of Lorraine, 1, bd Arago-57078 METZ, Cedex 3, France
[4] Laboratory LGCES, University 20 August 1955-Skikda, Algeria
[*] *ibtissem-k21@hotmail.fr*

2.2. Preparation of Activated Carbons

Bean peel (BP), acorn peel (AP) and *Pistacia lentiscus* (PL) were collected in the northeastern region of Algeria. After collecting, these adsorbents were cut into small pieces with a clean chisel, then washed thoroughly with distilled water to remove dirtiness, dried in sunlight, and finally crushed and filtered at 250 μm.

Pistacia lentiscus was soaked in hexane to remove residual oils, then filtered and washed several times with distilled water, dried in an oven at 353 K for 12 h, and cooled at a room temperature. After that, BP, AP and PL were carbonized at 623, 923 and 853 K, respectively, for 1 h in an oven. The chars produced were soaked in potassium hydroxide solution with an impregnation (char:KOH ratio was 1:1.75 % w/w) [7].

The activation step was carried out in glass tubes placed in a microwave oven (Monowave Extra Anton Paar MAS24 type; the frequency 2.45 GHz). The microwave power was adjusted at 800 W, the irradiation time was selected as 7 min for each sample, and the stirring speed was set at 600 rpm [8].

The activated products were then washed with hydrochloric acid of 0.1M and deionized water until the pH of the washing solution reached 7-8, then they were filtered and dried in an oven at 333 K for about 12 h [9].

2.3. Characterization

The thermal decomposition of BP, AP and PL was studied using thermal balance 2050 TGA v5.4 A from TA Instruments. In order to visualize the morphology of the activated carbons before and after the activation process, we have used scanning electron microscopy (TESCAN type).

3. Results and Discussion

3.1. Characterization of the Adsorbent

3.1.1. Thermogravimetric analyses

Thermal decomposition curves are illustrated below in Fig. 1.

TGA thermal curve that corresponds to BP (Fig. 1a), comprises four stages of the mass loss process. The first weight loss of 11.5 % is due to the release of the adsorbed water at 329 K. Next, three other peaks follow: the decomposition reaction with weight loss of about 28 % was observed at 563 K, which corresponds to the hemicellulose departure, also a weight loss of about 20 % is observed at 598 K, corresponding to the departure of the cellulose, while the last loss of about 14 % took place at 713 K, corresponding to the departure of the lignin [10, 11].

TGA thermal curve that corresponds to AP (Fig. 1b), contains four stages of the mass loss process. The first stage extends from the beginning of the analysis to 350 K with weight loss of about 11 %. Three other peaks follow at 558, 613 and 678 K, with corresponding mass losses of 19, 13 and 8 % which indicates the thermal decompositions of the cellulose, hemicellulose, and lignin, respectively [12, 13].

TGA thermal curve that corresponds to PL is shown in Fig. 1c. Three stages of mass loss were observed. The first stage of weight loss (2.42 %) was observed at 337 K, corresponding to the departure of the physisorbed water. The second stage that had a mass loss of 33 % was observed at 551 K, corresponding to the departure of the hemicellulose and cellulose. The last loss of about 8 % occurs at 663 K, corresponding to the departure of the lignin.

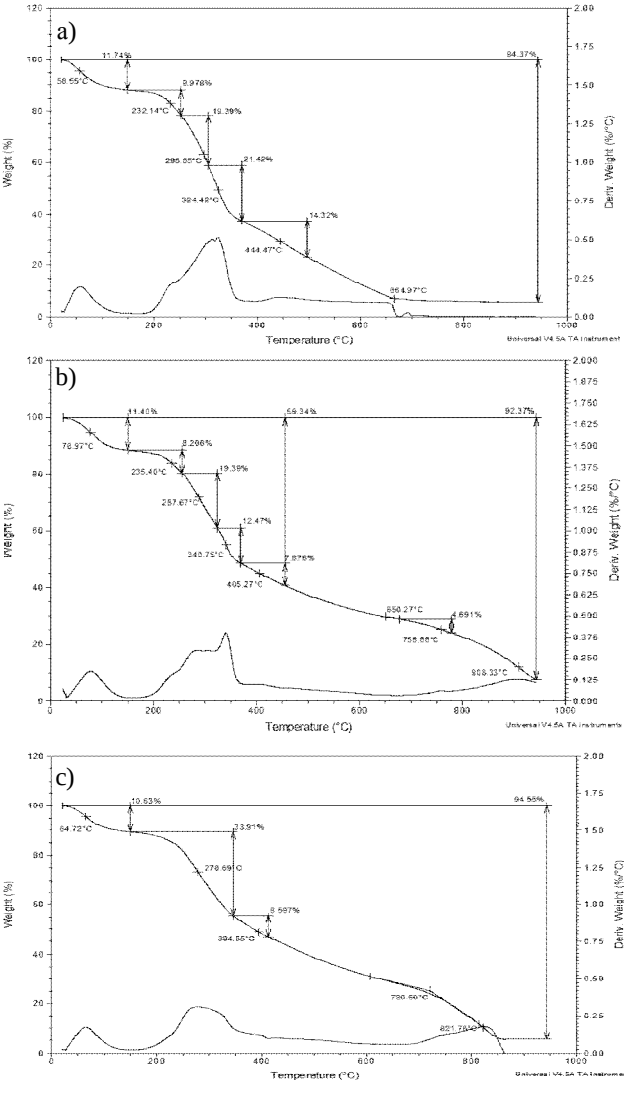

Fig. 1. TGA/DTG analysis of BP (a), AP (b) and PL (c)

3.1.2. Scanning electron microscopy studies

In order to estimate the textual structure of adsorbents, scanning electron microscope analysis has been used before and after the activation process *via* microwave assisted KOH activation.

It can be seen that the surface morphology of activated carbon from BP (Fig. 3a) has developed uniform surface, forming an orderly pore structure.

However, the surface morphology of activated carbons from AP and PL was a gathering of fine particles, which has no regular and fixed shape and size. The particles were of different dimensions and included a large number of kinks on the external surface.

3.2. Adsorption Kinetics Studies

Kinetic experiments were carried out in Erlenmeyer flasks including 100 ml aqueous solution of methylene blue with a known number of different adsorbents at ambient temperature. Solutions were stirred at 250 rpm during selected laps time. After that, the solution was centrifuged in order to remove the adsorbent dispersion and analyzed by UV spectrometry (Analytik Jena (AG) spectrophotometer).

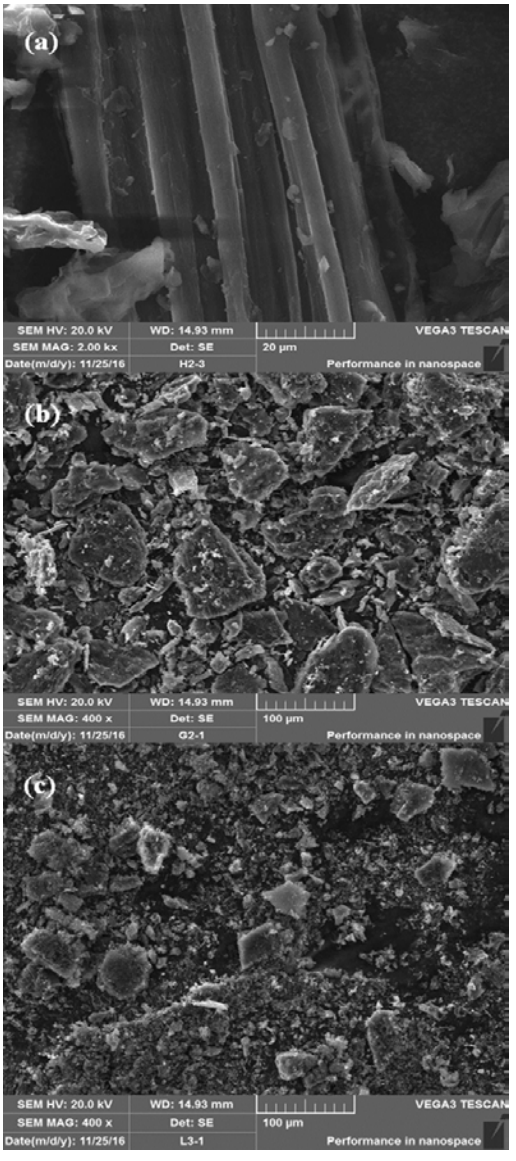

Fig. 2. SEM micrographs of chars: BP (a), AP (b) and PLC (c)

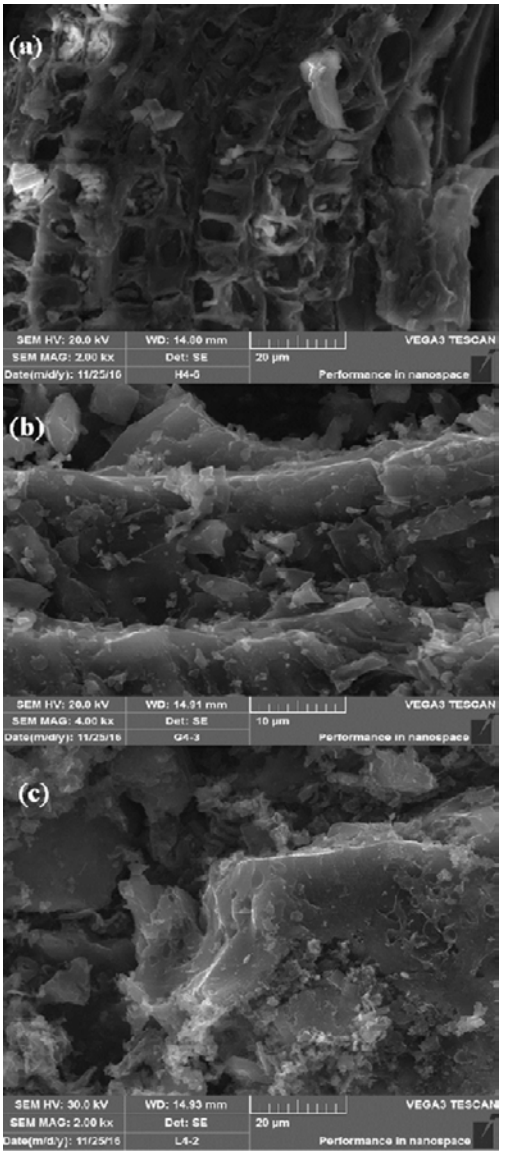

Fig. 3. SEM micrographs of activated carbons: BP (a), AP (b) and PL (c)

The amount of dye adsorbed onto adsorbents at time *t*, q_t (mg/g) was computed by the mentioned mass balance relationship:

$$q_t = (C_0 - C_e) \cdot \frac{V}{m} \quad (1)$$

$$R\% = \frac{(C_0 - C_e)}{C_0} \cdot 100 \quad (2)$$

where q_t is the adsorption capacity; *R*% is the adsorption percentage; C_0 and C_e are the initial and equilibrium concentrations, mg/l; *V* is the volume of the solution, l; *m* is the mass of adsorbent used, g.

Fig. 4 presents the kinetics adsorption obtained at room temperature with the adsorbate initial concentration of 10 mg/l. The mass of activated carbons was 50 mg within all experiments.

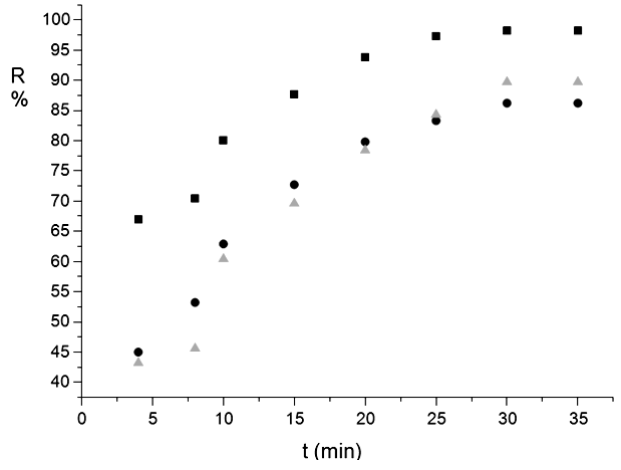

Fig. 4. Kinetics adsorption MB on BP (**n**), AP (●) and PL (▲)

Fig. 4 shows the variation of the adsorbed MB amount as a function of time on BP, AP, and PL. It can be seen from Fig. 4 that the adsorption efficiency increases with the contact time because a large number of vacant surface sites are present for adsorption. Equilibrium is reached for three adsorbents after 30 min. The maximum adsorption percentage for activated carbons was 98.2 % for BP, 86.2 % for AP and 89.7 % for PL.

Kinetic studies are important to estimate the efficiency and mechanism of sorption process. Adsorption kinetics defines the nature of adsorption interaction dependence of the adsorbents with species [14].

Constants from two kinetic models, pseudo first-order and pseudo second-order ones, were fit for experimental data to examine the adsorption of MB by activated carbons BP, AP and PL.

The first one was the linear form of the pseudo first-order model of Lagergren [15, 16], generally expressed as follows:

$$Ln(q_e - q_t) = Ln(q_e) - k_1 t \quad (3)$$

where q_e and q_t are the amounts of MB adsorbed at equilibrium and after time *t*, respectively. We noticed the rate constant of adsorption as k_1, min^{-1}.

The pseudo-second-order model [17]:

$$\frac{dqt}{dt} = k_2 (qe - qt)^2 \quad (4)$$

where k_2 is the equilibrium rate constant of the pseudo-second-order, $g \cdot mg^{-1} \cdot min^{-1}$.

We separated variables in Eq. (4) and then integrated for the boundary conditions $q_t = 0$ to $q_t = q_t$ and $t = 0$ to $t = t$ yields to the expression that we can rearrange to the following linear formula:

$$\frac{t}{q_t} = \frac{1}{k_2 q_e^2} + \frac{t}{q_e} \quad (5)$$

The slope and the intercept allow us to establish q_e and k_2, respectively.

Kinetic model parameters together with R^2 correlation coefficients are presented in Table 1.

The pseudo-second-order model gives a better fit. The correlation coefficients of the pseudo-second-order kinetics have higher values than those of the pseudo-first-order. Moreover, the value of q_e obtained with pseudo-second-order model is in a good agreement with the experimental value of $q_{e\ exp}$. Therefore, the adsorption of MB onto activated carbons BP, AP and PL follows second-order reaction kinetics.

The results propose that the adsorption of MB takes the path of the pseudo-second-order kinetics, showing that the rate-determining step of the adsorption process can be chemical adsorption or chemisorption [18].

Table 1

Pseudo-first order and pseudo-second-order kinetics parameters of BP, AP, and PL

Adsorbent	Pseudo-first-order				Pseudo-second-order		
	k_1, min^{-1}	$q_{e\ calc}$, mg/g	$q_{e\ exp}$, mg/g	R^2	k_2, $g \cdot mg^{-1} \cdot min^{-1}$	$q_{e\ calc}$, mg/g	R^2
BP	0.1598	17.34	19.64	0.90	0.0141	21.69	0.98
AP	0.1288	16.33	17.24	0.98	0.0078	20.70	0.98
PL	0.1051	17.15	17.94	0.96	0.0047	22.72	0.98

3.3. Adsorption Isotherms

The adsorption isotherms of MB on activated carbons BP, AP, and PL have assessed the exact identical experimental setup as with kinetic experiments. In each experiment, samples of 50 mg of BP, AP, and PL were equilibrated for 30 min at 298 K with 100 ml of the dye aqueous solution of initial concentrations between 5 and 30 mg/l.

The adsorption isotherms of MB on adsorbents are plotted in Fig. 5. We noted that they have a generally similar appearance, indicating that when the initial concentration of the MB increases, the adsorbed amount increases to almost a plateau indicating the saturation of all the sites on the adsorbents surface. The isotherms have been classified according to the classification of Giles *et al.* [19].

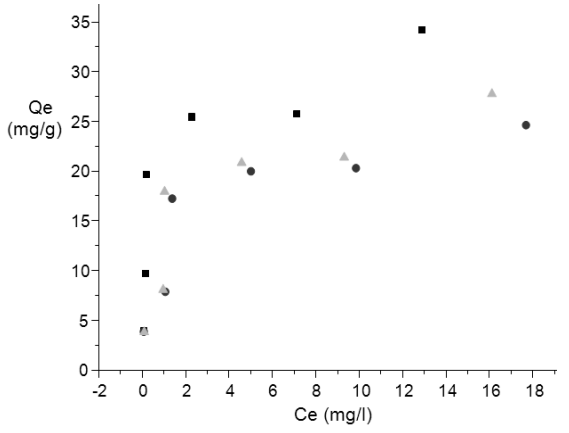

Fig. 5. Isotherms of MB on BP (■), AP (●) and PL (▲)

3.3.1. Langmuir isotherm model

The Langmuir model [20] presumes that an adsorption may happen at specific homogeneous sites on the adsorbent and is used successfully in many monolayer adsorption processes [21].

The Langmuir equation has the following form

$$\frac{C_e}{q_e} = \frac{1}{q_m b} + \frac{C_e}{q_m} \tag{6}$$

where q_m is the theoretical maximum monolayer adsorption capacity, mg·g^{-1}; b is the Langmuir constant, l·mg^{-1}.

Langmuir isotherm can be expressed with respect to a dimensionless separation factor R_L, which is expressed as:

$$R_L = \frac{1}{1 + bC_0} \tag{7}$$

where C_0 is the maximum initial MB concentration, mg/l.

The value of R_L points to the shape of Langmuir isotherm to be either unfavorable ($R_L > 1$), linear ($R_L = 1$), irreversible ($R_L = 0$), or favorable ($0 < R_L < 1$).

3.3.2. Freundlich isotherm model

Freundlich isotherm is settled on the assumption of a heterogeneous surface with a non-uniform heat distribution of the sorption on the surface [22, 23].

The Freundlich model is expressed as follows:

$$q_e = K_F C_e^{1/n} \tag{8}$$

where K_F (mg·g^{-1}·(l·mg^{-1})$^{1/n}$) and n are Freundlich constants related to the multilayer adsorption capacity and the surface heterogeneity, respectively. If ($n < 1$) the adsorption is unfavorable, ($n = 1$) the adsorption is homogeneous and ($n > 1$) the adsorption is favorable.

All of the correlation coefficients and the constants calculated from both models are listed in Table 2.

We can notice from Table 2 that the correlation factor R^2 is close to the unity for both models, however with a better fit of the experimental data [21].

It can be seen that the values of Freundlich constant n are over 2, which indicates that BP, AP, and PA are good adsorbents for MB.

The value of R_L between 0–1 proves that the adsorption of the MB on BPA, APA and PLA is favorable.

3.4. Effect of pH

pH of MB solution has been detected to be one of the most important factors affecting sorption process because of its influence on surface charge of adsorbent and solubility of MB [24, 25].

The influence of pH on the MB adsorption was studied for the different adsorbents. For this purpose, 100 ml of 10 mg/l solution contaminated with MB and the optimum dose of the adsorbent were introduced. Each solution was stirred for a time corresponding to the equilibrium time of the dye, and the value of pH was varied. The acidic and basic pH values obtained were justified by the addition of 1M HCl to acidify and 1M NaOH to basify.

Table 2

Langmuir and Freundlich isotherm parameters for MB adsorption

Adsorbent	Langmuir				Freundlich		
	q_m, mg·g^{-1}	b, l·mg^{-1}	R^2	R_L	K_F, mg·g^{-1}·(l·mg^{-1})$^{1/n}$	n	R^2
BP	45.45	1.83	0.93	0.051	16.726	3.215	0.73
AP	17.54	4.38	0.90	0.022	10.175	2.932	0.89
PL	19.60	2.68	0.92	0.035	10.633	2.702	0.86

Fig. 6 shows the variation of MB removal on BP, AP, and PL at various initial pH of the solution.

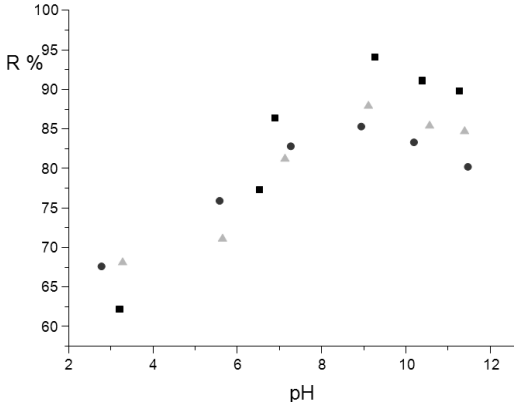

Fig. 6. Influence of pH on the adsorption yield on BP (**n**), AP (●) and PL (▲)

The behavior of MB dye adsorption on three activated carbons was studied over a wide range of pH (2–12). It can be seen from Fig. 6 that the maximum quantity of MB removal for three adsorbents was at pH 9; after that we can notice a decrease in the adsorbed capacity of the MB between pH 10 and 12. This behavior may be due to the fact that the surface of the adsorbents at pH < 9 is negatively charged, which promotes the adsorption of the methylene blue cationic dye. On the other hand, for pH values above 9, the surface of the adsorbents is positively charged and therefore capable of repelling the dye cations.

As the pH value decreases, the number of negatively charged sites also diminishes and the number of positively charged sites increases [26].

4. Conclusions

In this work, we have demonstrated that activated carbons prepared from agricultural wastes of bean peel, acorn peel and *Pistacia lentiscus* under microwave induced KOH chemical activation are good adsorbents for the removal of methylene blue from aqueous solutions. Equilibrium is reached for all activated carbons BP, AP, PL after 30 min. The elimination ratios of these compounds were ranged from 86.2 to 98.2 % for all new activated carbons BP, AP, and PL. The experimental adsorption data of Langmuir and Freundlich isotherm model have proven that the adsorption of MB on BP, AP and PL is favorable.

The calculated kinetic parameters of activated carbons BP, AP and PL from the pseudo first-order and pseudo second-order plots indicate that the pseudo-second-order model shows a better fit.

The attractive features of activated carbons *via* microwave assisted KOH can reduce the time and save energy for activated carbons preparation. Moreover, the activated carbons BP, AP, and PL are environment friendly, effective and of a low cost.

References

[1] Batzias F., Sidiras D.: Bioresour. Technol., 2007, **98**, 1208. https://doi.org/10.1016/j.biortech.2006.05.020
[2] Tan I., Hameed B., Ahmad A.: Chem. Eng. J., 2007, **127**, 111. https://doi.org/10.1016/j.cej.2006.09.010
[3] Ghosh D., Bhattacharyya K.: Appl. Clay Sci., 2002, **20**, 295300. https://doi.org/10.1016/S0169-1317(01)00081-3
[4] Robinson T., McMullan G., Marchant R., Nigam P.: Bioresour. Technol., 2001, **77**, 247. https://doi.org/10.1016/S0960-8524(00)00080-8
[5] Robinson T., Chandran B., Nigam P.: Water Res., 2002, **36**, 2824. https://doi.org/10.1016/S0043-1354(01)00521-8
[6] Qi J., Li Z., Guo Y., Xu H.: Mater. Chem. Phys., 2004, **87**, 96. https://doi.org/10.1016/j.matchemphys.2004.05.008
[7] Foo K., Hameed B.: Biomass Bioenerg., 2011, **35**, 3257. https://doi.org/10.1016/j.biombioe.2011.04.023
[8] Foo K., Hameed B.: Chem. Eng. J., 2012, **187**, 53. https://doi.org/10.1016/j.cej.2012.01.079
[9] Foo K., Hameed B.: Chem. Eng. J., 2012, **184**, 57. https://doi.org/10.1016/j.cej.2011.12.084
[10] Djilani C., Zaghdoudi R., Modarressi A. *et al.*: Chem. Eng. J., 2012, **189-190**, 203. https://doi.org/10.1016/j.cej.2012.02.059
[11] Ozdemir I., Sahin M., Orhan R., Erdem M.: Technol., 2014, **125**, 200.
[12] Farinella N., Matos G., Arruda M.: Technol., 2007, **98**, 1940.
[13] Deiana A., Sardella M., Silva H. *et al.*: J. Hazard. Mater., 2009, **172**,13. https://doi.org/10.1016/j.jhazmat.2009.06.095
[14] Ghaedi M., Biyareh M., Kokhdan S. *et al.*: Mater. Sci. Eng. C, 2012, **32**, 725. https://doi.org/10.1016/j.msec.2012.01.015
[15] Zhu L., Chen B., Shen X.: Environ. Sci. Technol., 2000, **34**, 468. https://doi.org/10.1021/es990177x
[16] Dogan M., Ozdemir Y., Alkan M.: Dyes Pigments, 2007, **75**, 701. https://doi.org/10.1016/j.dyepig.2006.07.023
[17] Eftekhari S., Habibi-Yangjeh A., Sohrabnezhad S.: J. Hazard. Mater., 2010, **178**, 349. https://doi.org/10.1016/j.jhazmat.2010.01.086
[18] Dawood S., Kanti Sen T.: Water Res., 2012, **46**, 1933. https://doi.org/10.1016/j.watres.2012.01.009
[19] Giles C., MacEwan T., Nakhwa S., Smith D.: J. Chem. Soc., 1960, **10**, 3973. https://doi.org/10.1039/jr9600003973
[20] Gurses A., Dogar C., Yalcin M. *et al.*: J. Hazard. Mater., 2006, **131**, 217. https://doi.org/10.1016/j.jhazmat.2005.09.036
[21] Langmuir I.: J. Am. Chem. Soc., 1918, **40**, 1361. https://doi.org/10.1021/ja02242a004
[22] Mechati F., Bouchelta C., Medjram M. *et al.*: J. Environ. Chem. Eng., 2015, **3**, 1928. https://doi.org/10.1016/j.jece.2015.07.007
[23] Hamdaoui O., Naffrechoux E.: J. Hazard. Mater., 2007, **147**, 381. https://doi.org/10.1016/j.jhazmat.2007.01.021
[24] Abuzer C., Gizem Ilgun E., Bozkurt H.: Chem. Eng. J., 2012, **191**, 228. https://doi.org/10.1016/j.cej.2012.03.007
[25] Kumar P., Ramalingam S., Senthamarai C. *et al.*: Desalin., 2010, **261**, 52. https://doi.org/10.1016/j.desal.2010.05.032

[26] Tahir S., Rauf N.: Chemosphere, 2006, **63**, 1842. https://doi.org/10.1016/j.chemosphere.2005.10.033

Received: March 29, 2018 / Revised: April 20, 2018 / Accepted: September 12, 2018

ВИДАЛЕННЯ МЕТИЛЕНОВОГО СИНЬОГО АДСОРБЦІЄЮ НА АКТИВОВАНОМУ ВУГІЛЛІ ОДЕРЖАНОГО З СІЛЬСЬКОГОСПОДАРСЬКИХ ВІДХОДІВ ПІД ДІЄЮ АКТИВОВАНОГО МІКРОХВИЛЯМИ КОН

Анотація. *Для видалення барвника метиленового синього з водних розчинів досліджено нове недороге активоване вугілля, одержане з лушпиння бобів (ЛБ), жолудя (ЛЖ) та мастикового дерева (ЛМ) під дією активованого мікрохвилями КОН. Проведено аналіз одержаних зразків з використанням термогравіметричного аналізу та скануючої електронної мікроскопії. Адсорбційні властивості вуглецю визначені з урахуванням впливу pH, часу контакту, кількості адсорбента та його початкової концентрації. Показано можливість використання ЛБ, ЛЖ та ЛМ як екологічних ефективних та недорогих адсорбентів для видалення метиленового синього барвника з водного розчину.*

Ключові слова: *активоване вугілля, сільськогосподарські відходи, адсорбція, метиленовий синій, мікрохвилі.*

Chem. Chem. Technol., 2019,
Vol. 13, No. 3, pp. 372–376

Chemical
Technology

IMPROVEMENT OF ADSORPTION-ION-EXCHANGE PROCESSES FOR WASTE AND MINE WATER PURIFICATION

***Myroslav Malovanyy*[1, *]*, Kateryna Petrushka*[1]*, Ihor Petrushka*[1]

https://doi.org/10.23939/chcht13.03.372

Abstract. The increase of ecological safety level of the hydrosphere as a result of the improvement of the adsorption processes for waste and mine water purification by using natural sorbents and desalting processes *via* electrodialysis has been investigated. The optimal parameters of improved sorption processes with natural sorbents have been established. The mechanism of diffusion was studied by the "kinetic memory" method. Effective coefficients of pore diffusion were determined during sorption of pollutants by natural sorbents. The optimal parameters of electrodialysis with intermembrane filling by ion exchangers for demineralization of waste and mine water have been established.

Keywords: ecological safety, electrodialysis, natural sorbents, sorption, waste and mine water, intermembrane filling.

1. Introduction

Ukraine belongs to the least water-dependent countries of Europe, since the local reserves of river runoff is about 1000 m^3/year per person. The main reason of surface water pollution is the dumping of untreated and insufficiently treated industrial waste water. Wastewater of light or mining industries is especially dangerous because it is not only highly mineralized, but also contains high molecular compounds in significant concentrations. Among them there are organic dyes from textile enterprises. The specific volume of wastewater from painting industry is 150–489 m^3/t. In some mining regions of Ukraine there is a shortage of drinking water, whereas a large amount of mine water is pumped out from underground openings and negatively affects the environment. Using purified mine water would help to solve two problems at once: to reduce its negative impact on the environment and to overcome the shortage of technical water in the regions with poor water resources.

Effective method for purification of municipal wastewaters and landfill filtrates are aerobic biological methods [1, 2]. One of the promising methods of waste and mine water demineralization is electrodialysis, due to which desalting and concentration of water with a salt content of up to 12,000 mg/l can be achieved; the purification efficiency would be up to 94 %. As a result, the initial solution can be concentrated by almost 20 times. It is important that the service life of the membranes is economically attractive and durable [3-7].

The high effect is achieved by using ion exchangers. Electrodialysis is an effective desalination method, in particular for seawater which may be used in drinking water supply. Electrochemical, as well as reagent methods are versatile, well exposed to automation and provide high efficiency of purification [8-10].

Adsorption using natural sorbents of mineral and plant origin is also economically viable method of waste and mine water purification [11-13]. The prospect of using natural minerals in the process of wastewater treatment is determined not only by their high adsorption capacity but also by the existence of effective methods for improving the adsorption properties of minerals and the nature of their surfaces *via* modification. Exhausted natural adsorbents often do not require regeneration (the sorbents saturated with the withdrawn component receive new qualitative characteristics and can be used in other technologies).

Therefore, the investigations aimed at improving the adsorption-ion-exchange processes of waste and mine water purification are relevant and important for increasing the ecological safety of the hydrosphere.

The aim of this work is to increase the ecological safety level of the hydrosphere as a result of the improvement of the adsorption processes for waste and mine water purification by using natural sorbents and desalting processes *via* electrodialysis.

2. Experimental

The kinetics of dyes sorption by natural sorbents was investigated in a thermostated apparatus equipped

[1] Lviv Polytechnic National University,
12, S.Bandery St., 79013 Lviv, Ukraine
[*] *mmal@lp.edu.ua*

with a stirrer using activated bentonite, glauconite and palygorskit as the sorbents. The design of the setup allowed to vary the speed of rotation of the mixing device for various experiments. The contaminated media were artificially prepared wastewater, contaminated with anionic red 8C and active scarlet 4ZhT dyes. In the experiments with interrupted stirring, the mixing device was stopped after 5 min, the interruption time was 10 min ($\Delta\tau$ = 10 min).

A method for comparing experimental values with the theoretical ones for intradiffusion sorption process on the basis of effective coefficients of pore diffusion was that adsorption occurred in the volume of the fluid, which in a weight ratio significantly exceeded the content of the solid phase (sorbent). It means that at the initial moment of time the concentration of pollutions in the fluid changes slightly. In the beginning of the process, it is accepted as a constant on the surface of the adsorbent grain, and the mathematical problem was formulated as a problem of diffusion with the first-type boundary conditions.

To investigate ion-exchange processes for highly mineralized waste and mine water purification the model system of ion exchange resin KU 2–NH_4Cl solution was used. The ion exchanger was placed in a measuring cell (U-shaped tube) and alternately led to the equilibrium with the test solution (solutions of 0.1–0.5 M were investigated). The values of back resistance of the pure solution and the ionite–solution system depending on the solution concentration ($1/R$) were plotted. The point of intersection of the received dependences allowed to determine the concentration of the iso-conductive solution (under which the concentration conductivity is the same as that of ion exchanger). Then the resin was transferred to a centrifuge cell (the ion exchange cell with a porous bottom and two platinum electrodes, folded against each other in the cell wall). The equilibrium solution was removed by centrifugation. The centrifugation of the cell lasted 15 min at the increase in gravity by 373 times. Using an AC bridge (1000 Hz), the resistance of the cell (R_x) was measured, the value of which was used to calculate the specific electrical conductivity of the ion exchanger. The obtained results allow to study the concentration dependence of the resin specific conductivity in the NH_4Cl solution.

3. Results and Discussion

The selectivity of adsorption by clay minerals is caused not only by the presence of micro-, meso-, macropores, but also by participation of nanotubes in the adsorption processes and formation of the pores between them. It was investigated that the pore radius of the modified bentonite of the Ilnitsky deposit shifts toward the transition pores and macropores [14], which suggests an expansion of selective sorption range. The increase in the number of transition pores indicates that the main mass transfer occurs precisely in these pores. In addition, the capillary condensation is observed in such pores, which takes place when the non-compensated superficial forces act over the pores entire volume.

Forecasting of the adsorption kinetics on the example of direct dyes sorption from wastewater can determine the speed of achieving the process equilibrium and its mechanism, as well as the maximum sorption capacity of the adsorbent. In this case, the possibility of calculating the diffusion coefficients of mass transfer allows to construct an optimization profile of the industrial process.

The solution of the problem for the intradiffusion adsorption process at the initial concentration in the solution (τ = 0; C_0) and in the adsorbent grain C_{a0}, and the first-type boundary conditions, with the assumption that the particles shape being spherical, is the equation that determines the change in the component concentration in the liquid phase with time [15]:

$$\frac{C_1}{C_0} = 1 - \frac{1}{1+a}\left[1 - \sum_{n=1}^{\infty} \frac{6a\,(1+a)\exp\left(-m_n^2 t\right)}{9 + 9a + a^2 m_n^2}\right] \quad (1)$$

$$\frac{tg m_n}{m_n} = \frac{3}{3 + a \cdot m_n^2} \quad (2)$$

where C_0 is the initial concentration of the component in the solution, g/dm^3; C_1 is the component concentration at the given moment of time, g/dm^3; μ_n are positive roots of characteristic equation; a is the coefficient of adsorbent pores filling by an adsorbate.

Theoretical calculations of the coefficient of pore filling in natural sorbents by direct dyes (Fig. 1) are carried out taking into account the hydrodynamic conditions of the process and the effective coefficients of pore diffusion. The granulometric composition of sorbents and their distribution by fractions are the same.

From the presented graphic dependences it is observed that the maximum coefficient of pores filling by direct dyes for natural adsorbents is achieved at n = 6 s^{-1}. On the basis of constructed dependences, calculated effective coefficients of pore diffusion and the shape of kinetic curves, we may assert that the process transfers from the external diffusion or mixed area to pore diffusion area, which is characterized by Bio number Bi $\to$ 0.

$$Bi = \frac{b\,R}{D_p} \quad (3)$$

where β is the mass transfer coefficient, m/s; D_p is the coefficient of pore diffusion, m^2/s; R is the radius of the adsorbent grain, m.

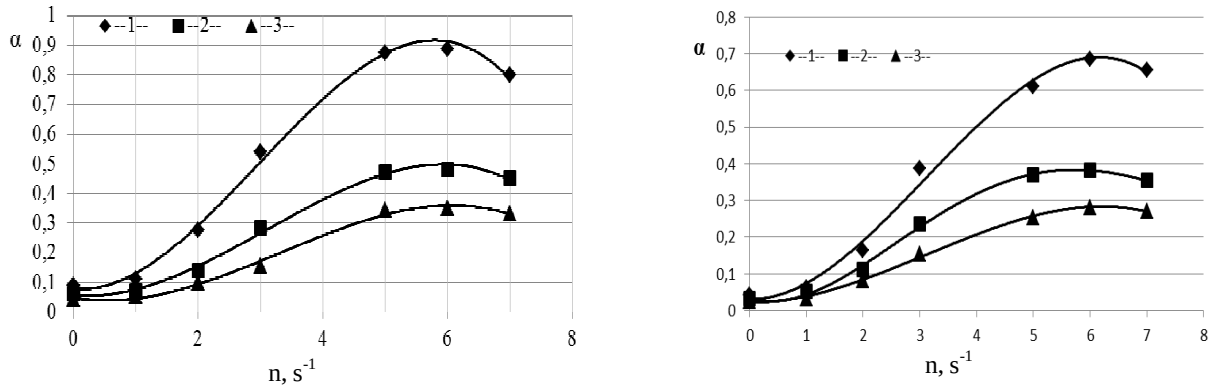

Fig. 1. Effect of the process hydrodynamic conditions on the coefficient of pore filling of the adsorbent (activated bentonite (1); palygorskit (2); glauconite (3)) by anionic red 8C (a) and active scarlet 4ZhT (b)

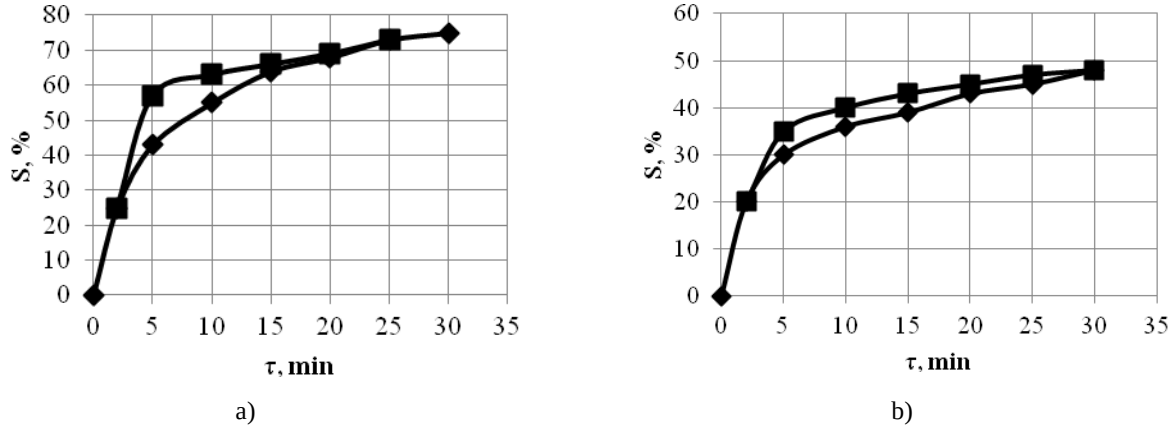

Fig. 2. Kinetic curves of anionic red 8C (a) and active scarlet 4ZhT (b) sorption by activated bentonite for variable stirring modes (◆ – continuous; ■ – periodical)

At the external diffusion Bi > 50. Within the range of Bi = 0.2–50 the diffusion mixed area takes place and at Bi $\rightarrow$ 0 there is a pore diffusion.

In order to confirm the diffusion mechanism, we used an interrupt method, or the so-called "kinetic memory" method, the essence of which is described above. Concentration gradients in the adsorbent grain were aligned during the period of contact between the sorbent and the solution, *i.e.*, when the diffusion process was retarded. After the contact was restored, the mass transfer rate increased in comparison with that before interruption. Thus, the increase in the sorption rate confirms the proceeding of pore diffusion (Fig. 2).

To calculate the level of achievement of adsorption equilibrium (*F*), we used a model of gel diffusion from a limited volume to the elementary spheroidal particle of the adsorbent [16]:

$$F = 1 - \frac{6}{p^2} \cdot e^{\frac{-p^2 \cdot D_p \cdot t}{R^2}} \quad (4)$$

where *t* is the adsorption time, s.

If the process approaches the equilibrium one, the final value of the component concentration in the solution has the form:

$$\frac{C_{1f}}{C_0} = \frac{a}{1+a} \quad (5)$$

Parameter *t* is the dimensionless value which is similar to the Fourier number ($Fo = \frac{D \cdot t}{R^2}$) and takes into account physical and sorption characteristics of the sorbent:

$$t = \frac{D \cdot t}{R^2} \cdot \frac{e_p}{1-e_p} \cdot \frac{C_0}{r_s \cdot q_0} \quad (6)$$

where t is the adsorption time, s; D is the diffusion coefficient, m^2/s; R is the particle radius, m; ρ_s is the density of solid porous phase, kg/m^3; ε_p is the particle porosity, m^3/m^3.

Obviously, the low values of the exponential correspond to the high time values, therefore, since some time we can neglect the roots of the characteristic equation m_n. Eq. (4) can be submitted as a straight dependence:

$$\ln\left(\frac{C_1}{C_0}-\frac{a}{1+a}\right)=\ln B-m^2t \qquad (7)$$

We determine the effective diffusion coefficient using a slope angle:

$$D=\frac{tga\,R^2}{m_1^2}\cdot\frac{1-e_p}{e_p}\cdot\frac{r_s q_0}{C_0} \qquad (8)$$

The obtained results allow to determine effective diffusion coefficients of pollutants sorption by natural sorbents in the modified form and to estimate the intensity of the adsorption process.

To determine the parameters of the external diffusion process of adsorption, we proposed a model based on the theory of local isotropic turbulence for apparatus with a mechanical stirring [16]. This theory is applied to describe dissolution of the solid particles, the sizes of which exceed the thickness of the diffusion boundary layer. The theoretical coefficient of mass transfer is calculated according to the dependence:

$$b_{theor}=0.267\cdot(e_0\cdot n)^{1/4}\cdot Sc^{3/4} \qquad (9)$$

where e_0 – specific energy of dissipation; n – kinematic viscosity, m^2/s; $Sc=\frac{n}{D}$ – the Schmidt number.

The diffusion coefficient of dissolved pollutants (D_d, m^2/s) is determined according to Wilk-Chang equation:

$$D_d=7.4\cdot10^{-8}\frac{T(x\cdot M_{water})}{m\cdot u^{0.6}} \qquad (10)$$

where T is the temperature, K; x is an initial concentration of pollutant in water, g/dm^3; M_{water} is the molecular weight of water, g/mol; m is a dynamic viscosity of water, Pa·s; u is a volumetric molecular weight of the pollutant, cm^3/mol.

The specific energy of dissipation e_0, and mixing power N were determined according to known dependences:

$$e_0=\frac{N}{r\cdot V} \qquad (11)$$

$$N=K_N\cdot r\cdot n^3\cdot d^5 \qquad (12)$$

where K_N is the coefficient of mixing, which depends on the Reynolds number; ρ is the density of the fluid, kg/m^3; d is a diameter of the mixer, m; n is the number of mixer revolutions, 1/s.

According to Ref. [16], an increase in the coefficient of mass transfer is observed compared to the calculated Eq. (9) due to the radial separation of solid particles. Theoretical values of β were compared with those determined experimentally.

Fig. 3 shows the experimental and calculated values of the coefficients of mass transfer β depending on the number of revolutions n. The obtained graphic dependences allow us to confirm the adequacy of the proposed calculating method in order to predict the intensity of the sorption process.

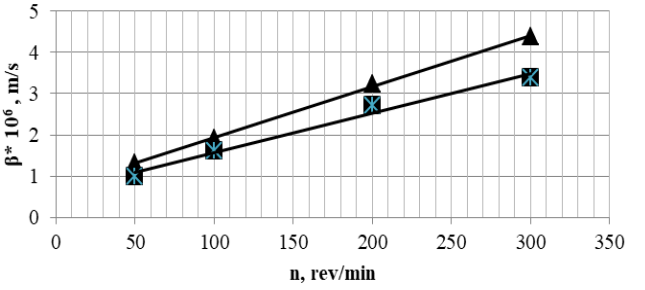

Fig. 3. Coefficient of mass transfer *vs.* number of revolutions for the model solution "pollutant-sorbent": ▲ – theoretical results; ■ – experimental results

The character of the kinetic curves in Fig. 3 confirms the dominant mechanism of pore diffusion in the adsorption process of direct dyes from wastewater by natural sorbents. Thus, using the correction factor k_β, which takes into account the radial separation of the sorbent solid fraction in a limited volume of fluid, the value of the experimental coefficient of mass transfer will approach the theoretical value.

Reverse water supply systems contain ions of sodium, phosphates, chlorides and sulfates. It is important to choose how to remove these ions in a form easy to be used. It is expedient to recycle sodium chloride *via* electrodialysis to obtain alkali and active chlorine. Electrodialysis with filling the intermembrane space by ion-conducting turbulators, *e.g.* granulated ion exchange materials, is a promising method. The role of these ion-exchange materials is that irreversible dissociation of water occurs on their heteropolar boundaries with ion-exchange membranes, during which hydrogen and hydroxyl ions are generated, which are involved in the continuous electrochemical regeneration of the ion-exchange material. There is a combined transport with ions of water mineral impurities. The use of insulating fillers results in a significant increase of the voltage drop and decrease of the membranes working surface. Therefore, the use of ion exchangers in the form of granules as intermembrane filling is of considerable interest. But for the successful application of insulating

fillers for the electrodialysis, a prerequisite is the preliminary study of the electrical conductivity of materials that will be used for intermembrane filling.

We obtained dependences for the pure solution (1) and the system ionite – solution (2), allowing to determine the concentration of insulating solution. They are shown in Fig. 4. The point of intersection of the resulting dependences allows to determine the concentration of the insulating solution, which is equal to 0.51 mol/dm^3.

When using the dependence of specific electric conductivity of NH_4Cl solution y = 11.136x+0.061 we found k_{iso} = 5.8296 Ohm^{-1}·m^{-1} or S/m.

The cell constant is calculated according to Eq. [17]:

$$\Gamma = k_{iso} \cdot R_{iso} \qquad (13)$$

where Γ is the cell constant, determined by the known electrical conductivity of the ionite at the point of isoelectric conductivity, R_{iso} is the measured resistance of the cell after centrifugation with resin, brought to equilibrium with an isoelectric conductivity solution. So, Γ = 5.8229 Ohm^{-1}·m^{-1} · 596 Ohm = 3474.442 m^{-1}.

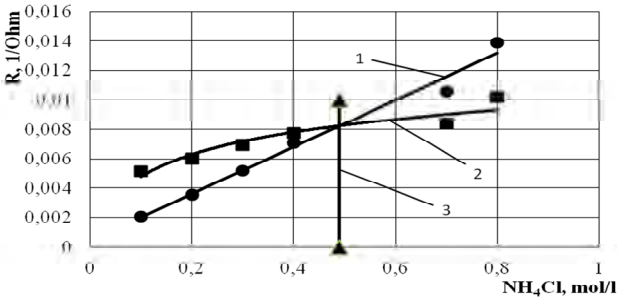

Fig. 4. Determination of the isoelectric conductivity point of KU-2 resin in a U-shaped tube: NH_4Cl solution (1); ionite (2) and line of isoelectric conductivity (3)

The obtained data can be used to calculate the electrodialysis process of solutions with NH_4Cl, using intermembrane filling by the ion exchanger KU-2.

4. Conclusions

The proposed mathematical models of the adsorption process, which are based on the calculation of external and pore diffusion parameters, allow us to determine the limiting step of adsorption. This enables to predict the degree of pollutants absorption from wastewater. The experimental results regarding the electrical conductivity of KU-2 resin, which will be used for intermembrane filling during electrodialysis, allowed to determine the cell constant and establish the concentration dependence of the KU-2conductivity. The obtained results can be used for the calculation of real processes.

References

[1] Malovanyy M., Zhuk V., Sliusar V. *et al.*: East Eur. J. Adv. Technol., 2018, **1**, 23. https://doi.org/10.15587/1729-4061.2018.122425
[2] Malovanyy M., Shandrovych V., Malovanyy A. *et al.*: J. Chem., 2016, **2016**, 9. https://doi.org/10.1155/2016/6874806
[3] Tedesco M., Brauns E., Cipollina A. *et al.*: J. Memb. Sci., 2015, **492**, 9. https://doi.org/10.1016/j.memsci.2015.05.020
[4] Daniilidis A., Vermaas D., Herber R., Nijmeijer K.: Renew. Energy, 2014, **64**, 123. https://doi.org/10.1016/j.renene.2013.11.001
[5] Tufa R., Curcio E., van Baak W. *et al.*: RSC Adv., 2014, **4**, 42617. https://doi.org/10.1039/C4RA05968A
[6] Chang D., Choo K., Jung J. *et al.*: Desalination, 2009, **236**, 152. https://doi.org/10.1016/j.desal.2007.10.062
[7] Wang Q., Yang P., Cong W.: Separ. Purif. Technol., 2011, **79**, 103. https://doi.org/10.1016/j.seppur.2011.03.024
[8] Nosachova Yu., Zeleniuk O., Gomelya M.: Khim. Inzhener. Ekolohiia ta Resursozb., 2010, **1**, 48.
[9] Bezdieniezhnykh L., Sviatenko A.: Ekol. Bezpeka, 2015, **2**, 78.
[10] Gomelya M., Trus I., Shabliy T.: Chem. Chem. Techol., 2014, **8**, 197. https://doi.org/10.23939/chcht08.02.197
[11] Melnyk L., Bessarab O., Matko S., Malovanyy M.: Chem. Chem. Technol., 2015, **9**, 467. https://doi.org/10.23939/chcht09.04.467
[12] Malyovanyy M., Sakalova G., Chornomaz N. *et al.*: Chem. Chem. Technol., 2013, **7**, 355. https://doi.org/10.23939/chcht07.03.355
[13] Shmandii V., Bezdenezhnykh L., Kharlamova E. *et al.*: Chem. Chem. Technol., 2017, **11**, 242. https://doi.org/10.23939/chcht11.02.242
[14] Petrushka I., Malovanyy M., Yatchyshyn Y., Petrushka K.: Naukovi Pratsi ONAKhT, 2015, **47**, 48.
[15] Kul A., Caliskan N.: Adsorpt. Sci. Technol., 2009, **27**, 85. https://doi.org/10.1260/026361709788921632
[16] Brahynskyi L., Behachev B., Barabash B.: Peremeshyvanye v Zhydkykh Sredakh. Khimik, Leninhrad 1984.
[17] Gnusin N., Grebenyuk V., Pevnitskaya M.: Elektrokhimiya Ionitov. Nauka, Novosibirsk 1972.

Received: March 26, 2018 / Revised: October 01, 2018 / Accepted: October 15, 2018

УДОСКОНАЛЕННЯ АДСОРБЦІЙНО-ЙОНООБМІННИХ ПРОЦЕСІВ ОЧИЩЕННЯ СТІЧНИХ ТА ШАХТНИХ ВОД

Анотація. *Досліджено підвищення рівня екологічної безпеки гідросфери в результаті удосконалення адсорбційних процесів очищення стічних та шахтних вод від забруднень із застосуванням природних сорбентів та процесів знесолювання електродіалізом. Встановлені оптимальні параметри удосконалення процесів сорбції забруднень природними сорбентами. Механізм дифузії досліджений методом «кінетичної пам'яті». Визначені ефективні коефіцієнти внутрішньої дифузії в процесі сорбції забруднень природними сорбентами. Встановлені оптимальні параметри реалізації електродіалізу із міжмембранною засипкою йонітом для демінералізації стічних та шахтних вод.*

Ключові слова: *екологічна безпека, електродіаліз, природні сорбенти, сорбція, стічні та шахтні води, міжмембранна засипка.*

Chem. Chem. Technol., 2019, Vol. 13, No. 3, pp. 377–383

Chemical Technology

PREPARATION OF SECONDARY pH OF PHTHALATE BUFFER SOLUTION USING DIFFERENTIAL POTENTIOMETRIC CELL: METHOD VALIDATION AND APPLICATION

Ayu Hindayani[1], Oman Zuas[1, *], Sujarwo[2], Fransiska S. H. Krismastuti[2], Nuryatini[1]

https://doi.org/10.23939/chcht13.03.377

Abstract. A secondary pH of phthalate buffer was prepared by differential potentiometry method using a Baucke cell which is separated by sintered glass disk in the middle of cell – so called two-half cells. The method has been validated at 298 K with the purpose to evaluate its suitability for meeting the application requirement. The method validation parameters include accuracy (bias), precision (repeatability), and estimation of measurement uncertainty. It was found that both accuracy and precision of the method were good, which is indicated by their very low standard deviation (SD). The measurement uncertainty value of the method was estimated. Application of the validated analytical method for the measurement of phthalate buffer in an international comparative test (APMP.QM-K91) showed that the result was close to the APMP.QM-K91's Key Comparison Reference Value.

Keywords*:* differential potentiometric cell, pH, phthalate buffer, method validation, international key comparison.

1. Introduction

Scientifically, pH is defined as a value of $-\log a_H$, involving a single ion quantity and activity of hydrogen ion [1]. Practically, the pH is used to specify acidity or basicity properties of any substance that are mainly in the form of their aqueous solution. Determination of pH is one of the most common and frequent quantitative measurement in the field of chemical analyzes [2]. The common application of the pH measurement is to control industrial processes with the purposes to preserve product quality, reduce the corrosion rate in plant equipment, and protect the aqueous environment by helping wastewater discharge process to meet regulatory limits [3].

Measurement of pH is a process applying the physico-chemical principle and it can be performed by using various methods such as colorimetry and potentiometry. To date, potentiometry is widely used due to its simplicity and accuracy in comparison to other methods [4]. Potentiometric method is measuring the potential difference between two electrodes that are simultaneously immersed in the solution to be examined [5], by which those glass electrodes must be regularly calibrated before use by using pH buffer standard solution.

A reliable data of a pH measurement process having a traceability property to the International System of Units (SI) is extremely required [2]. For pH measurement, the traceability chain can be established by linking the pH data resulted from a measurement to the pH value of a primary pH buffer standard solution [6]. This buffer standard is obtained from the primary method [2]. It is widely known that the primary pH buffer standard solution for the calibration purpose is characterized by its long-term stability, high purity and good reproducibility [6]. However, the use of primary pH buffer standard solution by common testing and calibration laboratories is costly; thus secondary pH buffer standard solution is an alternative which is widely used by the laboratories to keep the traceability of their pH measured data [2].

So far, the pH value of secondary pH standard buffer solution is commonly determined by secondary method using differential potentiometric cell or called as Baucke cell. This method was firstly introduced in 1994 by F. Baucke, whose name was then used for naming the cell [2]. Schematic design of Baucke cell is presented in Fig. 1 [6].

[1] Metrology in Chemistry Laboratory, Centre for Research and Human Resource Development,
National Standardization Agency of Indonesia (BSN),
Kawasan PUSPIPTEK Build. 420, Serpong15314, Tangerang Selatan-Banten, Indonesia
[2] Research Centre for Chemistry-Indonesian Institute of Sciences (RCChem-LIPI)
Kawasan PUSPIPTEK Build. 452, Serpong15314, Tangerang Selatan-Banten, Indonesia
[*] *oman@bsn.go.id; zuas.oman@gmail.com*

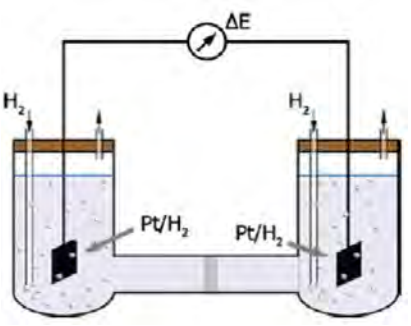

Fig. 1. Schematic diagram of Baucke cell [6]

Baucke cell is U-shaped cell separated by a sintered glass disk in the middle of the cells, called as two-half cells. One cell contains the primary buffer solution (as a standard solution) and platinum/hydrogen (Pt/H_2) electrode. Another cell contains secondary buffer solution (as a sample solution) and Pt/H_2 electrode. These two buffer solutions must have the same nominal composition. Similarly, two Pt/H_2 electrodes must have as similar characteristic as possible. Since the hydrogen in the half cells is about the same, liquid junction potential (LJP, developed in the junction between the two half cells) can be neglected [2]. The pH of secondary buffer can be calculated by Eq. (1) [2]:

$$\mathrm{pH}_s = \mathrm{pH}_p - \frac{\Delta E_{cell} F}{RT \ln 10} \quad (1)$$

where pH_p is pH value from primary buffer standard solution; ΔE_{cell} is potential difference between two Pt/H_2 electrodes after stabilization (V); F is Faraday constant (96,485 $C \cdot mol^{-1}$), R is the universal gas constant (8.314 $J \cdot K^{-1} \cdot mol^{-1}$); T is solution temperature (K) [2].

In Indonesia, most of industrial and testing laboratories used imported and traceable buffer standard solutions in their pH measurement activities [7]. The use of traceable secondary pH buffer standard solutions is extremely important to keep the traceability of the measurement to the SI unit. However, an imported buffer standard solution is economically disadvantageous due to being costly and the import process is also time consuming. Therefore, providing the industries and testing laboratories with secondary buffer standard solution to meet the local need is essential.

In pH measurement, the phthalate buffer is one of the most commonly used in comparison to other buffer standard solutions because it is readily commercial available, relatively stable and pH value is markedly non-sensitive to a temperature change [8]. In addition, the phthalate buffer standard solution can be easily prepared from readily available certified material.

In this study, a phthalate buffer solution as a secondary pH buffer standard solution was developed by LIPI. The secondary pH buffer standard solution was prepared by using gravimetric method and the pH values were determined by the differential potentiometry method using a Standard Reference Material® potassium hydrogen phthalate (SRM® 185i) as the traceable reference standard. It is important to notice that methods for the preparation and pH measurement must be validated before determining the pH value and producing the phthlate buffer solution in a large scale. The purpose of the method validation is not only to meet its suitability requirement for application but also to evaluate the method's performance [9], by which the results are presented and discussed in this paper.

2. Experimental

2.1. Materials

All chemicals were of analytical grade, otherwise stated, and used as received without any further purification. Hydrogen (H_2) gas (99.9 % purity) was purchased from SII Gas Indonesia. Chloride acid (37 % purity), nitric acid (65 % purity), lead (II) acetate (99.5 % purity), Certipure® Certified Reference Material (CRM) potassium hydrogen phthalate (1019650025) were purchased from Merck, Germany. Palladium (II) chloride (anhydrous, Pd basis 60 %) was purchased from Sigma-Aldrich, USA. The SRM® 185i was purchased from National Institute of Standards and Technology (NIST), USA. Demineralized water (0.05 μs/cm) was produced from a Thermo Scientific Barnsted Smart2 pure water purification system and used in all experiments.

2.2. Equipment

For the investigations we used: analytical balance with accuracy of 1 mg (PR5003 Dual Range, Mettler Toledo Switzerland), oven (Heraeus Instruments, Germany) and a direct current (DC) power supply 0.01 A (Ad-8723D, China), a digital multimeter 0.01 mV (34461A, Agilent Technologies Sdn Bhd, Malaysia), waterbath 0.1 K (Thomas T-N22D, Japan), chiller (Thomas TRL-117NF, Japan), hot plate and magnetic stirer (Cimarec 2, Barnstead Thermolyne Corp. USA), fume hood (LFH-2120V, Daihan Labtech Korea), digital thermometer (MKT50, Anton Paar GmBH, Germany), Baucke Cell, Pt electrode, and chamber (Japan), stopwatch, and clean glasswares.

2.3. Procedure

2.3.1. Preparation of buffer solution

Standard buffer solution was made from phthalate buffer solution (0.05 molal) SRM® 185i by adopting a

procedure from [10]. In a typical experiment, the SRM®NIST 185i was firstly dried at 383.15 K for 2 h followed by storing in a desiccator until use, aiming to remove the water content because the SRM® 185i is stable only in a dry environment. After that, 9.8 g of SRM 185i was transferred into a clean and dry beaker glass (1 l). Demineralized water was then added into the beaker glass until the mass reach 959.293 g. The solution was shaken thoroughly until the solid was totally dissolved. This gravimetric preparation could eliminate the need to weigh exactly predetermined mass of solid samples.

Another buffer solution (0.05 molal), as a sample, was made from Certipure® CRM potassium hydrogen phthalate in accordance with the procedure described in [11]. The CRM was dried by placing in an oven at 383.15 K for 2 h in order to remove the water content. After that, 10.21 g of CRM was dissolved in 800 ml of water and made up to 1 l. The solution was shaken thoroughly until the solid was totally dissolved.

2.3.2. Preparation of Pt electrode

The use of clean Pt electrodes in pH measurements by differential potentiometric cell is considered very important. In this study, the Pt electrodes were cleaned using hot aqua regia in order to achieve a sufficiently small of potential bias [12] and to remove any impurities from the electrode surface, by which the possible interference during the measurement can be diminished [13]. After that, a palladinizing process for the Pt electrode to minimize reduction of phthalate was carried out by coating method using palladium black solution [8]. Typically, palladium black solution was a solution mixture consisting of palladium chloride, lead acetate and chloride acid, where the Pt electrodes were coated by electrolytic method [12]. The presence of the palladium black on the electrode surface may increase the effectiveness of a hydrogen electrode [14]. Preliminary results showed that a slightly coated electrode surface was found to be more stable than thick coated one [8]. To determine the best surface coating of the electrodes, the effect of palladinizing parameters such as current and time were studied. The variation of the current and time was ranging within 0.3–0.5 A and 2–5 min, respectively.

2.3.3. pH Measurements

The pH of phthalate buffer 0.05 molal (both standard and sample) were measured by using differential potentiometric cell. The potential difference between SRM®185i as a standard and Certipure® CRM potassium hydrogen phthalate as a sample was assigned as ΔE_{cell}. Both buffer solutions were placed in the Baucke cell, followed by inserting the palladinized Pt electrodes into each cell. After that, the Baucke cell was immersed into the waterbath (298 K). The hydrogen gas was then fed into each cell with the flow rate of 500 ml/h [12]. It should be noticed that the hydrogen gas was firstly pre-humidified before entering the Baucke cell by passing through the hydrogen into two chambers containing phthalate buffer solution [2]. The palladinized Pt electrodes were then connected to digital multimeter and the ΔE_{cell} value was recorded after stabilization. A schematic diagram of the differential potentiometric cell system used in this study is shown in Fig. 2. In this study, one hour was required to stabilize the potential and the measurement was then conducted every 10 min. Finally, the mean value of ΔE_{cell} was used for calculating the pH values by using Eq. (1).

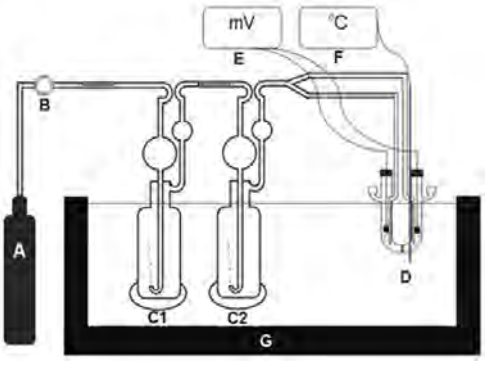

Fig. 2. Schematic diagram of differential potentiometric cell system: hydrogen gas (A), gas controller (B), chambers containing phthalate buffer (C1 and C2), Baucke cell and Pt electrodes (D), digital multimeter (E), digital thermometer (F) and water bath (G)

2.3.4. Validation method

Validation of an analytical method is a process of defining an analytical requirement and confirming that the method under consideration has capabilities and is consistent with its application requirements [9]. In this study, differential potentiometric cell was used for the preparation of secondary reference material for pH measurement; thus, validation of the method is extremely required to meet its application purposes. In general, validations of the method are conducted to evaluate the performance characteristics of the method in term of its selectivity, limit of detection (LOD) and limit quantification (LOQ), working range, analytical sensitivity, accuracy (bias), precision (repeatability), robutsness, and estimation of measurement uncertainty [9]. However, in analytical pH measurement, the validation method is only limited to such parameters as accuracy (bias), precision (repeatability) and measurement of the uncertainty.

Accuracy is referred to how close the mean of measurement result (produced by method) is to the

reference value. This assessment is commonly quantitatively expressed as bias [9]. Determination of bias (b) relies on the different between the mean of measurement results ($\overline{X}$) and the reference value stated in CRM's certificate (X_{CRM}). The value of b is determined by using Eq. (2) [9].

$$b = \left| \overline{X} - X_{CRM} \right| \quad (2)$$

In this study, the mean from 10 times of measurements was used. The method is categorized as not to be bias, when the value falls within the range of measurement precision value ($\pm 2s$) (Eq. (3)) with calculation of s (Eq. (4)) at 95% confidence level [15].

$$-2s < b < +2s \quad (3)$$

$$s = \sqrt{U_{CRM}^2 + \frac{S_w^2}{n}} \quad (4)$$

where U_{CRM} is standard uncertainty from certificate; S_w is standard deviation, and n is a number of measurements.

Precision (also called as repeatability) is a measure of how close the measurement results are one to another [9]. Precision is usually expressed by a standard deviation obtained from several measurement replications. In the pH measurement using differential potentiometric cell, a good repeatability is achieved when the value of standard deviation is equal or less than $6.0 \cdot 10^{-5}$ V. This criterion is based on our experiences in the measurement using differential potentiometric cell to decrease the measurement uncertainty.

Moreover, for estimating the uncertainty of the measurement, identification of the uncertainty sources which contribute to the measurement uncertainty value is the initial step. After that, estimation of the uncertainty from each individual source was conducted followed by combining such individual uncertainties to give an overall estimation of measurement uncertainty [16].

3. Results and Discussion

In the BSN, the electrochemistry laboratory is a part of metrology in chemistry group which has responsibility for the development of reference material in electrochemistry field such as buffer. The developed buffer reference materials are used to keep the traceability of pH measurement (at national level) to SI. It might be an acceptable idea that every method must be validated before coming into use for a routine measurement. In this study, the measurement of the phthalate buffer was determined by secondary method using differential potentiometric cell and the method was validated in term of the measurement accuracy (bias), precision (repeatability), and its measurement uncertainty estimation.

3.1. Palladinizing Pt Electrodes

Optimization of palladinizing Pt electrode is an important step and it has to be conducted to increase the work efficiency of the Pt electrode, because in homogeneities such as tiny spots on the electrode surface may affect the measurement results. Therefore, any surface dirt must be removed by cleaning procedure [12]. Besides, in the differential potentiometry, the surface condition of two Pt electrodes must be as similar as possible [2].

Fig. 3 shows the ΔE_{cell} dependency on the electrical current used in the palladinizing Pt electrode. It can be seen from Fig. 3 that the obtained ΔE_{cell} value significantly decreases when the electrical current increases up to 0.4 A and then increases. This phenomenon can be described as follows: at a low current (below 0.4 A) in palladinizing, only a small number of metal was deposited on the surface of Pt electrode and that was a non-optimum condition to minimize the reduction process of phthalates, leading to a very large ΔE_{cell} value. In contrast, at a high current (above 0.4 A), the ΔE_{cell} value is significantly increased. These high ΔE_{cell} values might be due to the high current used in the palladinizing resulting in inhomogeneity of deposited metal on the electrode surface [17]. Consequently, two Pt electrodes were unidentical and those electrodes did not meet the requirement of the electrodes used in potential differential potentiometric cell. Moreover, when palladinizing at the current of 0.4 A, the ΔE_{cell} was found to be the smallest value, indicating that two half cells were similar, having homogenous deposition of metal on the electrode surface. Based on this finding, a value of 0.4 A was used as the optimal current in palladinizing the Pt electrodes.

Fig. 4 displays the effect of time variation on the ΔE_{cell} value. As it can be seen from Fig. 4, ΔE_{cell} decreases in 2–4 min and then increases in 5 min. For 2 min, the ΔE_{cell} was found to have a relatively high value. It was assumed that due to the short time of palladinizing process a very small amount of metal is deposited on the electrode surface (data are not shown here). Thus, the reduction of phthalates cannot be minimized. On the contrary, longer palladinizing time may decrease the ΔE_{cell} value and the lowest value of ΔE_{cell} is achieved in 4 min, indicating that the metal deposited on the electrode surface was in a homogenous and optimum condition. Consequently, the smallest ΔE_{cell} value confirms that the optimum palladinizing time is 4 min.

So, it can be concluded that the optimum electrical current and reaction time were 0.4 A and 4 min, respectively. The Pt electrode obtained under this optimum condition was then used for the measurements in the validation of the analytical method.

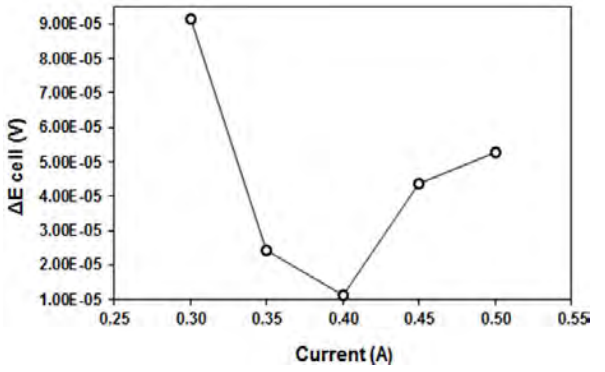

Fig.3. The dependence of ΔE_{cell} on the electrical current in Pt electrodes palladinizing

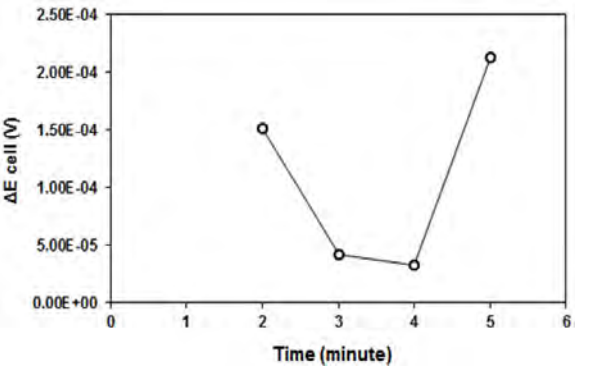

Fig. 4. Optimization of time in Pt electrodes palladinizing

3.2. Validation Method

In this study, the validation of the measurement method was conducted in terms of accuracy (bias), precision (repeatability) and measurement uncertainty estimation. For the accuracy, the evaluation was taken by estimating the bias of the mean true value from 10 measurement replications. The results of the method accuracy are presented in Table 1. It can be seen from Table 1 that the mean of pH value of the CRM was found to be 4.0052, while the certificate value of the secondary phthalate buffer was 4.0070; thus the bias of the method was 0.0018. This bias value is relatively small and lies in the range of the precision value $\pm 2\sigma$ (with 95% confidence level), implying that the analytical method is accurate [15].

Table 1

Accuracy data of the analytical method

Measurements	pH at 298 K
1	4.0045
2	4.0051
3	4.0050
4	4.0056
5	4.0057
6	4.0057
7	4.0053
8	4.0056
9	4.0050
10	4.0049
Mean ($\bar{X}$)	4.0052
Standard deviation (S_w)	0.0004
U_{CRM}	0.0015
X_{CRM}	4.0070
$b = \lvert \bar{X} - X_{CRM} \rvert$ (Eq. 2)	0.0018
$\sigma = \sqrt{U_{CRM}^2 + \frac{S_w^2}{n}}$ (Eq. 4)	0.0015
Criteria $-2s <<$ (Eq. 3)	-0.0030 < 0.0018 < 0.0030
Status	OK

Precision (repeatability) is a measure of how close the measurement results are to each other [9]. The precision is usually expressed by standard deviation from several measurement replications. In this study, repeatability was carried out by measure of the sample in 10 replications and the results are listed in Table 2. From the Table 2, it was found that the standard deviation for the measurement is $3.0 \cdot 10^{-5}$ which is lower than acceptance criteria value ($6.0 \cdot 10^{-5}$ V) of our experience in measurement using differential potentiometric cell. Hence, it can be concluded that the analytical method used in this study is precise (repeatable). Moreover, for the measurement uncertainty estimation, all possible sources of the uncertainty contributor were identified and schematically displayed using Ishikawa diagram as shown in Fig. 5 [2].

Table 2

Precision/repeatability data of the analytical method

Measurements	ΔE_{cell} at 298 K, V
1	0.00009
2	0.00001
3	0.00005
4	0.00004
5	0.00002
6	0.00005
7	0.00008
8	0.00008
9	0.00001
10	0.00008
Mean ($\bar{X}$)	0.00005
Standard deviation (S_w)	$3.0 \cdot 10^{-5}$
Criteria	equal or less than $6.0 \cdot 10^{-5}$
Status	OK

Table 3 shows the measurement uncertainty estimation for secondary pH measurement. From Table 3, it can be seen that the expanded uncertainty for the secondary pH measurement using differential potentio-

metric cell at 298 K is 0.001 (95 % confidence level), which is lower than the IUPAC recommended value (0.004 at 95 % confidence level) [1]. Extremely small uncertainty of the primary buffer used might be the reason for small uncertainty obtained in this study, indicating that uncertainty of the primary buffer is very important [2].

3.3. Application

Validation method of the secondary pH measurement using differential potentiometric cell is to check the suitability of the differential potentiometry method with the application required and evaluate the method's performance. In this regard, participation in an international key comparison (APMP.QM-K91) was conducted. In short, the comparison results indicated that differential potentiometric cell can be used in the pH measurements of phthalate buffer at 298 K. The measured value (4.006) is close to the APMP.QM-K91's key comparison reference value (KCRV), that is 4.00765. The results are graphically displayed in Fig. 6 [18].

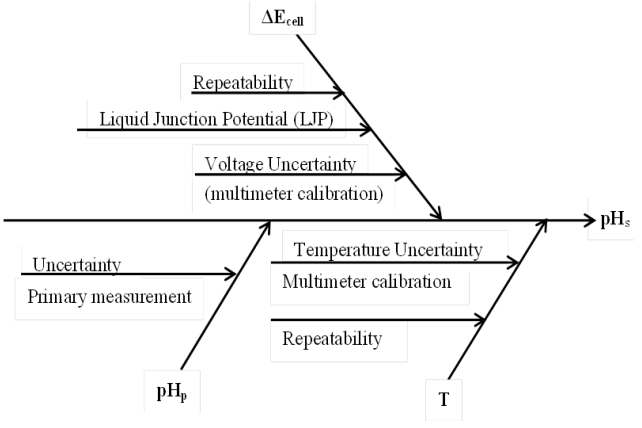

Fig. 5. Ishikawa diagram [2]

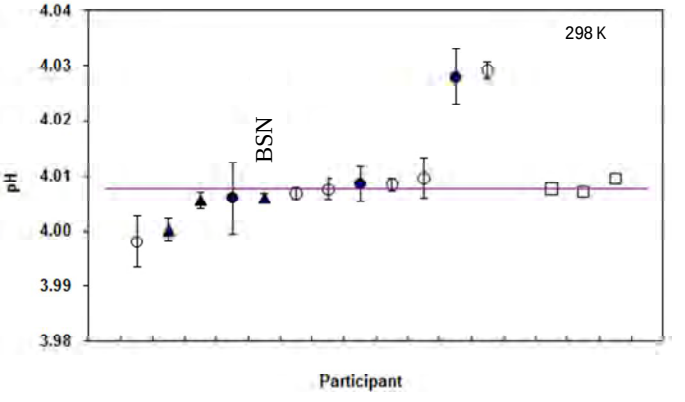

Fig. 6. Results of pH measurements of phthalate buffer at 298 K compared with APMP.QM-K91 [18]

Table 3

Data for uncertainty estimation of secondary pH measurement using differential potentiometric cell at 298 K

Sources	Standard uncertainty (u_i)	Unit	Sensitivity coefficient (c_i)	Unit	$u_i \cdot c_i$
Primary buffer	0.0004	–	1	–	0.0004
ΔE_{cell}					
$E_{cal.}$	$5.50 \cdot 10^{-7}$	V	-16.91	V^{-1}	$-9.30 \cdot 10^{-6}$
$E_{res.}$	$5.77 \cdot 10^{-7}$	V	-16.91	V^{-1}	$-9.76 \cdot 10^{-6}$
$E_{stab.}$	$2.00 \cdot 10^{-5}$	V	-16.91	V^{-1}	$-3.38 \cdot 10^{-4}$
Repeatability	$3.23 \cdot 10^{-6}$	V	-16.91	V^{-1}	$-5.46 \cdot 10^{-5}$
LJP	$3.53 \cdot 10^{-6}$	V	-16.91	V^{-1}	$-5.96 \cdot 10^{-5}$
Temperature					
$T_{cal.}$	0.02	K	$2.0 \cdot 10^{-6}$	K^{-1}	$3.0 \cdot 10^{-8}$
$T_{res.}$	0.06	K	$2.0 \cdot 10^{-6}$	K^{-1}	$1.15 \cdot 10^{-7}$
Stability	0.06	K	$2.0 \cdot 10^{-6}$	K^{-1}	$1.20 \cdot 10^{-7}$
Homogeneity	0.04	K	$2.0 \cdot 10^{-6}$	K^{-1}	$8.0 \cdot 10^{-8}$
				Combined uncertainty (u_c)	0.0005
				Expanded uncertainty (U), $k = 2$	0.001

4. Conclusions

The result of validation shows that the differential potentiometry method is appropriate for the pH measurement of phthalate buffer at 298 K, with the value of the bias and precision found to be 0.0018, and $3.0 \cdot 10^{-5}$, respectively, having an estimated uncertainty value of 0.001 ($k = 2$). The validated method of pH has been tested by participating in the international comparison (APMP.QM-K91) and the result was excellent, confirming that the method is valid.

Acknowledgments

The author would like to thank Mrs. Eli Susilawati for the help during laboratory experiments and data collection. The LIPI support of the study through the project "Strengthening chemical metrology competency and infrastructure" is highly acknowledged.

References

[1] Buck R., Rondinini S. *et al.*: Pure Appl. Chem. 2002, **74**, 2169. https://doi.org/10.1351/pac200274112169
[2] Gonzaga F., Dias J., Jehnert D. *et al.*: Electroanal., 2013, **25**, 1955. https://doi.org/10.1002/elan.201300135
[3] Laongsri B., Boonyakong C., Tangpaisarnkul N., Cherdchu C.: Accred. Qual. Assur., 2017, **12**, 194. https://doi.org/10.1007/s00769-006-0210-0
[4] Wu Y., Koch W., Marinenko G.: J. Res. Nat. Bur. Stand., 1984, **89**, 395.
[5] European Pharmacopoeia, 4th edn. Council of Europe, Strasbourg 2002.
[6] Spitzer P., Pratt K.: J. Solid State Electrochem., 2011, **15**, 69. https://doi.org/10.1007/s10008-010-1106-9
[7] Nuryatini, Sujarwo, Hindayani A.: J. Standardisasi, 2015, **18**, 35.
[8] Hetzer H., Durst R.: J. Res. Nat. Bur. Stand., 1977, **81A**, 21.
[9] Magnusson B., Örnemark U. (Eds.): Eurachem Guide: The Fitness for Purpose of Analytical Methods – A Laboratory Guide to Method Validation and Related Topics, 2nd edn., 2014. www.eurachem.org.
[10] Gonzalez C., Watters Jr. R.: Certificate of Analysis SRM®NIST 185i Potassium Hydrogen Phthalate pH Standard, Department of Commerce United States of America 2013.
[11] Yildirim A.: Certificate of Analysis Certipure® Certified Reference Material Potassium Hydrogen Phthalate, MERCK, Germany 2015.
[12] Baucke F.: J. Electroanal. Chem., 1994, **368**, 67. https://doi.org/10.1016/0022-0728(93)03024-J
[13] Mustopo Y.: Effect of Time on Thickness and Adhesivity Layer in Electroplating Process of Chrome Decorative without Basic Layer with Copper Basic Layer and Copper-Nickel., Department of Mechanical Engineering, Technical Faculty of UNS, Solo, Indonesia 2011.
[14] Hamer W., Acree S.: J. Res. Nat. Bur. Stand., 1944, **33**, 87.
[15] Budiman H.: Warta Kimia Analitik., 2014, **20**, 18.
[16] Bell S.: Measurement Good Practice Guide (Issue 2), National Physical Laboratory, United Kingdom 2001.
[17] Subangga B., Sutikno E., Ariseno A.: Effect of Anode Variation and time of Electroplating on Wear Rate of Grinding Ball., Department of Mechanical Engineering University of Brawijaya Malang.
[18] Hioki A., Asakai T., Maksimov I. *et.al.*: Metrologia, 2017, **54**, 08002. https://doi.org/10.1088/0026-1394/54/1A/08002

Received: March 13, 2018 / Revised: April 03, 2018 / Accepted: August 30, 2018

ПРИГОТУВАННЯ ВТОРИННОГО pH-СТАНДАРТУ ДЛЯ ФТАЛАТНОГО БУФЕРНОГО РОЗЧИНУ З ВИКОРИСТАННЯМ ДИФЕРЕНЦІАЛЬНОЇ ПОТЕНЦІОМЕТРИЧНОЇ КОМІРКИ: ВАЛІДАЦІЯ МЕТОДУ ТА ЗАСТОСУВАННЯ

Анотація. *Методом диференційної потенціометрії із застосуванням електрохімічної комірки Бауке, розділеної посередині пористою скляною дисковою перегородкою на так звані дві напівкомірки, приготований фталатний буферний розчин як вторинний стандарт для величини pH. Правильність цього методу перевірена за температури 298 K з метою оцінки його придатності. Параметри валідації методу включають точність (відхилення від істинного значення), прецизійність (повторюваність) та оцінку невизначеності вимірювань. Виявлено, що і точність, і прецизійність методу були на належному рівні, що підтверджується дуже низькими величинами стандартних відхилень. Проведено оцінку величини невизначеності вимірювання цього методу. Застосування валідованого аналітичного методу для вимірювання величини pH фталатного буферного розчину згідно міжнародного порівняльного випробування (APMP.QM-K91) показало, що результат був близьким до паспортної (сертифікованої) величини, яка використовується як референтна для порівняння в рамках випробування APMP.QM-K91.*

Ключові слова: *диференціальна потенціометрична комірка, pH, фталатний буферний розчин, валідація методу, порівняння з міжнародною референтною величиною.*

Chem. Chem. Technol., 2019,
Vol. 13, No. 3, pp. 384–390

Chemical
Technology

KINETIC MODELING STUDIES OF ENZYMATIC PURIFICATION OF GLUCOMANNAN

Dyah Hesti Wardhani[1, *], Andri Cahyo Kumoro[1], Azafilmi Hakiim[2], Nita Aryanti[1], Heri Cahyono[1]

https://doi.org/10.23939/chcht13.03.384

Abstract.[1] Purification of glucomannan by hydrolising starch – the main contaminant – was studied. Hydrolysis removed 88.7 % of starch. The highest glucomannan content was found to be 73.35 %. The sample showed the comparable infrared spectra to those of the commercial glucomannan. The kinetics of enzymatic hydrolysis was evaluated using the Michaelis-Menten model.

Keywords: α-amylase, *Amorphophallus oncophyllus*, glucomannan, hydrolysis, purification, starch.

1. Introduction

Amorphophallus oncophyllus is a type of tuber that grows wildly and recently being commercially cultivated in the forest edge of Indonesian. The tuber contains calcium oxalate, which is associated with itching and irritations in the mouth that makes the tuber underutilized for human consumption. Being a member of the philodendron (arum) family, the native *A. oncophyllus* flour (NAoF) was reported to contain glucomannan up to 60 % [1]. Unfortunately, most of the Indonesian farmers sell the tubers as dried chips or low-quality tuber flour [2]. Low glucomannan content reflects a low economic value of those products. The international standards have ratified that the top grade glucomannan flour should contain minimum 70 % of starch. Hence, it is important to explore glucomannan purification method in order to improve the economic value.

Glucomannan of *Amorphophallus* sp. is a linear heteropolysaccharide composed of β-1,4-linked D-mannose and D-glucose monomers with 1 to 1.6 of glucose/mannose ratio and certain short side branches at the C-3 position of the mannoses through β-1,6-glucosyl units. The acetyl groups along the backbone are located at the C-6 position on average every 9–19 sugar units. Glucomannan is widely utilized as food ingredients, including emulsifier and stabilizer as well as functional foods and drug excipient [1, 3, 4].

Purification methods of glucomannan from NAoF strongly affect the properties and structure of the purified glucomannan, which finally influence the scope of applications of glucomannan. Therefore, it is important to develop an efficient and convenient isolation method to produce high purity glucomannan. The isolation of glucomannan is commonly conducted using dry (mechanical) and wet methods. The mechanical purification methods include blowing and sieving, which result in flour with low glucomannan content [5]. Water, ethanol, and 2-propyl alcohol are common solvents used for impurities removal in wet methods [6]. However, the latter method demands a high volume of solvent. Due to the weakness of these previous methods, another alternative method was proposed.

Starch, cellulose, and nitrogen-containing materials are the main impurities, which encapsulate glucomannan granules [6]. High glucomannan content can be achieved by maximizing the removal of impurities. Starch is the highest impurity of NAoF, which seriously affects the purity and quality of glucomannan, such as reducing viscosity and increasing turbidity [7]. Hence removing of starch is expected to be the most efficient method to increase the quality of glucomannan. As far as literature survey being conducted, only α-amylase has been used to enzymatically modify starch and its derivatives by cleaving α-1,4 glycosidic [8]. Due to the specific properties of the enzyme, α-amylase is expected to only cleave α-1,4 glycosidic linkage of starch and leaves α-1,4 glycosidic of glucomannan uncleaved. Application of enzymatic method on glucomannan purification was still not fully studied. Hence, the objective of this work was to study the effect of enzymatic hydrolysis of starch on glucomannan purification from NAoF. In addition, the kinetics of enzymatic hydrolysis was evaluated using the Michaelis-Menten model.

[1] Department of Chemical Engineering, Faculty of Engineering, University of Diponegoro,
Jl Prof. Soedarto, SH, Tembalang Semarang, Indonesia
[2] MSc Study Program on Chemical Engineering, University of Diponegoro
Jl. Prof. Soedarto, SH, Tembalang Semarang, Indonesia
[*] *dhwardhani@che.undip.ac.id*

2. Experimental

2.1. Materials

The main material used in this study was NAoF obtained from the local farmer (Sidoharjo, East Java-Indonesia). The content of starch and glucomannan in the flour were 7.92 and 66.3 %, respectively. α-Amylase (EC 3.2.1.1) was isolated from *Bacillus subtilis* and working at pH 6.0–7.0 with 4,000 U/g activity (Suntaq International Limited). *B. subtilis* is one of the bacteria which has been used to produce enzymes for human and animal feed [9]. 2-Propyl alcohol (IPA) solution (70 %) was used for washing the suspension after the hydrolysis. Other chemicals used in this work were of analytical grade and used directly without pre-treatment.

2.2. Enzymatic Hydrolysis

The enzymatic hydrolysis was conducted based on the method of Wardhani [1]. A flour suspension (400 ml) was prepared by diluting a predetermined amount of NAoF in distilled water at 343 K to obtain a certain concentration of the flour (1.5, 2.0, 2.5, and 3.0 % w/v). Starch and water in the flour suspension were allowed to react with the assistance of α-amylase (0.03 g/g flour). The enzyme concentration referred to the best concentration of Wardhani [1]. The suspension was maintained at pH 6.8 during the hydrolysis. Each of the suspension was conducted for different period of hydrolysis (0, 25, 50, 75, 100 and 150 min) under continuous stirring at 350 rpm. Once the reaction completed, 2-propyl alcohol (200 ml, 70 %) was added to the suspension and stirring was continued at 350 rpm for 30 min. After filtration of the suspension, a creamy solid cake was obtained. The cake was then dried and powdered. The obtained powders were subjected for further analyses.

2.3. Analytical Methods

The powder samples obtained from enzymatic hydrolysis were subjected to starch determination using Fehling solution to obtain the glucose concentration. The conversion factor (0.9) was used to obtain starch concentration [10]. Reducing sugar was determined using Somogyi-Nelson method with D-glucose as a standard [11]. Glucomannan determination was conducted following the method of Chua based on 3,5-dinitro-salicylic acid colorimetric assay with D-glucose as a standard [4]. The sample was extracted using formiat–NaOH before hydrolysis using sulfuric acid. Both the extract solution and the hydrolysate solution were subjected to colorimetric reaction and the absorbances were read at 550 nm. Glucomannan concentration (*GM*) was calculated as:

$$GM\,(\%) = 5000\varepsilon\cdot(5T\text{-}T_0)/m \qquad (1)$$

where ε is the correction factor (0.9); m is a sample weight, mg; T and T_0 are glucose in hydrosilate and in extract sample, respectively.

The analyses were done in triplicates. In addition, the powder sample with the highest glucomannan was subjected to Fourier Transform Infrared Spectrometry (FTIR) for functional groups characterization and Scanning Electron Microscope (SEM) for particles microstructure observation. FTIR spectrum of the samples was recorded under dry air condition at room temperature in the range of 4000-400 cm^{-1} by using IR Prestige Shimadzu. The peaks were assigned by comparison with the literature data. The powder granules morphology was observed using SEM apparatus (FEI Inspect S50) at a certain magnification. Prior to SEM analysis, a dry sample was placed on a stub and coated with gold.

2.4. The Kinetics Modeling

The Michaelis-Menten model was applied to study the kinetic model of enzymatic starch hydrolysis on NAoF using *a*-amylase at the first 25 min of the reaction. The Michaelis-Menten mechanism was developed based on the interaction between the enzyme (*E*) and the substrate (*S* – starch), leading to an intermediary enzyme-substrate complex (*ES*), from which the reaction product (*P* – reducing sugar) is generated (Eq. (2)).

$$E + S \underset{k-1}{\overset{k1}{\Leftrightarrow}} ES \overset{k2}{\rightarrow} E + P \qquad (2)$$

where k_1 is a reaction rate constant for enzyme-substrate linking; k_{-1} is a reaction rate constant for enzyme-substrate complex dissociation, and k_2 is a reaction rate constant for product generation.

Three stages of reaction can be identified in the Michaelis-Menten mechanism [12]:

i. The first stage is a rapid bi-molecular reversible one, leading to the formation of an enzyme-substrate complex.

ii. The second stage is the reverse of the first one, the intermediate complex, having a relatively short lifetime.

iii. The third stage leads to the final product by the irreversible conversion of enzyme-complex, while the free enzyme goes again to the first stage, linking another substrate molecule.

The kinetic constants, *i.e.* K_m and V_{max}, were determined from an initial rate of hydrolysis production at various starch concentrations by optimization of their

values by fitting the model to the experimental data using solver facilities of Ms-Excel. The model was statistically validated through the R^2 value.

3. Results and Discussion

The effort to increase glucomannan content of NAoF through the removal of starch as the main impurities of the flour has been conducted by an enzymatic hydrolysis. The purified flour was determined for starch, reducing sugar, and glucomannan content.

3.1. Starch Content

The effect of time and flour concentration on starch contents of hydrolyzed products is depicted in Fig. 1a. The figure shows that the starch content decreased in line with time at all NAoF concentrations. At longer reaction time, the enzyme was able to create more active sites for the substrate to be cleaved resulted in lower starch concentrations in the flour. This result was in line with that reported by Simsek and El [13]. As expected, Fig. 1a also shows that hydrolysis of NAoF at higher flour concentrations results in lower starch content. This phenomenon reveals that the enzyme concentration (0.03 g/g NAoF) used in this research provides enough active sites to promote hydrolysis of the starch in the range of 1.5–3 % of NAoF. This result was supported by Wardhani who found that increasing the enzyme concentration up to 0.03 g/g NAoF showed a positive effect in reducing the starch [1]. However, reverse effect was observed when the enzyme concentration was over than that one. This could be due to increasing starch competitor compounds which were produced during the starch hydrolysis [1].

At all initial NAoF concentrations studied in this work, about a half of the starch content could be removed in the first 50 min, and then followed by a slower starch removal rate. During enzymatic hydrolysis, the initial period corresponds to the rapid hydrolysis of the most amorphous part of the starch granules, whereas in the latter stage, the more crystalline parts are slowly degraded [14]. In addition, the high concentration of reducing sugar as the hydrolysis product in the reaction medium during the hydrolysis of starch leads to a significant decrease of the hydrolysis rate due to its competition with the starch in occupying the same active sites of *a*-amylase [15]. As a result, the degradation rate decreased after 50 min. Moreover, it was observed that after 100 min of hydrolysis, the suspension system became more viscous. This increase in viscosity limited molecules movements resulted in lower opportunities of the starch granules to contact with an enzyme which subsequently reduces the starch degradation. A similar trend was reported by Hera [16], Zhang [17], and Zheng [18] who found there is no significant difference of starch hydrolysis rate after 90–100 min.

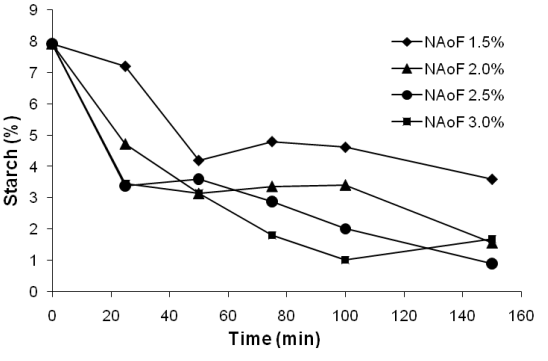

a)

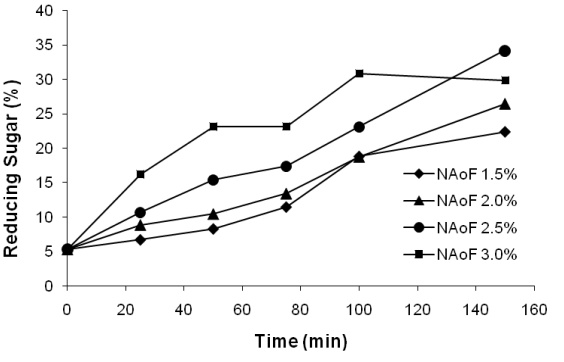

b)

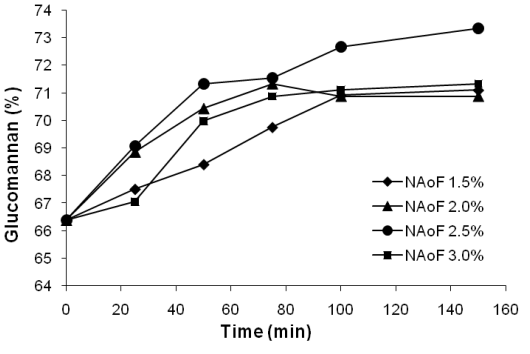

c)

Fig. 1. The effect of reaction time and the concentration of native *A. oncophyllus* flour on starch concentration (a), reducing sugar (b) and glucomannan (c) of the purified flour. Reactions were conducted using *a*-amylase 0.30 g/g flour at 343 K

In this study, the lowest starch concentration was observed at hydrolysis using 2.5 % w/w NAoF concentration for 150 min. In this condition, about 88 % of the initial starch was hydrolyzed. The removal of starch in this research was lower than the previous report Nurjanah [19] who managed to reach 96 % of starch conversion. The difference in results is possibly due to thermostable α-amylase which allows to be applied at a higher temperature (368 K) and converts more starch in a shorter time. Fig. 1a also shows some residual starch was still detected at 150 min which was difficult to be completely hydrolyzed. Lopez [20] reported that 90 % starch hydrolysis conversion was achieved within 2 h. However, the total hydrolysis is still not achieved even after 48 h of incubation time.

3.2. Reducing Sugar

Depending on the chain length, hydrolysis of starch results in reducing sugar and other derivative products. Fig. 1b shows that concentration of reducing sugars increased with the reaction time at all initial concentration of NAoF. A similar result was reported by Rodriguez and Bernik [21] who found that reducing sugar still significantly increased even after 240 min during hydrolysis of high amylose maize starch Hylon VII using α-amylase from human origin Type XI. Higher initial NAoF concentration leads to a higher production of reducing sugar at all reaction times. This result agreed well with Khawla [22] who hydrolyzed potato peel flour. However, the reducing sugar of 3 % NAoF decreased after 100 min which could be due to the possibility of reducing sugar degradation as a consequence of prolonged time [23] and high concentration of reducing sugar during the hydrolysis of starch led to a significant decrease of the hydrolysis rate [15]. In addition, increasing the viscosity of the system might also reduce the effectiveness of enzymatic hydrolysis. Wu and Zhong [24] reported that viscosity of glucomannan still maintains to increase even after 6000 s of stirring. The highest reducing sugar (20.34 %) was obtained from the reaction of 2.5 % w/w NAoF concentration for 150 min.

3.3. Glucomannan Content

Fig. 1c presents the effect of reaction time and initial concentration of NAoF on glucomannan content of hydrolyzed *A. oncophyllus* flour. In general, a longer reaction time resulted in higher glucomannan content. The rise in glucomannan purity was a result of α-amylase activity, which specifically attacked only the α-1,4-glycosidic linkage of the starch. Since glucomannan is a heteropolysaccharide molecule consisting of D-mannose and D-glucose linked by β-1,4 bond, it was not hydrolyzed. The enzyme helped in cleaving and removing starch coating the glucomannan granules and subsequently led to release the glucomannan granules. Fig. 1c shows the highest glucomannan purity (73.35 %) was attained at enzymatic hydrolysis of 2.5 % w/w flour for 150 min. The glucomannan purity increased about 10 % from NAoF. In this condition, the purified flour sample contained 0.9 % of starch and 20.34 % of reducing sugar. Nurjanah [19] reported higher increase of glucomannan content from 28.75 to 80.53 %. Meanwhile, Mulyono [25] obtained the glucomannan content increased from 31.99 to 93.75 %. Both authors used NAoF with lower initial glucomannan content than that used in this study. NAoF with lower glucomannan content may suggest that NAoF contains higher starch content. The higher starch content in the initial NAoF showed the higher potential of the impurities removal, which subsequently resulted in a higher increase in glucomannan content.

3.4. Enzymatic Hydrolysis Kinetic Model

Fig. 2 shows the correlation between the initial starch concentrations of NAoF and the initial rates of a product formation according to the Michaelis-Menten model. The constants of the model were determined by a nonlinear regression method. The optimized value of K_m and V_{max} were 32.84 and 0.905 g/l·min, respectively.

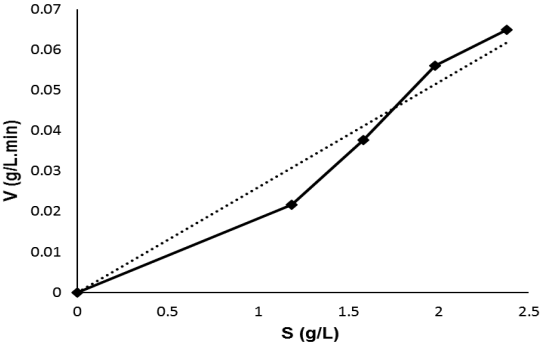

Fig. 2. Plotting between initial starch concentration in the suspension system and initial velocity of reducing of *A. oncophyllus* flour suspension data (solid-line) and model according to Michaelis-Menten equation (dot-line)

Michaelis-Menten constant (K_m) is the concentration of substrate at which the enzyme active sites are filled half-full. Thus, K_m measures a substrate concentration required for significant catalysis reaction to occur. High K_m value indicates a weak bond between the enzyme and the substrate in the formation of the complex compounds ES or low apparent affinity of the enzyme for the substrate. Hence, the enzyme requires a higher substrate concentration to reach 50% saturation. In this study, K_m value was higher than the concentrations of starch in the system observed (1.19–2.37 g/l). This

implied that a constant rate of complex dissociation is faster than that of complex production (Eq. (2)). In this condition, the Michaelis-Menten equation for starch hydrolysis in the glucomannan enzymatic purification becomes:

$$V = \frac{V_{\max}[S]}{K_m} \quad (3)$$

Eq. (3) suggests that the rate of the reaction is proportional to the substrate concentration. Hence, the enzymatic starch hydrolysis in glucomannan purification followed the first-order kinetics.

Meanwhile, maximum velocity (V_{max}) is a theoretical maximum rate of the reaction, which is never achieved in reality. It shows the number of substrate molecules converted to the product by the enzyme per unit time when the enzyme active site fully filled with the substrate. V_{max} values are proportional to the rate constants of the product formation k_2 [12]. As expected, the V_{max} value obtained in this study was much higher than the rate constants of the product formation obtained from the experiments (0.031–0.061 g/l·min). The statistical parameter showed a good agreement ($R^2 = 0.956$) between the experimental data and modeling results using the Michaelis-Menten model.

3.5. FTIR Analysis

Comparison of IR spectra of NAoF, the purified sample (obtained from hydrolysis of 2.5 % substrate concentration for 150 min) and the commercial glucomannan (Patrick Holford, 98 % glucomannan content) in the wavelength range of 4000–400 cm^{-1} is presented in Fig. 3. The spectra were in good agreement with those reported by An [3] and Chua [4]. The IR spectra of all samples demonstrated similar peak ranges of wavelength but difference in the intensity of the absorbance. In general, the absorbance values of the purified flour sample were between NAoF and commercial glucomannan.

All samples showed a peak attributed to broad bands located at 3000–3700 cm^{-1}, which indicated the presence of O–H groups of glucomannan [17]. These hydroxyl groups were laid on characteristically by methyl groups located at ~2900 cm^{-1} which assigned to –CH stretch vibration and 1720 cm^{-1} which attributed to C=O stretching vibration. The existence of β-1,4 linked glucose and mannose of glucomannan was indicated by the carbonyl (C=O) stretch vibration located at ~1650 cm^{-1} [26]. While peaks at ~1150 and ~1050 cm^{-1} referred to C–O–C stretch vibrations from ether groups in the pyranose rings, which indicate the presence of β-1, 4 glucosidic and β-1,4 mannosidic linkages in glucomannan [27].

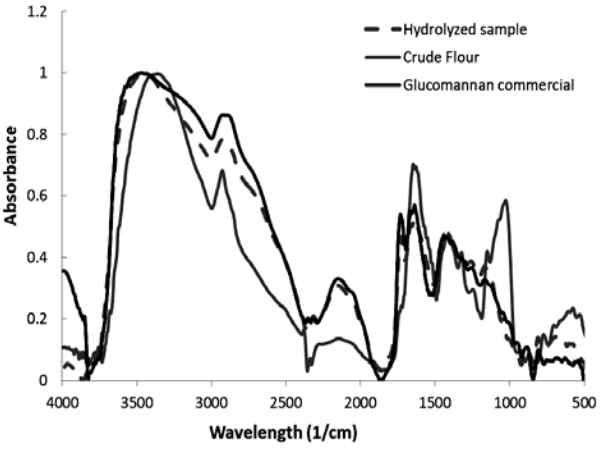

Fig. 3. Comparison of IR spectra of the native *A. oncophyllus* flour (grey solid-line), the purified flour (grey dash-line), and the commercial glucomannan (black solid-line)

3.6. Granules Morphology

The morphological observation was conducted to investigate the effect of hydrolysis on the microstructure of glucomannan granules. Fig. 4 (top) shows the granules morphology of NAoF observed at different magnifications. The NAoF granules displayed polygonal shapes with an average size of 600 µm. The figure indicates the presence of exposed biomaterials covering some parts of NAoF surface as a result of grinding and milling of *A. oncophyllus* dried chips into flour (Fig. 4, top left). These biomaterials were likely to be the impurities, which covered up the glucomannan granules. This fact is in accordance with the results [6] reported that glucomannan granules were encapsulated by impurities including starch, cellulose and nitrogen-containing material.

Meanwhile, Fig. 4 (bottom) shows the morphology of the hydrolyzed *A. oncophyllus* flour sample at 100 and 450 magnifications. After enzymatic hydrolysis, the hydrolyzed flour granules were irregular in shapes with an average size of 900 µm. The hydrolyzed flour granules degraded on their external part leading to the formation of a number of hollows. This phenomenon indicates that hydrolysis took place by exo-corrosion, and it was not uniform for all flour granules in which some regions were much more susceptible to enzymes attack than the others. The hydrolysis resulted in sharper edges and the cleaner surface of the flour granules than that of NAoF. Franco and Ciacco [27] also reported the enzymatic attack on the large granules of cassava and corn starches (> 16 µm) as indicated by remarkable corrosion of granule surface, primarily in the radial direction. The removal of impurities by enzymatic hydrolysis resulted in the significant increase of glucomannan content in the flour.

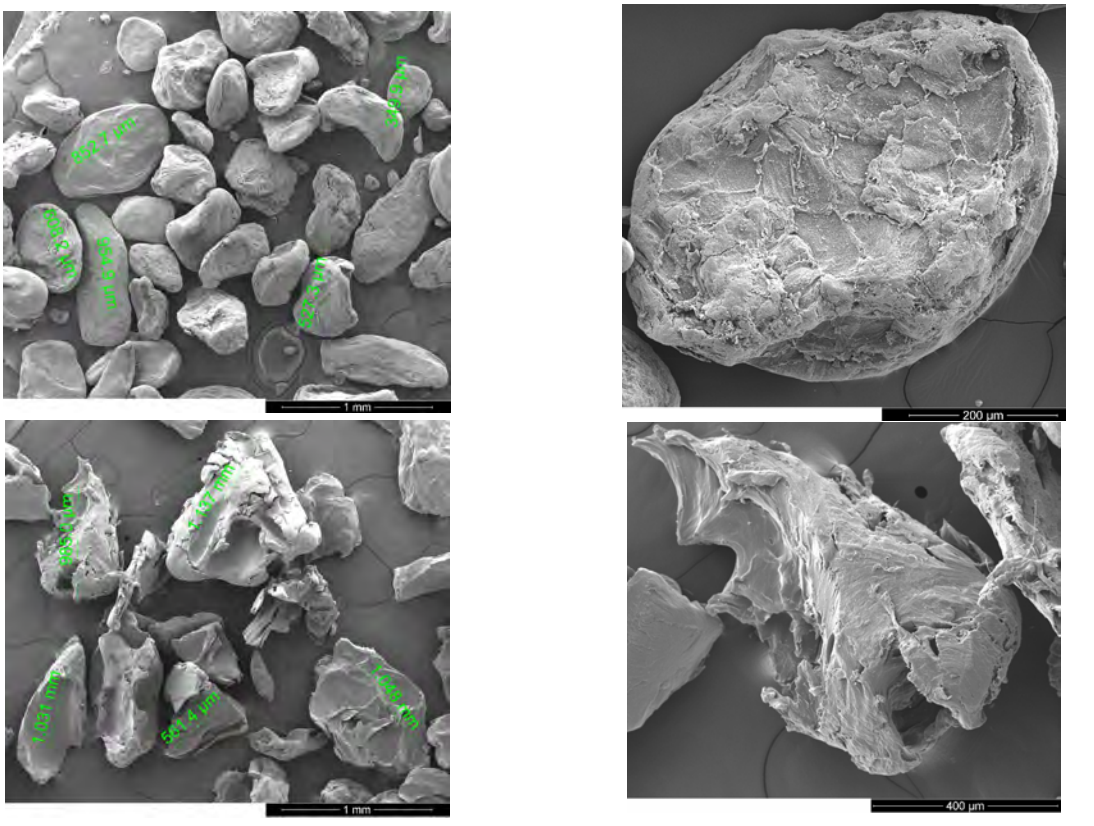

Fig. 4. Granule morphology of native *A. oncophyllus* flour (top) and the purified sample (bottom), at 100 (left) and 450 (right) magnifications

4. Conclusions

The overall results suggested that hydrolyzing 2.5 % w/w of NAoF for 150 min successfully removed 88.7 % of starch and increased 10% glucomannan concentration. The final product contained 73.35 % of glucomannan, 0.9 % of starch, and 20.34 % of reducing sugar. K_m and V_{max} values of Michaelis-Menten model were 32.84 g/l and 0.905 g/l·min, respectively with R^2 = 0.956. The enzymatic starch hydrolysis in glucomannan purification followed the first-order kinetics. The hydrolyzed flour sample with the highest glucomannan showed a comparable IR spectrum to that of commercial glucomannan. The morphology analysis confirmed the removal of NAoF impurities from the flour granules as well as the rupture of NAoF granule after hydrolysis.

Acknowledgements

This research was funded by Directorate of Research and Community Service, Directorate General of Higher Education, Ministry of Research, Technology and Higher Education of the Republic of Indonesia through Fundamental Scheme (Grant no. 140-16/UN7.5.1/PG/2015).

References

[1] Wardhani D., Vazquez J., Ramdani D., *et al.*: Biosci. J., 2019, **35**, 277. https://doi.org/10.14393/BJ-v35nla2019-41766.
[2] Harmayani E., Aprilia V., Marsono Y.: Carbohydr. Polym., 2014, **112**, 475. https://doi.org/10.1016/j.carbpol.2014.06.019
[3] An N., Thien D., Dong N. *et al.*: Carbohydr. Polym., 2011, **84**, 64. https://doi.org/10.1016/j.carbpol.2010.11.021
[4] Chua M., Baldwin T., Hocking T., Chan K.: Carbohydr. Polym., 2012, **87**, 2202. https://doi.org/10.1016/j.carbpol.2011.10.053
[5] Hakiim A..: MSc Thesis, University of Diponegoro, Indonesia 2015.
[6] Ohashi S., Shelso G., Moirano A., Drinkwater W.: Pat. US 6162906A, Publ. Dec. 19, 2000.
[7] Xu W., Wang S., Ye T. *et al.*: Food Chem., 2014, **158**, 171. https://doi.org/10.1016/j.foodchem.2014.02.093
[8] Patel A., Singhania R., Pandey A.: Curr. Opin. Food Sci., 2016, **7**, 64. https://doi.org/10.1016/j.cofs.2015.12.002
[9] Vincent S., Diane S., Lori G. *et al.*: Ind. Biotechnol., 2016, **12**, 295. https://doi.org/10.1089/ind.2016.0011
[10] AOAC 2005. Official of Analysis of the Association of Official Analytical Chemistry. Washington: AOAC Inc.
[11] Sadasivam S., Manickam A.: Biochemical Methods, 3rd edn. New Age International Pvt Ltd Publishers. New Delhi 2008.
[12] Muntean E.: Bulletin UASVM Agricult., 2011, **68**, 344.
[13] Simsek S., El S.: Carbohydr. Polym., 2012, **90**, 1204. https://doi.org/10.1016/j.carbpol.2012.06.039

[14] Yook C., Robyt J.: Carbohydr. Res., 2002, **337**, 1113. https://doi.org/10.1016/S0008-6215(02)00107-6
[15] Kolusheva T., Marinova A.: J. Univ. Chem. Technol. Metall., 2007, **42**, 93.
[16] Hera E., Gomez M., Rosell C.: Carbohydr. Polym., 2013, **98**, 421. https://doi.org/10.1016/j.carbpol.2013.06.002
[17] Zhang H., Yin L., Zheng Y., Shen J.: Food Hydrocolloid., 2016, **54**, 23. https://doi.org/10.1016/j.foodhyd.2015.09.018
[18] Zheng Y., Zhang H., Yao C. *et al.*: Food Hydrocolloid., 2015, **48**, 312. https://doi.org/10.1016/j.foodhyd.2015.02.036
[19] Nurjanah Z.: BSc thesis, Bogor Agricultural Institute, Indonesia 2010.
[20] Lopez C., Torrado A., Fucinos P. *et al.*: Enzyme Microb. Technol. 2006, **39**, 252. https://doi.org/10.1016/j.enzmictec.2005.10.012
[21] Rodriguez S., Bernik D.: LWT-Food Sci. Technol., 2014, **59**, 635. https://doi.org/10.1016/j.lwt.2014.05.034
[22] Khawla B., Sameh M., Imen G. *et al.*: Ind. Crops Prod., 2014, **52**,144. https://doi.org/10.1016/j.indcrop.2013.10.025
[23] Nikolic´ S., Mojovic´ L., Rakin M., Pejin D.: Fuel, 2011, **88**, 1602. https://doi.org/10.1016/j.fuel.2008.12.019
[24] Wu J., Zhong Q.: J. Food Eng., 2016, **175**, 104. https://doi.org/10.1016/j.jfoodeng.2015.12.010
[25] Mulyono E.: Centre of Research and Development of Agricultural Post Harvest. Indonesia: Program of application research intensive, 2010.[26] Widjanarko S., Nugroho A., Estiasih T.: Afr. J. Food Sci., 2011, **5**, 12.
[27] Franco C., Ciacco C.: Starch, 1992, **44**, 422. https://doi.org/10.1002/star.19920441106

Received: March 12, 2018 / Revised: April 29, 2018 / Accepted: August 23, 2018

КІНЕТИЧНІ МОДЕЛЬНІ ДОСЛІДЖЕННЯ ЕНЗИМАТИЧНОГО ОЧИЩЕННЯ ГЛЮКОМАННАНА

Анотація. *Вивчено процес очищення глюкоманнана гідролізом крохмалю – основного забруднювача. Встановлено, що гідролізом усувається 88,7 % крохмалю. Одержано найвищий вміст глюкоманнану 73,35 %. Проведено порівняльні дослідження ІЧ-спектрів дослідженого і комерційного глюкоманнана. За допомогою моделі Міхаеліса-Ментена описано кінетику ензиматичного гідролізу.*

Ключові слова: *α-амілаза, Amorphophallus oncophyllus, глюкоманнан, гідроліз, очищення, крохмаль.*

Chem. Chem. Technol., 2019,
Vol. 13, No. 3, pp. 391–398

Chemical
Technology

DETERMINATION OF THE CHEMICAL COMPOSITION OF THE EXTRACT OF APRICOT POMACE *(Prunus Armeniaca L.)*

***Victoria Vorobyova*[1, *]*, *Anastasiia Shakun*[1]*, *Olena Chygyrynets'*[1]*, *Margarita Skiba*[2]**

https://doi.org/10.23939/chcht13.03.391

Abstract. The objective of this study was to investigate a comprehensive characterization of composition profiles of the apricot pomace extract (*Prunus armeniaca L*) depending on the used solvent systems. The propan-2-ol, decamethylcyclopentasiloxane and the mixture of the apricot pomace extracts are characterized by IR, UV-visible spectroscopy and gas chromatography-mass spectrometry (GC-MS) techniques.

Keywords: apricot pomace, extract, propan-2-ol, decamethylcyclopentasiloxane, aldehydes, terpene alcohols.

1. Introduction

In connection with the change in the environmental situation in the market, it becomes more and more important to purchase environmentally friendly products, that is, with the maximum replacement of synthetic components by natural ones. Many chemically active substances are found in plant raw materials [1, 2]. Many studies have been carried out on some plants which resulted in development of natural "green" products. However, scientific information on the component composition of various plants, particularly those that are less widely used in medicine or food, industry is still scarce. So, it is an interesting and useful task to find new sources for highlighting naturally active compounds and to obtain various products [3-7]. One of the types of plant raw materials of industrial importance, is the waste of processing fruit and berry crops. The use of agricultural and food by-products is an economical solution for chemical industry. However, large amounts of fruit waste are discarded yearly at processing plants. This not only wastes a potentially valuable resource but also aggravates an already serious disposal problem [8].

[1] National Technical University of Ukraine "Igor Sikorsky Kyiv Polytechnic Institute",
37, Peremogy Ave., 03056 Kyiv, Ukraine
[2] Ukrainian State Chemical-Engineering University,
8, Gagarina Ave., 49066 Dnipro, Ukraine
[*] *vorobyovavika1988@gmail.com*

Apricot (*Prunus armeniaca L.*) is one of the most widely grown fruit trees with a total world production of about $3.4 \cdot 10^6$ tons. Current production of apricot in Ukraine is about 160 000 tons per year. Large amounts of fruit resides resulting in the pressing of apricots are available in Ukraine. With this harvest, there are about 4000 tons of apricot pomace per year. These residues, called pomaces, are mostly composed of fruit skins, pulp and seeds, and are considered as wastes of no value. At present in Ukraine there is no systematic collection and utilization of pomace; thus, a valuable product with a large industrial potential remains unexploited.

In the literature there are several references to the polyphenolic composition of apricot by-products obtained by extraction with water [8, 9]. However different solvent systems may be used to extract active components from plant materials [10]. In the majority of studies only the water extract profile was studied sufficiently, while the information about compound composition of alcoholic extract is very limited. It's common knowledge, that the concentration and composition of chemically active substances in apricot pomace extract significantly depend on the type of solvent which has been selected for the extraction. Under the same conditions of extraction time and temperature, the type of solvent used is the most important factor [11]. Water, aqueous mixtures of ethanol, methanol, 2-propanol and acetone are commonly used to extract active compounds from plant materials [12]. There are numerous successful reports about uses of various extracts of plant materials, including the pomace of apricot, in different branches of "green" chemical technology. The main ones are the cosmetic and food industry, as well as the production of nanosilver particles, the development of environmentally friendly corrosion inhibitors [4-6], the creation of an alternative to synthetic antioxidants and preservatives [13-15]. At the same time there is a lack of information to compare the effects of different solvents on the extraction of major classes compound of the apricot pomace.

The aim of this work was to carry out a comprehensive characterization of composition profiles of

the apricot pomace extract depending on the used solvent systems to provide a comprehensive assessment of opportunities for use in chemical industry. This research provides much beneficial information for the food and cosmetic industry to choose suitable conditions for extracting desirable components from apricot pomace, and serves as a good base for other researchers.

2. Experimental

The object of research is crushed dried of apricot pomace. One apricot (*Prunus armeniaca L.*) cultivar known under local name "Favorite" was harvested (during July 2017) in two geographical regions of Ukraine (Kherson, Nikolaev). Before the extraction, this raw material is subjected to grinding to particles of 5×10^{-1} mm in size in order to increase the efficiency of mass transfer of the active components from the plant material to the solvent. For a more complete extraction, a series of gravimetric analysis experiments were performed to determine the dry residue, from which it can be stated that the hydromodule of plant raw materials to the extractant 2:1 is predominant for this type of material. Extraction was carried out with Soxhlet apparatus. Three frequently used solvent systems, including propan-2-ol, decamethylcyclopentasiloxane (silicone (D5)), and propan-2-ol and decamethylcyclopentasiloxane (1/1), were selected for comparisons.

Identification and quantification of the main compounds were performed by the method of chromatography and mass spectrometry (GC-MS). Analytical conditions: HP- 5MS capillary column (30×0.25 mm), helium as a carrier gas, thickness of the phase 0.25 µm, flow of the carrier gas 1.5 ml/min. The injector temperature was maintained at 523 K; the detector temperature was held at 553 K. The column oven temperature was programmed as follows: an initial temperature of the column was 373 K; heating rate of the column (temperature gradient) was 10 K/min up to 553 K, the mass range was monitored from 30 to 500 m/z; the sample was introduced with a split flow of 15 ml/min; the volume of the sample was 2 µl. The components were identified by comparing the peak retention times in the chromatogram and the complete mass-spectra of individual components with the corresponding results for pure compounds in the NIST-5 Mass Spectral Library.

IR spectra of the extract were measured by a Bruker Tensor 27 FTIR spectrometer with a diamond crystal accessory using a spectral range of 4000–600 cm^{-1} with the resolution of 4 cm^{-1}. IR-reflectance spectra of the mild steel sample surface after immersion in an inhibited solution were recorded in the range of 4000–600 cm^{-1} using IR reflectance spectrophotometry (Perkin Elmer).

Identification of extractable compounds was conducted using a Shimadzu UV-1601 PC scanning double beam UV-Vis spectrophotometer (Shimadzu Corporation, Kyoto, Japan). The UV-Vis spectra were recorded within 200–800 nm.

3. Results and Discussion

According to the obtained chromatographic-mass spectral analysis data, the composition of propan-2-ol extract of dry pomace of apricot contains 38 individual components present in an amount of more than 0.54 %. (Fig. 1, Table 1). Mass spectra and structures of apricot pomace extracts main components identified by GC-MS are presented in Fig. 2.

All of them are known compounds and are easily identified by mass spectrum and linear retention indices. The main components are aldehydes: hexanal (1.32 %), (E)-2-hexanal (3.10 %), (Z)-2-heptenal (3.65 %), heptanal (2.18 %), 2-phenylacetaaldehyde (1.29 %), *β*-cyclocitral (5.17 %), (E,E)-2,4-decadienal (3.65 %), also ketones: 2-hexanone (1.03 %), 3-hexanone (0.54 %). The class of alcohols is presented by (Z)-3-hexenol (0.76 %), (E)-2-hexenol (1.87 %), hexanol (5.67 %). In a minor amount, the extract contains esters, such as (E)-2-hexenyl acetate (2.78 %), (Z)-3-hexenyl butanoate (1.51 %), hexyl hexanoate (2.12 %). Also, the kernel of the fruit contains many acids, this class is represented by octadecanoic acid (6.02 %), (9*Z*,12*Z*)-octadeca-9,12-dienoic acid (4.2 %), hexadecanoic acid (5.4 %), (9*Z*)-octadec-9-enoic acid (6.1 %), (9*Z*,12*Z*,15*Z*)-9,12,15-octadecatrienoic acid (0.63 %).

The extract of apricot pomace contains an increased content of terpene alcohols: linalool (3.06 %), *α*-terpineol (5.98 %), nerol (3.02 %), geraniol (8.54 %), isoborneol (1.03 %), nerolidol (8.54 %), farnesol (1.38 %) and others. These compounds represented over 18 % of the total volatiles in apricot pomace.

Investigation of the composition of silicone (D5) extract of apricot waste showed that it identifies the same number of compounds, but with different quantitative content. The main number of identified compounds is duplicated with an alcohol extract. It also contains limiting and unsaturated aldehydes, alcohols, esters, but terpene compounds are present in smaller quantity. Nevertheless, in the silicone extract there is an increased amount of fatty acids, even new compounds such as 1-tetradecanoic acid (9Z)-hexadec-9-enoic acid have been found in comparative to propan-2-ol extract of apricot.

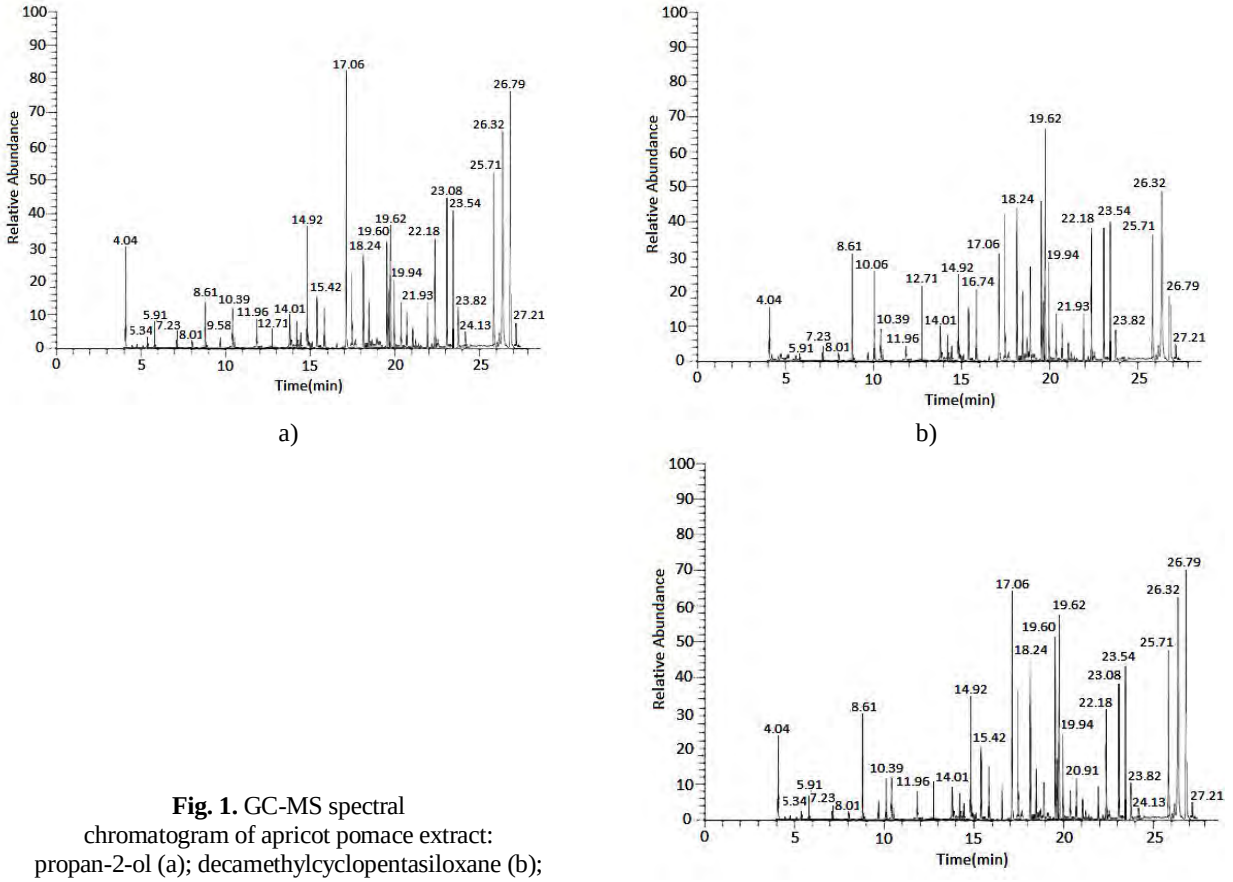

Fig. 1. GC-MS spectral chromatogram of apricot pomace extract: propan-2-ol (a); decamethylcyclopentasiloxane (b); propan-2-ol and decamethylcyclopentasiloxane (c)

Table 1

Component composition of volatile substances of extracts squeezes of apricot

№	Retention time, min	Name of the compound	Molecular formula	Molecular weight, g/mol	Quantitative ratio, %		
					propan-2-ol	silicone (D5)	propan-2-ol - D5
1	2	3	4	5	6	7	8
1	4.04	Hexanol	$C_6H_{14}O$	102	5.67	2.94	3.79
2	5.34	(Z)-3-Hexenol	$C_6H_{12}O$	100	0.76	-	0.57
3	5.91	(E)-2-Hexenol	$C_6H_{12}O$	100	1.87	0.62	1.64
4	7.23	2-Hexanone	$C_6H_{12}O$	100	1.03	0.94	1.00
5	8.01	3-Hexanone	$C_6H_{12}O$	100	0.54	0.53	0.63
6	8.61	(Z)-2-Heptenal	$C_7H_{12}O$	112	3.65	4.78	4.39
7	9.58	Hexanal	$C_6H_{12}O$	100	1.32	0.79	1.21
8	10.06	Benzaldehyde	C_7H_6O	106	1.94	3.92	2.60
9	10.39	(E)-2-Hexanal	$C_6H_{12}O$	98	3.10	1.97	2.64
10	11.96	Heptanal	$C_7H_{14}O$	114	2.18	1.02	1.76
11	12.71	2-Phenylacetaldehyde	C_8H_8O	120	1.29	3.06	2.46
12	14.01	(E)-2-Hexenyl acetate	$C_8H_{14}O_2$	142	2.78	1.53	2.37
13	14.37	5-Butyloxolan-2-one (γ-octalactone)	$C_8H_{14}O_2$	142	2.03	1.98	1.99

Table 1 (continued)

1	2	3	4	5	6	7	8
14	14.43	endo-1,7,7-Trimethyl- bicyclo[2.2.1]heptan-2-ol (isoborneol)	$C_{10}H_{18}O$	154	1.03	1.09	1.07
15	14.92	2,6,6-Trimethylcyclohexene-1-carbaldehyde (β-cyclocitral)	$C_{10}H_{16}O$	152	5.17	4.27	4.71
16	15.42	(2E,4E)-Deca-2,4-dienal	$C_{10}H_{16}O$	152	3.65	2.81	3.19
17	15.86	(Z)-3,7-Dimethyl-2,6-octadien-1-ol (nerol)	$C_{10}H_{18}O$	154	3.02	2.74	2.85
18	16.74	(9*Z*,12*Z*,15*Z*)-9,12,15-Octadecatrienoic acid (α-linolenic acid)	$C_{18}H_{30}O_2$	278	0.63	3.94	2.17
19	17.06	(2E)-3,7-Dimethyl-2,6-octadien-1-ol (geraniol)	$C_{10}H_{18}O$	154	8.54	4.52	6.94
20	17.29	(9*Z*,12*Z*)-Octadeca-9,12-dienoic acid (linoleic acid)	$C_{18}H_{32}O_2$	280	4.20	5.34	4.78
21	18.24	Hexadecanoicacid (palmitic acid)	$C_{16}H_{32}O_2$	256	5.40	5.98	5.63
22	18.32	3,7-Dimethylocta-1,6-dien-3-ol (linalool)	$C_{10}H_{18}O$	154	3.06	2.71	2.89
23	18.94	1-Tetradecanoic acid	$C_{14}H_{28}O_2$	228	–	4.35	2.01
24	19.60	Octadecanoic acid (stearic acid)	$C_{18}H_{36}O_2$	284	6.02	6.17	6.11
25	19.62	(9*Z*)-Octadec-9-enoic acid	$C_{18}H_{34}O_2$	182	6.10	6.88	6.59
26	19.94	5-Hexyloxolan-2-one (γ-decalactone)	$C_{10}H_{18}O_2$	170	3.65	3.65	3.63
27	20.67	(7aR)-5,6,7,7a-Tetrahydro-4,4,7a-trimethyl-2(4H)-benzofuranone	$C_{11}H_{16}O_2$	180	2.05	2.18	2.07
28	20.91	5-Pentyl-5-pentanolide (δ-decalactone)	$C_{10}H_{18}O_2$	170	2.87	1.91	2.52
29	21.09	(Z)-3-Hexenyl butanoate	$C_{10}H_{18}O_2$	170	1.51	1.24	1.36
30	21.23	(9Z)-Hexadec-9-enoic acid	$C_{16}H_{30}O_2$	254	–	0.56	0.54
31	21.93	Hexyl hexanoate	$C_{12}H_{24}O_2$	200	2.12	2.26	2.20
32	22.18	(1R,2S,6S,7S,8S)-8-Isopropyl-1,3-dimethyltricyclo[4.4.0.0]dec-3-ene (α-copaene)	$C_{15}H_{24}$	204	4.02	4.53	4.38
33	23.08	3-Cyclohexen-1-ol, 4-methyl-1-(1-methylethyl) (4-terpineol)	$C_{10}H_{18}O$	154	4.98	4.50	4.61
34	23.54	2-(4-Methylcyclohex-3-en-1-yl)propan-2-ol (α-terpineol)	$C_{10}H_{18}O$	154	5.98	4.82	5.47
35	23.82	(3E)-4-(2,6,6-Trimethylcyclohex-1-en-1-yl)but-3-en-2-one (β-ionone)	$C_{13}H_{20}O$	192	1.97	1.24	1.79
36	24.13	4-(2,6,6-Trimethylcyclohexa-1,3-dienyl)butan-2-one (dihydro-β-ionone)	$C_{13}H_{22}O$	194	0.98	–	0.54
37	25.71	3,7-Dimethyl-2,6-octadien-1-yl acetate	$C_{13}H_{22}O$	170	6.10	4.25	5.72
38	26.32	Dihydro-5-octyl-2(3H)-furanone	$C_{12}H_{22}O_2$	198	7.65	5.91	6.74
39	26.79	3,7,11-Trimethyl-1,6,10-dodecatrien-3-ol (nerolidol)	$C_{15}H_{26}O$	222	8.54	2.3	7.04
40	27.21	(2E,6E)-3,7,11-Trimethyldodeca-2,6,10-trien-1-ol (farnesol)	$C_{15}H_{26}O$	222	1.38	0.69	0.87

In the extract, which was obtained using a mixture of propan-2-oland decamethylcyclopentasiloxane, 40 compounds discovered in the previously described extracts were found. This extract contains the predominant amount of both fatty acids and aldehydes of different nature, alcohols, as well as terpenoid compounds. A complete list of identified compounds is given in Table 1.

It has been established that with the extraction by a group of solvents, the total yield of extractive substances was in the following order from high to low: decamethylcyclopentasiloxane 114.92; isopropyl alcohol 123.11; mixture solvents 125.47. These results suggest that 50% mixture of 2-propanol and decamethyl-cyclopentasiloxane (1:1) give the highest yields among 3 solvents for compounds from the apricot pomace extract.

The presence of the functional groups of the higher organic compounds in the extract is confirmed by the analysis of the liquid phase of the extract of the apricot grinders by IR spectroscopy. The IR spectrum (Fig. 3, Table 2) is a classical spectrum with a good resolution of lines and an even base, which indicates the chemical stability of the sample. The colloidal systems in extracts often distort the baseline. The moisture content of the sample greatly broadens the peaks. In the spectrum, it is possible to distinguish absorption bands in the region of 3000–2800 cm^{-1}, which probably indicates the presence of an intermolecular hydrogen bond. The presence of aliphatic CH_3 and CH_2 groups is indicated by a strong absorption in the 2930–2850 cm^{-1} region (valence vibrations of CH_3 and CH_2 groups) and in the region of

1463–1377 cm^{-1} (deformation vibrations). A number of signals in the region of 902 cm^{-1} indicate the vibrations of the CH bonds. There are also absorption bands in the range of 1611–1617, 1505 and 3400 cm^{-1}, characteristic for vibrations of aromatic structures. It should be noted that along with aromatic compounds there are compounds with conjugated double bonds (such as conjugated dienes), that are evidenced by the presence of the absorption band in the spectrum at 1653 and 973 cm^{-1}.The IR spectrum of all extracts have intense absorption bands in the 1700–1735 cm^{-1} region, which is characteristic of valence vibrations of $\nu_{C=O}$ groups.

A joint examination of this region and the region of 3800–2600 cm^{-1}, where the valence vibrations bands of OH groups are located, suggests that all fractions contain carboxylic acids. The proof is the presence of a very wide band with a maximum at 2650 cm^{-1}, related to the vibrations of the ν_{OH} carbonyl groups, and an intense band at 1700–1735 cm^{-1}, related to the valence vibration of $\nu_{C=O}$ carboxylic acids. Concerning the remaining oxygen-containing compounds, it is impossible to draw clear conclusions, since the picture in the 3200–3800 cm^{-1} region is complicated by the presence of bounded water in the composition of the fractions.

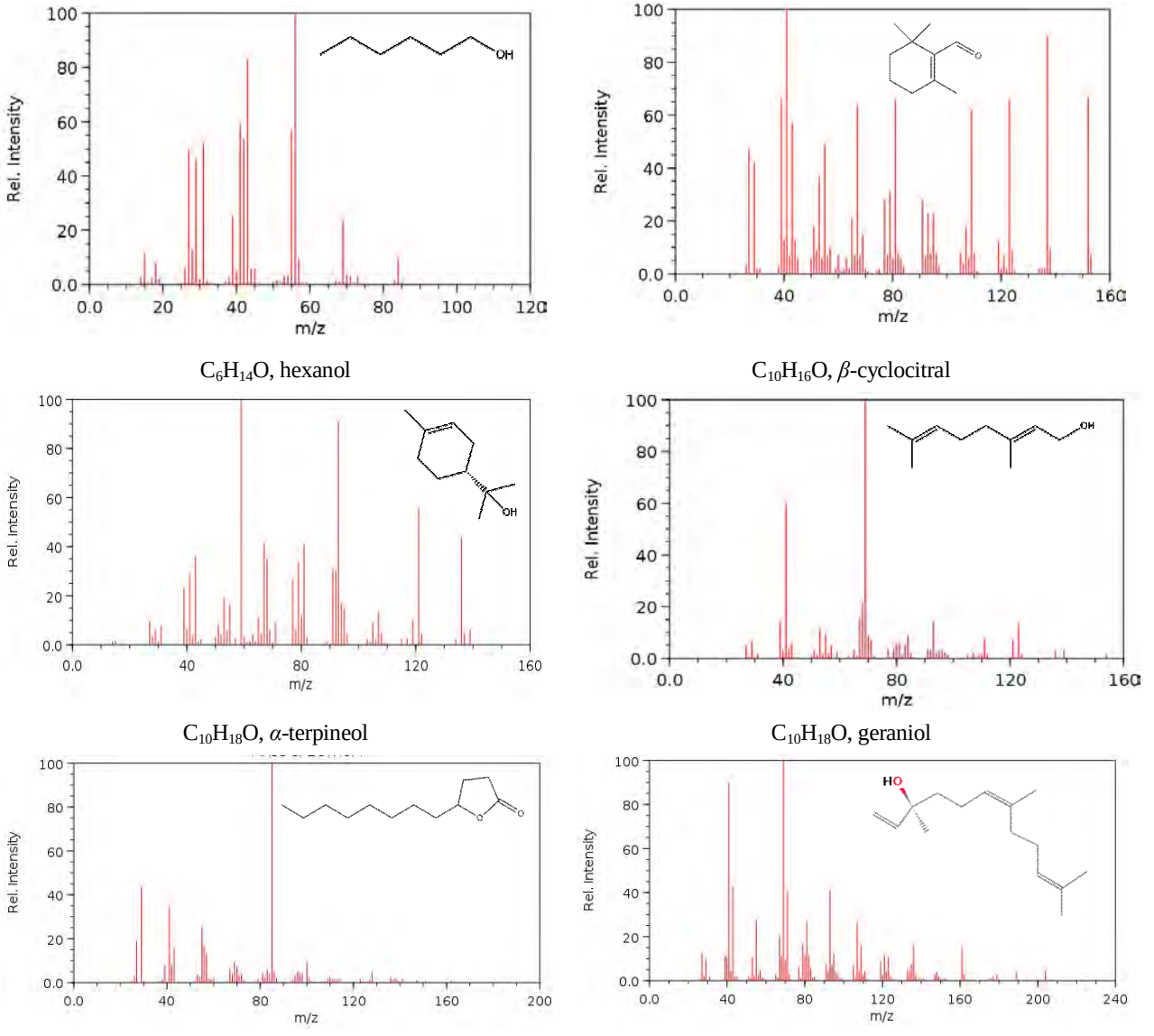

$C_6H_{14}O$, hexanol

$C_{10}H_{16}O$, β-cyclocitral

$C_{10}H_{18}O$, α-terpineol

$C_{10}H_{18}O$, geraniol

$C_{12}H_{22}O_2$, γ-dodecalactone

$C_{15}H_{26}O$, nerolidol

Fig. 2. Mass spectra and structures of the apricot pomace extracts main components identified by GC-MS

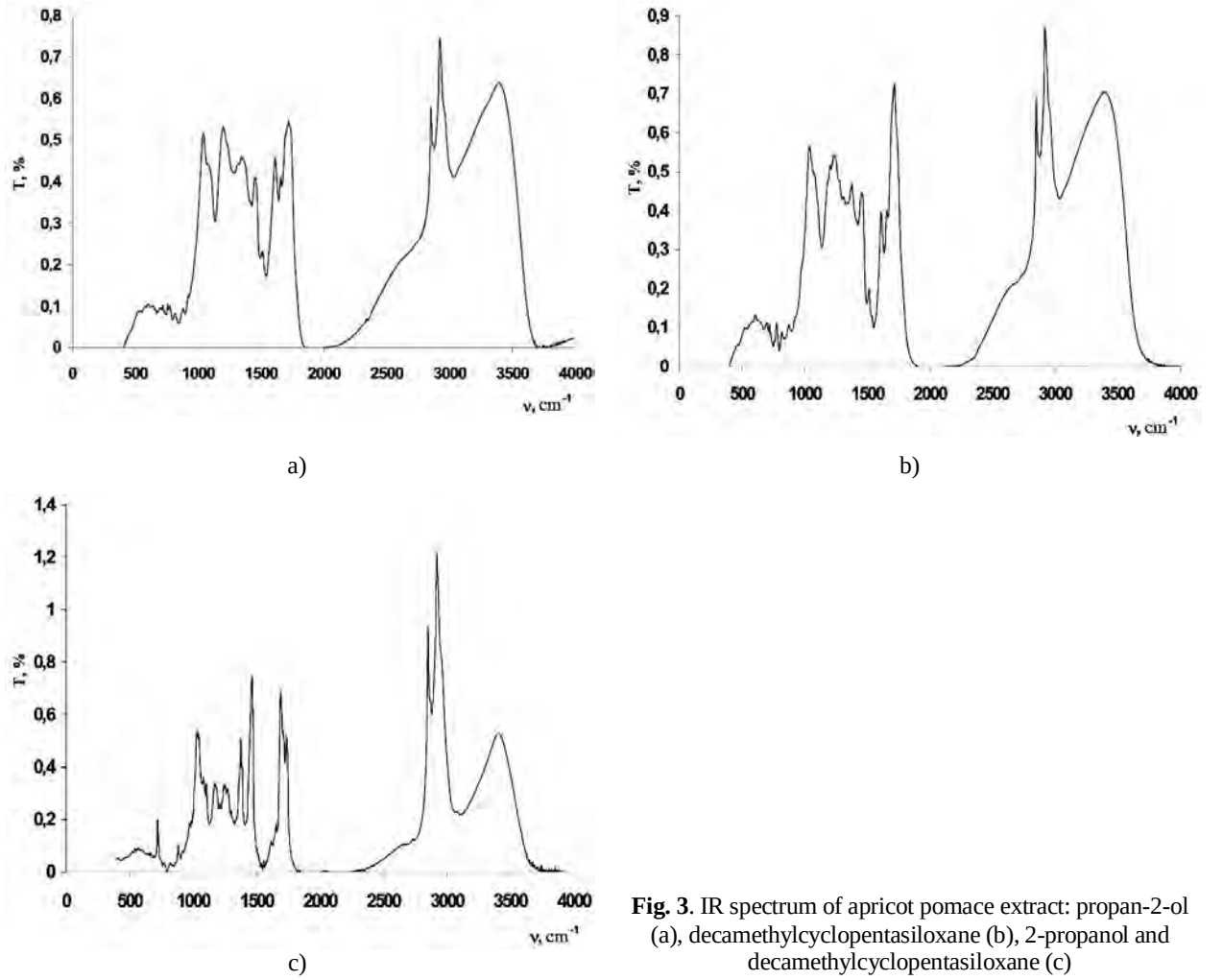

Fig. 3. IR spectrum of apricot pomace extract: propan-2-ol (a), decamethylcyclopentasiloxane (b), 2-propanol and decamethylcyclopentasiloxane (c)

Table 2

Assignment of absorption bands (cm^{-1}) in IR spectra of the apricot pomace extracts

Absorption band for functional groups		Apricot pomace extract		
		propan-2-ol	D5	propan-2-ol-D5
ν(C-H (aromatic))	3460–3205	3394	3389	3403
ν(CH_3)	2975–2810	2960	2960	2960
ν(CHOaldehydes, (2 bands))	2900–2820; 2775–2700	2921, 2850	2919, 2850	2919, 2850
ν(OHconnected by H bond)	2700-2500	~2600	~2650	~2650
ν(C=O)	1750–1600	1718	1714	1735
ν(C=C (unsaturated))	1620–1680	1654	1654	1653
ν(C=C (aromatic))	1705–1660	1611, 1505	1611, 1510	1617, 1505
δ(CH_2)	1470–1430	1456	1456	1463
δ(CH_3)	1380–1370	1345	1376	1375
γ (CH (pendulum oscillation))	982–970	–	–	973
Pendulum oscillations	720–710	719	719	719

The analysis of the observed bands in the 1000–1200 cm^{-1} region, together with the absorption at 1735 cm^{-1} in the carbonyl region, suggest the presence of keto-ether compounds in the extracts. This is most clearly seen for the silicone extract.

The UV-Vis spectroscopic method is one of the main methods of qualitative determination of chemical compounds that are present in plant phyto-constituents. The qualitative UV-Vis spectrum profile of the extract was selected at a wavelength of 200–800 nm (Fig. 4).

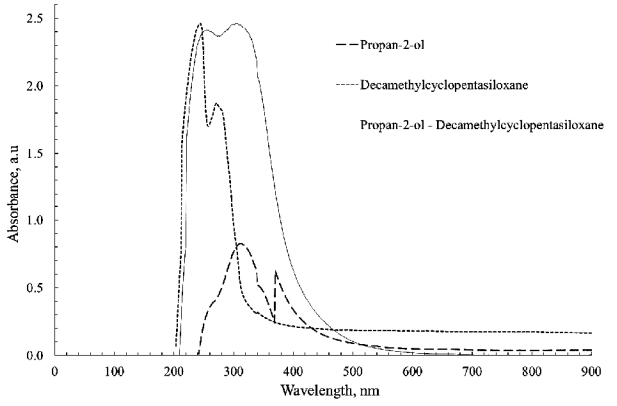

Fig. 4. UV–visible absorbance spectra of apricot pomace extracts

For the correct reproduction of the UV spectroscopic data, both the solvents and the extracts themselves were investigated. After analyzing the spectrum obtained in the selected region, it was found that the spectrums are actively affected by the solvent, so the spectroscopy of the samples was performed, with the compensation of the propan-2-ol, decamethylcyclopentasiloxane and the mixture of propan-2-ol and D5 (50%/50%) established in the subtraction channel. At the same time, the maximum significance of the spectrums was achieved.

Different compounds have their characteristic wavelength of maximum absorption. For propan-2-ol extract the peak values at 313 and 370 nm indicate terpenoid compounds and their derivatives. According to the GC/MS, the extract contains the most abundant terpenoid compounds, namely geraniol and nerolidol. For the silicone extract, peaks at 244 and 271 nm were detected, indicating the presence of fatty acids in its composition. On the UV spectrum of the extract obtained with a mixture of propan-2-ol and decamethylcyclopentasiloxane, 2 peaks at 248 and 319 nm are shown, indicating the prevalence of compounds in the class of fatty acids and terpenoids. Therefore, analysis of the UV spectrum of the obtained extract confirmed the presence of compounds with a predominant content in the isopropanol extract of apricot pomace.

The unique composition of extracts determines the possibility of their application in different branches of chemical technology. Extracts can be used as a finished product, and also extract individual substances from the extracts, which have their own specific functional application (Table 3). Thus, the extract can be used in medicine for the treatment of many types of diseases and as a component of food, cosmetic products that have a curative-prophylactic effect [16-18]. The presence of these phyto chemicals makes apricot pomace a potential source of bioactive compounds.

Table 3

Nature and the biological activities of phyto constituents of the entire plant parts of apricot pomace extracts

Retention time, min	Name of the compound	Compound nature	Uses
4.04	Hexanol	Alcohol	Antifoams, hydrotropic substances, antiseptic and irritant
14.92	*β*-Cyclocitral	Monoterpene acyclic aldehyde	Fragrant, flavor, antiseptic and anti-inflammatory agent
17.06	Geraniol	Terpenoid	Fragrant substance, antifungal, shows the properties of antibiotics
18.24	Hexadecanoic acid	Saturated fatty acid	Anti –inflammatory, nematicide, antioxidant
19.60	Stearic acid	Aliphatic monobasic carboxylic acid	Emulsifying agent, stabilizer
19.62	(9Z)-Octadec-9-enoic acid	Monounsaturated fatty acids	Emulsifying agent
22.18	*α*-Copaene	Tricyclic sesquiterpenes.	In perfumery, fragrant substances and odor fixers, as well as in medicine, for example, as anthelmintic agents
23.08	4-Terpineol	Monoterpene alcohol	Solvent, plasticizer, flotation agent; has antimicrobial properties.
23.54	*α*-Terpineol		
25.71	Geranylacetone	Terpenoid	Fragrant substances, antibacterial agent
26.32	*γ*-Dodecalactone	Lactone	Fragrant substances
26.79	Nerolidol	Terpenoid	Odor fixer, fragrant substances

4. Conclusions

The results clearly showed that significantly different classes of compounds and their number were extracted by different solvent systems. Different solvents may need to be used to study the characteristics of various compositions of active compounds in different chemical technology. The most efficient solvent for total extraction compounds from apricot pomace was the mixture of propan-2-ol and D5. The presence of aldehydes, and terpene alcohols in the apricot pomace extracts was confirmed in this study.

Thus, it can be concluded that the waste of the common apricot (*Prunus armeniaca L*) is promising for its further study and for using raw materials as a source in the development of new functional products. This preliminary study gives an idea to isolate the major active constituents present in the pomace apricot and also helps to develop biologically active compounds from raw materials.

References

[1] Islam T., Yu X., Badwal T., Xu B.: Chem. Cent. J., 2017, **11**, 59. https://doi.org/10.1186/s13065-017-0287-z
[2] Gokbulut I., Karabulut I.: Food Chem., 2012, **132**, 1098. https://doi.org/10.1016/j.foodchem.2011.11.080
[3] Roussos P., Sefferou V., Denaxa N. *et al*.: Scientiahorticulturae, 2011, **129**, 472. https://doi.org/10.1016/j.scienta.2011.04.021
[4] Zhang T., Wei X., Miao Z. *et al*.: Chem. Cent. J., 2016, **10**, 47. https://doi.org/10.1186/s13065-016-0195-7
[5] Chyhyrynets O., Fateev Y., Vorobiova V. *et al*.: Mater. Sci., 2016, **51**, 644. https://doi.org/10.1007/s11003-016-9886-4
[6] Vorob'iova V., Chyhyrynets' O., Vasyl'kevych O.: Mater. Sci., 2015, **50**, 726. https://doi.org/10.1007/s11003-015-9778-z
[7] Chygyrynets' E., Vorobyova V.: Chem. Chem. Technol., 2014, **8**, 235.
[8] Gündoğdu M., Kan T., Gecer M.: HortScience, 2013, **48**, 696.
[9] Svarcova I., Jan H., Valentova K.: Biomedical Papers, 2007, **151**, 163. https://doi.org/10.5507/bp.2007.031
[10] Karapetyan T., Mirzoyan V., Hanisyan R., Sahakyan N.: The New Armenian Medical Journal, 2011, 5, 44.
[11] Dragovic-Uzelac V., Levaj B., Mrkic V. et al.: Food Chem., 2007, 102, 966. https://doi.org/10.1016/j.foodchem.2006.04.001
[12] Melgarejo P., Calín‐Sánchez Á., Carbonell‐Barrachina Á. et al.: J. Sci. Food Agricult., 2014, 94, 85. https://doi.org/10.1002/jsfa.6201
[13] Khodadadi B., Bordbar M., Nasrollahzadeh M.: J. Colloid Interf. Sci., 2017, **409**, 1. https://doi.org/10.1016/j.jcis.2016.11.032
[14] VasileDulf K., Vodnar D., Dulf E., PinteaA.: Chem. Cent. J., 2017, **11**, 92. https://doi.org/10.1186/s13065-017-0323-z
[15] Erdogan-Orhan I., Kartal M: Food Res. Int., 2011, **44**, 1238. https://doi.org/10.1016/j.foodres.2010.11.014
[16] Solís-Solís H., Calderón-Santoyo M., Schorr-Galindo S. *et al*.: Food Chem., 2007, **105**, 829. https://doi.org/10.1016/j.foodchem.2007.01.061
[17] Lapornik B., Prošek M., Wondra A.: J. Food Eng., 2005, **71**, 214. https://doi.org/10.1016/j.jfoodeng.2004.10.036
[18] Cheaib D., El Darra N., Rajha H. *et al*.: Antioxidants, 2018, **7**, 11. https://doi.org/10.3390/antiox7010011

Received: March 06, 2018 / Revised: April 12, 2018 / Accepted: August 12, 2018

ВИЗНАЧЕННЯ ХІМІЧНОГО СКЛАДУ ЕКСТРАКТУ АБРИКОСОВОГО ЖМИХА (*Prunus armeniaca* L.)

Анотація. *Вивчено комплексну характеристику компонентних профілів екстракту абрикосового жмиха (Prunus armeniaca L.) залежно від використовуваних систем розчинників. За допомогою ІЧ-спектроскопії, УФ-спектроскопії та газової хромато-мас-спектроскопії проаналізовані екстракти, отримані пропан-2-олом, декаметилциклопентасилоксаном та сумішшю силікону і пропан-2-олу абрикосового жмиха.*

Ключові слова: *абрикосовий жмих, екстракт, пропан-2-ол, декаметилциклопентасилоксан, альдегіди, терпенові спирти.*

Chem. Chem. Technol., 2019, Vol. 13, No. 3, pp. 399–406

Chemical Technology

REMOVAL OF PETROLEUM FROM AQUEOUS SYSTEMS BY POLY(DIVINYLBENZENE) AND POLY(METHYL METHACRYLATE-DIVINYLBENZENE) RESINS: ISOTHERMAL AND KINETIC STUDIES

Carla Silva[1, *], Paulo Rocha[1], Thiago Aversa[2], Elizabete Lucas[1, 3]

https://doi.org/10.23939/chcht13.03.399

Abstract. In this study, the performance of two polymer resins was evaluated, one composed of methyl methacrylate-divinylbenzene (MMA-DVB) and the other of only divinylbenzene (DVB), for adsorption of oil in synthetic oily wastewater. The tests were carried out using two processes: (i) continuous flow, to assess the quantity of oily water that can be eluted until reaching the saturation point of resins; and (ii) batch, to obtain information about the best-fitting kinetic and isotherm models for the two resins. The results for both resins showed better fits to the Freundlich isotherm model and the pseudo-second-order kinetic model. The low activation energy values found suggest physical adsorption between the resins and oil. Although DVB resin has presented slightly better oil removal efficiency than the MMA-DVB one, the results showed that DVB resin can be industrially replaced by MMA-DVB resin, due to the latter advantages: lower cost, lower toxicity and easy regeneration, as indicated by the kinetic and isotherm studies.

Keywords: oily water treatment, adsorption, porous polymer resins, isotherm model, kinetic model.

1. Introduction

The process of petroleum production is accompanied by continuous production of water. This produced water is a byproduct, the complex composition of which depends on the type of oil, age of the field and extraction procedure. In general, this water contains high concentrations of different salts, a large quantity of dispersed and emulsified oil, solids from the rock formation and chemical products added to improve the extraction process, such as biocides, antifoam agents and corrosion inhibitors [1-6]. Therefore, the produced water needs to be treated before being discharged in the environment because toxic properties or used for other purposes [7]. The treatment method depends on this final destination: discharge or reuse in other activities, such as irrigation, steam generation for tertiary oil recovery or power generation [8-10], and reinjection in producing wells [11-12]. For discharge, in Brazil the concentration of oil must be reduced to 0.029 kg/m^3, according to the rules issued by the National Environmental Council [13]. For reuse and reinjection, the levels of contaminants must be smaller than for discharge, making it necessary to use more complex treatment methods, such as nanofiltration and reverse osmosis membranes.

Produced water treatment by physico-chemical processes, involving gravitational separation, hydro-cycloning and/or ultrafiltration, is very common, but in some cases these methods are unable to reduce the concentrations of contaminants to acceptable levels, even for discharge. Various alternatives have been studied to "polish" this water, with processes involving adsorption being the most suitable and widely studied [14-15]. Among filtering methods, the use of crushed walnut shells and other plant materials can be mentioned. In adsorption processes, materials like charcoal, organic clays and polymer resins are being used [16-19]. Polymer resins have several advantages, such as thermal, mechanical and chemical stability and reusability. They can also be tailored to the type of contaminant to be removed [20-22]. In adsorption processes in general, polymer resins have presented satisfactory results, and although they can be obtained with varied compositions [23-26], those based on divinylbenzene (DVB) and styrene (STY) having the greatest application. Several studies of the use of STY-DVB resins to treat produced water have been published [27-29]. Since crude oil is a complex mixture of compounds with different characteristics, some studies have been published investigating the efficiency of resins made from methyl methacrylate (MMA) and DVB [30-32]. These resins show as advantages the lower

[1] Universidade Federal do Rio de Janeiro, Instituto de Macromoléculas, Av. Horácio Macedo, 2030, block J, Cidade Universitária, 21941-598, Rio de Janeiro, RJ, Brazil
[2] Instituto Federal de Educação, Ciência e Tecnologia do Rio de Janeiro (IFRJ), Av. República do Paraguai, 120, 25050-100, Duque de Caxias, RJ, Brazil
[3] Universidade Federal do Rio de Janeiro, COPPE/PEMM, Av. Horácio Macedo, 2030, block F, Cidade Universitária, 21941-598, Rio de Janeiro, RJ, Brazil
* *michele.frota@gmail.com*

toxicity of MMA in relation to STY and slightly more polar character of MMA [33], inducing more effective adsorption of other types of molecules that compose crude oil. In previous studies, preliminary tests of continuous flow treatment of oily water allowed establishing parameters to obtain the best efficiency of this type of resin to remove oil from synthetic wastewater samples [34-35]. However, to the best of our knowledge, no studies have been published involving the physico-chemical adsorption of oil by MMA-DVB resin, to shed more light on the interaction aspects. Therefore, this paper presents the results of tests to evaluate the removal of oil from synthetic oily water (oil-in-water emulsion) with an MMA-DVB polymer resin in comparison with a DVB resin, through continuous flow and batch processes, indicating the isothermal and kinetic parameters that best fit the systems. The study of these aspects is of great importance for more effective treatment of produced water so that it can be discharged or reused.

2. Experimental

2.1. Chemicals

The crude oil sample was donated by the Petrobras Research Center (CENPES), Rio de Janeiro, Brazil, and is identified as "Petroleum B" (density 927 kg/m^3 and ºAPI = = 20.35, at 293 K). Hexane, sodium chloride and calcium chloride (P.A. purity grade) were supplied by Vetec Química Fina Ltda, Duque de Caxias, Brazil, and used as received. Two kinds of mesoporous polymer resins, previously synthesized and characterized, were used as adsorbents: (i) polydivinylbenzene (DVB) (surface area $567 \cdot 10^3$ m^2/kg; pore volume $1.28 \cdot 10^{-4}$ m^3/kg; pore diameter 79.5 Å); and (ii) poly(methyl methacrylate-divinyl benzene) (MMA-DVB) (molar ratio 77–23; surface area $72 \cdot 10^3$ m^2/kg; pore volume $3.9 \cdot 10^{-4}$ m^3/kg; pore diameter 218.9 Å). Distilled and deionized water was produced with a Gehaka OS10LX reverse osmosis system.

2.2. Preparation of the Water Contaminated with Crude Oil

Firstly, synthetic saline water was prepared containing NaCl and $CaCl_2$ in the ratio of 10:1, respectively, with the total salt concentration of 55 kg/m^3. The salts were dissolved in half the total volume of water, by magnetic stirring, and after their total dissolution the rest of the water was added to the system [31, 35]. This concentration of salts was chosen because it is near the salinity of the water typically found in oil fields [36]. The crude oil was then slowly added to half the volume of the saltwater, under stirring at 13,000 rpm with an Ultra-Turrax T-25. Finally, the remaining saltwater was poured into the system and stirred for 900 s at 15,000 rpm [31, 35].

2.3. Determination of Total Oil and Grease (TOG) by Fluorescence Spectroscopy

Fluorescence spectroscopy was used to analyze the total oil and grease (TOG) concentration, using a Turner Designs TD-3100 bench top fluorometer [31, 34, 36]. Aliquots of $4.5 \cdot 10^{-5}$ m^3 of oily water were collected in $5 \cdot 10^{-5}$ m^3 graduated cylinder tubes, followed by addition of $5 \cdot 10^{-6}$ m^3 of hexane. The tubes were shaken vigorously for about 300 s to extract the maximum of the oil phase by the hexane.

After complete separation of the phases, the organic phase (containing oil and grease) was isolated for subsequent analysis. The excitation wavelength was set at 350 nm and the emission spectra were obtained in the range of 360–600 nm, in line with the data obtained in a previous study [34]. The fluorescence emission of the mono and polyaromatic hydrocarbons contained in crude oil typically occurs in the region of (430 ± 30) nm. The device was calibrated using the reading for pure hexane and a solution of oil in hexane at the concentration of 0.025 kg/m^3, as specified in the instruction manual.

2.4. Batch Adsorption Experiments

In these experiments, we evaluated the following factors that influence the adsorption process: contact time, adsorbent mass, and temperature. The equilibrium data were fitted in two isotherm models: Langmuir and Freundlich [39], in their linearized versions. The kinetic data were fitted in the pseudo-first-order and pseudo-second-order models [40, 41].

The analysis was carried out by immersing the adsorbent in the oily water and mechanically shaking the solution in a Haake SWB25 shaker, at 100 rpm. The temperature was thermostatically controlled using a bath coupled to the shaker (Thermo Haake C25P). All analyzes were done in duplicates for the two systems studied.

2.4.1. Equilibrium adsorption studies

For this study, five test tubes were prepared, each containing 50 lL of oily water at 0.030 kg/m^3 and a different mass of resin ($5 \cdot 10^{-5}$, $1 \cdot 10^{-4}$, $3 \cdot 10^{-4}$, $7 \cdot 10^{-4}$, $1 \cdot 10^{-3}$ kg). The tubes were agitated at 298, 308, 318 and 323 K. The oily concentration in solution, C_e (kg/m^3) was quantified by fluorescence.

2.4.2. Adsorption kinetics studies

To analyze the adsorption kinetics, six test tubes were prepared, each containing $5 \cdot 10^{-5}$ m^3 of the oily water at 0.15 kg/m^3 and $3 \cdot 10^{-4}$ kg of resin. The tubes were agitated at 298, 308, 318 and 323 K, with different contact times: 900, 1800, 3600, 5400, 7200 and 14400 s. The oil concentration in solution, C_e (kg/m^3), was quantified by fluorescence.

2.5. Data Analysis

For both the equilibrium and kinetics studies, the concentration of adsorbed solute per mass unit (q_e) was calculated by Eq. (1):

$$q_e = \frac{(C_i - C_e)\cdot V}{m} \quad (1)$$

where C_i is the initial solute concentration in the solution, kg/m^3; C_e is the solute concentration in the solution under equilibrium, kg/m^3; V is the solution volume, m^3; and m is the adsorbent mass, kg.

2.5.1. Isotherm models

The Langmuir and Freundlich isotherm models were adopted to analyze the equilibrium data. The Langmuir isotherm is valid for monolayer adsorption and serves as the starting point for many adsorption studies in catalytic applications [39]. The Langmuir model is described by Eq. (2):

$$\frac{1}{q_e} = \frac{1}{Q_0} + \frac{1}{bQ_0C_e} \quad (2)$$

where q_e is the mass of adsorbate per unit mass of adsorbent, kg/kg; Q_0 indicates the maximum adsorbate mass that can be retained in the adsorbent; b is the Langmuir constant, which is related to the bonding energy; and C_e is the solute concentration in equilibrium, kg/m^3.

Eq. (3) describes the equilibrium of heterogeneous adsorption systems proposed by the Freundlich isotherm model [39]:

$$\log q_e = \log K_F + \frac{1}{n}\log C_e \quad (3)$$

where q_e is the mass of adsorbate per unit mass of adsorbent, kg/kg; K_F is a constant that indicates the relative adsorption capacity of the adsorbent, kg/kg; n is a dimensionless constant that indicates the adsorption intensity; and C_e is the solute concentration in equilibrium, kg/m^3).

2.5.2. Kinetic models

The pseudo-first-order model follows Eq. (4):

$$\ln(q_e - q_t) = \ln q_e - K_1 t \quad (4)$$

where q_e is the mass solute adsorbed per unit of adsorbent mass in equilibrium, kg/kg; q_t is the concentration of solute adsorbed per unit of adsorbent mass (kg/kg) at time t (s); and K_1 is the adsorption velocity constant, s^{-1}.

The angular coefficient of $\ln(q_e - q_t)$ *versus* time plot provides the first-order velocity constant (K_1). The values of $\ln(q_e - q_t)$ were calculated from the linear portion of the graph of q_t *vs.* t. The activation energy of the process was obtained by plotting the graph of $\ln K_1$ as a function of $1/T$ from the Arrhenius equation (Eq. (5)) [42, 43].

$$\ln K_1 = -\frac{E_a}{RT} + \ln A \quad (5)$$

where K_1 is the adsorption velocity constant, s^{-1}; E_a is the activation energy, kJ/mol; R is the universal gas constant (8.314 J/mol·K); and A is the pre-exponential factor.

The pseudo-second-order model follows Eq. (6):

$$\frac{t}{q} = \frac{1}{K_2 q_e^2} + \frac{1}{q_e}t \quad (6)$$

where q_e is the concentration of solute adsorbed per unit of adsorbent mass in equilibrium, kg/kg; q is the concentration of solute adsorbed per unit of adsorbent mass at time t, kg/kg; and K_2 is the pseudo-second-order velocity constant, kg·kg·s^{-1}.

2.6. Retention Experiments Under Continuous Flow

The resins were first placed in water to swell for 24 h at room temperature. Then with the aid of a packing tool, stainless steel columns (11 mm inner diameter × 30 mm height – bed volume equal to $2.85\cdot10^{-6}$ m^3) were packed with resins at the water flow rate of $1.67\cdot10^{-8}$ m^3/s for 3600 s, using a Jasco PU-1580 chromatographic pump. At each hour, the flow rate was increased by $8.3\cdot10^{-9}$ until reaching $1.67\cdot10^{-7}$ m^3/s. The system was kept at this condition for 1 h and then 1 h more at 1 ml/min.

Oily water at concentrations of about 0.2 kg/m^3 (previously quantified) was eluted through the column at the flow rate of $1.17\cdot10^{-7}$ m^3/s. After each $2.0\cdot10^{-4}$ m^3 of solution, aliquots were collected to determine TOG by fluorimetry.

3. Results and Discussion

3.1. Studies of Oil Retention by Batch Adsorption

The batch experiments had the objective of obtaining the parameters for fitting an isotherm model, for efficient interpretation of the equilibrium and kinetics of the resins. The relative errors were of the order of 5 %.

3.1.1. Adsorption equilibrium

To assess the influence of resin mass on the adsorption efficiency, experiments were performed in which the mass and temperature were varied, maintaining the initial adsorbate concentration and adsorbate-adsorbent contact time constant. This experiment allowed obtaining information on the minimum quantity of adsorbent needed to achieve maximum adsorption.

With respect to the efficiency in removing each mass of adsorbent at a given temperature (Fig. 1), the DVB resin was more efficient than the MMA-DVB resin. At 298 K, with $5\cdot10^{-5}$ kg of DVB (Fig. 1a), the adsorption efficiency reached 50 %, while with $7\cdot10^{-5}$ kg the efficiency was 80 %. For masses above this value, no substantial increase in efficiency was observed. In the case of MMA-DVB (Fig. 1b), there was a greater dependence

between the mass and adsorption efficiency. The initial efficiency was 23 % with $5 \cdot 10^{-5}$ kg of resin, which increased to the maximum of 58 % with resin mass of $1 \cdot 10^{-3}$ kg. The performance profile was the same for all the other temperatures tested, where larger resin masses produced higher adsorption efficiencies. This behavior can be attributed to the larger surface areas due to the increase in mass.

The better efficiency of DVB resin *versus* MMA-DVB resin can be explained by the higher specific surface area of DVB in relation to MMA-DVB. This is an important factor for a material to be a good adsorbent. The DVB resin has a specific surface area about eightfold that of MMA-DVB. However, the adsorption results for MMA-DVB were not proportionally lower in relation to its smaller surface area, showing that the adsorption depends not only on specific surface area, but also on other factors, such as pore size and volume, particle size and type of adsorbent-adsorbate interaction in terms of polarity, hydrophobicity and crosslinking degree, among other factors [44, 45].

With respect to the effect of temperature on the oil adsorption capacity of the resins, this capacity for both resins declined with rising temperature (Fig. 1). This can be attributed to the fact that adsorption is exothermal [46].

These data were used to plot the adsorption isotherms, providing information on how effectively the resins adsorb the oil present in the water, by estimating the quantity adsorbed in function of concentration in equilibrium (C_e). For both adsorbents, the concentration of solute adsorbed per unit of mass (q_e) was initially calculated according to Eq. (1), and these values were used to plot graphs of q_e *versus* C_e (Fig. 2), which depict the adsorption isotherms of oil in the DVB and MMA-DVB resins at all studied temperatures.

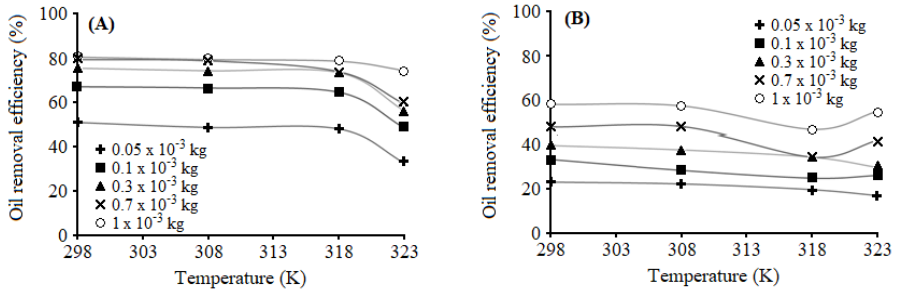

Fig. 1. Effect of temperature on the oil adsorption efficiency of DVB (a) and MMA-DVB (b), using resin masses of $0.05 \cdot 10^{-3}$, $0.1 \cdot 10^{-3}$, $0.3 \cdot 10^{-3}$, $0.7 \cdot 10^{-3}$ and $1.0 \cdot 10^{-3}$ kg and oil concentration of 0.03 kg/m^3

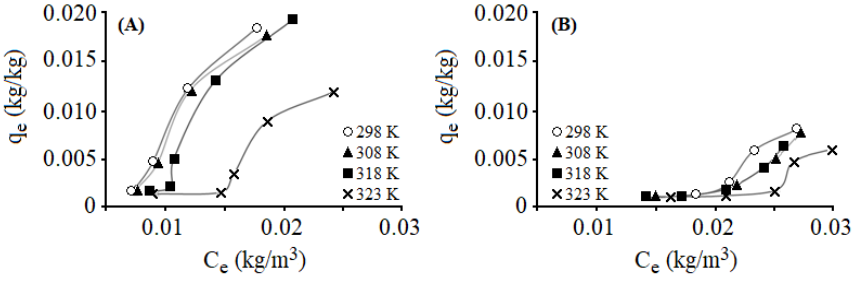

Fig. 2. Adsorption isotherms of DVB (a) and MMA-DVB (b). Initial oil concentration of 0.03 kg/m^3, temperature range of 298–323 K, contact time of 18000 s; q_e is the mass of oil adsorbed per mass of adsorbent in equilibrium, and C_e is the concentration of oil in water in equilibrium

Table 1

Parameters of the Langmuir and Freundlich models of adsorption of oil by the DVB and MMA-DVB resins, at initial oil concentration of 0.03 kg/m^3, masses of $5 \cdot 10^{-5}$ and $1 \cdot 10^{-3}$ kg and contact time of 18000 s

Adsorbent	Temperature, K	Model					
		Langmuir			Freundlich		
		b	Q_0, kg/kg	R^2	K_F	n	R^2
DVB	298	-62.35	-0.0022	0.8390	104.71	0.45	0.9211
	308	-59.81	-0.0022	0.8110	1348.96	0.36	0.8982
	318	-51.66	-0.0022	0.7920	2511.89	0.34	0.8684
	323	-31.02	-0.0030	0.7530	112.20	0.40	0.7902
MMA-DVB	298	-33.62	-0.00094	0.9020	6309.60	0.26	0.8870
	308	-31.81	-0.0010	0.9542	1995.30	0.28	0.9204
	318	-31.91	-0.0010	0.9526	501.20	0.31	0.9042
	323	-25.98	-0.0012	0.8289	199.50	0.33	0.7825

As previously mentioned, the profile of the isotherms shows that the quantity of oil adsorbed was inversely proportional to the increase in temperature, explained by the exothermal nature of the adsorption processes, and the difference in the isotherm profiles of the two resins is probably due to factors like porosity and chemical structure of the adsorbents [47]. The data from the isotherms were fitted to the Langmuir and Freundlich models to identify the one that best represented the adsorption process of the systems studied. We employed the equations of Langmuir (2) and Freundlich (3) in their linearized forms to obtain the parameters of each isotherm model (Table 1).

For the Langmuir model, the MMA-DVB resin presented the highest correlation values, but they were not very close to 1. Besides this, for both resins the calculated values for the parameters b and Q_0 were negative, suggesting that the systems studied cannot be represented well by this model. In turn, for the Freundlich model, the resins presented correlation coefficient values that were not very high (< 0.95), indicating that the isotherms were unfavorable and revealing a weak interaction between the resins and oil. Of the parameters obtained, n is related with the interaction of the adsorbate and adsorbent and K_F is related with the adsorption capacity. We also observed that the temperature has a stronger influence on the adsorption of MMA-DVB, because with increasing temperature, the values of K_F decreased.

3.1.2. Adsorption kinetics

Figs. 3a and 3b show the results of the mass of oil adsorbed per mass of adsorbent (q_e) in function of contact time, for DVB and MMA-DVB resins, respectively. From these data on adsorption efficiency in function of contact time it is possible to predict the behavior of the adsorbents through kinetic models.

Initial analysis of the graphs allows noting that the largest removal occurred in the initial contact periods. The adsorption took place quickly at first and then gradually slowed until reaching the equilibrium, at about 60 min for DVB and 30 min for MMA-DVB. The latter resin, although less efficient in adsorbing oil, reached equilibrium in less time. This can be explained by the porosity characteristics, where although MMA-DVB has smaller surface area than DVB, the average pore diameter is larger, allowing easier access of the oil particles to the pores.

By applying the kinetic pseudo-first-order model [48] (Eq. (4)), in its linearized form (Eq. (5)), it was possible to obtain graphics (Fig. 4) with good correlation coefficients. For DVB, the values were nearer to 1, while for MMA-DVB they varied from 0.92 to 0.98. These results indicate that the oil adsorption process of the adsorbents evaluated can be represented by the Lagergren model. Based on the data from the graphs in Fig. 4, we calculated the constant K_1 (adsorption velocity constant) and $q_{e(calc)}$ (concentration of solute adsorbed per unit of adsorbent mass in equilibrium), presented in Table 2.

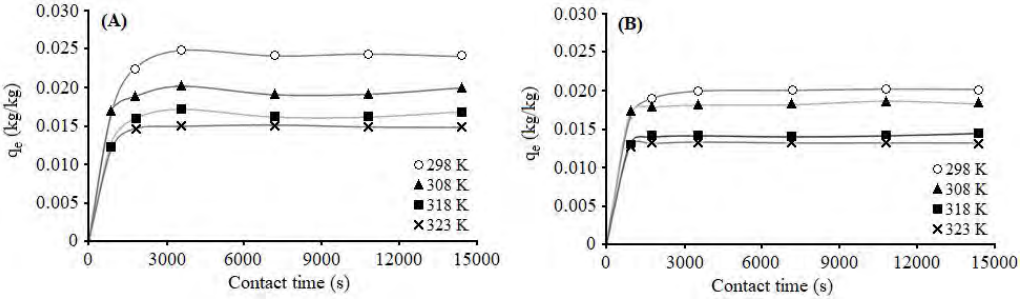

Fig. 3. Adsorption kinetics of DVB (a) and MMA-DVB (b). Initial oil concentration of 0.15 kg/m^3, resin mass of $3 \cdot 10^{-4}$ kg and temperature range of 298–323 K; q_e is the mass of oil adsorbed per adsorbent mass

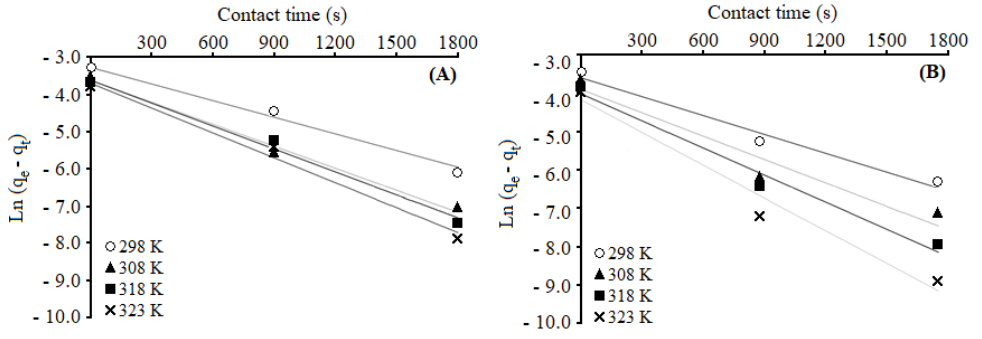

Fig. 4. Linearization of the pseudo-first-order adsorption kinetics of DVB (a) and MMA-DVB (b). Initial oil concentration of 0.15 kg/m^3, resin mass of $3 \cdot 10^{-4}$ kg and temperature range of 298–323 K

Comparison of the values of R^2 and $q_{e(calc)}$ of the two kinetic models studied indicates that the pseudo-second-order better describes the kinetic behavior of the systems evaluated than the pseudo-first-order model. According to the literature, the pseudo-second-order model is able to describe the adsorption kinetics in a wide time range, but only for low solute concentrations, unlike the other model [40, 49, 50].

The initial adsorption velocity values (h) indicate that in general the velocity increased with rising temperature and that MMA-DVB adsorbed the oil molecules in water faster than DVB at all temperatures studied.

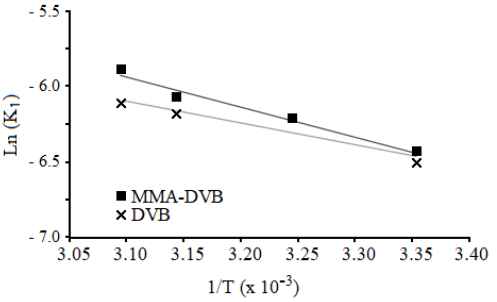

Fig. 5. Determination of the activation energy for adsorption of oil in the DVB and MMA-DVB resins

Table 2

Pseudo-first-order kinetic constants for adsorption of oil by the adsorbents DVB and MMA-DVB

Adsorbent	Temperature, K	K_1	$q_{e(exp)}$, kg/kg	$q_{e(calc)}$, kg/kg	R^2
DVB	298	0.0015	0.02415	0.02545	0.9964
	308	0.0020	0.01937	0.01791	0.9942
	318	0.0021	0.01637	0.01801	0.9921
	323	0.0022	0.01492	0.01668	0.9909
MMA-DVB	298	0.0016	0.01992	0.01825	0.9899
	308	0.0020	0.01818	0.01348	0.9221
	318	0.0023	0.01410	0.01199	0.9820
	323	0.0028	0.01314	0.01026	0.9712

Table 3

Activation energy values (E_a) for the adsorbents DVB and MMA-DVB

Adsorbent	Equation	$-E_a/R$	E_a, kJ/mol	R^2
DVB	$y = -1403.2x + 1.7475$	–1403.2	11.67	0.8791
MMA-DVB	$y = -2101.1x + 0.5858$	–2101	17.47	0.9131

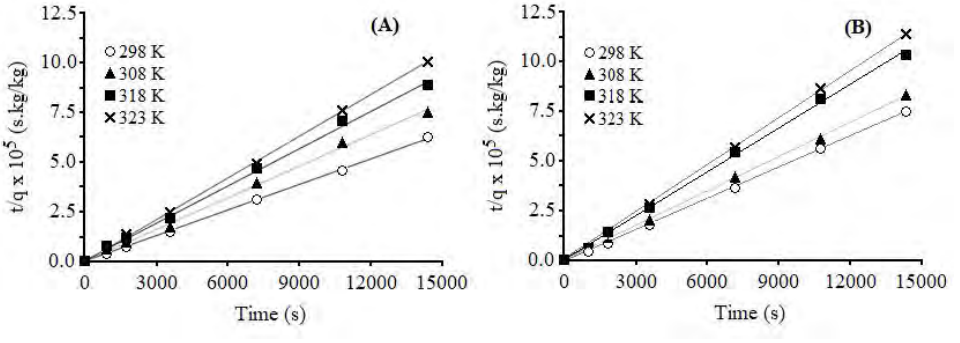

Fig. 6. Linearization of the pseudo-second-order adsorption kinetics of DVB (a) and MMA-DVB (b). Initial oil concentration of 0.15 kg/m^3, resin mass of $3 \cdot 10^{-4}$ kg, temperature range of 298–323 K, and contact time of 14400 s

Table 4

Pseudo-first-order kinetics constant for adsorption of oil by the adsorbents DVB and MMA-DVB

Adsorbent	Temperature, K	K_2, kg·s^{-1}	$q_{e(exp)}$, kg/kg	$q_{e(calc)}$, kg/kg	h, kg/kg^{-1}·s^{-1}	R^2
DVB	298	0.3464	0.024	0.024	0.00021	0.9992
	308	0.5650	0.019	0.020	0.00022	0.9989
	318	0.5575	0.016	0.017	0.00016	0.9988
	323	1.5767	0.015	0.015	0.00035	0.9997
MMA-DVB	298	0.5031	0.019	0.020	0.00020	0.9999
	308	1.2686	0.018	0.18	0.00042	0.9998
	318	0.9469	0.014	0.014	0.00019	0.9997
	323	11.0777	0.013	0.013	0.00187	1.0000

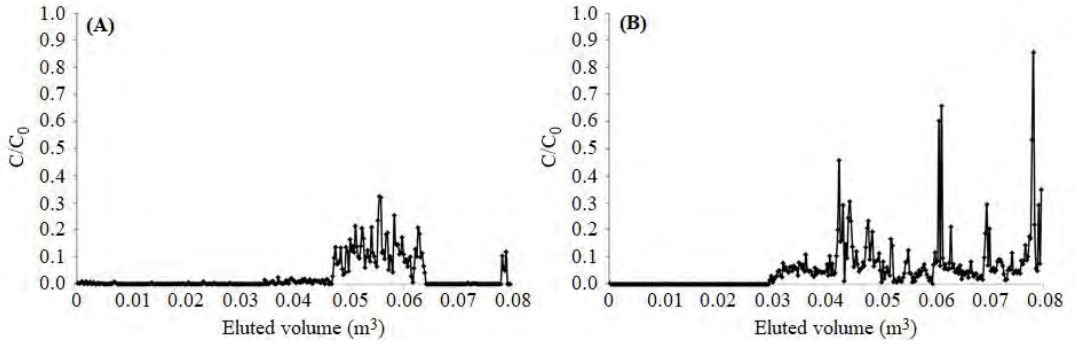

Fig. 7. Oil removal profile of DVB (a) and MMA-DVB (b) by the continuous flow process

3.2. Studies of Oil Retention Under Continuous Flow

The objective of this investigation of adsorption under continuous flow was to determine the saturation point of the adsorbents. Although this point is normally defined as the point where the quantity of oil in the water after treatment is the same as before treatment, here we considered the saturation point to be that where the concentration of oil in the eluted water was greater than or equal to 0.029 kg/m^3.

The tests were conducted using synthetic oily water at 0.2 kg/m^3, where the total oil and grease (TOG) concentration was measured before and after elution, allowing plotting C/C_0 *versus* volume eluted graphs. C/C_0 corresponds to the ratio between the TOG in the eluted water (C) and the water before elution (C_0). Aliquots of eluted water were collected each $2.0 \cdot 10^{-4}$ m^3.

Both resins showed high efficiency in removing oil from the water. In the system composed of the MMA-DVB resin (Fig. 7b), the removal efficiency was 100 % after elution of the first 30 l of water (10,316 bed volumes). After this volume, oil started to be detected in the eluted water, but the TOG value higher than 0.029 kg/m^3 was only detected after elution of approximately $4.2 \cdot 10^{-2}$ m^3 of water, corresponding to 14,700 bed volumes.

In turn, for the system formed by DVB, 100 % adsorption efficiency was achieved after elution of 47 l of oily water, corresponding to approximately 16,500 bed volumes. As of that point, the TOG concentration of the eluted water increased, with subsequent return to concentrations near zero, as shown in Fig. 7a.

The differences in the elution profiles of the two resins can be associated with their structures. MMA-DVB, because it contains ester groups, has higher polarity than DVB, which is basically composed of aromatic rings. These are probably capable of establishing more favored interactions with the compounds present in the oil, allowing better adsorption. The tests with both resins were conducted until elution of $8.0 \cdot 10^{-2}$ m^3 of oily water, the volume at which a sharp saturation peak was observed for MMA-DVB.

4. Conclusions

Both systems, DVB and MMA-DVB (70:30), adsorb oil in multilayers through physisorption, since their behaviors better fit the isotherm model proposed by Freundlich than that proposed by Langmuir. The adsorption occurring by physical interactions was confirmed by the kinetic study, whose results better fitted to the pseudo-second-order model, and low activation energy values for the adsorbate-resin interactions were obtained. For both resins, the adsorption process was fast, allowing their industrial application through the continuous flow process. The DVB resin presented slightly better oil removal efficiency than the MMA-DVB resin, probably because the larger surface area presented by the former: the water eluted through the columns contained 5 % of the original quantity of oil in eluted volumes of $4.8 \cdot 10^{-2}$ m^3 for DVB and $3.2 \cdot 10^{-2}$ m^3 for MMA-DVB. Such difference can be counterbalance by using slightly larger amount of the MMA-DVB in the column. Therefore, DVB resin can be industrially replaced by MMA-DVB resin to remove oil from oily water, due to the follwoing advantages: lower cost, lower toxicity and easy regeneration, as indicated by the kinetic and isotherm studies.

Acknowledgments

The authors thank Petrobras and the Brazilian Agencies: ANP, FINEP, CAPES, CNPq and FAPERJ.

References

[1] Stephenson M.: Soc. Pet. Eng., 1992, **44**, 548.
[2] Fakhru'l-Razia A., Pendashteha A., Abdullaha L. *et al.*: J. Hazard. Mat., 2009, **170**, 530. https://doi.org/10.1016/j.jhazmat.2009.05.044
[3] McCormack P., Jones P., Hetheridge M., Rowland S.: Wat. Res., 2001, **35**, 3567. https://doi.org/10.1016/S0043-1354(01)00070-7
[4] Lucas E., Mansur C., Spinelli L., Queirós Y.: Pure Appl. Chem., 2009, **81**, 473. https://doi.org/10.1351/PAC-CON-08-07-21

[5] Srinivasan A., Viraraghavan T.: Bioresour. Technol., 2010, **101**, 6594. https://doi.org/10.1016/j.biortech.2010.03.079
[6] Lucas E., Spinelli L., Khalil C.: Polymers Applications in Petroleum Production [in:] Mark H. (Ed.), Encyclopedia of Polymer Science and Technology. John Wiley & Sons, Inc., 2015. https://doi.org/10.1002/0471440264.pst641
[7] Rajakovic V., Aleksic G., Radetic M., Rajakovic L.: J. Hazard. Mat., 2007, **143**, 494. https://doi.org/10.1016/j.jhazmat.2006.09.060
[8] Barrufet M., Burnett D., Mareth D.: SPE Annual Techn. Conf. and Exhib., Dallas 2005, 9.
[9] Tao F., Hobbs R., Sides J. *et al.*: SPE/EPA Exploration and Production Environmental Conference, San Antonio, 1993, 3.
[10] Souza A., Furtado C.: Bol. Tec. Prod. Petrol. Rio de Janeiro, 2006, **1**, 215.
[11] Robinson D.: Filtration + Separation, 2013, **50**, 38. https://doi.org/10.1016/S0015-1882(13)70168-X
[12] Bataee M., Irawan S., Ridha S. *et al.*: SPE Journal, 2017, **22**, 1. https://doi.org/10.2118/183627-PA
[13] CONAMA (Conselho Nacional do Meio Ambiente) – Resolution number 393, 2007.
[14] Den Broek W., Plat R., Der Zande M.: SPE Int. Oil and Gas Conf. and Exhib. in China, Beijing 1998.
[15] Munirasu S., Haija M., Banat F.: Proc. Saf. Environ. Prot., 2016, **100**, 183. https://doi.org/10.1016/j.psep.2016.01.010
[16] Masqué N., Galià M., Borrull F.: Chromatographia, 1999, **50**, 21. https://doi.org/10.1007/BF02493612
[17] Sokker H., El-Sawyb N., Hassan M., El-Anadoul B.: J. Hazard. Mat., 2011, **190**, 359. https://doi.org/10.1016/j.jhazmat.2011.03.055
[18] Okiel K., El-Sayed M., El-Kady M.: Egypt. J. Pet., 2011, **20**, 9.
[19] Igunnu E., Chen G.: Int. J. Low Carbon Technol., 2014, **9**, 157. https://doi.org/10.1093/ijlct/cts049
[20] Li H., Jiao Y., Xu M. *et al.*: Polymer, 2004, **45**, 181. https://doi.org/10.1016/j.polymer.2003.11.013
[21] Huang J., Huang K., Wang A., Yang Q.: J. Colloid Interf. Sci., 2008, **327**, 302. https://doi.org/10.1016/j.jcis.2008.09.006
[22] Fontanals N., Galiá M., Cormack P. *et al.*: J. Chromatogr. A, 2005, **1075**, 51. https://doi.org/10.1016/j.chroma.2005.04.010
[23] Dumont P., Fritz J.: J. Chromatogr. A, 1995, **691**, 123. https://doi.org/10.1016/0021-9673(94)00766-3
[24] Nash D., McCreath G., Chase H.: J. Chromatogr. A, 1997, **758**, 53. https://doi.org/10.1016/S0021-9673(96)00710-8
[25] Iayadene F., Guettaf H., Bencheikh Z. *et al.*: Eur. Polym. J., 1998, **34**, 219. https://doi.org/10.1016/S0014-3057(97)00099-2
[26] Bouvier E., Meirowitz R., McDonald P.: Pat. US 6254780. Publ. Jul. 3, 2001.
[27] Zhou Y., Chen L., Hu X., Lu J.: Ind. Eng. Chem. Res., 2009, **48**, 1660. https://doi.org/10.1021/ie8012242
[28] Zhou Y., Tang X., Xiao-Men H. *et al.*: Sep. Pur. Technol., 2008, **63**, 400. https://doi.org/10.1016/j.seppur.2008.06.002
[29] Kundu P., Mishra I.: Sep. Pur. Technol., 2013, **118**, 519. https://doi.org/10.1016/j.seppur.2013.07.041
[30] Clarisse M., Queirós Y., Barbosa C. *et al.*: Chem. Chem. Technol., 2012, **6**, 145.
[31] Aversa T., Queirós Y., Lucas E., Louvisse A.: Polímeros, 2014, **24**, 45. https://doi.org/10.4322/polimeros.2013.048
[32] Silva C., Rocha Q., Rocha P. *et al.*: J. Environ. Manag., 2015, **57**, 205. https://doi.org/10.1016/j.jenvman.2015.04.025
[33] Cardoso A., Lucas E., Barbosa C.: Polímeros, 2004, **14**, 201. https://doi.org/10.1590/S0104-14282004000300017
[34] Queirós Y., Clarisse M., Oliveira R. *et al.*: Polímeros, 2006, **16**, 224. https://doi.org/10.1590/S0104-14282006000300012
[35] Aversa T., Silva C., Rocha Q., Lucas E.: J. Environ. Sci. Health A, 2016, **51**, 634. https://doi.org/10.1080/10934529.2016.1159872
[36] Tibbetts P., Buchanan I., Gawel L., Large R.: A Comprehensive Determination of Produced Water Composition [in:] Ray J., Engelhardt F. (Eds.), Produced Water: Technological/Environmental Issues and Solutions. Springer Science & Business Media, New York 1992. https://doi.org/10.1007/978-1-4615-2902-6_9
[37] Galkin A.: J. Anal. Chem., 2004, **50**, 1078.
[38] Rendell D.: Fluorescense and Phosforescence. John Wiley & Sons, Bristol 1987.
[39] Adamson A.: Physical Chemistry of Surfaces. John Wiley & Sons, California 1990.
[40] Ho Y., McKay G.: Chem. Eng. Res. Design, 1998, **76**, 332.
[41] Sho Y., Wase J. A. D., Forster F. C.: Environ. Technol., 1996, 17, 71. https://doi.org/10.1080/09593331708616362
[42] Smith F., Hashemi J.: Fundamentos de Engenharia e Ciência dos Materiais. McGraw Hill Brasil, Porto Alegre 2012.
[43] Huang J., Jin X., Mao J. *et al.*: J. Hazard. Mat., 2012, **217**, 406. https://doi.org/10.1016/j.jhazmat.2012.03.053
[44] Cheng S., Tang H., Yan H.: J. Appl. Polym. Sci., 2006, **102**, 4652. https://doi.org/10.1002/app.24702
[45] Drechny D., Trochimczuk A.: React. Funct. Polym., 2006, **66**, 323. https://doi.org/10.1016/j.reactfunctpolym.2005.10.024
[46] Kennedy L., Vijaya J., Sekaran G., Kayalvizhi K.: J. Hazard. Mat., 2007, **149**, 134. https://doi.org/10.1016/j.jhazmat.2007.03.061
[47] Teixeira V., Coutinho F., Gomes A.: Quim. Nova, 2004, **27**, 754. https://doi.org/10.1590/S0100-40422004000500015
[48] Guimarães D., Leão V.: J. Hazard. Mat., 2014, **280**, 209. https://doi.org/10.1016/j.jhazmat.2014.07.071
[49] Azizian S.: J. Colloid Interf. Sci., 2004, **276**, 47. https://doi.org/10.1016/j.jcis.2004.03.048
[50] Plazinski W., Dziuba J., Rudzinski W.: Adsorption, 2013, **19**, 1055. https://doi.org/10.1007/s10450-013-9529-0

Received: February 07, 2018 / Revised: March 16, 2018 / Accepted: June 03, 2018

ВИДАЛЕННЯ НАФТИ З ВОДНИХ СИСТЕМ ПОЛІДИВІНІЛБЕНЗЕНОВИМИ ТА ПОЛІМЕТИЛМЕТАКРИЛАТ-ДИВІНІЛБЕНЗЕНОВИМИ СМОЛАМИ: ІЗОТЕРМАЛЬНІ ТА КІНЕТИЧНІ ДОСЛІДЖЕННЯ

Анотація. *Досліджені метилметакрилат-дивінілбензенова (ММА-ДВБ) та дивінілбензенова (ДВБ) смоли для адсорбції нафти в штучному середовищі нафта-вода. Дослідження проводили для двох процесів: (i) безперервний процес для оцінювання кількості води з нафтою, яку можна елюювати до досягнення межі насичення смол; і (ii) періодичний процес для одержання кінетичної та ізотермічної моделі двох смол., Встановлено, що для обох смол результати найкраще відповідають ізотермі Фройндліха та кінетичній моделі псевдодругого порядку. Знайдені значення низької енергії активації свідчать про фізичну адсорбцію між смолами та нафтою. Показано, що незважаючи на непогану ефективність ДВБ смоли щодо видалення нафти, її можна замінити промисловою смолою ММА-ДВБ, завдяки таким перевагам як менша вартість, токсичність та легкість регенерації.*

Ключові слова: *оброблення нафтовмісної води, адсорбція, пористі полімерні смоли, ізотерма, кінетична модель.*

Chem. Chem. Technol., 2019,
Vol. 13, No. 3, pp. I

Events

IN MEMORY OF PROFESSOR JACEK NAMIESNIK
1949–2019

On April 14, 2019 suddenly died Professor Jacek Namiesnik, Rector of Gdansk University of Technology (Poland).

This sincere and intelligent person left warm recollections and deep gratitude for his contribution to the establishment and enhancement of cooperation in science and education, particularly among Lviv Polytechnic National University and Gdansk University of Technology.

Prof. J. Namiesnik was a Polish chemist, full professor of Gdansk University of Technology, specialist in the field of analytical chemistry, environmental chemistry and green analytical chemistry. He published above 900 scientific works, was the author of 10 patents. He has won numerous awards for outstanding scientific achievements. Jacek Namiesnik was the director of Doctoral Studies at the Faculty of Chemistry. The supervisor of 65 PhD thesis.

He was also an active member of several editorial boards of scientific and scientific-technical journals, including *Chemistry & Chemical Technology*.

He was also very active outside of the home institution, as is evidenced by the large number of functions he performed in various academic and professional associations: Polish Chemical Society, International Union of Pure and Applied Chemistry, Romanian Society of Analytical Chemistry, Steering Committee International Society of Environmental Analytical Chemistry, Member of Scientific Board Institute of Oceanology, Institute of Nuclear Chemistry and Technology, European Academy of Sciences and Arts.

Prof. Namiesnik was a scientist who no only concentrated his efforts on the introduction of native university into a prestigious group of higher education institutions, but also made it possible for Ukrainian scientists to teach at the Gdansk University of Technology, and for Ukrainian students to study there in the framework of program Erasmus+.

With great sadness we perceived the tragic news of the death of this unique man and great scientist who connected his entire career with Gdansk University of Technology and was one of the most famous Polish scientists.

Editorial Board
journal *Chemistry & Chemical Technology*